The Biological Activities of Benzimidazole-Based Fluorophores

Chloe Louise Howells

This dissertation is submitted for the degree of Doctor of Philosophy

March 2022

Department of Chemistry

Word count:

This Thesis is dedicated to

Marion Patricia Howells

And

Mansel Gordon Howells.

Love and miss you more more more xxx

Declaration

This thesis has not been submitted in support of an application for another degree at this or any other university. It is the result of my own work and includes nothing that is the outcome of work done in collaboration except where specifically indicated. Many of the ideas in this thesis were the product of discussion with my supervisor Dr. Nick Fletcher.

Abstract

Investigating Benzimidazole Based Fluorophores for Their Biological Activities

Chloe Louise Howells

This research thesis concerns the synthesis of novel mononuclear ruthenium(II) polypyridyl complexes with one ligand functionalised with benzimidazole groups, and the investigation into their ability to interact with DNA and various anions using different techniques, such as UV/Vis absorbance and emission, ^{1}H-NMR and circular dichroism spectroscopies.

Various complexes of the form [Ru(bpy/phen)$_2$(L)]$^{2+}$ {where bpy = 2,2´-bipyridine, phen = 1,10-phenanthroline, L = 4,4′-bis(benzimidazol-2-yl)-2,2′-bipyridine (bbib), 4,4'-*bis*(amidobenzimidazol-2-yl)-2,2'-bipyridine (bbaib), 4,4′-*bis*(benzimidazole-2-yl-methyl)-2,2′-bipyridine (bbimb), 4,4′-*bis*(benzimidazole-2-yl-carbonyl)-2,2′-bipyridine (bbimbo)} were synthesised in their racemic forms.

Absorbance, fluorescence and ^{1}H-NMR titrations studies were used to investigate the interaction between the complexes and dihydrogen phosphate, acetate, chloride and bromide anions. The results indicated that [Ru(bpy)(bbib)]$^{2+}$, [Ru(phen)(bbib)]$^{2+}$ [Ru(bpy)(bbaib)]$^{2+}$, [Ru(phen)(bbaib)]$^{2+}$, [Ru(bpy)(bbimb)]$^{2+}$ and [Ru(bpy)(bbimbo)]$^{2+}$ have high levels of interaction with dihydrogen phosphate and acetate in aqueous environments and no interaction with bromide and chloride. Stability constants calculated for [Ru(bpy)(bbib)]$^{2+}$, [Ru(phen)(bbib)]$^{2+}$ [Ru(bpy)(bbaib)]$^{2+}$ and

$[Ru(phen)(bbaib)]^{2+}$ suggest a 2:1 guest:host stoichiometry for dihydrogen phosphate and a 1:1 guest:host stoichiometry with acetate.

UV/Vis absorption, luminescence and circular dichroism (CD) titration studies with calf thymus DNA (*ct*-DNA) were used to analyse the binding between the racemic complexes and *ct*-DNA. The results were insufficient to confirm whether interaction occurs between $[Ru(bpy)(bbib)]^{2+}$, $[Ru(phen)(bbib)]^{2+}$ $[Ru(bpy)(bbaib)]^{2+}$, $[Ru(phen)(bbaib)]^{2+}$, $[Ru(bpy)(bbimb)]^{2+}$ and $[Ru(bpy)(bbimbo)]^{2+}$ and *ct*-DNA. CD Thermal denaturation studies indicated a decrease in stability of *ct*-DNA structure in the presence of $[Ru(bpy)(bbib)]^{2+}$, $[Ru(phen)(bbib)]^{2+}$ $[Ru(bpy)(bbaib)]^{2+}$ and $[Ru(phen)(bbaib)]^{2+}$. Equilibrium membrane dialysis studies were employed to determine whether enantioselective binding occurs between complex and *ct*-DNA. The results gave no indication that there are enantioselective interactions between $[Ru(bpy)(bbib)]^{2+}$, $[Ru(phen)(bbib)]^{2+}$ $[Ru(bpy)(bbaib)]^{2+}$ and $[Ru(phen)(bbaib)]^{2+}$ and *ct*-DNA. Viscosity studies with *ct*-DNA showed no change in relative viscosity of *ct*-DNA with $[Ru(bpy)(bbib)]^{2+}$, $[Ru(phen)(bbib)]^{2+}$ $[Ru(bpy)(bbaib)]^{2+}$ and $[Ru(phen)(bbaib)]^{2+}$.

Acknowledgements

First and foremost, I would like to give my thanks to Dr. Nick Fletcher for the time, effort given and for often being my shoulder to cry on! Thank you for giving me such an awesome opportunity to develop my skills and taking so many chances on me. I cannot express how grateful I am to have had you as my PhD supervisor. We're at the end now!

Thank you to all the technical staff and other members of the department that have given up their time to help me through this! Especially, a shout out to Dr. David Rochester, Dr. Geoff Aiken (the amount of troubleshooting you've done has practically saved this project!) and Dr. Nathan Halcovitch. Thanks to the great people that have populated C21 over the years and given me so many laughs when I felt near to tears! Thank you to Josh and Bette especially, who have shared so many vents and laughs and made lab work that much more enjoyable!

To Mum and Tony, and Dad and Kays, thank you so, so much for putting up with me being a poor university student for over nine years, supported me when I needed it most and helped me so much. Thank you to my lovely nieces and nephew, Willow, Lola and Rohan for putting up with Aunty Chloe living far away!

Thank you to my best friends since high school, Lydia, Jenny, Amy and Amber for giving me a reason to look forward to coming back to Wales and for always listening to my rants!

My biggest thanks and love go to Nan and Grandad. You were my biggest fans throughout all of this, and I hope I've made you proud. I did this all for you and I couldn't have done it without you.

Table of Contents

Glossary of Words

4,4΄-bbib

4,4΄-bbaib

4,4΄-bbimb

4,4΄-bbimbo

A

BP

Bpy

C

CD

COSY

ct DNA

d

DCM

dd

ddd

DMF

DMSO

DNA

Dppz

EtBr

EtOH

G

IR

K_b

LC

LDA

LMCT

m

M

MC

MLCT

Chapter One

Chapter One – Introduction

1.1 Overview

Deoxyribonucleic acid (DNA) is considered to be one of the most important components of life. It is a large chemical structure containing the information required to maintain healthy cells within an entity, in the form of genetic coding. This data can be replicated, transcribed/processed as RNA and translated into essential proteins.[1] These processes are very specific and are regulated by binding of site-specific molecules to the nucleic acids. This makes DNA a worthwhile target for pharmaceutical research, where the synthesis of molecules that can bind to nucleic acid sites can be put forward for therapeutic uses, such as distamycin (Figure 1.1), a groove binder used in the treatment of cancer.[2]

Transition metal complexes have been of great interest for medicinal use for a number of years, with the most well-known example of this being cis-platin, a platinum(II) complex used in the treatment of several cancers (Figure 1.1).[3] However this drug, and many others like it, comes with severe disadvantages such as unwanted side-effects and development of resistance, resulting in the need for new and improved drugs to be available.[4] Transition metals complexes have distinct advantages over organic compounds as anti-cancer drugs, as they have a wide range of characteristics that can be finetuned to specific purposes or targets, either by changing the metal centre or variation in the attached ligands.[5-7] There are multiple ways in which these molecules can bind to DNA, and establishing the binding mode is imperative to tuning characteristics to suit need. Recent developments have included ruthenium complexes

as potential therapeutics in the fight against cancer, such as RAPTA-C, a piano-stool ruthenium (II) complex which is currently undertaking clinical trials (Figure 1.1).[8] This introduction will introduce the concept of DNA/RNA structures, evaluate the use of transition metal complexes in targeting them, along with the introduction of the use of these complexes in anion binding in a biological setting.
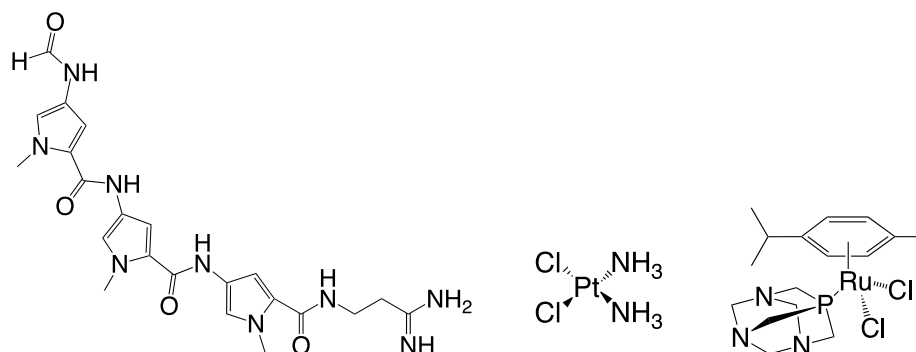
Figure 1.1 – The structures of distamycin, cisplatin and RAPTA-C.

1.2 DNA

1.2.1   Nucleic Acid Structure

DNA stores all genetic information for healthy cells to maintain and replenish themselves, in the form of strands made up of a long chain of components called nucleotides. These have three constituent parts, consisting of a 2'-deoxy-D-ribose sugar, which bonds to phosphate groups via the 3' and 5' positions (Figure 1.2). At the 5' position, a nitrogenous base is linked onto the sugar via a β-glycosidic bond and for DNA, is either adenine (A), thiamine (T), cytosine (C) or guanine (G). The sugar is replaced with D-ribose in ribonucleic acid (RNA), and uracil (U) replaces thiamine.
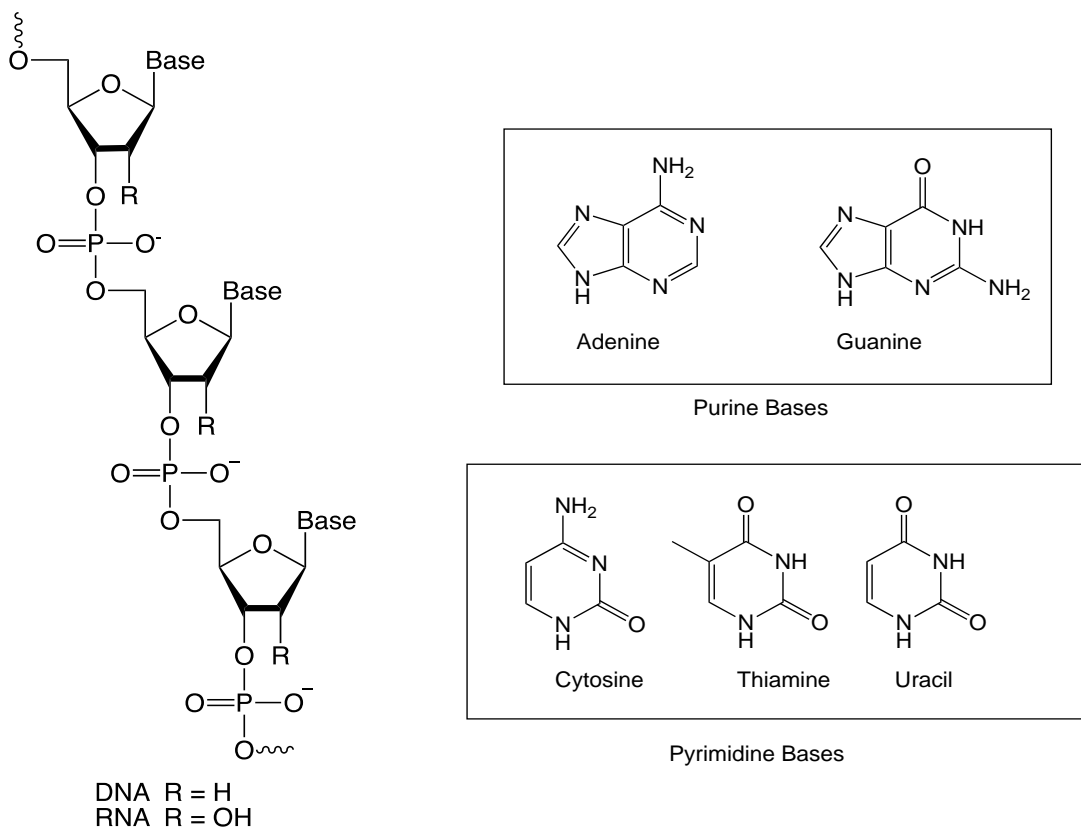
Figure 1.2 *- Polynucleotide structure and base structures for DNA and RNA.*

The 3D duplex structure of DNA that we have come to understand was originally proposed by Watson and Crick in 1953 using the X-ray data obtained by Franklin.[9] Two antiparallel nucleotide chains (strands) are affixed by perpendicular hydrogen bonding between base pairs, A and T or G and C. As the chains run opposite directions, the grooves formed are not equal in size, known as major and minor grooves. The major groove is understood to interact with proteins in order to regulate several gene expression mechanisms, whereas the minor groove is more known as a target in medicinal chemistry, including transition metal complexes, although endogenous proteins can also interact here. There are three main forms of double stranded DNA, known as A-form, B-form and Z-form (Figure 1.3).

The most common type of DNA structure is the B-form, which arises in highly hydrated environments, where there is a low salt concentration. It is a right-handed helix, with 10.4 base pairs per turn and a diameter of 23.7 Å. This is the form found by Franklin in her X-ray crystallography work and is represented by the Watson-Crick model. A-form is produced where there is less hydration, and salt concentration is slightly higher than for B-form. Like B-form DNA it is a right-handed helix, but is slightly wider, with 11 base pairs per turn and a diameter of 25.5 Å. Finally, Z-form is the least common arrangement of DNA. Found in areas of high salt concentration, it is made of a left-handed helix, with a smaller diameter of 18.4 Å, but has 12 base pairs per turn. The name Z-form comes from the "zig-zag" structure that the phosphate groups create.
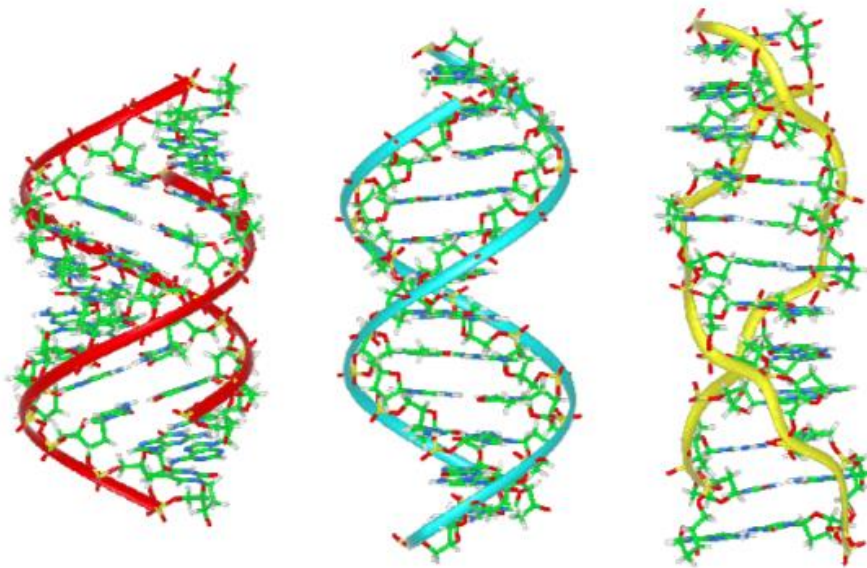
Figure 1.3 - *Illustrations of A-, B- and Z-forms of DNA (source - Wikipedia).*

The variations in structure between the three forms of DNA result in large differences in the size and depth of the major and minor grooves, caused by sugar puckering when opposing base pairs form hydrogen bonds (Figure 1.4). The major groove of B-form DNA has a similar depth to its minor groove but is much broader. Comparatively, A-

form DNA has a much narrower and deeper major groove with a wide and shallow minor groove, and Z-form has a flat major groove and a narrow, deep minor groove.
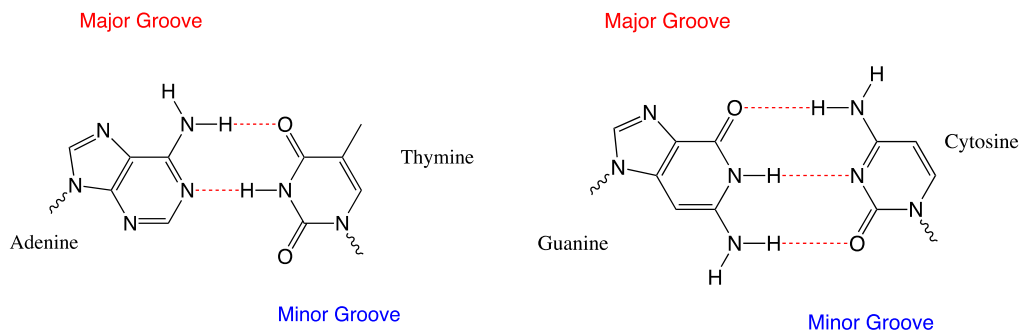
Figure 1.4 *Hydrogen bonding of DNA.*

The main structural difference between DNA and RNA is the 2'-hydroxyl group on the RNA sugar group, and because of this RNA favours to form other secondary structures. This means that RNA is more likely to hydrolyse as the 2'-OH can act as a nucleophile when deprotonated and attack the adjacent phosphorus of the phosphate backbone, and prefers to form single-stranded structures with itself, although it can still adopt the double stranded form. These single-stranded motifs include bulge sites and hairpin loops, where Watson-Crick base pairs form within the same strand, leaving regions where pairs are unable to form motifs.

Bulge sites are unpaired stretches of nucleotides formed by hydrogen-bonded bases of a single strand within a nucleic acid duplex. They can vary in size from singular unpaired residues to a bulge of several nucleotides that can form flexible extrusions from the double helix, creating unique recognition sites in the three-dimensional structures of DNA and RNA.[10] Hairpin loops consist of two structural elements, a double stranded DNA or RNA stem (often containing mismatches and bulge sites) and a terminal loop where the single strand doubles back on itself like the shape of a hairpin.

These are the most common form of secondary structures found, especially in RNA. These loops can guide RNA folding, determine interactions in a ribozyme, protect mRNA from degrading or act as an substrate for enzyme interaction.[11]

1.2.2 Nucleic Acid Interactions

New, improved drug candidates are always a hot topic in the field of medicinal chemistry. Often this involves establishing an initial candidate and modifying it in order to minimise any negative effects. A thorough understanding of any interactions that occur between candidate and its target is essential, as they might result in side effects (possibly due to inhibition of interactions between DNA and proteins or other nucleic acid structures). Drugs that target nucleic acids are often tested using DNA alone due to the various regions of potential drug targets. Interactions that occur between nucleic acid and a drug may be electrostatic, a result of hydrogen bonding and hydrophobic interactions within either major or minor grooves (groove binding), intercalation of aromatic areas of a complex into DNA, or formation of covalent bonds between complex and sugar or base of DNA strands.

1.2.2.1 Electrostatic Interactions

DNA electrostatic interactions are essential in many biological processes that maintain and regulate cell functions in eukaryotic cells. Spermine (Figure 1.5), a polycationic organic molecule, has been found to play a major role in cell proliferation via its electrostatic interactions with DNA.[12-13] In cellular environments, spermine is found as a fully protonated species (tetracationic), enabling both hydrogen bonding and long-range electrostatic interactions to form with the double helix, particularly in the hydrophobic regions of the major groove and the negatively charged phosphate

backbone.[14] In these areas, hydrogen bonds form between primary amines and the available oxygens and between secondary amines and N7 guanine positions, and change the spatial positioning of oxygens on the phosphate backbone to better enable hydrogen bonding.[15] Spermine, like the cations K^+ or Mg^{2+}, can also cause the DNA to switch between secondary structures, which can control other DNA interactions such as protein binding in order to regulate important biological systems e.g. DNA condensation.[16]
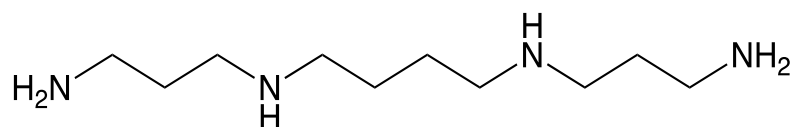
Figure 1.5 *- Structure of spermine.*

1.2.2.2   Covalent Interactions

The formation of covalent adducts between DNA and a drug is a well-established mechanism used in chemotherapy. The formation of these non-reversible adducts introduce defects into the DNA structure such as cross-strand linkages, resulting in disruption of key mechanisms in cell replication. This disruption causes cell cycle (the process through which a cell grows and divides) arrest as essential proteins can potentially no longer bind to DNA, leading to apoptosis.[17]

It is thought that NAMI-A (Figure 1.6), a pseudo-octahedral Ru(III) complex containing an imidazole moiety, uses covalent interactions in order to achieve cell death. It is the first ruthenium complex to undergo clinical trials for use as a chemotherapeutic.[18-19] The complex is hydrolysed twice to form the active species upon cellular uptake. This has been found to react with the guanine N7 position, an electron-rich atom, forming bifunctional interstrand adducts, which are capable of preventing RNA synthesis from occurring.[20] However, despite the evidence of DNA binding, it is debated whether this

is the main mechanism that results in apoptosis, as there are also observations that NAMI-A interacts with extracellular collagen and serum proteins, potentially disrupting vital biological processes in this manner.[21-22]
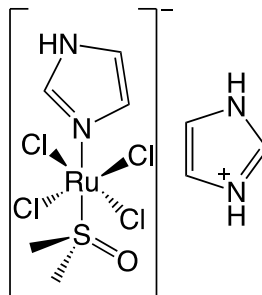
Figure 1.6 - The structure of NAMI-A.

1.2.2.3   Intercalation

Intercalation is high affinity binding mechanism, where a highly aromatic region of a molecule inserts itself between adjacent base pairs in the DNA double helix.[23] This action forces the bases apart, altering the helical structure and ultimately lengthening the strands, causing the DNA to unwind. The distortion can cause inhibition of key processes in DNA replication, such as transcription, as protein binding is no longer possible.[24] Intercalators are usually electron deficient planar complexes with polyaromatic planar groups. Electrostatic interactions initially occur as the molecule approaches the DNA. This insertion is stabilised by high levels of π-stacking between the aromatic base pairs and the ligand, and furthermore so by the formation of hydrogen bonds and van der Waals interactions.[25]

An example of an intercalator used in chemotherapy is doxorubicin (Figure 1.7). This organic compound is used in the treatment of many cancers, including lymphoma. The intercalation of doxorubicin into the DNA results in prevention of the progression of topoisomerase II by stabilising the DNA-enzyme complex after the double helix has

been cleaved, which inhibits the next steps in DNA replication.[26] The aromatic ligand sits between the base pairs while the six membered sugar sits within the minor groove and forms electrostatic interactions with the adjacent base pairs, strengthening the interaction.[27]
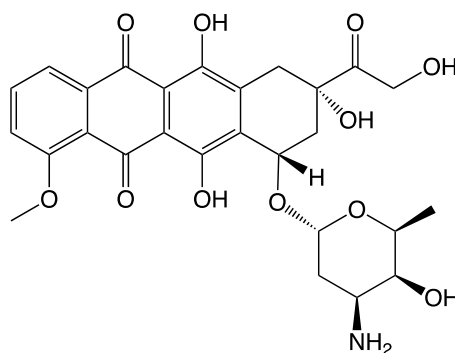
Figure 1.7 - *The structure of doxorubicin.*

1.2.2.4   Groove binding

Groove binding interactions are reversible electrostatic that occur specifically in the grooves of the DNA double helix. The main difference between the major and minor grooves are their widths and depth, which are caused by sugar puckering (hydrogen bonding between Watson-Crick base pairs). Within the major groove, the N7 and O6 of guanine, N7 of adenine and O4 of thiamine act as hydrogen bond acceptors and the exocyclic NH_2 groups of adenine and cytosine are hydrogen bond donors. In the minor groove, the hydrogen bond acceptors are the N3 of adenine and guanine and the O2 of thiamine and cytosine, and the exocyclic amine group of guanine acts as a hydrogen bond donor (Figure 1.4).

The use of groove binding differs depending on which groove is the target. Major groove binding tends to be utilised in biological mechanisms such as steps in DNA replication which require sequence-specific DNA binding proteins, e.g. histones and

transcription factors.[28] Minor groove binding agents have a varied use, from antibiotics and antivirals to anticancer agents, although endogenous proteins can also interact here. Lexitropsins (Figure 1.8), analogues of distamycin and netropsin, are highly researched minor groove binders. It has been observed crystallographically that they bind to DNA in A-T rich regions, anti-parallel and side by side in the minor groove.[29] The data also showed that the N-H amide groups lie towards the groove, enabling hydrogen bonds to form with A-T base pairs, spanning 5+1 base pairs.[30] The crescent shape of the lexitropsins is a very important factor in their ability to bind in the minor groove, fitting neatly into the proportions. The shape and charge of the molecule maximise the stability of the binding via electrostatics, hydrogen bonding and Van der Waals interactions.[31]

R = CH, N
R' = CH, N
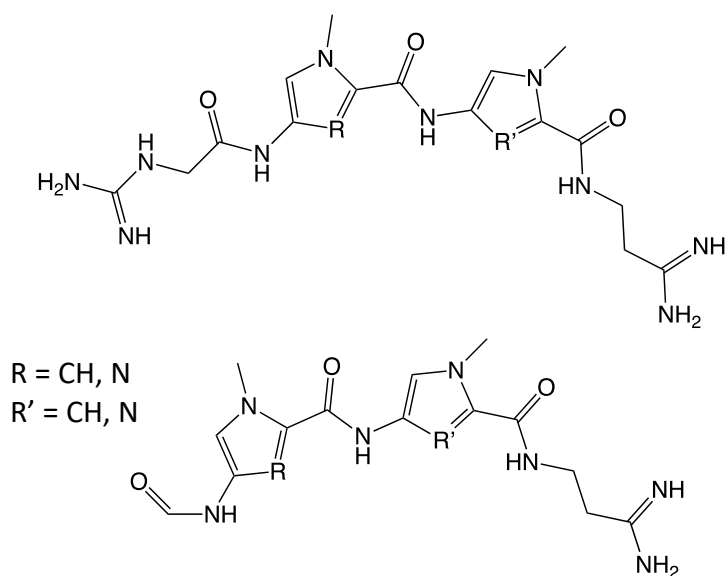
Figure 1.8 - Structural examples of Lexitropsins.

1.3 Imidazoles and Benzimidazoles as Dyes and Drugs

Many important natural products contain imidazole rings aside from nucleic acids. One of the most prevalent structures is the amino acid histidine (Figure 1.9), consisting of an α-amino group and an imidazole side chain. This amino acid is essential for the biosynthesis of proteins and is a common ligand in metalloproteins.[32] It is also the

11

precursor for the imidazole-based hormone histamine, which makes up part of the immune response system amongst other important roles.[33,34] With so many examples of imidazoles occurring in the body, it is understandable that so many drugs used today include imidazole moieties.
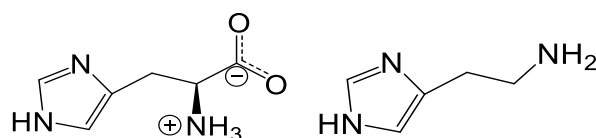
Figure 1.9 – The structures of histidine and histamine respectively.

Perhaps some of the most well-known minor groove binding molecules are the Hoechst stains, such as Hoechst 33258 (Figure 1.10). These synthetic dyes contain a bis-benzimidazole and are functionalised by a methylpiperazine on one end and another group opposing, which varies between dyes. In the case of Hoechst 33258, the functionalisation comes from a phenol group. They are blue fluorescent dyes used in many applications for the staining of B-DNA in bacterial and eukaryotic cells.[35] In order to bind within the minor groove, the NH groups of the bis-benzimidazole rings form hydrogen bonds with O2 of thymine and N3 of adenine, which are then further stabilised by van der Waals interactions between the molecule and the minor groove floor.[36,37] The fluorescent properties of Hoechst stains are greatly enhanced when the drug is bound to A-T rich regions within the minor grooves when compared to interactions with G-C rich regions in the same environment.[38]
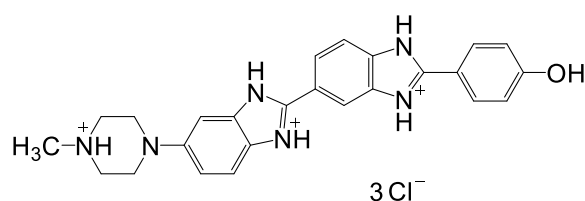
Figure 1.10 – The structure of Hoechst 33258.

Not all imidazole-containing drugs target DNA grooves as their primary mechanism of action. Metronidazole (Figure 1.11) is a nitroimidazole prodrug with a methyl group at the 2 position, a nitro group at the 5 position and an ethyl alcohol group on N1. It is classified as an antibiotic, used to treat anaerobic bacterial infections, e.g. pelvic inflammatory disease and protozoal infections.[39] The molecule enters the bacterial cell via passive diffusion across the cell wall/membrane where the nitro group is immediately reduced by the pyruvate:ferredoxin oxidoreductase system, resulting in the formation of a nitro radical.[40,41] The reduction only occurs within the cell itself, creating a positive concentration gradient therefore pulling more of the inactive drug into the cell.[42] The nitro radical is also thought to be the means by which the drug destroys cells, by inhibiting DNA synthesis and repair and causing breaks within the strands via oxidative stress.[43,44] Metronidazole is quite commonly used as the first port of call for a lot of infections due to its inaction in aerobic cells. This is because only anaerobic and microanaerobic cells have the redox potential required to reduce the nitro group from the inactive to the active form.[43]
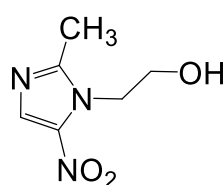
Figure 1.11 – *The structure of Metronidazole.*

Azole-based agents are very commonly used to combat fungal infections. Clotrimazole (Figure 1.12) is commonly prescribed to treat various *Candida* infections and is comprised of two benzene rings, a 2-chlorobenzene ring and an imidazole ring, all surrounding a central carbon atom. The drug is introduced into the fungal cell, where it

binds to the active site of lanosterol 14α-demethylase, through a haem cofactor where the sixth position of the iron is occupied by the imidazole nitrogen.[45,46] This binding inhibits the enzyme so it can no longer demethylate lanosterol, halting the biosynthesis of ergosterol, an essential component of the fungal cell wall.[46] The cell wall has a much higher permeability without this lipid, causing intracellular constituents to leak out, resulting in cell lysis.[47]
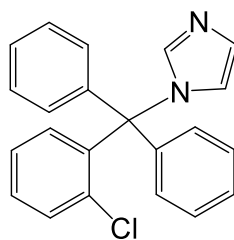
Figure 1.12 – *The structure of Clotrimazole.*

Clotrimazole has also been investigated for its potential in fighting cancerous cells. In 1995, Benzaquen *et al.* found that the drug could inhibit cancer cell proliferation and tumour growth *in vivo.*[48] Multiple targets have been established that contribute to the anticancer activity, however the main mechanism of action of clotrimazole is as an inhibitor of hexokinase, a major enzyme overexpressed in malignant tumours. Hexokinase normally protects the cell from apoptosis (a form of programmed cell death where biochemical events lead to cell death) when bound to voltage dependant anion channels by blocking released cytochrome c from the mitochondrial outer membrane. This blocking causes detachment of mitochondrial-bound hexokinase, resulting in cell death.[48] Another mechanism suggested to contribute to anticancer activity is the inhibition of calcium binding proteins resulting in the depletion of Ca^{2+} stores from the cell that cannot be replenished through normal cell mechanisms.[49] This interaction interferes with the Ca^{2+} activated potassium channels of the cell, meaning that translation cannot occur therefore slowing tumour growth.[50] More recent studies have

attempted to put clotrimazole onto a metal centre, such as ruthenium or platinum, and test the resulting complexes on cell lines. In many cases, the metal-bound drug was found to cause higher levels of apoptosis than cisplatin or organic clotrimazole. [51-53]

1.4   Transition metal complexes and DNA

Transition metal (TM) complexes are considered excellent candidates for DNA binding chemotherapeutics. The initial breakthrough was serendipitous, when in 1965 Rosenberg *et al.* discovered the ability of cisplatin to control cell division, now understood that the platinum(II) complex achieves this by cross-linking itself into the double stranded DNA helix.[54] These cross-links form intra- and interstrand adduct, which causes bending and unwinding of the duplex, resulting in cell death.[55] Nowadays more and more TM complexes are reported for their abilities to interact with nucleic acids, leading to new and exciting methods in targeting and treating diseases.

Transition metal complexes have a distinct advantage over organic compounds in interacting with DNA. Their binding properties are characterised in such a way that they can be finetuned by substituting the ligands. Ligand choice when synthesising a complex able to bind to DNA can direct the mode of binding that is possible. Changing ancillary ligands can influence DNA binding too. Transition metal complexes that interact with nucleic acids often have bidentate ancillary ligands, such as 2,2ʹ-bipyridine (bpy) or 1,10-phenanthroline (phen). When included in tris(bidentate) TM complexes, these ligands are thought to weakly interact with DNA.[56] $[Ru(bpy)_3]^{2+}$ and $[Ru(phen)_3]^{2+}$ show interesting results when bound to nucleic acids. They are attracted into the minor groove and bind via ion pairing.[57] DNA is surrounded by a hydration

sphere, being in an aqueous environment, which is displaced when these complexes are introduced due to the hydrophobic orthogonal organic clefts created by the polypyridyl ligands.[58] However, for the 1,10-phenanthroline analogue, the story does not end here. It has been argued that one of the ligands partially intercalates between base pairs via the middle aromatic ring. Full intercalation cannot occur due to clashing between the DNA strand and the outer rings, i.e. the ligand does not project out enough to fully insert.[59,60]

Many transition metal complexes have DNA binding properties that result in photon emission when bound. This is beneficial to researchers as it can help to identify if a complex is targeting nucleic acids in cells, rather than other organelles or intracellular components. The most well-known example of this phenomenon is $[Ru(phen)_2(dppz)]^{2+}$ (Figure 1.14), which exhibits a "light switch" effect when bound to DNA. The intercalator shows no photoluminescence in aqueous solution alone, however in the presence of DNA a strong emission is observed indicative of interactions occurring.[61] This also has allowed for marking the site of intercalation and has helped to further understand the recognition properties of the complex.[62]
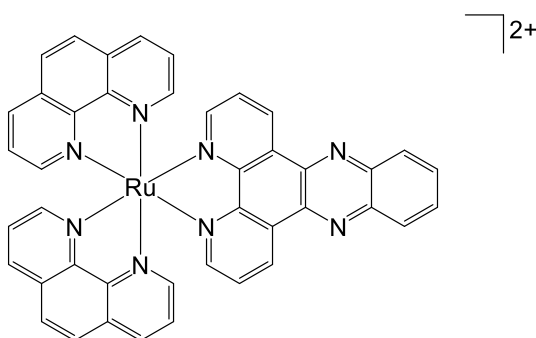
Figure 1.14 – The structure of [Ru(phen)₂(dppz)]²⁺(Ru-1).

More subtle changes to ligands can finetune DNA interactions further. Replacement with analogous or homologous forms of a ligand can result in changes in the strength and specificity of DNA binding by the complex. Consequently, vast libraries of complexes with subtle variations in the analogous ligands have been made with different properties to suit the needs of the user. Ru-2 (Figure 1.15) is a dicationic species, and is known to intercalate via the tpphz (tetrapyridyl [3,2-*a*:2',3',-*c*:3",2"-*h*:2"',3"'-*j*] phenazine) ligand into the DNA base stack. However, a small change to this ligand results in a complete change in binding properties. The addition of an ethylene linkage to form a terminal bipyridyldiylium moiety to make Ru-3 (Figure 1.15) and an overall tetracation transforms the interaction from one of intercalation to what has been suggested is groove binding.[63]
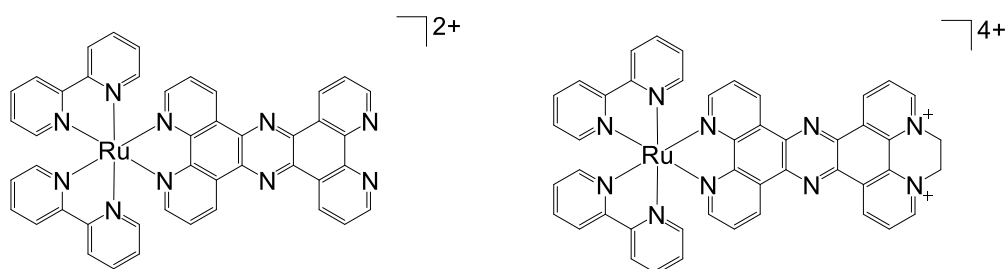
Figure 1.15 *– Structures of Ru-2 and Ru-3, derivatives of [Ru(bpy)$_2$(dppz)]$^{2+}$*

The choice of metal centre also has a large impact of the binding mode of a complex. [Ru(phen)$_2$(phi)]$^{2+}$ (Ru-4) (Figure 1.16) is an atypical DNA intercalator where the diamine groups allow for the aromatic moiety of the ligand phi to penetrate further into the major groove than in the case of phen. The ligand projects across the base pair rather than into the base stack as would be expected of a typical intercalator.[64] On the other hand, the rhodium analogue [Rh(phen)$_2$(phi)]$^{3+}$ (Rh-1) has the added ability to cleave the DNA at the site of intercalation when irradiated with short wavelength light (313-325 nm) by the formation of an intercalating ligand-based radical that takes a hydrogen

from a nearby deoxyribose. The degradation of the formed sugar radical causes direct DNA strand breakage.[65]
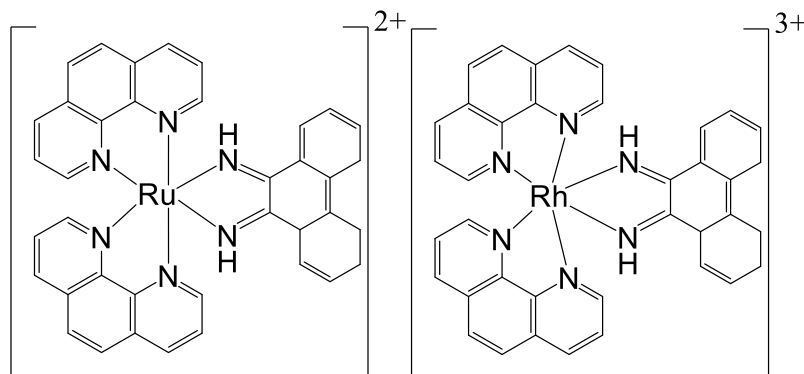
Figure 1.16 *– The structures of [Ru(phen)$_2$(phi)]$^{2+}$(Ru-4) and [Rh(phen)$_2$(phi)]$^{3+}$ (Rh-1) respectively.*

1.5 Anion Binding

Anions are incredibly important in everyday life, from the biological systems that sustain life to fertilization of crops. They are essential for the body to regulate itself, for example bicarbonates are necessary anions in the buffering of blood pH.[66] The introduction of anions into a system is not always beneficial. Hydrogen cyanide dissociates into the highly lethal cyanide anion when introduced into the body. It prohibits cellular respiration by acting as a non-competitive inhibitor for cytochrome c oxidase with high affinity.[67]

Anion binding occurs when a unit interacts with anions, charged atoms or a charged group of atoms with a net negative charge, usually via non-covalent means (hydrogen bonding, π-stacking, interhalogen binding, etc.). These interactions can result in a response within the recognising molecule which can be used to indicate anions, whether it be via NMR spectroscopy, colormetrics, changes in fluorescence or

electrochemically.[67] Testing for the presence for anions has a large number of applications, such as the testing of fluoride concentrations in potable water using boron-containing sensors (due to the reactivity of F⁻ to the Lewis acidity of boron).[68] Other uses include the medical testing of biological samples for anion levels to diagnose disorders (such as iodine levels indicative of thyroid issues), and testing the levels of chloride anions present in the body to monitor various illnesses such as heart or liver disease.[69-71]

Phosphate is a biologically essential anion. As mentioned previously it forms the backbone of DNA and RNA and is found in nucleotides (monomer DNA units) and adenosine triphosphate (ATP) and adenosine diphosphate (ADP) (Figure 1.17), along with many other biological molecules. ATP is considered the biological storage of energy in cells and it is conversion between the two forms via dephosphorylation that supplies energy for many metabolic processes. The removal of a phosphate anion is facilitated by the hydrolysis of the phosphoranhydride bonds, releasing the stored energy.[72]
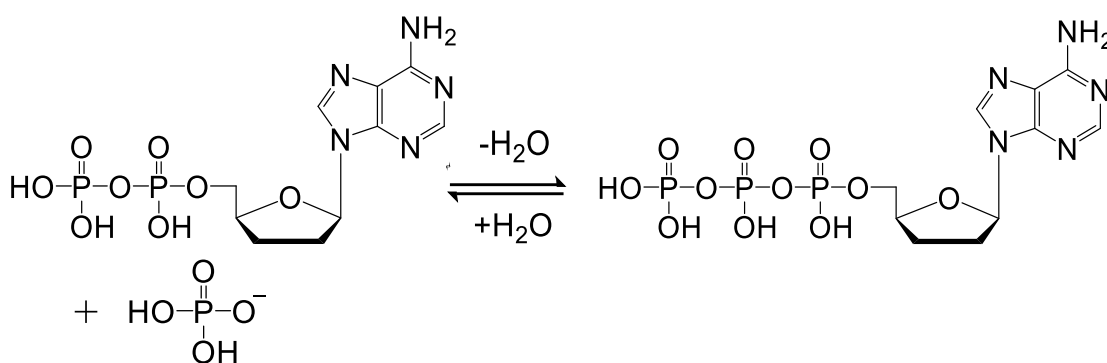
Figure 1.17: The conversion between ATP and ADP via hydrolysis.

There are numerous examples within biological systems where phosphate interacts with proteins. Histones, which are small basic proteins essential in cell reproduction as they pack and order DNA into nucleosomes.[73] Histones act as spools for the strands to wrap

around, stabilised by several interactions between the protein and DNA, mostly via the phosphate backbone.[74] These interactions include histone helix-dipoles forming α-helixes in several domains resulting in a net positive charge, enabling stability via interactions with the negative DNA phosphate groups.[75] Hydrogen bonds are thought to be formed between amide groups of the main peptide chains of and the phosphates, as well as salt bridges and further hydrogen bonding between the phosphate oxygens and basic amino acid side chains of lysine and arginine.[76]

Detection of phosphates in physiological conditions is essential in the diagnosis of hyperphosphatemia, an excess of serum phosphate, which increases the risk of hyperparathyroidism, soft tissue calcification and cardiovascular complications.[77] To improve methods of phosphate detection, research into supramolecular anion recognition chemistry has evolved to become a highly effective tool, where design of the receptors can be tuned in order to sense phosphate. However, there are still obstacles to overcome such as the environment in which the anions are contained. Although supramolecular anion sensors are very efficient at detecting phosphate in anhydrous organic media, competition arises in aqueous surroundings due to the high hydration energy of phosphates (ΔG_{hyd} of $H_2PO_4^- \approx 465$ kJ mol^{-1}).[78]

Another consideration that must be made for detection in aqueous solution is pH. Phosphate anions can exist in four forms, and these interchange depending on pH ($H_3PO_4 \rightleftharpoons H_2PO_4^- \rightleftharpoons HPO_4^{2-} \rightleftharpoons PO_4^{3-}$). In physiological conditions (~ pH 7.4) monohydrogen phosphate and dihydrogen phosphate are at equilibrium and therefore biological sensors normally target one of these. Phosphate anions in solution can also

form polyanionic species such as pyrophosphate which can pose a problem in detection.[79] With all these barriers to overcome, it is highly active research area.

Protonated or quaternised cationic pyridinium or imidazolium units are commonly used for organic acyclic anion sensors.[80] They are well known to interact via a range of non-covalent means, such as cation-anion electrostatic interactions and polarised hydrogen bonding interactions where the binding moiety is deprotonated by the anion, causing a detectable change.[81] These acyclic sensors have many forms, and are commonly monopodal or dipodal in nature, each arm containing a motif that can interact with anions (although these motifs may not be the same).

Ochoa-Lara and Ochoa-Terán have recently described a family of fluorescent dipodal anion sensors based on bis(napthylureylbenzamide) (Figure 1.18), where the dipodal arms differ between *ortho* and *meta* positions.[82] It was reported that both the length of the alkyl chain and the position of the urea and amide chains influence the fluorescent behaviours of the sensors in acetonitrile containing hydrogen phosphate (HP) and hydrogen pyrophosphate (HPP). The *ortho*-form displayed an OFF-ON response with both anions, showing maximum fluorescence with two equivalents of HPP, suggesting a 2:1 binding adduct. The *meta* family however showed an ON-OFF-ON response in similar conditions, where the addition of 0.5 equivalents of anion caused an initial quenching of emission, followed by an enhancement with higher stoichiometries. This behaviour has been rationalised as a formation of a 2:1 adduct on addition of 0.5 equivalents of anion, causing a quenching of the emission via electron transfer from the urea carbonyl oxygen leading to a partial negative charge. The anion then transfers the electron density to the oxygen via the hydrogen bonding. On increasing the anion

concentration, emission is enhanced due to partial deprotonation of the urea groups, also confirmed by ^{1}H-NMR titrations.
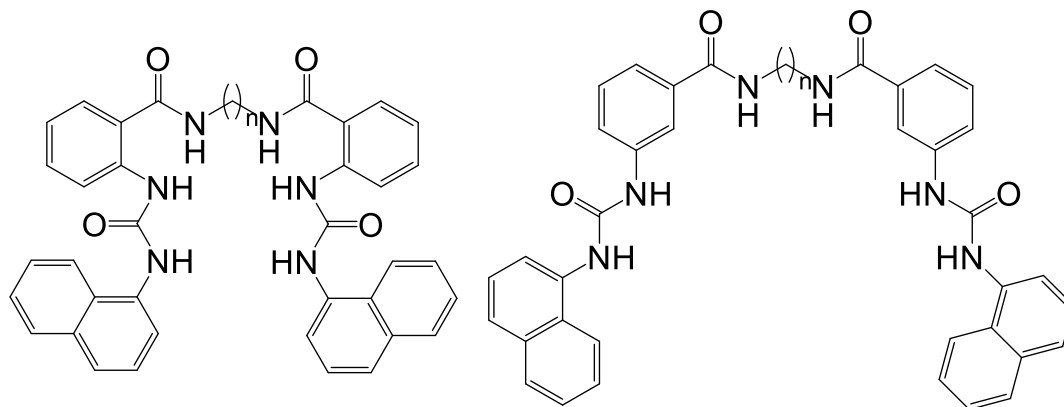

Figure 1.18: *The family of anion sensors reported by Ochoa-Lara and Ochoa-Terán, showing the ortho and meta positions.[80]*

In the last 20 years, an increased effort has been placed on the publishing of research into anion recognition devices based on transition metal complexes. Some of the most commonly researched metals in this area are ruthenium, iridium, osmium and rhenium as they have well defined emissive behaviour.[83] Ruthenium(II) polypyridyl complexes have been extensively researched in this regard, often functionalised with amide-containing motifs to act as hydrogen-bond donors at the anion recognition site.[84]

Recently, Ghosh *et al.* have described a case of selective phosphate recognition by a Ru(II) polypyridyl complex (Ru-5) containing a pendant urea functionalised pyridyl triazole (Figure 1.19).[85] ^{1}H-NMR titrations were undertaken in DMSO-d_6 with several anion species, including Cl^- and $H_2PO_4^-$ (using tetrabutylammonium as the counter cation). All anions used in the experiments, apart from phosphates and carboxylates, showed insignificant change in peak positions of both the triazole -CH and urea -NH protons, indicating that no interaction is occurring. However, in the case of $H_2PO_4^-$ and

$HP_2O_7^{3-}$, downfield shifts of the triazole – CH and urea -NH_b protons were observed (9.32 to 9.98 ppm and 8.62 to 10.52 ppm respectively) with a gradual broadening of the -NH_b peak, most likely due to a strong hydrogen-bonding interaction occurring without deprotonation. In this case a 1:2 host-to-guest stoichiometry is observed with TBA $H_2PO_4^-$, due to the ability to for the phosphate to associate with itself. The 1:2 host:guest stoichometry with $H_2PO_4^-$ was further confirmed via photophysical studies of the complex in acetonitrile, showing an enhancement in emission intensity on addition of two equivalents of dihydrogen phosphate anions. [85]
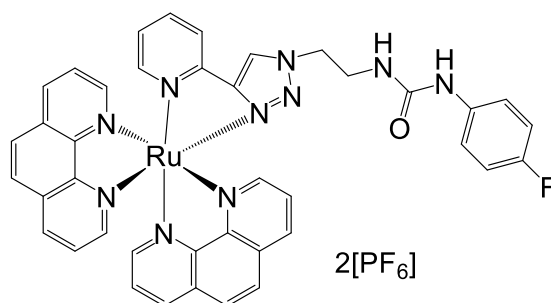
Figure 1.19: Ru-5, the ruthenium(II) polypyridyl complex reported by Ghosh and co-workers.[83]

Polynuclear complexes of ruthenium(II) are also popular for anion recognition and sensing.[86] These complexes hold some advantages over mononuclear species as they are tailorable to provide unique specificity, with the ability to easily introduce asymmetry into the frameworks via ancillary ligands or different metal centres or by using an asymmetrical bridge. Diruthenium complexes are often considered because of the facile electron transfer processes between multiple redox states (Ru(II), Ru(III), Ru(IV)) which are relatively accessible.[87]

Paul and co-workers have recently reported a series of luminescent trimetallic complexes, including a triruthenium complex (Ru-6) (Figure 1.20).[88] Each complex contains two imidazole -NH protons, enabling interactions with anions. These interactions were tested using a variety of optical tools. On addition of ten equivalents of TBA H_2PO_4, a colour change is observed with the naked eye, with the intensity of the colour change dependant on the electronic nature and basicity of the anions. Photoluminescence spectroscopy titrations with phosphates showed a large enhancement in emission intensity, and a shift in the λ_{max} (694 nm to 749 nm). Absorption spectra also show a change on addition of dihydrogen phosphate. Fitting of the experimental data showed a 1:1 binding behaviour in MeCN. However, in aqueous solution, no change is observed in UV/Vis or photoluminescence spectra on addition of as much as 20 equivalents of $H_2PO_4^-$, demonstrating the limitations of the detection of anions in protic media.
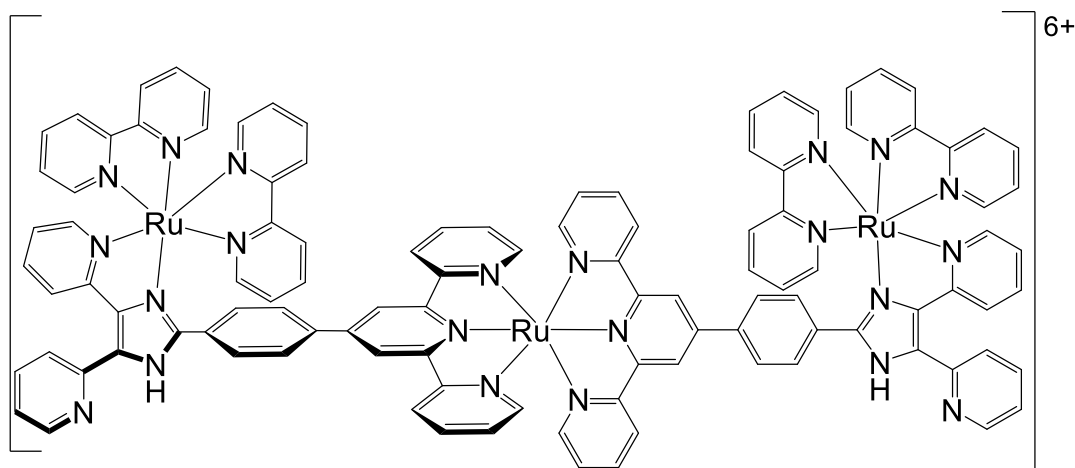
Figure 1.20: *Molecular structure of Ru-6 as reported by Paul and co-workers.[86]*

In 2014 Blackburn *et al.* reported interesting dihydrogen phosphate recognition by three novel thiourea-bridged dinuclear rhenium complexes bearing either a single thiourea group or two units separated by either a *para* or *meta*-substituted aromatic spacer (Figure 1.21).[89] ^{1}H-NMR titrations were undertaken in 50:50 CDCN and DMSO-d[6] and the spectra showed that TBA salts of NO_3^-, HSO_4^-, Br^- and ClO_4^- caused no shift in thiourea proton position in any of the three complexes, indicating that there is no measurable interaction occurring. The addition of one equivalent of fluoride salts showed a broadening of the peaks to a point where they could no longer be interpreted, indicative of proton exchange taking place. A small shift in the thiourea proton position was observed with chloride for the single thiourea containing complex ($\Delta\delta = 0.2$ ppm with ten equivalents). Acetate anions caused significant shifts of signals in all three complexes. A 1:1 stoichiometry was observed for the simpler complex, and a 2:1 stoichiometry for the *para* and *meta* complexes. The second bound anion showed a much greater association with the complex than the first, most likely due to the metal centre and associated carbonyl influences.
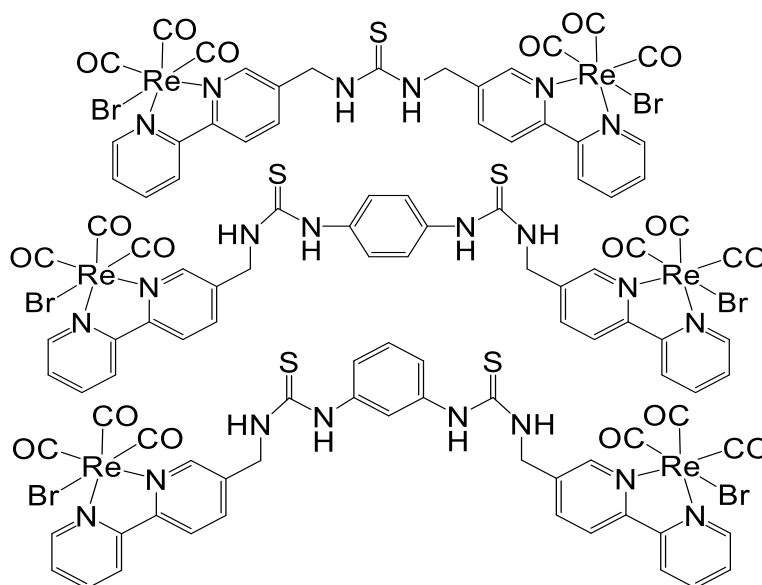
Figure 1.21 *– Re-1, Re-2and Re-3 respectively, as reported by Blackburn and coworkers.[87]*

Titration of $H_2PO_4^-$ salts with Re-1 gave a significant downfield shift of the NH proton signal and change in the methylene peak, both in signal position and gradual peak broadening from singlet to mutiplet. This implies a conformational change and a more rigid arrangement of the complex around the flexible CH_2 group, making the two protons diastereotopic. There is also a small downfield shift seen in the 3 and 4 positions of the bipyridine peaks. The calculated binding constant was considered too high to be accurate but is still indicative of a very strong binding interaction occurring. Dihydrogen phosphate titrations with the di-thiourea complexes were not successful as signal broadening would occur over one equivalent, thought to be caused by proton exchange.

UV/Vis absorbance titrations for Re-1, Re-2 and Re-3 (Figure 1.21) showed little to no perturbation with up to ten equivalents of the TBA salts of NO_3^-, Cl^-, HSO_4^-, Br^- or ClO_4^-, complimenting the data obtained from ^{1}H-NMR titrations. Acetate, fluoride and dihydrogen phosphate salts produced a decrease in LC transition thought to be caused by the anion deprotonating the thiourea moieties. Emission titrations of the three complexes (excited at 380 nm) showed little to no change in spectra with NO_3^-, Br^- or ClO_4^-. Adding TBA dihydrogen phosphate to the emission titrations of the complexes (Figure 1.21) resulted in interesting behaviour. Re-1 had an luminescence enhancement and blue shift of approximately 10 nm, then a subsequent slow quenching. Plotting of the integrated spectra revealed a sigmoidal titration curve, displaying a 2:1 guest:host stoichiometry, confirming the NMR titration data. The extended *para*-substituted complex showed a similar but more extreme response to $H_2PO_4^-$. Initially, emission increased with a blue shift of 20 nm up to 0.7 equivalents, before significant quenching. The extended *meta*-substituted system showed a similar but intermediate result, first an

enhancement and blue shift, then significant quenching. This behaviour is very interesting as the three systems appear to have two competing systems occurring. The anion seems to bind to begin with and enhances emission before deprotonation opens a non-emissive pathway. The strength of the dihydrogen phosphate binding is extremely high and the anion seems to behave more akin to acetate than other tetrahedral oxyanions like perchlorate, suggesting that cooperative binding is involved using the -OH groups of the phosphate to bind a second anion (which has been observed with acetate under certain conditions). This second binding strengthens the interaction of the first anion. It is hypothesised that this results from the formation of a hydrogen bond with the conjugate base. This insight into dihydrogen phosphate behaviour could potentially lead to new methods of selectively detecting the anion.

DNA can be considered as long polyanionic strands. However, hardly any complexes are known that directly recognise the negatively charged phosphate backbone. One of the main reasons for this potentially is due to the high levels of solvation in an aqueous buffering media. The water molecules surrounding the anion form hydrogen bonds and compete with the introduced complex. Nevertheless, "triplatin phosphate clamps" have been reported by Farrell and co-workers (Figure 1.22).[90] These polynuclear platinum(II) complexes are described as non-covalent DNA binding agents where phosphate backbone recognition is achieved via square planar tetra-amine/ammine Pt(II) coordination units forming bidentate NH-O-HN hydrogen bonds with the oxygen of the phosphate groups, resulting in a conformational change of the DNA.[91] This is potentially advantageous as a lack of covalent binding to DNA may potentially reduce the negative side effects when compared to similar complexes used currently in cancer treatment.
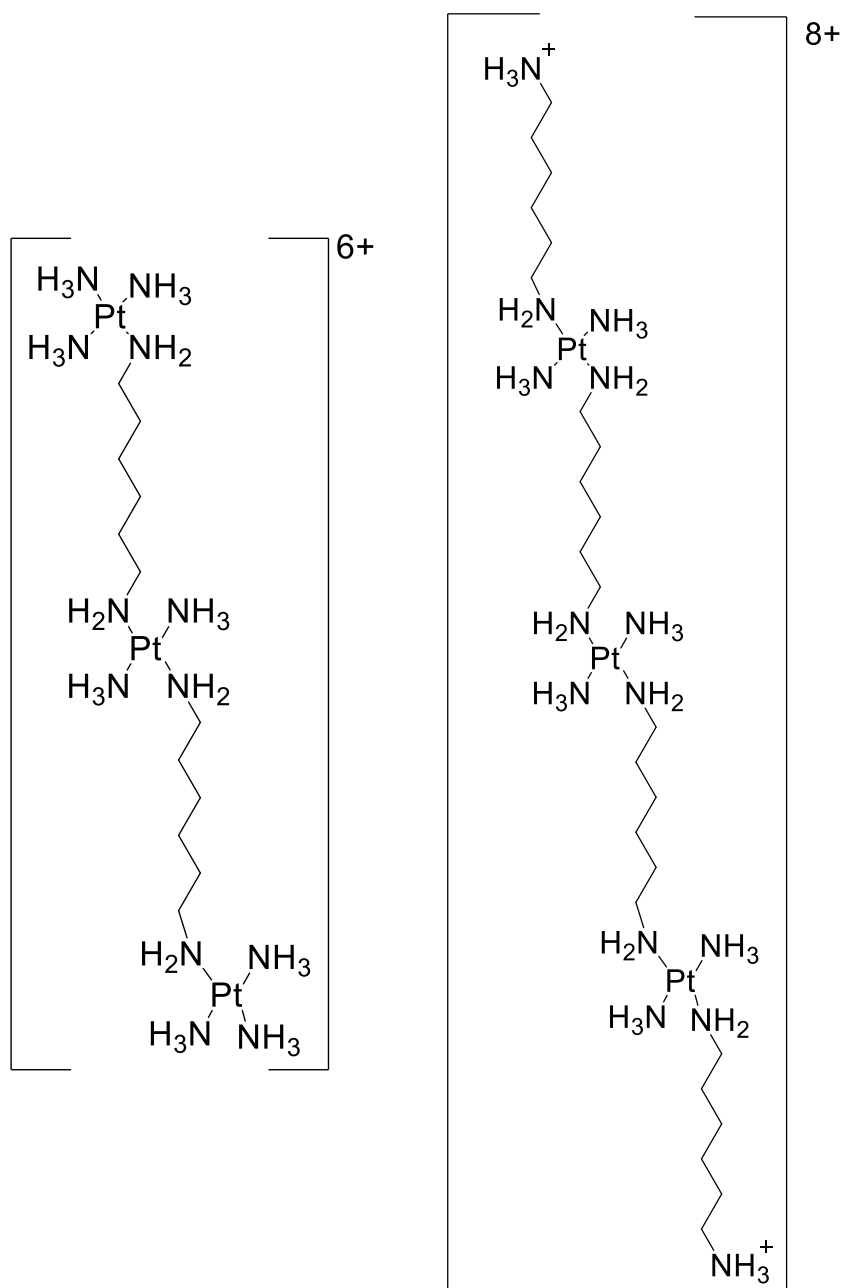
Figure 1.22: *Molecular structure of 2 phosphate clamps reported by Farrell et al. Left is TriplatinNC-A, right is TriplatinNC.*[85]

Triplatins are modular in nature, allowing for further fine-tuning of the design to enhance biological activities. These complexes demonstrate a sufficiently high binding affinity that ethidium bromide does not displace them from DNA, essentially making the conformational change irreversible, potentially leading to apoptosis.[92] They are

shown to selectively interact with phosphate oxygens over other oxygens, and against nitrogen atoms in a competitive environment.[93] This form of DNA-binding has been established as being discrete from both groove binding and intercalation, and the covalent-binding mode of cisplatin (on which the complexes are based). At the time of writing, no other examples of this form of DNA interaction were found, opening potential for new approaches for drug development.

1.6 Ruthenium(II) Polypyridyl Complexes

1.6.1 Introduction

Ruthenium(II) polypyridyl complexes have several advantages that other transition metal complexes do not have as DNA probes. These include, but are not limited to:

- A high stability

- Well documented spectroscopic activity

- The potential to be used as photodynamic therapy (PDT) agents

- Potential ligand functionalisation via known procedures

These advantages have resulted in several examples of investigations into Ru(II) polypyridyl complexes as potential DNA binders. One of the most researched examples is $[Ru(bpy)_3]^{2+}$ (Figure 1.23) for its exceptional properties of luminescence emission, reactivity, and redox activity, as well as a small affinity for DNA binding.[93,94] It is synthetically simple to functionalise this complex at one or more of the bipyridine ligands before or after it has been bound onto the metal. There are many well documented synthetic routes for functionalising bipyridine in order to fine tune the properties of the complex.[95]
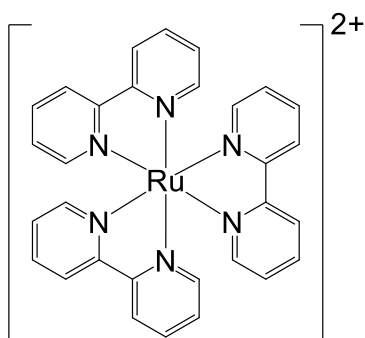
Figure 1.23: *The structure of [Ru(bpy)₃]²⁺ (Ru-7).*

A molecular orbital diagram for Ru-7 ([Ru(bpy)$_3$]$^{2+}$) shows the electronic transitions that the complex can undergo (Figure 1.24). Bipyridine-based ligands have large ligand field splitting abilities and can take part in metal back donation by acting as π-acceptors. Electron density can be donated from the ruthenium d-orbitals and placed into the ligand's low energy π* orbitals. The bipyridines have σ-donating orbitals localised on the nitrogen atoms, contributing towards the low spin d^6 ruthenium centre, as well as π-bonding and π* anti-bonding orbitals delocalised on the aromatic ring systems. Promoting an electron from $π_M$ to $π^*_L$ orbitals produces a metal to ligand charge transfer (MLCT), whereas promotion of an electron from $π_L$ to $π^*_L$ produces a ligand centred (LC) charge transfer. Laporte forbidden metal centred (MC) charge transfers occur when electrons are promoted from $π_M$ to $σ^*_M$.[96]
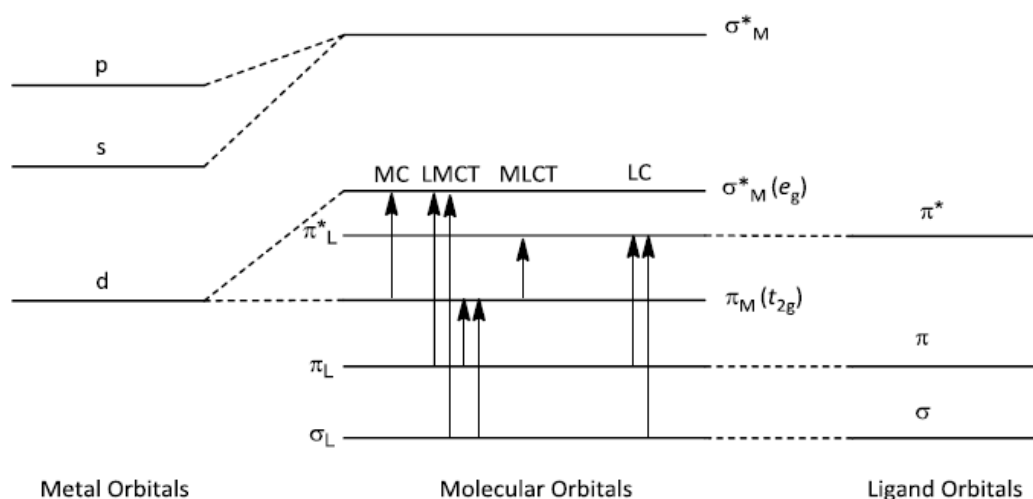
Figure 1.24 – *Simplified molecular orbital diagram of [Ru(bpy)₃²⁺ illustrating MC, LMCT, MLCT and LC transitions.*

The UV/Vis absorbance spectrum for $[Ru(bpy)_3]^{2+}$ (Figure 1.25) shows the LC, MC and MLCT regions described in the molecular orbital diagram (Figure 1.24). MLCT d-to-π^* transitions occur at approximately 452 and 244 nm. Two MC transitions are seen at around 353 and 323 nm whereas a strong LC transition can be observed at 288 nm. Exciting $[Ru(bpy)_3]^{2+}$ at 450 nm causes luminescence emission at around 610 nm. Emission quantum yield (ϕ) for the complex is calculated to be 0.062 in acetonitrile, which is used as the standard for measuring the emission of Ru(II) polypyridyl complexes.[97]
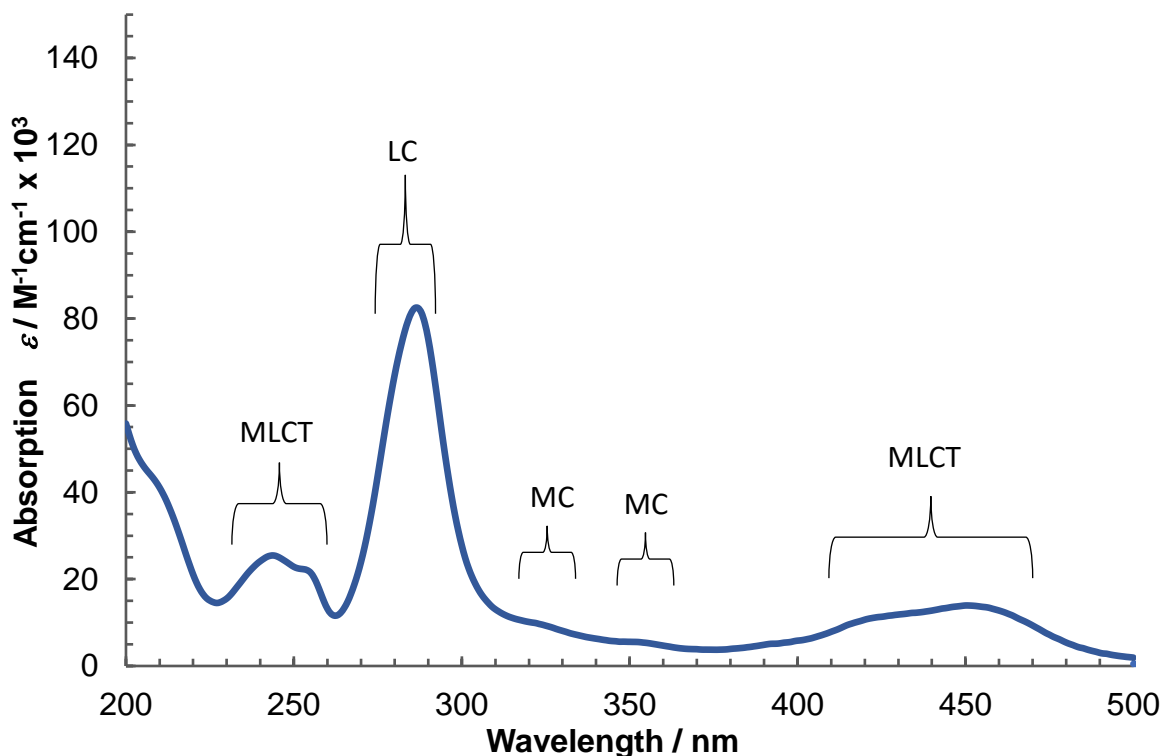
***Figure 1.25** – UV/Vis absorbance spectrum of [Ru(bpy)₃]²⁺.*

1.6.2 Chirality of Ru(II) Polypyridyl Complexes

Tris(bidentate) ruthenium(II) complexes of the formula $[Ru(L1)(L2)(L3)]^{2+}$ occur in two configurations, the left-handed/Λ form or the right-handed/Δ form (Figure 1.26). It is only possible to distinguish one from another using spectroscopic methods that are sensitive to chirality of molecules, such as circular dichroism (CD) spectroscopy. CD spectroscopy measures how much a compound absorbs right- or left-handed circularly polarised light, measured as a function of wavelength. If a negative CD spectrum is obtained, more right-handed circularly polarised light has been absorbed than left-handed, and vice versa for a positive spectrum.
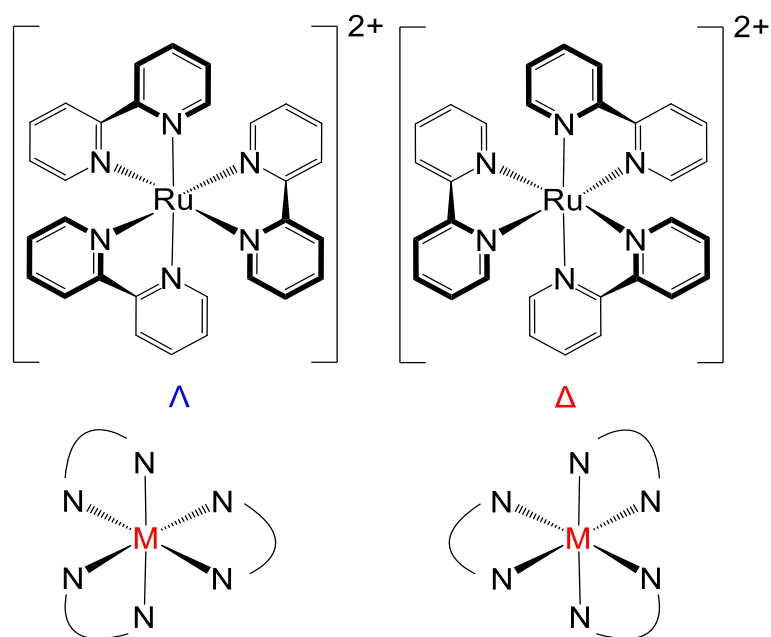
***Figure 1.26** – The Λ- and Δ-isomers of Ru-7.*

The chirality of these complexes needs to be considered when investigating their affinities for DNA. Although the isomers are treated as identical for many spectroscopic techniques, separately they may give different results when bound to DNA. This is because DNA itself is a chiral molecule, as established in Section 1.21. The handedness of the molecule could potentially influence binding to right-handed B-DNA, which needs to be established if possible.

The need to characterise individual isomers has led to the establishment of several methods to either separate or form enantiomerically pure ruthenium(II) tris(bidentate) complexes. Aldrich-Wright *et al.* synthesised a covalently bound DNA-silica adduct using calf-thymus DNA.[98] This was then placed on a HPLC column, which allowed for the separation of $[Ru(phen)_3]^{2+}$ and $[Ru(dpq)_3]^{2+}$. Several other methods have been developed to synthesise the separate enantiomers, including the use of glycopeptide antibiotics and capillary electrophoresis with chiral selectors.[99,100]

It is possible to chirally separate ruthenium(II) trisbipyridyl complexes using cation-exchange chromatography, using a chiral stationary phase and a solution mobile phase.[101,102] Combining the enantiomers with a chiral anion (such as ditolyl tartrate) forms two diastereoismeric salts, each with different retention times. These are then separated using ion exchange chromatography and the anion is removed by recrystalising the complexes with an achiral salt, such as KPF_6 following elution from the column.[103]

Fletcher *et al*. reported the use of cation-exchange column chromatography using a solid support of Sephadex^{TM} SP-C25 to separate $[Ru(L)_3]^{2+}$ complexes.[104,105] Sephadex^{TM} SP-C25 is a resin made of a 3D network of dextran bridged by epichlorohydrin. Each subunit has five chiral centres and is made up of cross linked α-D-glycopyranosides with very acidic propylsulphonates. Equilibrium establishes between the media where the bound cationic complex is retained in the solid phase. A sodium salt of a chiral eluent is usually used (e.g. sodium(+)-*O,O'*-dibenzoyl-D-tartrate or its counter sodium(-)-*O,O'*-dibenzoyl-L-tartrate) which competes with the stationary phase for the complex. The components separate as the lesser charged cations are bound weaklier to the Sephadex^{TM}, therefore they elute much more quickly than a higher charged complex. The chirality of the chosen eluent has an effect on the separation itself due to the cation interacting with the anionic auxiliary in multiple ways.[101] If using sodium(+)-*O,O'*-dibenzoyl-D-tartrate (DBT), Λ isomers will typically run faster and be collected first, followed by the Δ isomer. Use of the opposite salt will reverse this, and Δ will run the fastest of the two.

Further methods of separating the enantiomers involve the use of ruthenium(II) polypyridyl precursors such as $[Ru(bpy)_2(py)_2]^{2+}\pm DBT$, reacting them with a functionalised ligand.[102.106] The precursors can be chirally separated via the previously stated means beforehand, leading to the synthesis of enantiomerically pure forms of complex. It is beneficial to use this method as it is possible to create a stock of the chirally separated precursors to be used to create separate isomers (see Section 2.2.1.4).

1.6.3   Photodynamic Therapies and Ru(II) Polypyridyl Complexes

Photodynamic therapy (PDT) is a relatively recent developed treatment for some skin and eye conditions and for certain types of cancer. It involves the use of photosensitisers (PS) to kill cancer cells and tumours *in vivo* and many different infectious microorganisms.[107] A lot of commonly used PS are based around organic structures but now a higher focus has been placed on the research of inorganic complexes in the fight against disease.

PDT works on a principle that involved the absorption of a photon by a ground state PS, thus allowing it to be promoted into a singlet excited state.[108] This state is very short lived (ns) however it is enough time for intersystem crossing to occur to produce a much longer lived triplet excited state (µs). This extended time allows for photochemical reactions to happen between the PS and ambient oxygen.[109] There are two types of reaction that can occur during this time and these can happen simultaneously.[108] The first is electron transfer which results in the formation of superoxide, hydrogen peroxide and hydroxyl radicals. The other type is energy transfer where singlet excited state oxygen is produced. This system is preferrable due to the short half-life of the oxygen

species, which limits the diffusion distance, meaning that the PS will only affect molecules in close proximity.[107] Whether there is a dominant reaction is dependent on the structure and properties of the PS (particularly redox potential) and the concentration of oxygen in the environment.[106] The reactive oxygen species (ROS) formed then go on to react with biological molecules (nucleic acids, proteins and lipids) in the immediate vicinity, eventually leading to cell death.[109]

To treat tumours *in vivo* the PS must be given intravenously and the tumour location is then irradiated with (generally) red light.[110] There are three mechanisms by which cancer cell death occurs. Firstly, cancer cell death can occur just by the initial burst of ROS produced by the irradiation of the PS filled area. The oxygen reacts with the biological molecules within the cancer cells, resulting in oxidative damage to the cellular components and eventually autolysis.[111] PDT also affects the microvascular system that develops to support the tumour.[112] The oxidative damage caused by the ROS can cause the formation of thrombi or vascular leakage. It is important that this mechanism is mediated as if the vascular system shuts down too quickly, the supply of ambient oxygen is lost which will reduce the efficacy of the PS.[110] Finally, the oxidative damage caused by the ROS results in acute local inflammation and cytokine release, activating an innate immune system response. This causes the immune system to release neutrophils, macrophages and dendritic cells. If the tumour does not have immunosuppressive mechanisms and tumour antigens are present, the adaptive immune system may activate, producing a systemic anti-tumour immunity. [112]

PDT shows great promise as an effective treatment for tumours without surgery, however there are still limitations. Current photosensitisers require irradiation with red

light (around 600 – 800 nm), yet these wavelengths are too short for good tissue penetration.[113,114] Due to this, a high level of research has gone into PS that are excited at wavelengths that will also penetrate tissues. One of the current research areas is the investigation of transition metal complexes as photosensitisers.

Ruthenium(II) polypyridyl complexes are of special interest in PDT because of their unique properties outlined at the start of this section. Huang and co-workers reported modified $[Ru(bpy)_3]^{2+}$ complexes as potential PDT drugs (Figure 1.27).[115] These complexes contained the $[Ru(bpy)_3]^{2+}$ core, with substituted ammonium groups functionalised on the 4 and 4' positions of each bipyridine. The photostability of each complex was tested to ensure decomposition would not occur when irradiated in biological media. All three complexes showed no breaking down in bovine plasma after 72 hours (Figure 1.27). It was imperative to test that the compounds could generate ROS. This was investigated using 1,3-diphenylisobenzofuran (DPBF). The production of ROS results in a decrease in absorbance at 410 nm of DPBF, making a facile test with obvious results. In all three cases, the absorbance decreased with prolonged irradiation times at 450 nm, indicating DPBF had indeed been degraded by the generation of $^1O_2$. Electron spin resonance (ESR) was employed to verify whether other forms of ROS were being produced, i.e. radicals. It was confirmed that no radical ion signals were detected, only $^1O_2$ signals. Another essential aspect to acknowledge in PDT testing is the localisation of an agent within the cell using colocalization assays. Each complex tested showed good overlapping with the commercial lysosome dye used, with little overlapping with a mitochondrial dye or Hoechst 33342. Lysosomes are essential organelles and serve as the waste disposal centre of the cell.
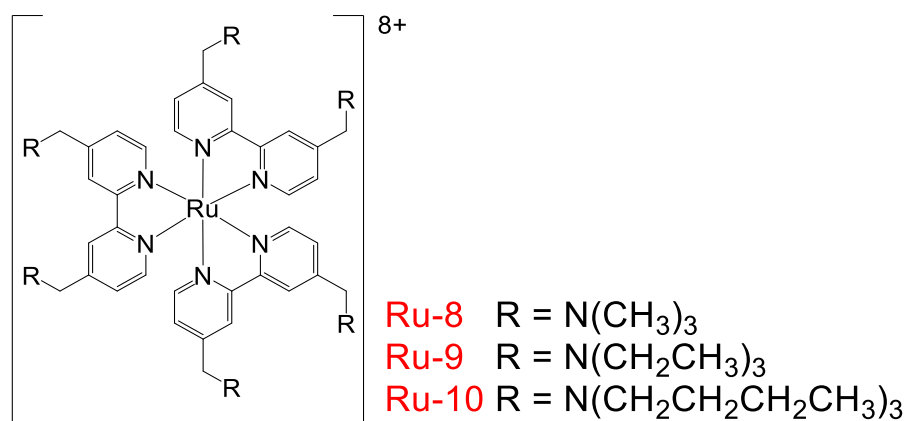
Figure 1.27 – *The (tris)bipyridyl complexes (Ru-8, Ru-9, and Ru-10) described by Huang et al.*[108]

The cytotoxicity and photocytotoxicity of Ru-8, Ru-9 and Ru-10 (Figure 1.27) were investigated using HeLa cell line via MTT assays (a colourmetric assay for assessing cell viability, proliferation and cytotoxicity). While all complexes were found to be non-toxic in the dark, Ru-10 was more cytotoxic than the others, probably caused by its higher cellular uptake efficiency. The photocytotoxicity was then established by irradiating the drug-containing cells at 450 nm. Ru-8 showed high levels of toxicity towards the HeLa cells, with an IC$_{50}$ value of 1.5 μM. Ru-9 and Ru-10 showed a lower efficiency than their counterpart towards the cells despite having a higher cellular uptake, attributed to a lower $^1O_2$ generating ability. Ru-8 as the most promising compound. Live cell staining showed examine cell viability, wherein calcein AM is used to stain HeLa cells. Micrographs taken showed that cell death was localised within the irradiated area. The next stage in PDT drug screening is to ascertain whether the candidate can produce ROS within the cellular environment. 2,7-Dichlorodihydrofluoroscein diacetate (DCFH-DA) is used as an indicator of ROS production as it reacts with $^1O_2$ to form the fluorophore DCF which emits strong green light. Ru-8 was shown to increase cell emission significantly, showing that the DCFH-DA was oxidising into DCF, therefore ROS must have been created.

More recently Hua *et al.* described potential PDT agents derived from [Ru(bpy)$_2$(dppz)][PF$_6$]$_2$ (Figure 1.28).[116] The two complexes are composed of two auxiliary bpy ligands and a dppz ligand attached to a pyrenyl group on either the 3 or 4 position (Ru-11 and Ru-12 respectively). Initial testing of ROS generation was done by monitoring the absorbance of DPBF in methanol. Ru-11 caused a significant decrease in absorbance when irradiated with 460 nm light, meaning that a large amount of ROS was produced by the system, even more so than [Ru(bpy)$_2$(dppz)][PF$_6$]$_2$. On the other hand, testing Ru-12 gave no decrease in absorbance, implying that there is little to no ROS generated. This is most likely down to R-12 having a much shorter T_1 excited state lifetime than R-11. *In vitro* cytotoxicity and photocytotoxicity were ascertained using A549 (human pulmonary adenocarcinoma cell) and MCF-7 (human breast cancer cell) cell lines via MTT assays. In the absence of irradiated light, both complexes were relatively non-toxic, which is highly important for PDT. However, when Ru-11 was irradiated at 460 nm, it killed the cancer cells, even at the lowest concentrations tested. IC$_{50}$ values were calculated to be 0.010 ± 0.001 μM for A549 and 0.004 ± 0.001 μM for MCF-7, showing that Ru-11 is an extremely potent photocytotoxic compound. Contrasting this, R-12 showed no photocytotoxic behaviour.

Ru-11   **R-12**
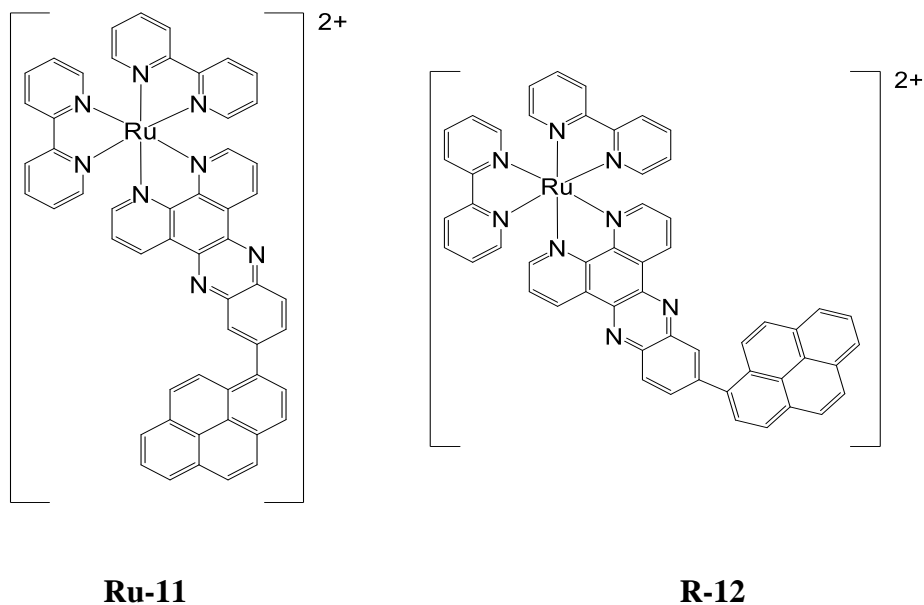
Figure 1.28 – The reported structures of the derived [Ru(bpy)₂(dppz)][PF₆]₂ complexes, Ru-11 and Ru-12, respectively.[113]

The photocytotoxicity of Ru-11 was further studied using live/dead cell co-staining assays. Calcein AM was used to stain live cells and propidium iodide used for dead cells. MCF-7 cells were used due to the higher toxicity of Ru-11 towards them. Very little MCF-7 cell death was seen in the absence of irradiated light but were almost wholly killed when irradiated, further showing the high PDT capabilities of R3. DCFH-DA was used as a probe to confirm that Ru-11 produces ROS in cells. No signal was observed without irradiation but when irradiated with 460 nm light, a strong green fluorescence was seen, confirming that ROS are indeed formed in a cellular environment. Overall, it has been confirmed that by tethering a pyrenyl group onto [Ru(bpy)₂(dppz)][PF₆]₂ creates a very potent potential PDT agent, and could stimulate development of other highly efficient ruthenium(II) polypyridyl complexes for this use.

1.6.4 Examples of Ru(II) and Recent Developments in the Area

Fairbanks *et al*. have reported a dinuclear ruthenium(II) polypyridyl complex (Ru-13) that is capable of threading B-DNA (Figure 1.29).[117] Resolution of the enantiomers has made it possible to further understand the potential of threading through the double helix and any affects this may have. Three enantiomers have been separated out, namely ΛΛ, ΔΔ (*rac*) and ΔΛ (*meso*) and these were examined for their DNA binding affinities. ^{1}H-NMR binding studies were undertaken by first titrating the unresolved complex into a DNA solution. This showed the complex in a slow-exchange regime indicating that any dissociation occurring is slow on an NMR time scale. The free complex has $2C_2$ symmetry, therefore the symmetrical protons have identical chemical shifts. However, when the compound is bound, each group of protons has at least four peaks, representing each stereoisomer and bound conformer, making it unassignable. To combat this, deuterated bipyridine was used in synthesis to remove ambiguity from the spectra.
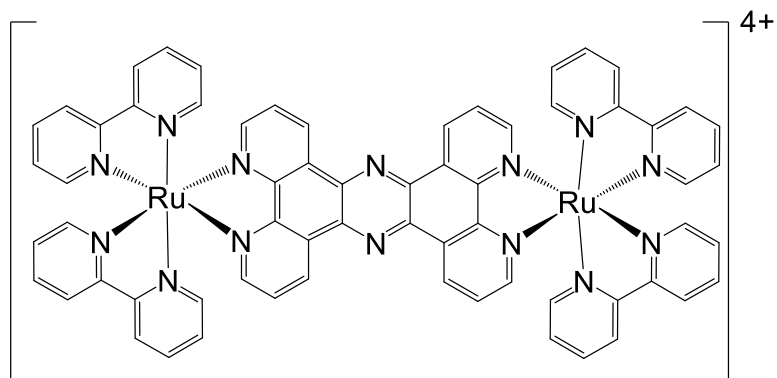
Figure 1.29 *– [Ru(bpy)₂(tppz)]²⁺ (Ru-13) as reported by Fairbanks et al.[115]*

Λ,Λ-Ru-13 was titrated into the DNA solution, resulting in two sets of ^{1}H-NMR resonances with a ratio of 2:1, implying that there are either two binding sites or two binding modes, both in slow exchange with free DNA. The major bound form showed large changes in the chemical shifts of DNA at the central (T4, A13)(A5,T12) base step resulting from the ring current of the highly aromatic complex. This preference for (T4,

A13)(A5,T12) is most likely due to the lower stability and higher levels of flexibility of A-T rich regions of DNA. There was also significant peak movement seen for adjacent thymidine methyl protons located in the major groove. Other shifts were observed for sugar protons within the minor groove, due to the minor bound form. Most likely, this enantiomer intercalates into two sites of the DNA, preferentially pyrimidine/AT/purine sequences. This is interesting as this type of sequence has the greatest flexibility of all dinucleotide sequences. The spectra from the titration of ΛΔ-Ru-13 into DNA solution indicated a 1:2 ligand to duplex ratio and two different binding modes or sites, as seen with ΛΛ-Ru-13.

The addition of ΔΔ-Ru-13 into DNA solution resulted in two sets of broadened signals in slow to intermediate exchange with free DNA. The spectra were generally unassignable due to the amount of exchange peaks present. TOCSY and COSY were employed to enable the assignment of thymidine methyl protons, and nuclear Overhauser effects (NOEs) were observed between these and ΔΔ-Ru-13 existing in one of the two observed conformations. A large shift change was also observed between the two bound conformers, with one set of resonances shifted upfield by approximately 0.6 ppm. Both the NOEs and these shift changes are indicative of a molecule threading though the DNA helix. The second conformer resulted in smaller peak shifts of the thymidine methyl protons, most likely resulting from binding within the minor groove. The isolation of the threading enantiomer means it may now be possible to further examine the effects on DNA without interference from non-threading forms, potentially leading to new forms of clinically accepted DNA binders for treatment of disease.

In 2020, Jiang and co-workers reported chiral ruthenium(II) polypyridyl complexes and their stabilising effects toward triplex RNA (Figure 1.30).[118] The structure consists of two 2,2'-bipyridine ligands and one dppz ligand, modified with an electron withdrawing -CF$_3$ group at the 7 position. The binding behaviours of the resolved enantiomers has been studied with triple stranded RNA of the form poly(U)·poly(A)*poly(U) where · represents Watson-Crick base pairing and * represents Hoogsteen base pairing. UV/Vis absorption titrations of each enantiomer were underetaken, where 15 µM of complex were added to RNA solutions. Δ-Ru-14 gave a 20.4% reduction in the MLCT region at 441 nm, with a 2 nm red shift (characteristic of dppz containing ruthenium(II) complexes). The spectrum of the opposite enantiomer was observed to have a similar result with the MLCT region reducing by 17.4%, along with the 2 nm red shift. This result indicated that association with triplex RNA is stronger with Δ-Ru-14 than Λ-Ru-14, which is backed up by the calculated larger binding affinity and smaller binding site values for Δ-Ru-14. This is mostly likely due to the chirality of the Δ isomer fitting better within the RNA structure, resulting in a stronger binding. It was expected that the strong electron-withdrawing properties of -CF$_3$ would have a noticeable effect on the binding affinity of the compound. However, both enantiomers have binding constants that are very similar to Δ-[Ru(bpy)$_2$(dppz)]$^{2+}$, suggesting that the -CF$_3$ group has little to no influence in the RNA binding capabilities.
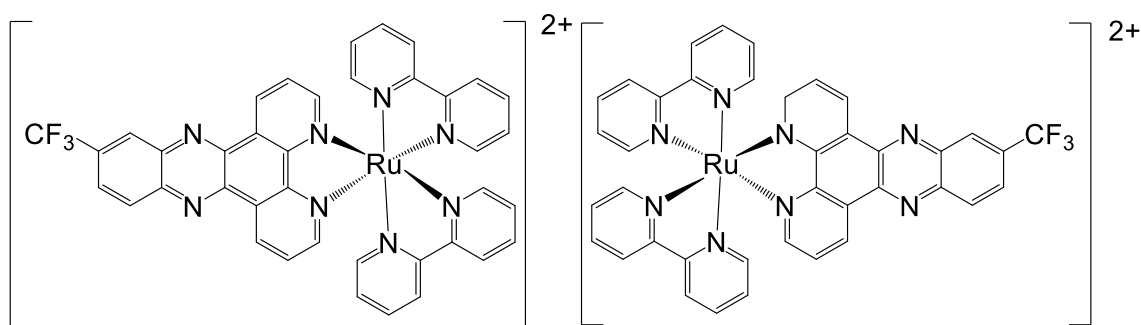
Figure 1.30 *– Δ-[Ru(bpy)₂(7-CF₃-dppz)]²⁺(Δ-Ru-14) and Λ-[Ru(bpy)₂(7-CF₃-dppz)]²⁺ (Λ-Ru-14)*

as reported by Jiang et al.[115]

Competitive binding experiments were carried out with an RNA triplex system. Both enantiomers of Ru-14 showed no emission in the absence and presence of RNA in phosphate buffer, unlike the parent dppz complex, which is a "light-switch". This is most probably caused by the addition of -CF₃, where the bulkiness of the group makes it more difficult for the ligand to fully intercalate into the RNA system. It is hypothesised that the two nitrogen atoms of the pyrazine ring do not sit within the helix and are able to hydrogen bond with solvent water molecules, opening a pathway for the emission to fully quench. However, both the Λ- and Δ- forms appear to displace ethidium bromide (EB) from the system, as observed from the quenching of fluorescence when they are added to a solution of EB and RNA triplex. Viscosity studies were carried with RNA triplex-bound complex. A significant increase of relative viscosity was observed for both enantiomers upon progressive addition, indicating that both enantiomers intercalate into the triple system. Larger increases were obtained from Δ-Ru-14, confirming that it has a more complimentary geometry for intercalation than its Λ counterpart.

Thermal denaturation studies were carried out to further confirm intercalation of Δ-Ru-14 and Λ-Ru-14 into RNA. The melting profile of triple stranded RNA was established to be biphasic, with the first melt temperature resulting from the removal of the third strand, and the second resulting from the splitting of the duplex. The Δ enantiomer increases both the first and second T_M from 35 °C to 38.9 °C and 44 °C to 48°C respectively, showing that it stabilises the triplex system. On the other hand, the Λ enantiomer decreases the first T_M from 35 °C to 34.5 °C but causes a large increase in the second from 44 °C to 51.4 °C, indicating that it destabilises the triplet system but stabilises duplex RNA. This difference in stabilising effects is possibly caused by the different geometries of the chiral structures, and the differences this fact causes in the two base pairing forms. The triplex major groove is different from that found in the RNA duplex form, as it is wider and forms two asymmetric parts: the smaller Crick-Hoogsteen groove and the wider Watson-Hoogsteen groove. It is thought that the Δ-enantiomer intercalates into the more flexible Watson-Hoogsteen groove, whereas the Λ-form intercalates into the Watson-Crick groove, potentially explaining why they stabilise different RNA structures.

Li *et al*. have described bifunctional ruthenium(II) polypyridyl complexes with curcumin based ligands and explored their potential as anticancer agents (Figure 1.31).[119] To firstly establish their cytotoxic behaviour, *in vitro* MTT assays were undertaken using A549 (human non-small cell lung cancer cell), MCF-7 (human breast adenocarcinoma cell) and SGC7901 (human gastric cancer cell) cell lines and [Ru(bpy)$_3$]Cl$_2$, cisplatin, curcumin and [Ru(bpy)$_2$(acac)]Cl$_2$ as reference compounds. Both Ru-15 and Ru-16 (Figure 1.31) showed significant toxicity against all three cell lines. Ru-16 showed a much higher level of cytotoxicity than all other complexes tested

whereas Ru-15 showed higher levels of cytotoxicity than only [Ru(bpy)$_2$(acac)]Cl$_2$ of the reference compounds. These results were further confirmed via live/dead cell co-staining using calcein AM and propidium iodide.
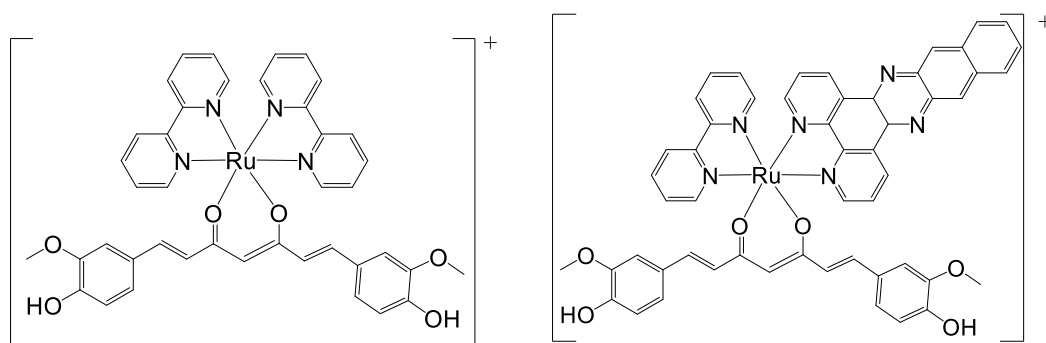
Figure 1.31 – Ru-15 and Ru-16 reported by Li and co-workers.[117]

The DNA interaction capabilities of the complexes were established via competitive binding experiments with ethidium bromide. A reduction in fluorescence from the ethidium bromide was observed on the continuous addition of both complexes, indicative of displacement of the binder by either intercalation or groove binding. Ru-16 reduced the fluorescence more than Ru-15, and calculated binding affinities indicate that 2 has a higher capability to bind DNA. Molecular docking studies were carried out using Autodock 4.2 to determine optimal binding between the duplex and complexes. It was determined that the best fit for Ru-15 was binding into the groove, lying in a parallel manner, whereas Ru-16 optimally bound via intercalation into the DNA strand via the dppn ligand. The binding energies were found to be higher for Ru-16 than Ru-15, which concurs with intercalation and groove binding.

Cellular uptake is an important factor in determining whether a potential antitumour agent is viable. ICP-MS was used in order to monitor this in A549 cell lines and it was

determined that Ru-16 had a 1.2x uptake than Ru-15, most likely because it has a much higher lipophilicity in order to pass through the cell membrane. These studies also determined that 56.9% of Ru-16 entered the cell nucleus as opposed to Ru-15, where only 30.1% ended up there, potentially explaining the difference in cytotoxicity. Flow cytometry with propidium iodide was then carried out to understand where in the cell cycle the complexes can interactComplimentarily to the previous experiments, Ru-16 was found to cause a higher percentage of cells in cycle arrest than complex 1. To confirm that cell death occurs via apoptosis, Hoechst 33358 stains were used with the A549 cell line. Introduction of complexes 1 and 2 resulted in cytoplasm shrinkage and fragmentation, along with a bright blue fluorescence, confirming apoptosis.

Spence and co-workers have reported a ruthenium(II) polypyridyl complex that is capable of detection of i-motif secondary structures in DNA, specifically an i-motif found in the promotor region of the death-associated protein gene (DAP).[120] $[Ru(bqp)_2]^{2+}$ (Ru-17) (Figure 1.32) was resolved into the *mer* and *fac* isomers, the latter being further resolved into *cis* and *trans* forms. Initial electronic absorption titrations were used to calculate binding constants, and the obtained data showed that the *cis* isomer had the higher binding affinity to the majority of DNA secondary structures, with the strongest binding occurring with i-motif DAP as well as double strand B-DNA. The *mer* isomer showed low binding constants for all tested DNA structures, which is consistent with the size and shape of the complexes. The *cis* isomer gave higher binding constants than its *trans* counterpart most likely due to the angle between the central pyridines (*cis* = 92 °, *trans* = 180 °). The smaller angle enables the *cis* isomer to be able to fit into tighter spaces, especially the smaller i-motif. Steady-state emission studies were used to further determine DNA binding capabilities. The *fac* isomers showed very

little emission in tris buffer alone with an increase on addition of DNA, *cis* especially so. The strongest increase in fluorescence came about from interactions with double stranded DNA, followed by i-motifs DAP and hTeloC (the i-motif formed from the human telomere). Unusually, there was no increase in emission observed when the experiments were undertaken in organic media, as opposed to water, indicating a different switch on mechanism for Ru-17 as opposed to other well known "light-switches". The *trans* isomer showed some enhancement of emission with all structures of DNA but not as strongly as the *cis* isomer. The *mer* isomer showed a very intense ^{3}MLCT emission in buffer which did not change when DNA was included. Fluorescent Intercalator Displacement (FID) assays were undertaken to understand the relative binding affinities of the complex using thiazole orange (TO). It was found that the *cis* isomer displaces TO better than the others across all tested DNA structures, especially i-motif DAP.
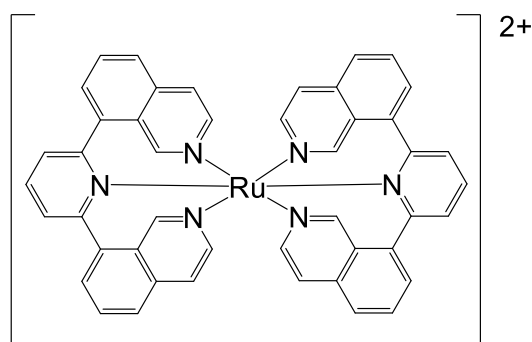
Figure 1.32 – The structure of [Ru(bqp)$_2$]$^{2+}$ (Ru-17) as reported by Spence et al.[118]

Luminescence lifetime experiments were carried out using multichannel scaling to probe the potential of i-motif recognition. In the absence of DNA the *mer* isomer of Ru-17 shows a biexponential decay from the ^{3}MLCT excited state with a long lived and high amplitude second component which is responsible for the overall emission. When DNA is added, this part becomes much longer lived but much less populated, and these

two characteristics balance each other out, leading to little observable change. The two *fac* isomers of Ru-17 exhibit much shorter decays without DNA but still display the ^{3}MLCT characteristic. The addition of DNA to the *trans* isomer of Ru-17 results in an increase of the 2nd component in both lifetime and population, giving the partial switch on effect seen in the steady state emission studies. The decay profile of the *cis* isomer changes from a two-component system to a three-component system in the presence of nucleic acids. This could be caused by the development of a new, previously inaccessible ^{3}MLCT state, or it could reflect on a subpopulation of bound chromophore that experiences a change in the ^{3}MLCT state. This new third component greatly lengthens the overall lifetime of the *cis* isomer, especially in the presence of DAP, where it is approximately ten times longer. This results in a clear indication of the presence of i-motifs in mixed solutions and can potentially enable new means by which to synthesise biosensors.

1.7 Objectives

Ruthenium(II) polypyridyl complexes that have a binding affinity for DNA are of great interest due to their unique properties and the potential as diagnostic and therapeutic agents. The potential for emissive complexes to recognise essential anions in aqueous environments is also highly researched for potential medicinal and environmental testing. Minor groove binding agents and phosphate recognition complexes are the focus of this research project.

Ruthenium(II) polypyridyl complexes were previously reported containing bipyridine and phenanthroline ligands functionalised with benzothiazole, benzoxazole or

benzimidazole groups (Figure 1.32).[121-122] These were observed to bind to double-stranded DNA in the minor groove. It was found that the benzothiazoles bound to DNA best when functionalised at the 4 and 4' position. No anion recognition testing has been attempted with any of these complexes. The ligands were proven to be very insoluble, and this stalled progress in the synthesis of these complexes. They were also found to have very weak luminescence, which would limit their applications as DNA binders.
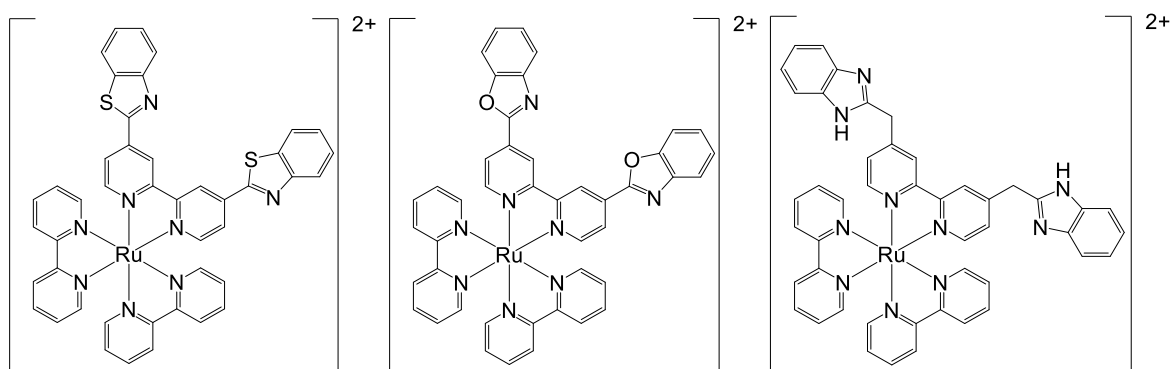
Figure 1.32 *– The structures of the previously reported minor groove binding complexes a.* *[Ru(bpy)2(bbtb)]$^{2+}$, b. [Ru(bpy)$_2$(bbob)]$^{2+}$ and c. [Ru(bpy)$_2$(bbimb)]$^{2+}$Ru-18, Ru-19 and Ru-20).*

The aim of this project was to synthesis a series of ruthenium(II) polypyridyl complexes in order to improve on the previously reported work. These will preferably bind DNA in the minor groove with the same affinity as, or better than, the previous work, and potentially be able to interact with anions in an aqueous environment.

The DNA binding affinities and anion recognition properties of mononuclear ruthenium(II) polypyridyl complexes will be determined using several methods. These comprise of ^{1}H-NMR spectroscopy titrations, UV/Vis absorbance, fluorescence

emission and circular dichroism titrations, relative viscosity studies and equilibrium dialysis testing. Calf thymus DNA will be used in these experiments as it is thought of as a model for mammalian DNA.

1.8 References

1 C. R. Calladine, H. R. Drew, B. F. Luisi and A. A. Travers, *Understanding DNA: The Molecule and How it Works: Third Edition*, Elsevier, 2004.

2 M. L. Kopka, C. Yoon, D. Goodsell, P. Pjura and R. E. Dickerson, *Proc. Natl. Acad. Sci. U. S. A.*, 1985, **82**, 1376 – 1380.

3 N. J. Wheate, S. Walker, G. E. Craig and R. Oun, *Dalton Trans.*, 2010, **39**, 8113 – 8127.

4 R. Oun, Y. E. Moussa and N. J. Wheate, *Dalton Trans.*, 2018, **47**, 6645 – 6653.

5 A. Bijelic, M. Aureliano and A. Rompel, *Angew. Chemie - Int. Ed.*, 2019, **58**, 2980 – 2999.

6 S. Bellemin-Laponnaz, *Eur. J. Inorg. Chem.*, 2020, **2020**, 10 – 20.

7 S. Fricker, *Dalton Trans.*, 2007, **43**, 4903 – 4917.

8 B. S. Murray, M. V. Babak, C. G. Hartinger and P. J. Dyson, *Coord. Chem. Rev.*, 2016, **306**, 86 – 114.

9 J. D. Watson and F. H. C. Crick, *Nature*, 1953, **171**, 737 – 738.

10 T. Hermann and D. J. Patel, *Structure*, 2000, **8**, R47–R54.

11 P. Svoboda and A. Di Cara, *Cell Mol Life Sci.*, 2006, **63**, 901–908.

12 B. G. Feuerstein, N. Pattabiraman and L. J. Marton, *Proc. Natl. Acad. Sci. U. S. A.*, 1986, **83**, 5948 – 5952.

13 A. A. Ouameur and H. A. Tajmir-Riahi, *J. Biol. Chem.*, 2004, **279**, 42041 – 42054.

14 K. Igarashi and K. Kashiwagi, *Int. J. Biochem. Cell Biol.*, 2010, **42**, 39 – 51.

15 S. Perepelytsya, J. Uličný, A. Laaksonen and F. Mocci, *Nucleic Acids Res.*, 2019, **47**, 12, 6084 – 6097.

16 A. G. Cherstvy, *Phys. Chem. Chem. Phys.*, 2011, **13**, 9942 – 9968.

17 R. K. Singh, S. Kumar, D. N. Prasad and T. R. Bhardwaj, *Eur. J. Med. Chem.*, 2018, **151**, 401 – 433.

18 V. Brabec and J. Kasparkova, *Coord. Chem. Rev.*, 2018, **376**, 75 – 94.

19 G. Sava, A. Bergamo, S. Zorzet, B. Gava, C. Casarsa, M. Cocchietto, A. Furlani, V. Scarcia, B. Serli, E. Iengo, E. Alessio and G. Mestroni, *Eur. J. Cancer*, 2002, **38**, 3, 427 – 435.

20 M. Groessl, Y. O. Tsybin, C. G. Hartinger, B. K. Keppler and P. J. Dyson, *J. Biol. Inorg. Chem.*, 2010, **15**, 5, 677 - 688.

21 H. A. Wee and P. J. Dyson, *Eur. J. Inorg. Chem.*, 2006, **20**, 4003 – 4018.

22 M. Liu, J. Z. Lim, Y. Y. Gwee, L. Aviva and P. A. Lay, *Angew. Chem. Int. Ed. Engl.*, 2010, **49**, 1661–1664.

23 B. M. Zeglis, V. C. Pierre and J. K. Barton, *Chem. Comm.*, 2007, 4565 – 4579.

24 M. Cusumano, M. L. Di Pietro, A. Giannetto and P. A. Vainiglia, *J. Inorg. Biochem.*, 2005, **99**, 560 – 565.

25 B. J. Pages, K. B. Garbutcheon-Singh and J. R. Aldrich-Wright, *Eur. J. Inorg. Chem.*, 2017, 12, 1613 -1624.

26 A. Mukherjee, R. Lavery, B. Bagchi and J. T. Hynes, *J. Am. Chem. Soc.*, 2008, **130**, 9747 – 9755.

27 B. Jawad, L. Poudel, R. Podgornik, N. F. Steinmetz and W. Y. Ching, *Phys. Chem. Chem. Phys.*, 2019, **21**, 3877 – 3877 – 3893.

28   W. Hu, C. Blecking, M. Kralj, L. Šuman, I. Piantanida and T. Schrader, *Chem. - A Eur. J.*, 2012, **18**, 3589 – 3597.

29   H. Y. Alniss, I. I. Witzel, M. H. Semreen, P. K. Panda, Y. K. Mishra, R. Ahuja and J. A. Parkinson, *J. Med. Chem.*, 2019, **62**, 10423 – 10440.

30   N. G. Anthony, B. F. Johnston, A. I. Khalaf, S. P. MacKay, J. A. Parkinson, C. J. Suckling and R. D. Waigh, *J. Am. Chem. Soc.*, 2004, **126**, 11338 – 11349.

31   S. Nakamura and T. Noguchi, *J. Am. Chem. Soc.*, 2017, **139**, 9364 - 9375.

32   M. Berlin, C. W. Boyce and M. De Lera Ruiz, *J. Med. Chem.*, 2011, **54**, 26 - 53.

33   R. Nirogi, A. Shinde, V. Tiriveedhi, L. Kota, S. K. Saraf, R. K. Badange, A. R. Mohammed, R. Subramanian, N. Muddana, G. Bhyrapuneni and R. Abraham, *Eur. J. Med. Chem.*, 2016, **108**, 655 – 662.

34   N. Ranjan, S. Story, G. Fulcrand, F. Leng, M. Ahmad, A. King, S. Sur, W. Wang, Y. C. Tse-Dinh and D. P. Arya, *J. Med. Chem.*, 2017, **60**, 4904 – 4922.

35   K. D. Harshman, P. B. Dervan, *Nucleic Acids Res.* 1985, **13**, 4825-4835.

36   P. G. Baraldi,A. Bovero, F. Fruttarolo, D. Preti, M. A. Tabrizi, M. G. Pavani, R. Romagnoli, R. *Med. Res. Rev.* 2004, **24**, 475-528.

37   D. E. Comings, *Chromosoma,* 1975, **52**, 229-243.

38   G. S. Khan, A. Shah, Zia-Ur-Rehman and D. Barker, *J. Photochem. Photobiol. B Biol.*, 2012, **112**, 115 – 118.

39   C. Mura, D. Valenti, C. Floris, R. Sanna, M. A. De Luca, A. M. Fadda and G. Loy, *Eur. J. Med. Chem.*, 2011, **46**, 4142 – 4150.

40   D. I. Edwards, *Biochem. Pharmacol.*, 1986, **35**, 53 – 58.

41   D. I. Edwards, *J. Antimicrob. Chemother.*, 1993, **31**, 9 – 20.

42   M. Müller, *Biochem. Pharmacol.*, 1986, **35**, 37 – 41.

43   A. Bolhuis and J. R. Aldrich-Wright, *Bioorg. Chem.*, 2014, **55**, 51 – 59.

44   A. M. Jarrad, T. Karoli, A. Debnath, C. Y. Tay, J. X. Huang, G. Kaeslin, A. G. Elliott, Y. Miyamoto, S. Ramu, A. M. Kavanagh, J. Zuegg, L. Eckmann, M. A. T. Blaskovich and M. A. Cooper, *Eur. J. Med. Chem.*, 2015, **101**, 96 - 102.

45   A. A. Sagatova, M. V. Keniya, R. K. Wilson, B. C. Monk and J. D. A. Tyndall, *Antimicrob. Agents Chemother.*, 2015, **59**, 4982 – 4989.

46   P. D. Crowley and H. C. Gallagher, *J. Appl. Microbiol.*, 2014, **117**, 611 - 617.

47   M. K. Kathiravan, A. B. Salake, A. S. Chothe, P. B. Dudhe, R. P. Watode, M. S. Mukta and S. Gadhwe, *Bioorganic Med. Chem.*, 2012, **20**, 5678 – 5698.

48   L. R. Benzaquen, C. Brugnara, H. R. Byers, S. Gattoni-Celli and J. A. Halperin, *Nat. Med.*, 1995, **6**, 534 - 540.

49   R. Palchaudhuri, V. Nesterenko and P. J. Hergenrother, *J. Am. Chem. Soc.*, 2008, **130**, 10274 - 10281.

50   G. Bartolommei, F. Tadini-Buoninsegni, S. Hua, M. R. Moncelli, G. Inesi and R. Guidelli, *J. Biol. Chem.*, 2006, **281**, 9547 - 9551.

51   H. Aktas, R. Flückiger, J. A. Acosta, J. M. Savage, S. S. Palakurthi and J. A. Halperin, *Proc. Natl. Acad. Sci. U. S. A.*, 1998, **95**, 8280 – 8285.

52   S. Betanzos-Lara, N. P. Chmel, M. T. Zimmerman, L. R. Barrón-Sosa, C. Garino, L. Salassa, A. Rodger, J. L. Brumaghim, I. Gracia-Mora and N. Barba-Behrens, *Dalton Trans.*, 2015, **44**, 3673 - 3685.

53   E. Robles-Escajeda, A. Martínez, A. Varela-Ramirez, R. A. Sánchez-Delgado and R. J. Aguilera, *Cell Biol. Toxicol.*, 2013, **29**, 431 – 443.

54   B. Rosenberg, L. Van Camp and T. Krigas, *Nature*, 1965, **205**, 698 - 699.

55   P. Jordan and M. Carmo-Fonseca, *Cell. Mol. Life Sci.*, 2000, **57**, 1229–1235.

56   T. C. Johnstone, K. Suntharalingam and S. J. Lippard, *Chem. Rev.*, 2016, **116**, 3436 - 3486.

57   L. Salassa, *Eur. J. Inorg. Chem.*, 2011, 4931 - 4947.

58   H. Gorner, A. Tossi, C. Stradowski and D. Schulte-Frohlinde, *J. Photochem. Photobiol. B Biol.*, 1988, **2**, 67 – 89.

59   C. V. Kumar, J. K. Barton and N. J. Turro, *J. Am. Chem. Soc.*, 1985, **107**, 5518 – 5523.

60   J. K. Barton, J. M. Goldberg, C. V. Kumar and N. J. Turro, *J. Am. Chem. Soc.*, 1986, **108**, 2081 - 2088.

61   P. Lincoln and B. Nordén, *J. Phys. Chem. B*, 1998, **102**, 9583 – 9594.

62   A. M. Pyle, J. P. Rehmann, R. Meshoyrer, C. V. Kumar, N. J. Turro and J. K. Barton, *J. Am. Chem. Soc.*, 1989, **111**, 3051–3058.

63   H. S. Derrat, C. C. Robertson, A. J. H. M. Meijer and J. A. Thomas, *Dalton Trans.*, 2018, **47**, 12300–12307.

64   G. Li, L. Sun, L. Ji and H. Chao, *Dalton Trans.*, 2016, **45**, 13261 – 13276.

65   C. Turro, A. Evenzahav, S. H. Bossmann, J. K. Barton and N. J. Turro, *Inorganica Chim. Acta*, 1996, **243**, 101 – 108.

66   N. H. Evans and P. D. Beer, *Angew. Chemie - Int. Ed.*, 2014, **53**, 11716 - 11754.

67   Z. Xu, X. Chen, H. N. Kim and J. Yoon, *Chem. Soc. Rev.*, 2010, **39**, 127 – 137.

68   P. Molina, F. Zapata and A. Caballero, *Chem. Rev.*, 2017, **117**, 9907 – 9972.

69   S. Sandhu, R. Kumar, P. Singh, A. Walia, V. Vanita and S. Kumar, *Org. Biomol. Chem.*, 2016, **14**, 3536–3543.

70   C. G. Collins, E. M. Peck, P. J. Kramer and B. D. Smith, *Chem. Sci.*, 2013, **4**, 2557–2563.

71   E. Galbraith and T. D. James, *Chem. Soc. Rev.*, 2010, **39**, 3831 – 3842.

72   M. W. Bowler, M. J. Cliff, J. P. Waltho and G. M. Blackburn, *New J. Chem.*, 2010, **34**, 784 - 794.

73   B. Biterge and R. Schneider, *Cell Tissue Res.*, 2014, **356**, 457 - 466.

74   J. S. Godde and K. Ura, *J. Biochem.*, 2008, **143**, 287 - 293.

75   M. Brehove, T. Wang, J. North, Y. Luo, S. J. Dreher, J. C. Shimko, J. J. Ottesen, K. Luger and M. G. Poirier, *J. Biol. Chem.*, 2015, **290**, 37, 22612 – 22621.

76   P. Tessarz and T. Kouzarides, *Nat. Rev. Mol. Cell Biol.*, 2014, **15**, 703 - 708.

77   L. Upadhyay and N. Verma, *Biotechnol. Lett.*, 2015, **37**, 1335–1345.

78   Y. Marcus, *Biophys. Chem.*, 1994, **51**, 111 - 127.

79   S. Pal, T. K. Ghosh, R. Ghosh, S. Mondal and P. Ghosh, *Coord. Chem. Rev.*, 2020, **405**, 213128 - 213184.

80   J. Zhao, D. Yang, X. J. Yang and B. Wu, *Coord. Chem. Rev.*, 2019, **378**, 415 - 444.

81   D. A. McNaughton, M. Fares, G. Picci, P. A. Gale and C. Galtagirone, *Coord. Chem. Rev.*, 2021, **427**, 213573 - 213616.

82   L. Lopez-Martinez, J. Garcia-Elias, A. Ochoa-Teran, H. Santacruz Ortega, K. Ochoa-Lara, C. U. Montano-Medina, A. K. Yatsimirsky, J. Z. Ramirez, V. Labastida-Galvan and M. Ordonez, *Tetrahedron*, 2020, **76,** 13805.

83 V. Balzani, A. Juris, M. Venturi, S. Campagna and S. Serroni, *Chem. Rev.*, 1996, **96**, 759 – 833.

84 T. Duff, A. Grussing, J-L. Thomas, M. Duati, J. G. Vos, *Polyhedron*, 2003, **22**, 775 – 780.

85 T. K. Ghosh, S. Chakraborty, B. Chowdhury and P. Ghosh, *Inorg. Chem.*, 2017, **56**, 9, 5371 – 5382.

86 S. Karmakar, D. Maity, S. Mardanya and S. Baitalik, *Dalton Trans.*, 2015, **44**, 18607 – 18623.

87 A. Das, T. Kundu, S. M. Mobin, J. L. Priego, R. Jiménez-Aparicio and G. K. Lahiri, *Dalton Trans.*, 2013, **42**, 13733 – 13746.

88 A. Paul, M. Bar, T. Ahmed and S. Baitalik, *Polyhedron*, 2020, **190**, 114772.

89 A. L. Blackburn, N. C. A. Baker and N. C. Fletcher, *RSC Adv.*, 2014, **4**, 18442 – 18452.

90 N. P. Farrell, *Chem. Soc. Rev.*, 2015, **44**, 8773–8785.

91 S. Komeda, T. Moulaei, K. K. Woods, M. Chikuma, N. P. Farrell and L. D. Williams, *J. Am. Chem. Soc.*, 2006, **128,** 16092 - 16103.

92 S. Komeda, T. Moulaei, M. Chikuma, A. Odani, R. Kipping, N. P. Farrell and L. D. Williams, *Nucleic Acids Res.*, 2011, **39**, 325 - 336.

93 S. Komeda, Y. Qu, J. B. Mangrum, A. Hegmans, L. D. Williams and N. P. Farrell, *Inorganica Chim. Acta*, 2016, **452**, 25 – 33.

94 Juris, A.; Balzani, V.; Barigelletti, F.; Campagna, S.; Belser, P.; von Zelewsky, A. *Coord. Chem. Rev.* 1988, **84**, 85-277.

95 P. D. Dayanidhi and V. G. Vaidyanathan, *Dalton Trans.*, 2021, **50**, 5691–5712.

96 Balzani, V.; Juris, A.; Venturi, M.; Campagna, S.; Serroni, S. *Chem. Rev.* 1996, **96**, 759-833.

97 V. Balzani, F. Barigelletti, L. Decola, *Top. Curr. Chem.* 1990, **158**, 31-71.

98 J.V. Caspar and T. J. Meyer, *J. Am. Chem. Soc.* 1983, **105**, 5583-5590.

99 J. R. Aldrich-Wright, I. Greguric, R. S. Vagg, K. Vickery, P. A. Williams, *J. Chromatogr. A* 1995, **718**, 436-443.

100 F. Gasparrini, I. D'Acquarica, J. G. Vos, C. M. O'Connor, C. Villani, *Tetrahedron-Asymmetr.* 2000, **11**, 3535-3541.

101 C. Jiang, M.-Y. Tong, D. W. Armstrong, S. Perera, Y. Bao, F. M. MacDonnell, *Chirality* 2009, **21**, 208-217.

102 Keene, F. R. *Chem. Soc. Rev.* 1998, **27**, 185-193.

103 T. J. Rutherford, P. A. Pellegrini, J. R. Aldrich-Wright, P. C. Junk, F. R. Keene, *Eur. J. Inorg. Chem.* 1998, 1677-1688.

104 N. C. Fletcher, F. R. Keene, *Dalton Trans.* 1998, 2293-2301.

105 N. C. Fletcher, F. R. Keene, *Dalton Trans.* 1999, 683-689.

106 X. Hua, A. von Zelewsky, *Inorg. Chem.* 1995, **34,** 5791-5797.

107 J. Liu, C. Zhang, T. W. Rees, L. Ke, L. Ji and H. Chao, *Coord. Chem. Rev.*, 2018, **363**, 17 - 28.

108 M. Jakubaszek, B. Goud, S. Ferrari and G. Gasser, *Chem. Commun.*, 2018, **54**, 13040 – 13059.

109 M. Dichiara, O. Prezzavento, A. Marrazzo, V. Pittalà, L. Salerno, A. Rescifina and E. Amata, *Eur. J. Med. Chem.*, 2017, **142**, 459 – 485.

110 T. Huang, Q. Yu, S. Liu, W. Huang and Q. Zhao, *Dalton Trans.*, 2018, **47**, 7628 – 7633.

111 Y. Wang, Z. Pan, X. L. Cheng, K. Zhang, X. Zhang, Y. Qin, J. Fan, T. Yan, T. Han, K. K. Shiu, S. C. K. Hau, N. K. Mak, D. W. J. Kwong, X. Liu, M.

Li, G. Deng, Q. Zheng, J. Lu and D. Li, *Eur. J. Med. Chem.*, 2021, **209**, 112867.

112   A. Machuca, E. Garcia-Calvo, D. S. Anunciação and J. L. Luque-Garcia, *Chem. - A Eur. J.*, 2020, **26**, 7685 – 7691.

113   J. Du, T. Shi, S. Long, P. Chen, W. Sun, J. Fan and X. Peng, *Coord. Chem. Rev.*, 2021, **427**, 213604.

114   V.-N. Nguyen, S. J. Park, S. Qi, J. Ha, S. Heo, Y. Yim, G. Baek, C. S. Lim, D. J. Lee, H. M. Kim and J. Yoon, *Chem. Commun.*, 2020, **56**, 11489–11492.

115   H. Huang, B. Yu, P. Zhang, J. Huang, Y. Chen, G. Gasser, L. Ji and H. Chao, *Angew. Chemie - Int. Ed.*, 2015, **54**, 14049 – 14052.

116   W. Hua, G. Xu, J. Zhao, Z. Wang, J. Lu, W. Sun and S. Gou, *Chem. - A Eur. J.*, 2020, **26**, 17495 – 17503.

117   S. D. Fairbanks, C. C. Robertson, F. R. Keene, J. A. Thomas and M. P. Williamson, *J. Am. Chem. Soc.*, 2019, **141**, 4644–4652.

118   L. Jiang, X. Liu and L. Tan, *J. Inorg. Biochem.*, 2020, **213**, 111263.

119   S. Li, G. Xu, Y. Zhu, J. Zhao and S. Gou, *Dalton Trans.*, 2020, **49**, 9454–9463.

120   P. Spence, J. Fielden and Z. A. E. Waller, *J. Am. Chem. Soc.*, 2020, **142**, 13856–13866.

121   C. B. Spillane, N. C. Fletcher, S. M. Rountree, H. van den Berg, S. Chanduloy, J. L. Morgan and F. R. Keene, *J. Biol. Inorg. Chem.* 2007, **12**, 797-807.

122   C. B. Spillane, M. N. V. Dabo, N. C. Fletcher, J. L. Morgan, F. R. Keene, I. Haq, N. J. Buurma, *J. Inorg. Biochem.* 2008, **102**, 673-683.

Chapter Two

Chapter Two: Synthesis and Binding Studies of Benzimidazole Functionalised Ruthenium(II) Polypyridyl Complexes

2.1 Introduction

Bipyridine and phenanthroline, along with other bidentate diimines, are excellent ligands for use in the synthesis of transition metal complexes due to their versatility in functionalisation. Adding substituents onto these scaffolds can result in dramatic changes in the properties of a coordinated metal complex. It is possible to tune and enhance certain aspects, such as anion interactions, and DNA binding. Previous work from within the Fletcher group has shown that functionalising bipyridine ligands with benzothiazoles and benzoxazoles (Figure 2.1) and subsequent coordination to ruthenium(II) polypyridyl complexes produces desirable minor groove DNA binding agents, for their potential use in theranostics.[1,2]
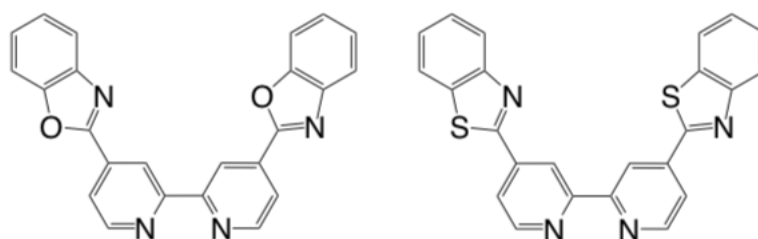
***Figure 2.1** – Benzoxazole and benzothiazole ligands previously synthesised by the Fletcher group.[1,2]*

It is well established that compounds with imidazole moieties are capable of interacting with DNA. Hoechst stains (Figure 2.2), a family of fluorescent dyes commonly used

to stain DNA, contain benzimidazoles at their cores.[3] Thorough studies of these molecules have established that the mechanism by which they interface with DNA is via binding into the minor groove of the double helix, showing selectivity for A-T rich regions as the NH groups of the benzimidazoles can make bridging three-centre hydrogen bonds between the N-3 of adenine and O-2 of thiamine on the edge of the base pairs.[4,5]
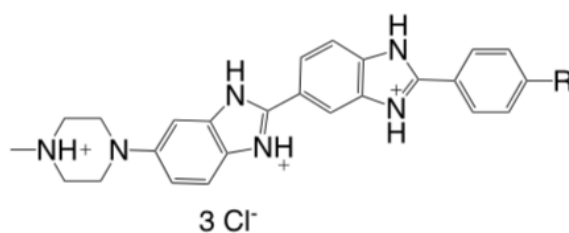
Figure 2.2 − *General chemical structure of Hoechst stains*

New complexes have been synthesised to build upon the previous work of the Fletcher group discussed above, with benzimidazole-functionalised bipyridine ligands to potentially improve ability to interact with the DNA minor groove. This has been accomplished by the addition of another hydrogen bond donor group. Replacing the ancillary ligands with 1,10-phenanthroline has also been considered, resulting in the synthesis of two complexes [Ru(bpy)$_2$(bbib)]$^{2+}$ (initially synthesised by Caitriona
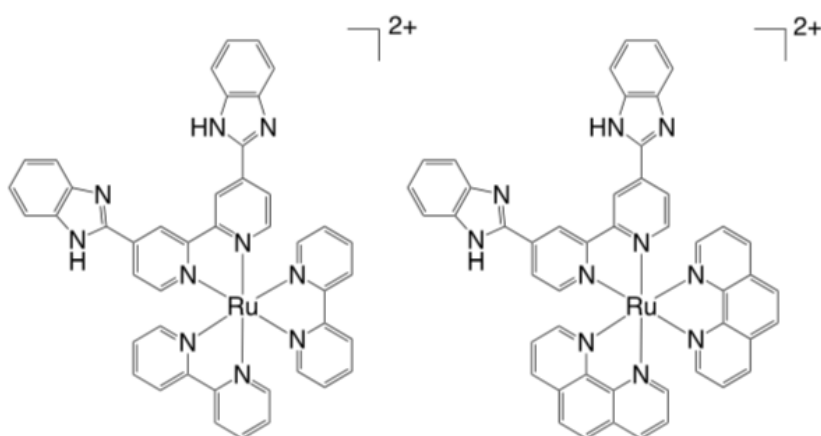
Figure 2.3 - *Target complexes*

Spillane) and $[Ru(phen)_2(bbib)]^{2+}$ (both Figure 2.3).[2] These have been for analysed for both their anion, and DNA, binding capabilities, which will be explored in this Chapter.

2.2 Synthesis and Characterisation of Benzimidazole Functionalised Ruthenium(II) Polypyridyl Complexes
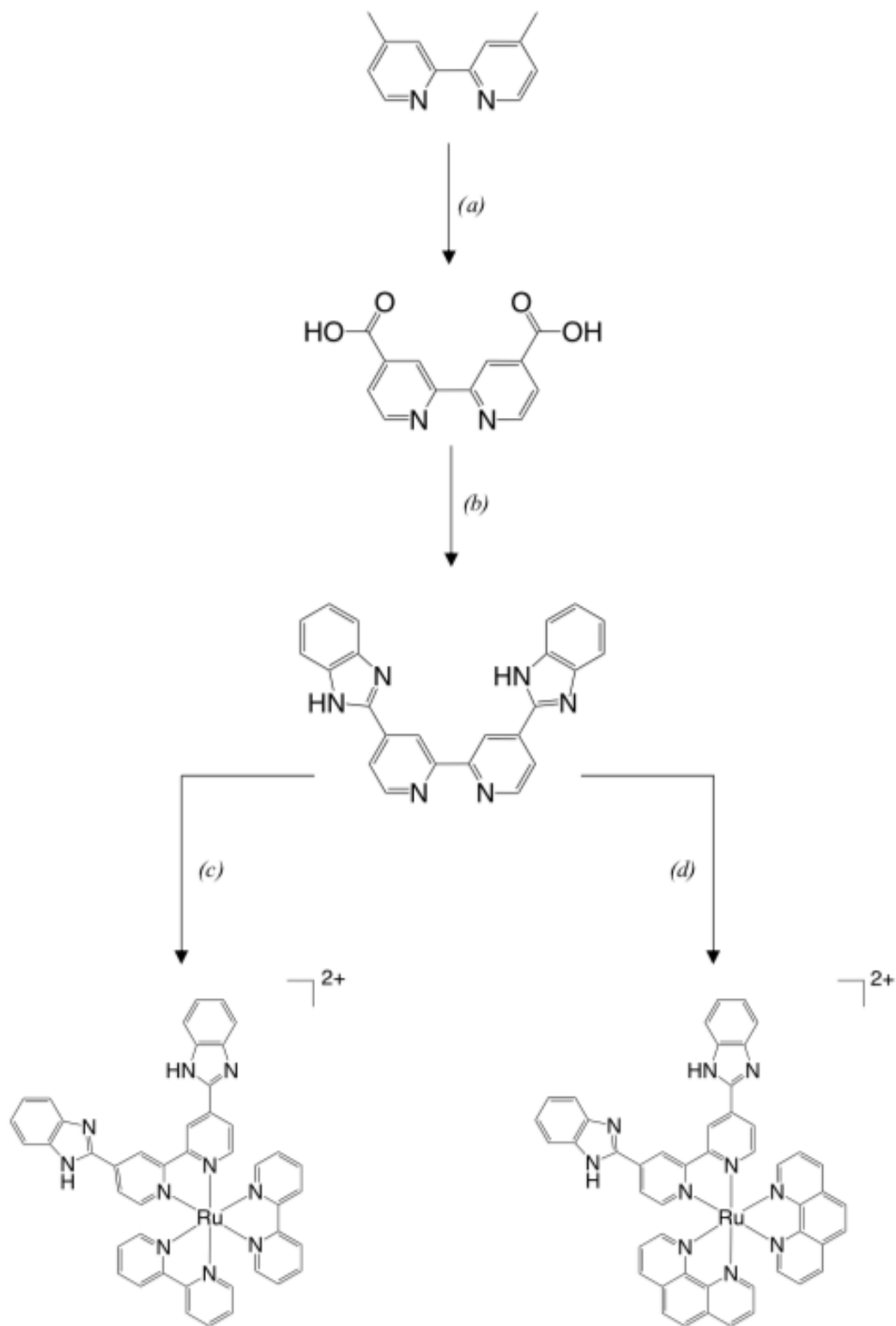
Scheme 2.1 *- Reaction scheme of the general synthesis of ligand and complexes. (a) CrO₃, H₂SO₄, RT; (b) 1,2-phenylenediamine, PPA, 200 ℃; (c) [Ru(bpy)₂Cl₂], triflic acid, ethylene gycol, 140 ℃; (d) [Ru(phen)₂Cl₂], triflic acid, ethylene glycol, 140 ℃.*

2.2.1 General Synthesis and Characterisation of Ligands and Complexes

2.2.1.1 Synthesis of 4,4'-bis(benzimidazol-2-yl)-2,2'-bipyridine

4,4'-Dicarboxylic acid-2,2'-bpy was synthesised from 4,4'-dimethyl-2,2'-bipyridine via a standard literature procedure and without further purification.[6,7] Conversion to bbib used *o*-phenylenediamine and polyphosphoric acid (PPA), acting as both solvent and dehydrating agent. This was stirred at 200 °C in a nitrogen atmosphere for 24 hours. Once cooled, the solution was slowly added to stirring aqueous saturated sodium carbonate solution, producing a brown solid which was used without further purification in 76% yield, confirmed by ^{1}H-NMR spectroscopy and mass spectrometry. Crystals were grown via evaporation of DMSO-D$_6$ and the structure was confirmed via single crystal x-ray crystallography (Appendix 7.1.1). The crystal structure shows that the ligand is highly planar with a degree of π-stacking occurring between the molecules (Figure 2.4).
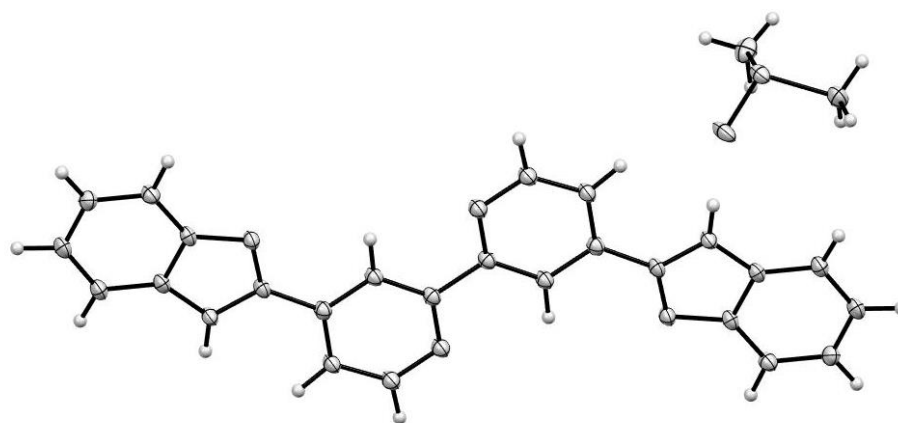
***Figure 2.4** – The crystal structure of bbib, co-crystallised with DMSO.*

2.2.1.3 ^{1}H-NMR Characterisation of bbib

The ^{1}H-NMR spectrum of bbib was recorded in DMSO-D$_6$. Despite the solubility issues of the ligand, sufficient dissolved using this solvent to permit characterisation. The spectrum for bbib (Figure 2.5) is similar to the benzoxazole and benzothiazole analogues synthesised by Spillane.[9] There are some differences aside from a peak just below 9.3 ppm, representative of the imidazole proton. In particular, the proton in the 3 position of the bipyridine (denoted as H^{3*}) is upfield significantly, due to the reduction of electron shielding around the proton. The proton in the 4 position of the benzimidazole group (denoted H^{Ar4}) is also upfield in a similar position to that of the proton in the 1 position (denoted H^{Ar1}).
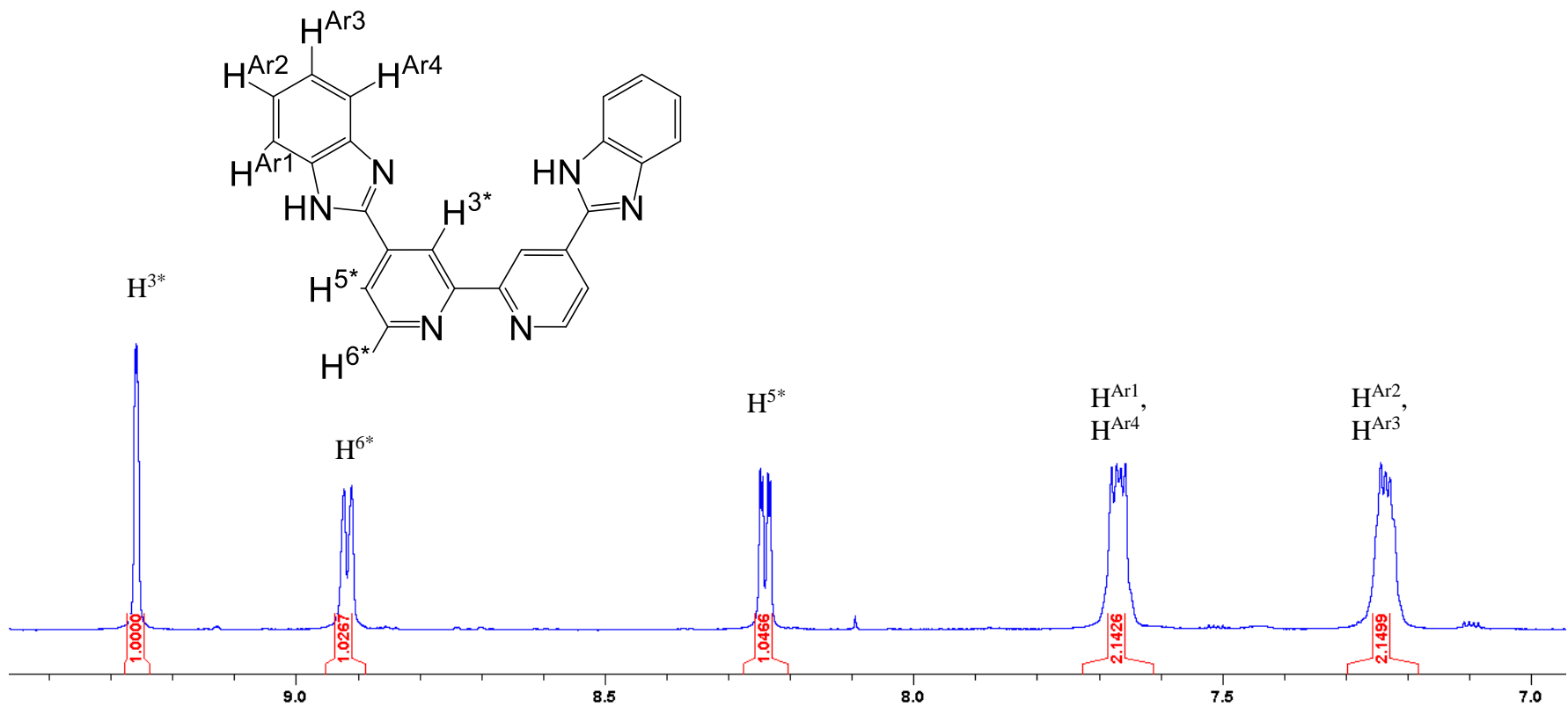
Figure 2.5 - *¹H-NMR Assignment of bbib in DMSO-D₆, 400 MHz, 25 ℃*

2.2.1.4 Synthesis of [Ru(bpy)$_2$(bbib)]$^{2+}$ and [Ru(phen)$_2$(bbib)]$^{2+}$

Complex preparation was completed by heating bbib, [Ru(bpy)$_2$Cl$_2$].xH$_2$O and trifluoromethanesulfonic acid at 140 °C in ethylene glycol for 4 hours in a nitrogen atmosphere. This formed a dark red solution. Once cooled, aqueous potassium hexafluorophosphate was added to precipitate the complex as a red brown PF$_6^-$ salt that was isolated by filtration. Size exclusion chromatography (Sephadex™ LH20) was used with a 1:1 acetone/methanol eluant to purify, obtaining the product as a brown solid in 79% yield, confirmed by ^{1}H-NMR spectroscopy and mass spectrometry. Subsequent conversion to the chloride salt was undertaken in water, stirring with Amberlite IRA-400 resin beads. [Ru(phen)$_2$Cl$_2$].xH$_2$O was used to synthesise [Ru(phen)$_2$(bbib)]$^{2+}$ in a similar method with a yield of 43%.

2.2.1.5 ^{1}H-NMR Characterisation of [Ru(bpy)$_2$(bbib)]$^{2+}$ and [Ru(phen)$_2$(bbib)]$^{2+}$

^{1}H-NMR spectra of [Ru(bpy)$_2$(bbib)][PF$_6$]$_2$ and [Ru(phen)$_2$(bbib)][PF$_6$]$_2$ were recorded in acetone-D$_6$. The spectrum for [Ru(bpy)$_2$(bbib)][PF$_6$]$_2$ (Figure 2.6) are again similar to those of the thiazole and oxazole analogues. The variations seen with the respective ligands are also seen in the spectra of the complexes. The spectrum of [Ru(phen)$_2$(bbib)][PF$_6$]$_2$ is very similar to that of the bipyridine analogue with additional peaks arising from the 1,10'-phenanthroline ligands, anticipated from the ^{1}H-NMR spectrum of [Ru(phen)$_3$][PF$_6$]$_2$.
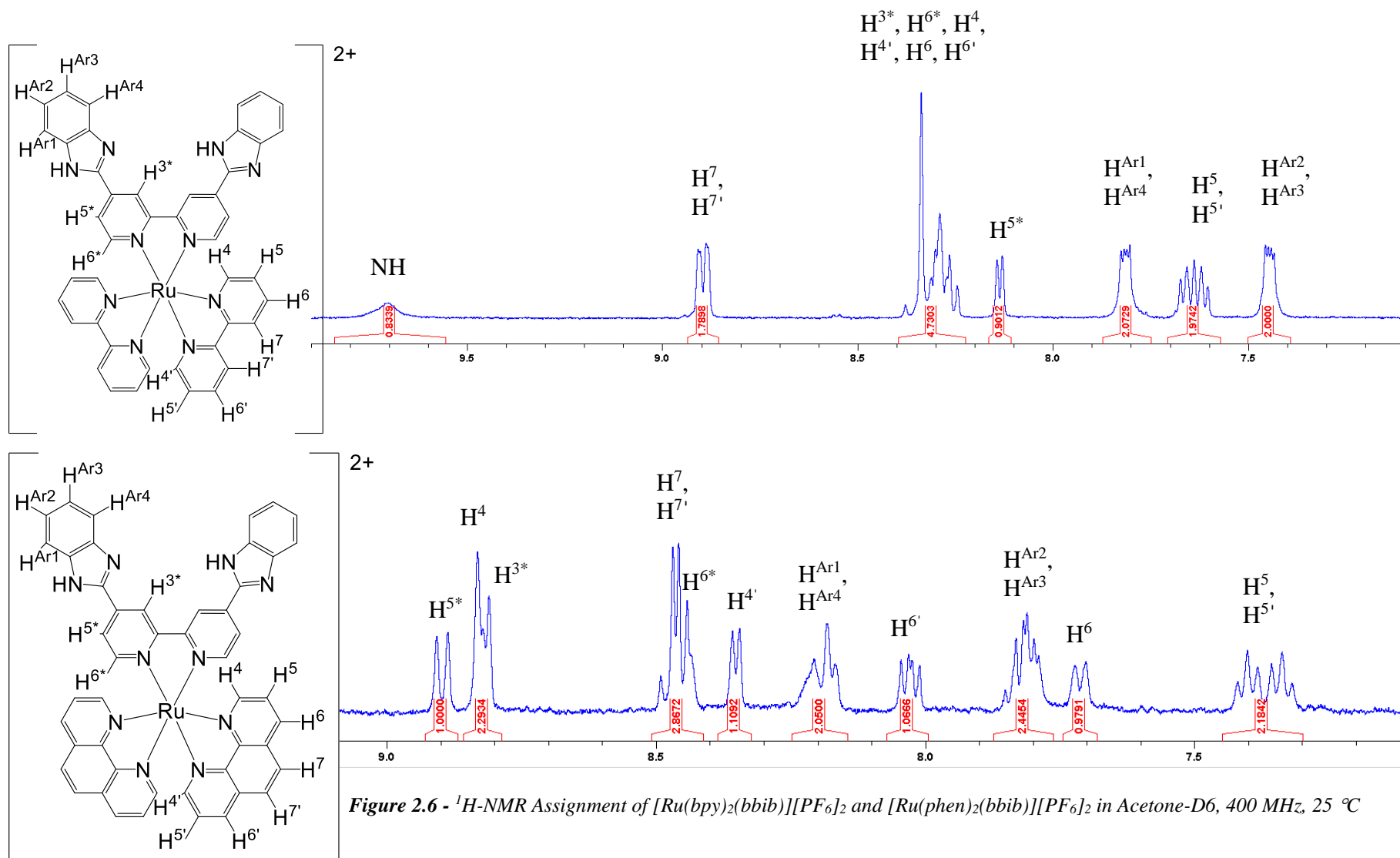
Figure 2.6 - ^{1}*H-NMR Assignment of [Ru(bpy)$_2$(bbib)][PF$_6$]$_2$ and [Ru(phen)$_2$(bbib)][PF$_6$]$_2$ in Acetone-D6, 400 MHz, 25 °C*

2.2.1.6 Attempted Synthesis of Complex Enantiomers

Previous attempts in the Fletcher group to separate the delta (Δ) and lambda (Λ) enantiomers of $[Ru(bpy)_2(bbib)][PF_6]_2$ via SP Sephadex C-25 cation exchange chromatography had proved to be unsuccessful, using chiral eluents *i.e.* 0.1 M sodium (+)/(-) di-O,O′-p-toluyl-D/L-tartrate solutions, 0.1 M sodium (+)/(-)-O,O′-dibenzoyl-D/L-tartrate solutions, 0.1 M sodium octanoate and sodium benzoate.[1,2] It is assumed that this is due to proton exchange on the imidazole. Therefore, different approaches were applied to attempt the isolation of the two enantiomers of $[Ru(bpy)_2(bbib)]^{2+}$.

The initial attempt to synthesise the Δ- and Λ- forms of $[Ru(bpy)_2(bbib)][PF_6]_2$ was via the use of proline as a chiral auxiliary, as outlined by Meggers.[7] However, it was not possible to retrieve the purified product off of the silica column without impurities (Scheme 2.2). Once the Meggers route was established as unsuccessful, an attempt was made to separately prepare the enantiomers via complexation of $[Ru(bpy)_2Cl_2]$ with pyridine to form $[Ru(bpy)_2(py)_2]^{2+}$, which was mixed with either L or D sodium dibenzoyl tartrate, forming an enantiorich precursor (Λ-$[Ru(bpy)_2(py)_2]$.DBT or Δ-$[Ru(bpy)_2(py)_2]$.DBT).[8] This was then complexed with bbib to form separate enantiomers of $[Ru(bpy)_2(bbib)][PF_6]_2$. Unfortunately when complexation was attempted, only racemic $[Ru(bpy)_2(bbib)][PF_6]_2$ was isolated which was confirmed via circular dichroism spectroscopy. This was most likely due to the high temperature of the reaction causing the enantiorich precursors to racemise. Hence it was decided, due to time constraints, to continue only with the racemic forms of complexes.

racemic

D-proline (2 eq.)   L-proline (2 eq.)
K_2CO_3 (0.5 eq.) K_2CO_3 (0.5 eq.)
180 - 190 ^oC 180 - 190 ^oC
Ethylene Glycol   Ethylene Glycol
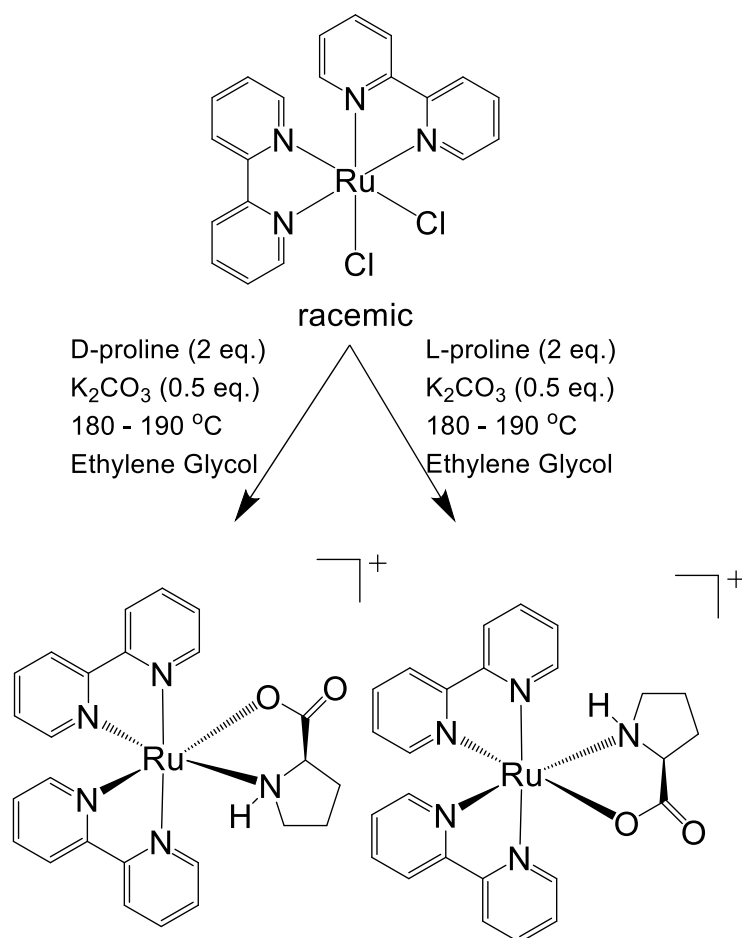
***Scheme 2.2** – The reaction scheme as proposed by Meggers et al. for preparation of enantioselected [Ru(bpy)₂(proline)]⁺, showing the major diastereomer formed.[7]*

2.2.3 Photophysical Properties of [Ru(bpy)₂(bbib)]²⁺ and [Ru(phen)₂(bbib)]²⁺

Table 2.1 - *A table to summarise the photophysical properties of [Ru(bpy)₂(bbib)]²⁺ and of [Ru(phen)₂(bbib)]²⁺*

	Absorption λ_{max} ± 1 nm	ε x10^{-3} (mol^{-1}cm^{-1})	Emission λ_{max} ± 1 n	Quantum Yield (ϕ_{em})*
[Ru(bpy)₂(bbib)]²⁺	293	7448	654	0.071
	374	3906		
	479	2269		
[Ru(phen)₂(bbib)]²⁺	266	17001	637	0.055
	293	9060		
	375	5340		
	485	3610		

*The spectra of the complexes were recorded as their hexafluorophosphate salts in acetonitrile at 298 K. The quantum yield of each complex was calculated relative to [Ru(bpy)₃](PF₆)₂ as a standard in acetonitrile (0.04).[10] λ_{ex} = 450 nm when absorption = 0.1 at 450 nm.

[Ru(bpy)₂(bbib)][PF₆]₂ and [Ru(phen)₂(bbib)][PF₆]₂ show similar absorbance and emission spectra. The absorption spectra of [Ru(bpy)₂(bbib)][PF₆]₂ consists of three well defined peaks in the range of 200-600 nm (Figure 2.7). Bands at 290 and 368 nm, assigned as ligand centred (LC) transitions, are most likely due to ancillary $\pi_{bpy} > \pi_{bpy}$* transitions and bbib $\pi \rightarrow \pi$* transition respectively. The peak at 290 nm is approximately twice the size of that of 368 nm. Intense bands at 250 nm and 479 nm can be accredited to metal to ligand charge transfer (MLCT) d $\rightarrow \pi$* transitions, one for the transition

between the metal centre and the functionalised ligand, and one for the transition between the metal centre and the identical ancillary ligands. In the absorbance spectra of [Ru(phen)$_2$(bbib)][PF$_6$]$_2$, a band is seen at 266 nm resulting from LC excited state of the ancillary $\pi_{phen} > \pi_{phen}*$ transition, replacing the $\pi_{bpy} > \pi_{bpy}*$ band.
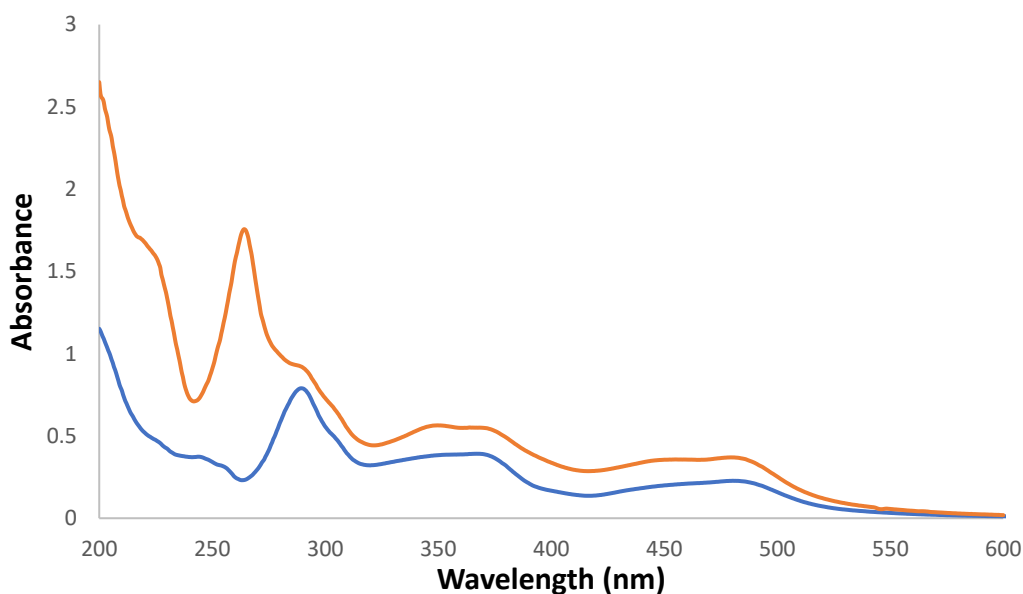
Figure 2.7 *– UV/Vis absorbance spectrum of [Ru(bpy)$_2$(bbib)][PF$_6$]$_2$ (blue) (50 μM) and [Ru(phen)$_2$(bbib)][PF$_6$]$_2$ (orange) (100 μM) measured at 25 ℃ in MeCN .*

The emission spectrum of [Ru(bpy)$_2$(bbib)][PF$_6$]$_2$ (Figure 2.8) was recorded between 500 and 850 nm at 25 °C, with the complex excitation wavelength of 450 nm. This produced a strong emission at 651 nm. [Ru(bpy)$_3$]$^{2+}$ was used as the standard luminophore (ϕ= 0.04).[10] From this, the relative emission quantum yield of [Ru(bpy)$_2$(bbib)][PF$_6$]$_2$ was calculated to be ϕ = 0.071. For [Ru(phen)$_2$(bbib)][PF$_6$]$_2$, run in comparable conditions, the emission was found to be at 636 nm, with a relative emission quantum yield of ϕ = 0.055, a lower value than for the bipyridine analogue. Both [Ru(bpy)$_2$(bbib)][PF$_6$]$_2$ and [Ru(phen)$_2$(bbib)][PF$_6$]$_2$ emit at a higher wavelength than that of [Ru(bpy)$_3$][PF$_6$]$_2$. This implies that the emission of [Ru(bpy)$_2$(bbib)][PF$_6$]$_2$ and [Ru(phen)$_2$(bbib)][PF$_6$]$_2$ are originating from a different transition than the emission

of [Ru(bpy)$_3$][PF$_6$]$_2$, i.e the excited state for [Ru(bpy)$_3$][PF$_6$]$_2$ is on the bipyridine ligand,

but for [Ru(bpy)$_2$(bbib)][PF$_6$]$_2$ and [Ru(phen)$_2$(bbib)][PF$_6$]$_2$, the excited state is on the

bbib ligand. This could also explain the increase in relative quantum yields. The two

complexes have relatively high quantum yields compared to [Ru(bpy)$_3$][PF$_6$]$_2$.
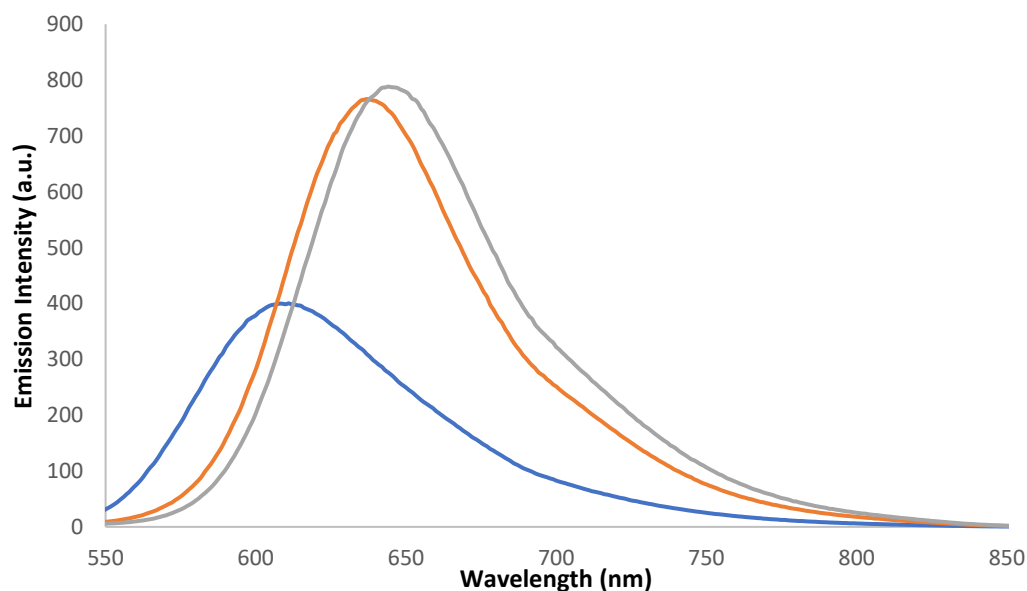
Figure 2.8 *- Emission spectra of [Ru(bpy)$_2$(bbib)][PF$_6$]$_2$ (grey), [Ru(phen)$_2$(bbib)][PF$_6$]$_2$ (orange) and [Ru(bpy)$_3$][PF$_6$]$_2$ (blue) excited at 450 nm at 25 °C in acetonitrile.*

2.2.4 Conclusions of Synthesis and Characterisation of Benzimidazole-functionalised Complexes

Two new ruthenium(II) polypyridyl complexes with benzimidazole based ligands have

been synthesised and characterised. These incorporate both the 1,10-phenanthroline and

2,2'-bipyridine analogues and enables comparison between these and similar

complexes and between themselves. The additional proton of the benzimidazole ligand,

compared to the previously reported benzoxazole or benzothiazole analogues has

caused difficulty in the chiral resolution in these ligands due to proton exchange

(Section 2.2.1.6), meaning that other routes had to be considered in order to synthesise

them separately, which have not been successful so far. The two ruthenium(II)

complexes have shown superior fluorescent properties over previously reported complexes and $[Ru(bpy)_3][PF_6]_2$, giving a greater potential for their uses as luminescent probes for DNA and anions.

2.3 pH Titrations

Changing the pH of an environment can affect the behaviour of a transition metal complex via modification of the ligand and charge. This can be examined experimentally via titration by measuring the variation of intensity and the wavelength of absorbance and emission.[11,12] This is a consequence of protonation/deprotonation events, usually of ligand functional groups.[13,14] Changing the surrounding pH can cause a "light-switch" effect for ruthenium complexes, which can be used for visual pH sensing.[15]

The pH of biological systems is critical for optimal function if to be used in a physiological setting. It affects the secondary structure of DNA and proteins, including enzymes, affecting their abilities to perform correctly.[16] A healthy cell typically operates at pH 7.4, whereas a diseased cell could have a different pH, for example, a cancer cell can have a pH range of 6.8 – 7.2.[17] Therefore, it is essential to understand how a complex behaves at several different pH levels.

The UV/Vis absorbance spectra and emission spectra of $[Ru(bpy)_2(bbib)]Cl_2$ and $[Ru(phen)_2(bbib)]Cl_2$ were taken over a pH range from 1.93 to 12.54 using a standardised 0.1 M Britton-Robinson buffer and adjusted by the addition of a 0.1 M NaOH solution, both containing the ruthenium complexes at 10 µM.
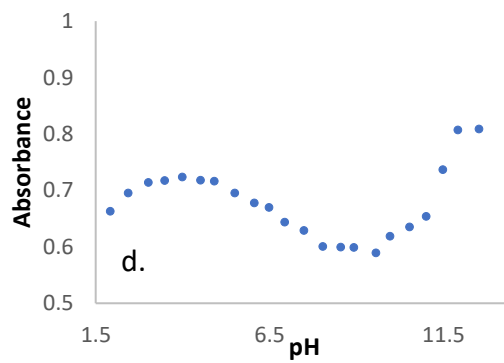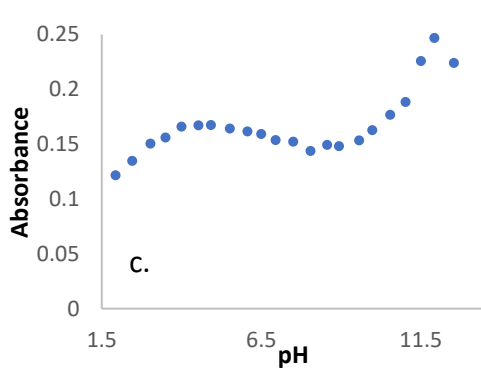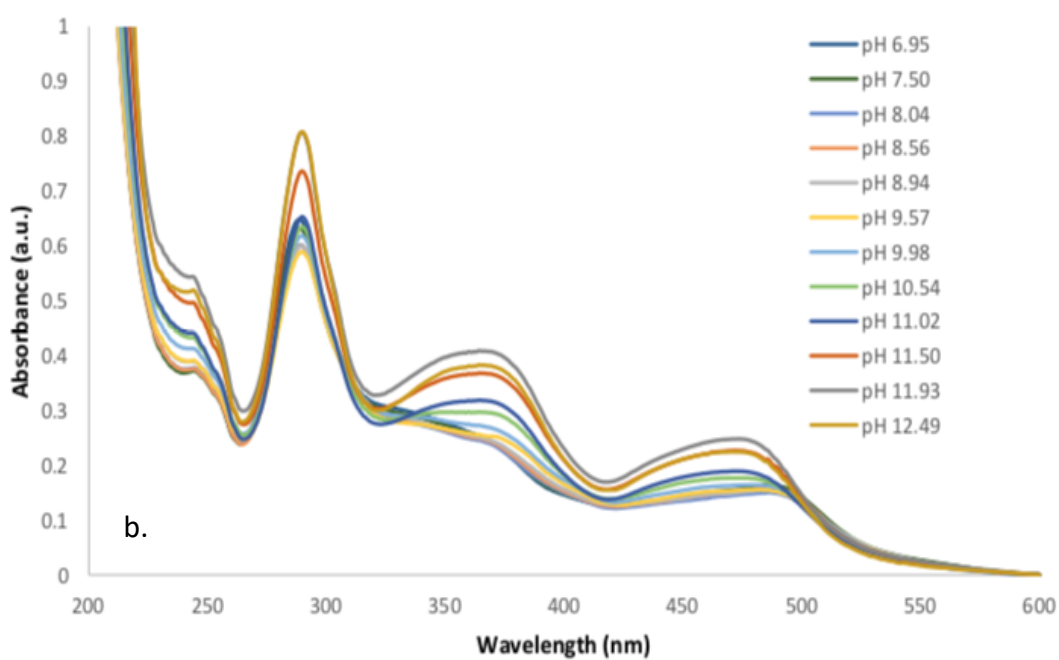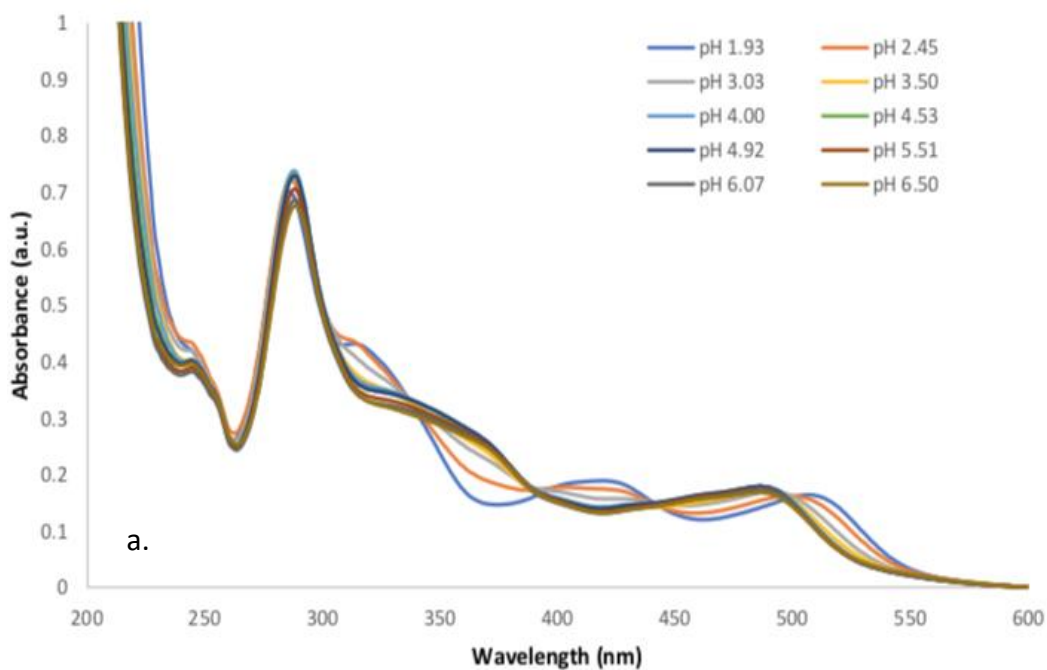
Figure 2.9 *- UV/Vis absorbance spectra of [Ru(bpy)$_2$(bbib)]Cl$_2$ at (a). pH ~2 to ~7, and (b). pH ~7.5 to ~12.5 and plotted absorbance values at (c). 290 nm and (d). 467.5 nm.*
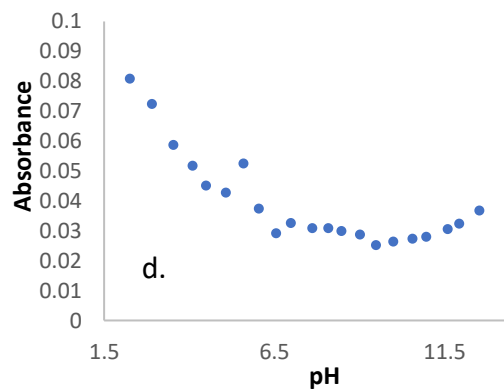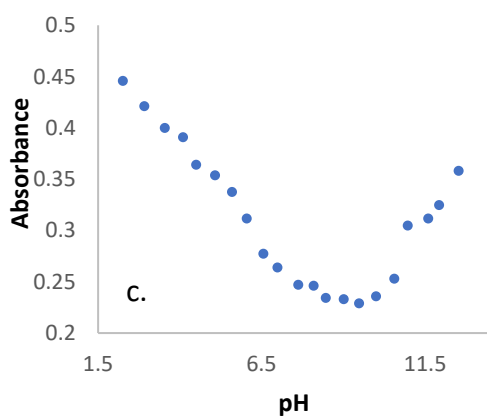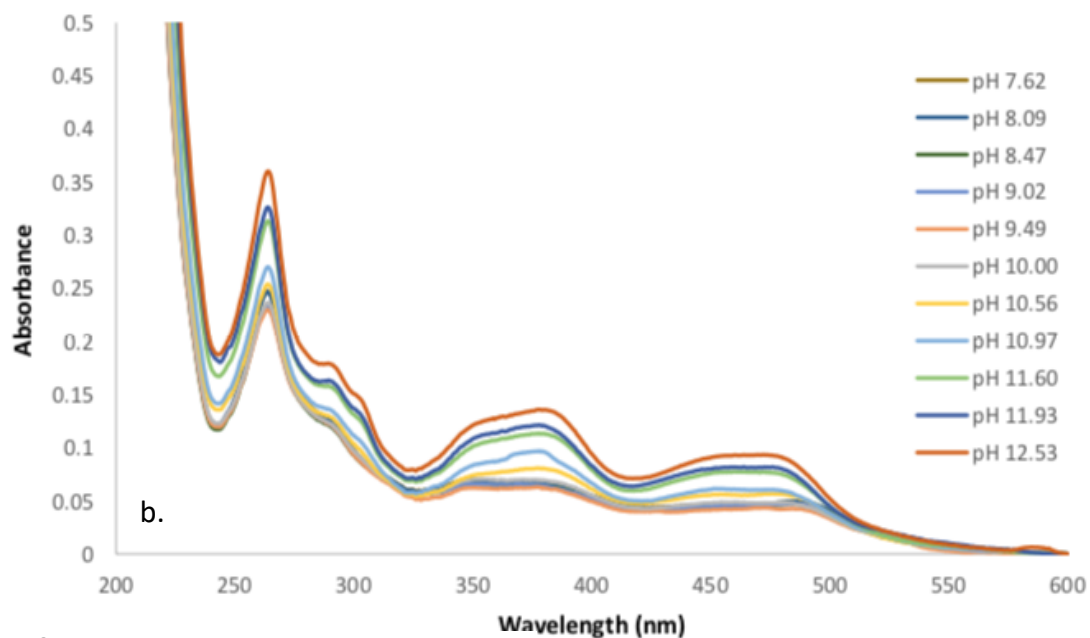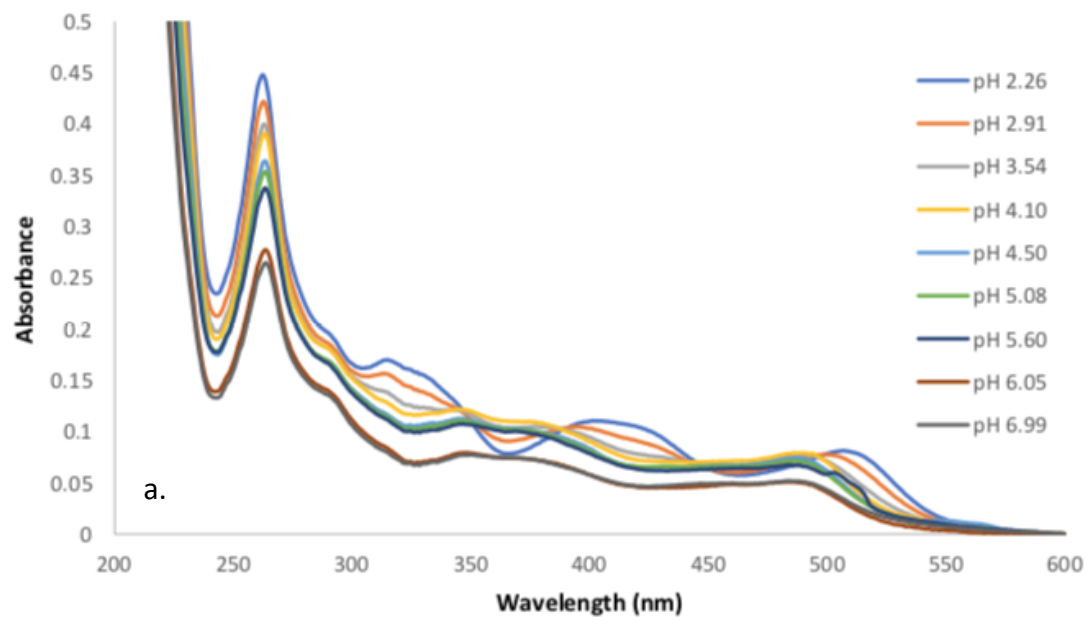
Figure 2.10 - *UV/Vis absorbance spectra of [Ru(phen)₂(bbib)]Cl₂ at (a). pH ~2 to ~7, and (b). pH ~7.5 to ~12.5 and plotted absorbance values at (c). 263 nm and (d). 467.5 nm.*

The UV/Vis absorbance spectra for both $[Ru(bpy)_2(bbib)]Cl_2$ (Figure 2.9) and $[Ru(phen)_2(bbib)]Cl_2$ (Figure 2.10) show several peaks which change with a variation in pH. This is most obvious in the regions that are considered to represent the bbib-LC transitions, 374 nm for $[Ru(bpy)_2(bbib)]Cl_2$ and 385 and 325 nm for $[Ru(phen)_2(bbib)]Cl_2$) and the MLCT region (499 – 515 nm for $[Ru(bpy)_2(BBIB)]Cl_2$, 479 – 515 nm for $[Ru(phen)_2(bbib)]Cl_2$). An increase of absorbance is observed with an increase of pH from 3 to 10 in these ligand-centred regions, possibly indicative of a deprotonation event, which would increase the energy gap between π - π^*_{bbib}. In acidic conditions, the complexes are protonated, resulting in a positive charge on the bbib ligand. This would mean that less energy is required for the $\pi_{bbib} - \pi^*_{bbib}$ transition to occur. This is visualised by the red shift in the wavelengths.

The MLCT peaks have both a change in absorbance and wavelength with varying pH. At pH 2.26, there is a peak at 515 nm representing the $d - \pi^*_{BBIB}$ MLCT. This band is not present at pH 7 and at pH 12 there is instead a peak at 479 nm for $[Ru(bpy)_2(bbib)]Cl_2$ and 499 nm for $[Ru(phen)_2(bbib)]Cl_2$, assigned to the $d - \pi^*_{bpy/phen}$ MLCT. This shift in peak wavelength suggests that there is a change in the position of the dominant MLCT from the $d - \pi^*_{bbib}$ transition to the d - $\pi^*_{bpy/phen}$ transition. In acidic conditions, the positive charge on the bbib ligand causes a decrease in energy requirement for electron promotion from the d-orbital of the metal centre into the π^*-orbital of bbib. As the conditions become more basic, the positive charge is removed, and eventually replaced with a negative charge via deprotonation (Figure 2.8). This infers a much higher energy needed for d - π^*_{bbib} to occur, while the energy required for $d - \pi^*_{bpy/phen}$ does not change. Therefore, it is implied that the MLCT order has changed, represented by change in MLCT peak from 515 nm to 479 nm and 499 nm for

[Ru(bpy)$_2$(bbib)]Cl$_2$ and [Ru(phen)$_2$(bbib)]Cl$_2$, respectively. Overall, this shows a significant change in the absorbance of the complex and can be seen by the naked eye. The acidic solution is orange, with the basic solution taking on a more yellow appearance.
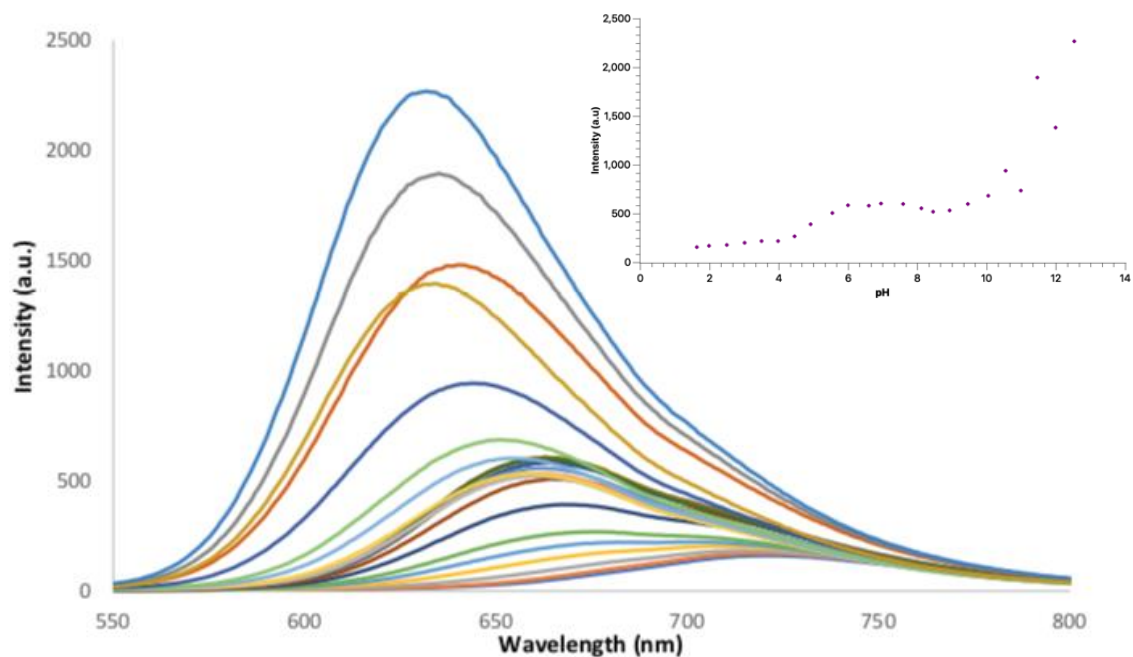
Figure 2.11 *– Emission spectra of [Ru(bpy)$_2$(bbib)]Cl$_2$ at pH ~2 to ~12.5. Solutions in 0.1 M Britton-Robinson buffer and 0.1 M NaOH, excited at 450 nm and spectra recorded at 25°C.*
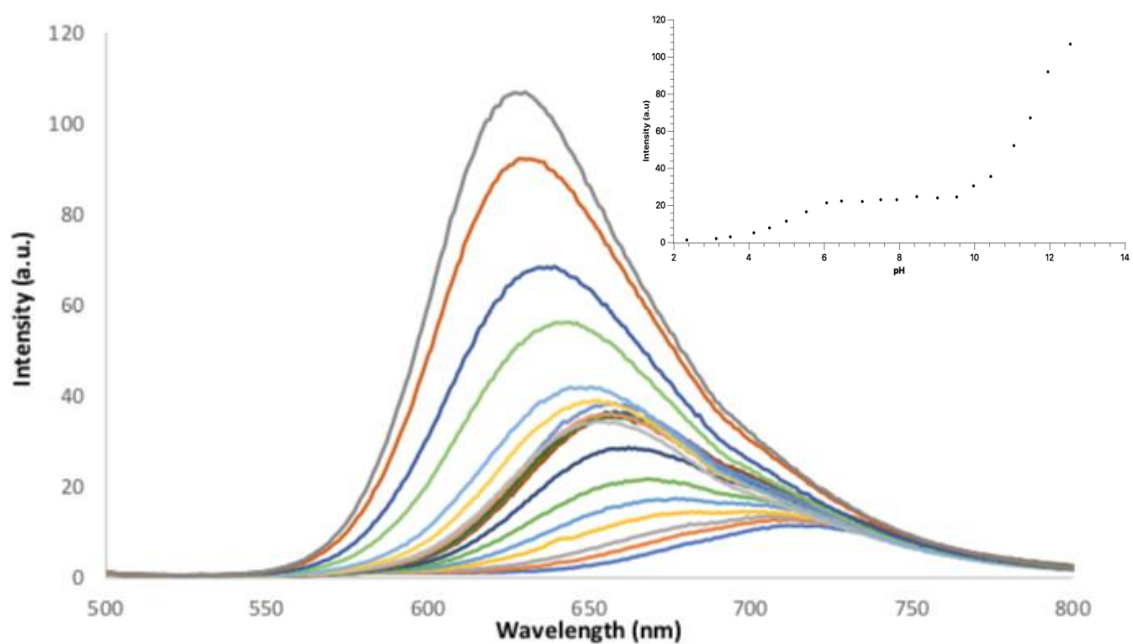
Figure 2.12 *– Emission spectra of [Ru(phen)$_2$(bbib)]Cl$_2$ at pH ~2 to ~12.5. Solutions in 0.1 M Britton-Robinson buffer and 0.1 M NaOH, excited at 450 nm and spectra recorded at 25°C.*

The emission spectra of [Ru(bpy)$_2$(bbib)]Cl$_2$ (Figure 2.11) and [Ru(phen)$_2$(bbib)]Cl$_2$ (Figure 2.12) show a substantial increase in intensity occurring as the solution moves from an acidic to basic pH. At approximately pH 2, λ_{max} is 720 nm for [Ru(bpy)$_2$(BBIB)]Cl$_2$ and 717 nm for [Ru(phen)$_2$(bbib)]Cl$_2$. This shifts bathochromically through 662 nm for [Ru(bpy)$_2$(bbib)]Cl$_2$ and 657 nm for [Ru(phen)$_2$(bbib)]Cl$_2$ at pH 7 and then to 631 nm for [Ru(bpy)$_2$(bbib)]Cl$_2$ and 632 nm for [Ru(phen)$_2$(bbib)]Cl$_2$ at around pH 12.5. These changes in emissive wavelength can be attributed to the fact that in an acidic pH the bbib ligand is protonated, which reduces the energy level for π^*_{bbib} – d transitions. This means that any radiative emission is originating from the d – π^*_{bbib} transition. As the pH increases, the energy requirement for the π^*_{bbib} – d transition also increases, until the energy level is greater than that of $\pi^*_{bpy/phen}$ – d transitions upon excitation. In this scenario, most emission is coming from the d – $\pi^*_{bpy/phen}$ transition (Figure 2.13).
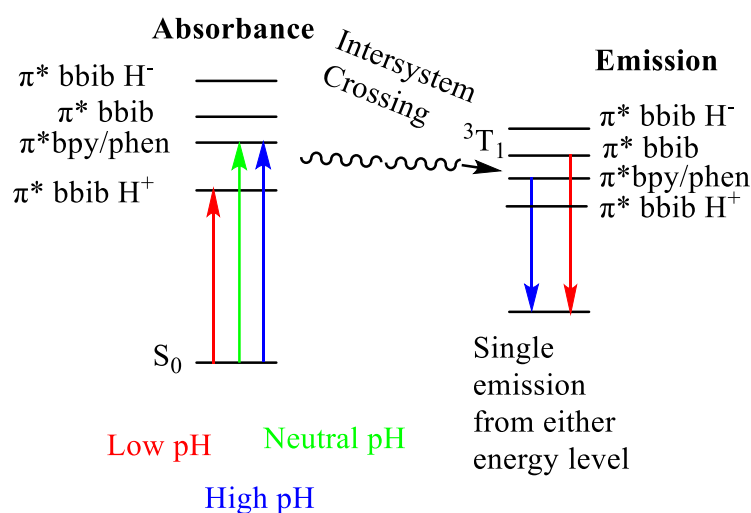
Figure 2.13 - *A Jablonski diagram to describe the changes in transitions for [Ru(bpy)$_2$(bbib)]$^{2+}$ and [Ru(phen)$_2$(bbib)]$^{2+}$ as a function of pH.*

There is a similar pattern in the decrease in emission intensity as the environment changes from basic to acidic, as there is also a change in the absorbance spectra (Figures 2.9 and 2.10), commensurate of two protonation/deprotonation events occurring (Figure 2.14). The change in intensity from acidic to basic pH is associated with the change in charge on the complex. As stated previously, the negative charge on the benzimidazole moieties of BBIB result in a much higher energy requirement for the $d - \pi^*_{BBIB}$ to occur, therefore it is thought that instead, the dominant transition is $d - \pi^*_{bpy/phen}$. This results in an increase in emission intensity due to bpy and phen ligands having a lower hydration/solvation sphere (attributed to bpy/phen being smaller and more hydrophobic than the bbib ligand), causing less quenching of the emission to occur as the electrons decay to the ground state. The positive charge of the bbib ligand in acidic environments would stabilise the excited state at $^3\pi^*_{bbib}$, therefore emission could be lost via solvent dissipation, due to the higher solvation sphere around the ligand. Another explanation for this increase in emission intensity is that simply the emission is not switching between the bbib ligand and the ancillary ligands, but the energy gap between $d\text{-}\pi^*_{bbib}$ is increasing, resulting in a decrease in wavelength and an increase in emission intensity.
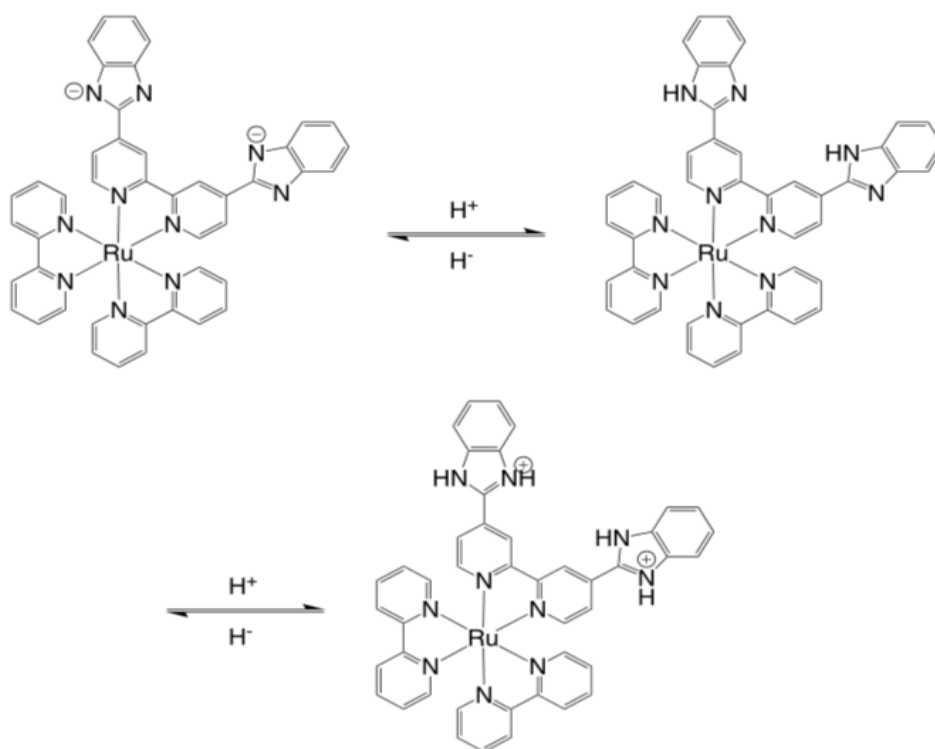
Figure 2.14 *– Proposed mechanism of protonation/deprotonation for [Ru(bpy)$_2$(BBIB)]$^{2+}$*

It must be considered that the Britton-Robinson buffer is a solution comprised of acetic acid, boric acid and, most importantly, phosphoric acid. Complexes bearing the bbib ligand have strong interactions with phosphate ions (as discussed subsequently), thus it is reasonable to assume that, at least partially, these results are representative of the phosphate-bound complex, although this may not be the case for the whole pH range. Phosphate ions, like the complexes, are subject to protonation/deprotonation with a change in pH and has conjugate acids i.e. dihydrogen phosphate. Above pH 10, it will be deprotonated, along with the complexes, therefore interactions are unlikely to occur. Similarly, below pH 4, both the complex and the ion would be protonated, and again, interactions are unlikely to happen. In between the two extremes of pH, however, the ion would have a slightly negative charge and the complex would be neutral. These charges are the "Goldilocks" conditions for interaction to occur, that is to say that they are just right (Figure 2.15)
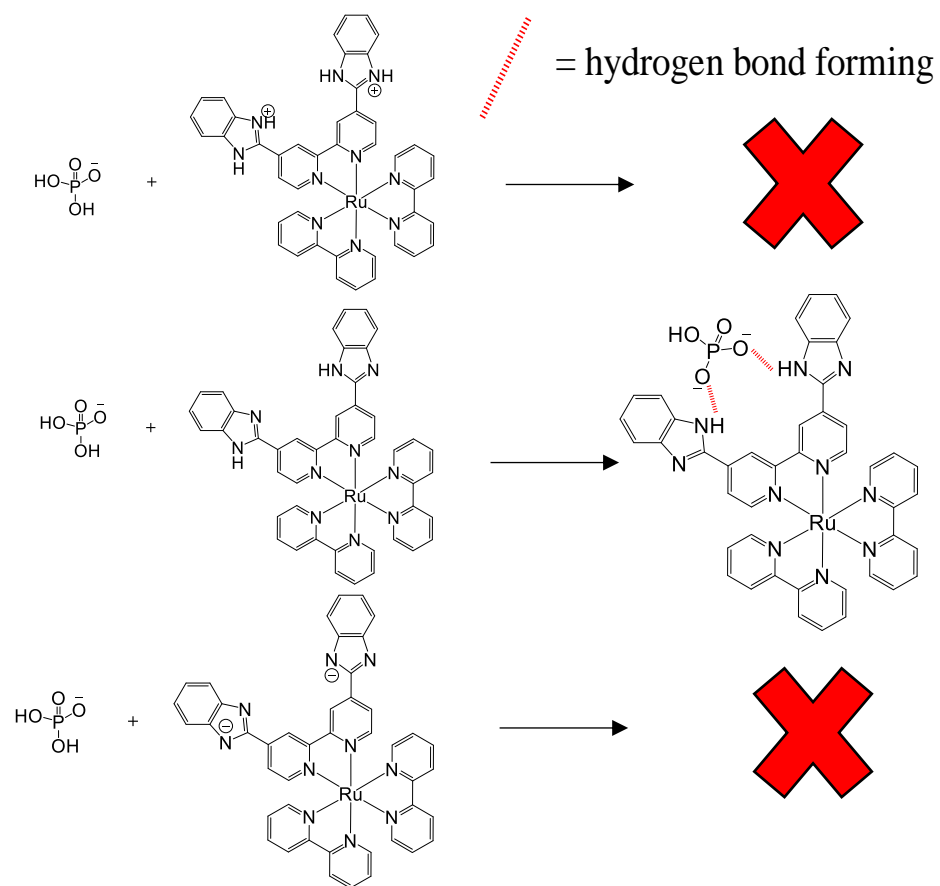
Figure 2.15 *– Diagram to illustrate pH effects on phosphate binding to BBIB ligand*

The pK_a and pK_b of both complexes have been estimated (Table 2.2) for both ground and excited states, via mid-point estimation of a line of best fit. When compared to the reported pK_a of benzimidazole and its conjugate acid (12.8 and 5.6 respectively), they are quite similar, indicating that the protonation/deprotonation is occurring on the benzimidazole. The pK_a and pK_b of the bbib ligand were not able to be determined due to solubility issues. It is possible that these values are given for the phosphate-bound adduct, rather than for the complex alone. The pK_a for the ground state of [Ru(bpy)$_2$(bbib)]Cl$_2$ is observed to be much lower than expected (a value of around 5 was to be expected), however this can be attributed to the limitations of the buffer used, which is optimal at pH levels above 3. There are slight differences in the pK_b estimation of the excited state between [Ru(bpy)$_2$(bbib)]$^{2+}$ and [Ru(phen)$_2$(bbib)]$^{2+}$. There are multiple potential reasons for this, such as the greater conjugation that the phenanthroline offer over that of the bipyridine.

Table 2.2 – Estimated experimental pKa and pKb values for [Ru(bpy)$_2$(bbib)]Cl$_2$ and [Ru(phen)$_2$(bbib)]Cl$_2$, determined via line of best fit using QTIPlot, compared to the literature values for the pKa and pKb of benzimidazole.

	pK_a of Ground State	pK_a of Excited State	pK_b of Ground State	pK_b of Excited State
[Ru(bpy)$_2$(bbib)]$^{2+}$	~2.5	~5	~10.5	~10.5
[Ru(phen)$_2$(bbib)]$^{2+}$	~5	~5	~11	~11
Benzimidazole	5.6	--	12.8	--

2.4 Anion Binding Studies

Assessing anion binding capabilities is important for complexes in a biological setting. Cellular cytoplasm contains many anions as they are used in many functions throughout the body and understanding any interactions that could occur is essential to appreciate complex behaviour within cells.[18,19] A major component of DNA/RNA is its backbone, which is made up of a long chain of phosphate anions (Section 1.2.1), all of which are capable of interaction with other entities.[20] An example of this is RNase, an enzyme acting as a catalyst in the degradation of RNA into its constituents. This protein contains phosphate binding sites, which cleave the nucleic acids at the phosphodiester bond between the 3'-phosphate group of a pyrimidine nucleotide (cytosine and uracil) and the 5' ribose of the adjacent nucleotide.[21] In the following experiments, the behaviours of $[Ru(bpy)_2(bbib)][PF_6]_2$ and $[Ru(phen)_2(bbib)][PF_6]_2$ have been examined in an environment containing $H_2PO_4^-$, Cl^-, Br^- and Ac^-, common anions found in cytoplasm.

2.4.1 UV/Vis and Emission Titrations

Transition metal complexes can also show change in photophysical properties when bound to anions. Therefore, a series of sequential addition titrations were monitored using UV/Vis and emission spectroscopy. Experiments were originally attempted in MeCN however precipitation occurred with $H_2PO_4^-$ and Ac^-, which is assumed to be the complex and anion interacting. To counteract this precipitation, each complex was then dissolved in a DMSO / 5% distilled water mixture (25 μM) and TBA salts were added (bromide, chloride, acetate and dihydrogen phosphate) sequentially up to 250 μM (10 equivalents). All data has been normalised to account for dilution effects.

2.4.2.1 Phosphate Titrations using UV/Vis and Emission Spectroscopy in MeCN

Initial attempts at UV/Vis and emission titrations in acetonitrile. $[Ru(bpy)_2(bbib)][PF_6]_2$

/ $[Ru(phen)_2(bbib][PF_6]_2$ (50 µM) were dissolved in MeCN with increasing

concentration of TBA $H_2PO_4^-$ (Up to 500 µM). The absorbance spectra for both

complexes show considerable scattering caused by precipitation (Appx 1 and 2). The

emission spectra of $[Ru(bpy)_2(bbib)][PF_6]_2$ and $[Ru(phen)_2(bbib)][PF_6]_2$, in the absence

of anions, display a high emission intensity. There is evidence that an interaction is

occurring, with the emission significantly quenched upon introduction of $H_2PO_4^-$ up to

approximately 2 equivalents (emission intensity was recorded as 233.94 – 11.90 a.u. for

$Ru(bpy)_2(BBIB)][PF_6]_2$ and 225.34 – 7.66 a.u. for $[Ru(phen)_2(BBIB)][PF_6]_2$ (Figure

2.16)). This decrease in emission could also be caused by the complex/anion adduct

precipitating out of solution, as it would decrease the concentration.

The quenching of emission in the acetate titrations stops occurring around one

equivalent for both $[Ru(bpy)_2(bbib)][PF_6]_2$ and $[Ru(phen)_2(bbib)][PF_6]_2$, therefore it is

reasonable to assume that one acetate anion is binding per each complex molecule

(Figure 2.17). However, in the case of dihydrogen phosphate, the emission is fully

quenched upon addition of two equivalents, suggesting that two anions are interacting

with one molecule of complex.
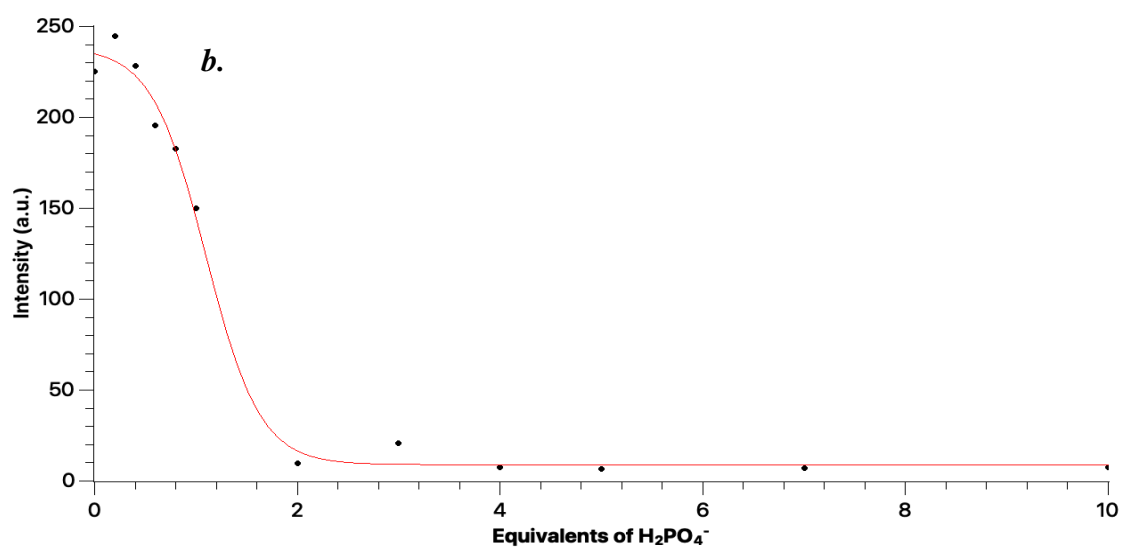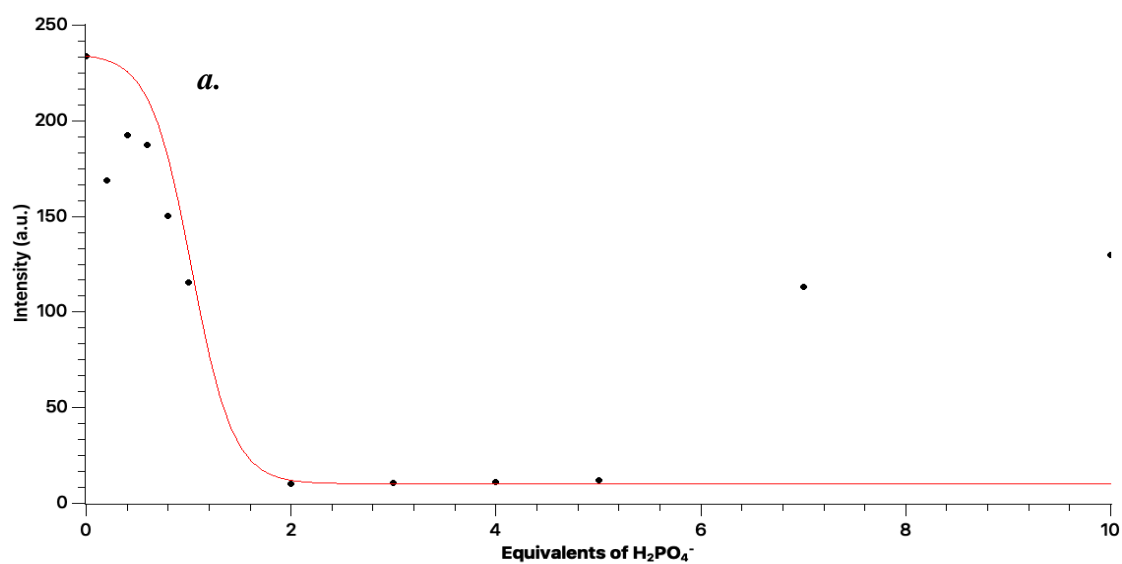
Figure 2.16 *- Maximum emissive wavelengths of (a.) [Ru(phen)₂(BBIB)[PF₆]₂ and (b)* *[Ru(phen)₂(BBIB)][PF₆]₂ with increasing H₂PO₄⁻ concentration. Spectra run at 25 °C in MeCN.*
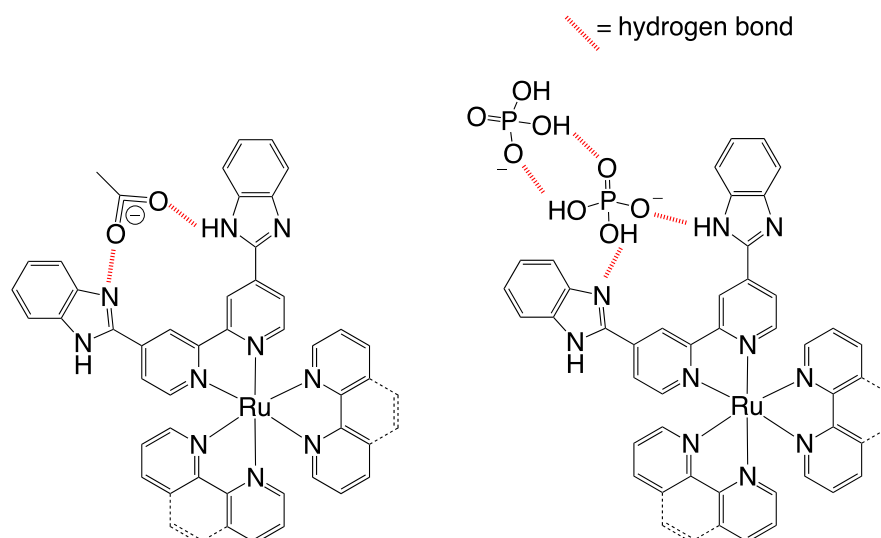
Figure 2.17 *– Hypothesised mechanism of interaction between Ru(phen)₂(bbib)][PF₆]₂/ [Ru(bpy)₂(bbib)][PF₆]₂ and acetate / dihydrogen phosphate anions.*

2.4.2.2 Anion Titrations using UV/Vis and Emission Spectroscopy in DMSO / 5% Deionised Water

In a wet DMSO solution, the addition of all anions tested ($H_2PO_4^-$, Ac^-, Cl^-, Br^-) resulted in no significant change in the absorbance spectra of either $[Ru(bpy)_2(bbib)][PF_6]_2$ and $[Ru(phen)_2(bbib)][PF_6]_2$ (25 µM) (Appx. 3 - 9). In the case of the dihydrogen phosphate and acetate ion titrations this infers that if there is an interaction, it does not result in a deprotonation event (see Section 2.3). There is no change in MLCT wavelength, suggesting that $d - \pi^*_{bbib}$ is still the lowest energy transition, leading to the ^{3}MLCT transition.
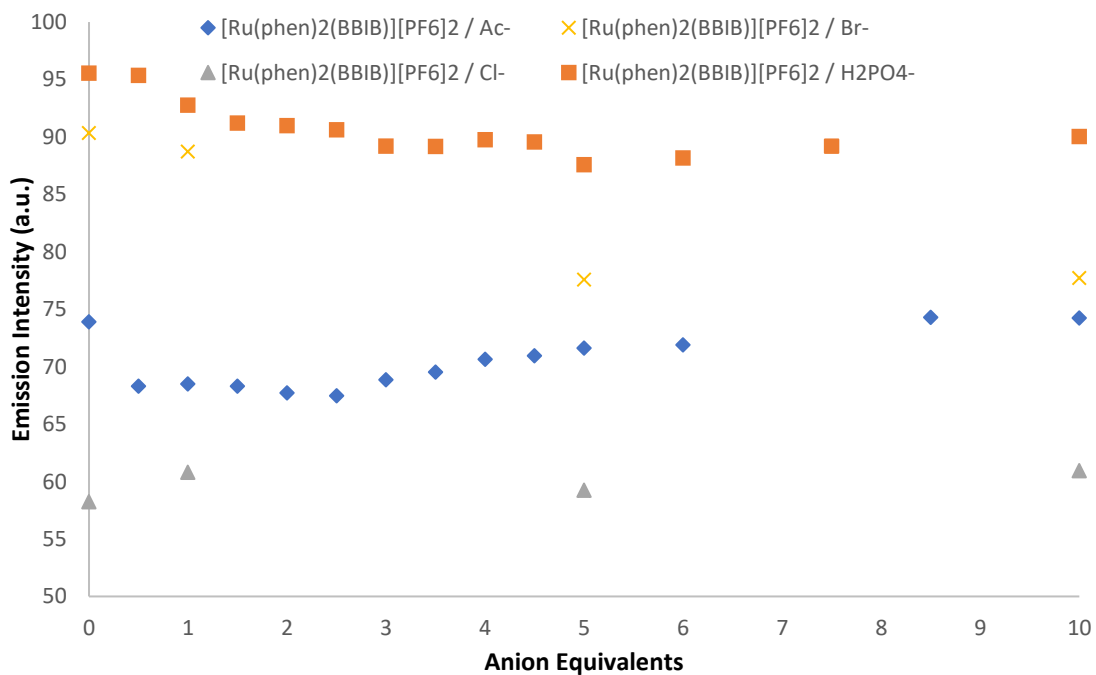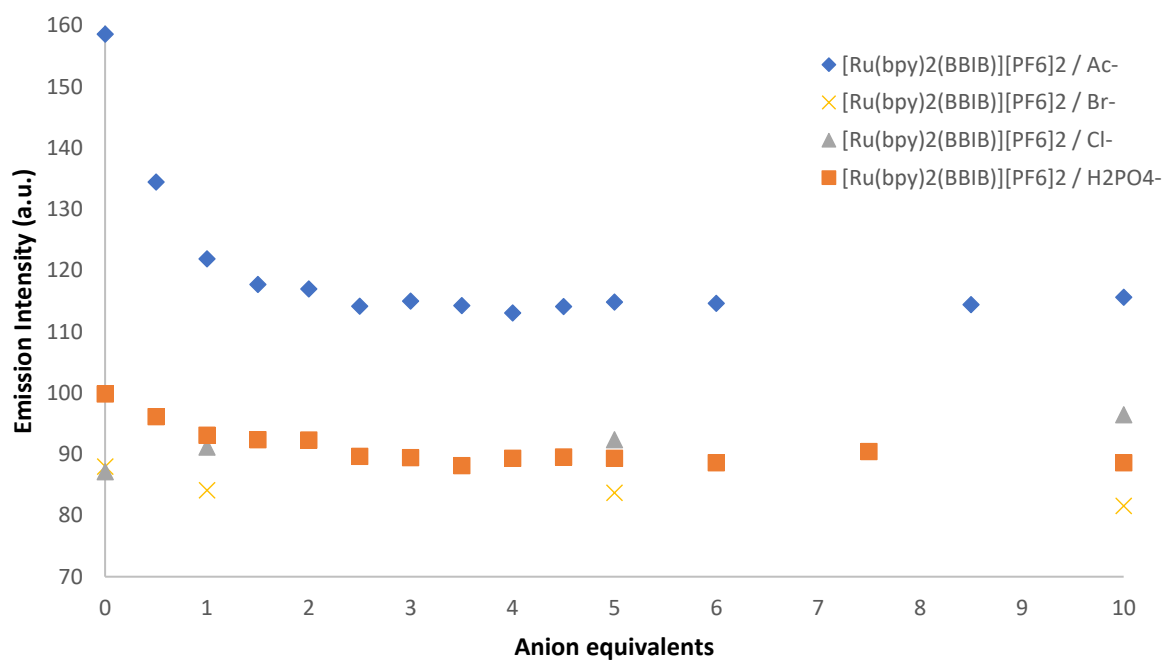
Figure 2.18 *– Maximum emissive wavelengths of (a.) [Ru(bpy)₂(bbib)] [PF₆]₂ and (b) [Ru(phen)₂(bbib)] [PF₆]₂ with increasing anion concentration (Ac⁻, Br⁻, Cl⁻, H₂PO₄⁻). Spectra run at 25 °C in DMSO / 5% deionised water.*

On addition of bromide or chloride ions, there is no observed change in emission intensity for [Ru(bpy)$_2$(BBIB)][PF$_6$]$_2$ or [Ru(phen)$_2$(BBIB)][PF$_6$]$_2$ (Figure 2.18), suggesting that there is no interaction occurring between the two. This is mostly likely due to the inability of the Br$^-$ and Cl$^-$ anions to form hydrogen bonds with the complex (Appx. 12 – 19).

Emission intensity was observed to decrease for [Ru(bpy)$_2$(bbib)][PF$_6$]$_2$ when dihydrogen phosphate and acetate are added (Figure 2.18) ([Ru(bpy)$_2$(bbib)][PF$_6$]$_2$: 100 – 89 and 159 – 116 a.u. for dihydrogen phosphate and acetate respectively). This indicates that an interaction is occurring. It is presumed that in the case of dihydrogen phosphate, hydrogen bonds form between the δ^+ imidazole proton and the negatively charged oxygen. The quenching, along with the unchanging absorbance spectra, indicate that interactions between anion and complex are opening up new, non-emissive pathways. While the quenching is weak, it is unusual as most phosphate sensors that rely on hydrogen bond formation do not work in aqueous environments.

There is no change observed with [Ru(phen)$_2$(bbib)][PF$_6$]$_2$ upon addition of dihydrogen phosphate and acetate anions (Figure 2.18). Also, the observed quenching for [Ru(bpy)$_2$(bbib)][PF$_6$]$_2$ is much lower than anticipated from the initial experiments run in acetonitrile. It is reasonable to assume that there is a hydration sphere surrounding the anions and complex when dissolved in the DMSO / 5% deionised water mixture, which is not present in the dry MeCN, a non-protic solvent. This sphere causes less radiative emission to occur, a result of solvent dissipation.

2.4.1 ^{1}H-NMR Spectroscopy Titrations

Anion binding studies of [Ru(bpy)$_2$(bbib)][PF$_6$]$_2$ and [Ru(phen)$_2$(bbib)][PF$_6$]$_2$ were undertaken via sequential addition titrations and followed by ^{1}H-NMR spectroscopy. Tetrabutylammonium salts of dihydrogen phosphate, acetate and chloride were used, and any interactions would show as a shift in peak position. Initially, the experiments were run in CD$_3$CN, however, this proved to be unsuccessful due to strong precipitation, albeit a visual indication of a possible interaction. The complexes (5 µM) were dissolved in 0.5 ml of DMSO-D$_6$ / 5% D$_2$O mixture to combat the precipitation, with aliquots of anion added up to the sum of 50 µM.

Dihydrogen Phosphate (H$_2$PO$_4^-$) and Acetate (AcO$^-$)

^{1}H-NMR spectroscopic titrations of [Ru(bpy)$_2$(bbib)][PF$_6$]$_2$ and [Ru(phen)$_2$(bbib)][PF$_6$]$_2$ (5 µM) (Figure 2.19, Appx. 20 - 24) were carried out with up to ten equivalents of TBA dihydrogen phosphate and TBA acetate (up to 50 µM). In both instances, shifts of several peaks are observed on addition of the anion, suggest that both the bpy and phen analogues interact with dihydrogen phosphate monobasic and acetate.

[Ru(bpy)$_2$(bbib)][PF$_6$]$_2$ showed a shift in the peak at 9.56 ppm with H$_2$PO$_4^-$, which corresponds to the H^3 proton of the benzimidazole on the functionalised ligand, to approximately 10 ppm. Downfield shifts indicate that hydrogen bonds have been formed between the anion (hydrogen bond donor) and this proton (a hydrogen bond acceptor), resulting in deshielding of the proton nucleus. An upfield shift is also observed for the peak at 7.34, which relates to the back two protons of the benzimidazole, implying a higher level of nuclear shielding, most likely due to a compensation of the hydrogen bond formation. There are no shift changes observed for any of the nonfunctionalized bipyridine protons and similar results are seen for [Ru(phen)$_2$(bbib)][PF$_6$]$_2$ with both dihydrogen phosphate and acetate. This implies that the ancillary ligands do not take part in the interaction, which takes place solely on the functionalised moiety.
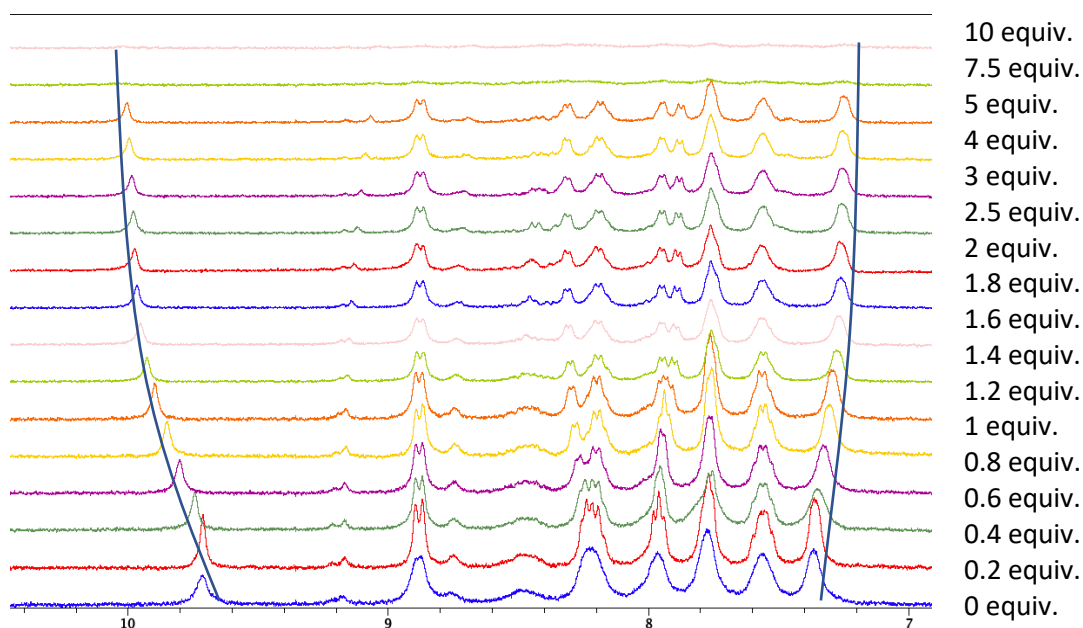
Figure 2.19 – *^{1}H-NMR titration of [Ru(bpy)$_2$(bbib][PF$_6$]$_2$ and H$_2$PO$_4^-$ in DMSO/5% deuterated water.*

Chloride (Cl⁻)

^{1}H-NMR spectroscopy titrations of [Ru(bpy)$_2$(bbib)][PF$_6$]$_2$ and [Ru(phen)$_2$(bbib)][PF$_6$]$_2$ (5 mM, 0.5 ml) with up to 10 equivalents of TBA chloride. No change in proton peak position was observed in the spectra on addition of the salt, suggesting that there is no significant interaction between the complexes and the anion.

Stability Constants

Stability constants for the ^{1}H-NMR titrations with dihydrogen phosphate and acetate were calculated by Dr. Fletcher using WINEQNMR[21] (Table 2.3) for a two anion to one complex binding ratio. The full mathematics of fitting ion and supramolecular bindings are well established and there are several pieces of software developed to do so.[21,22] The first stability constant *pK$_1$* relates to the first anion binding event, whereas Pβ_2 relates to the product of both the first and the second anions binding.

$$K_{stab1} \qquad\qquad K_{stab2}$$
$$\text{Host} + \text{ 2 anion} \; \rightleftharpoons \; \text{Complex:A } + \text{anion} \; \rightleftharpoons \; \text{Complex:A}_2$$

The data determines the values for pβ_1 and pβ_2 where: $\quad$ pβ_1 = $\log_{10}K_{stab1}$

$$\text{p}\beta_2 \;=\; \log_{10}(K_{stab1}K_{stab2})$$

Equation 2.1 – *The equation considered when using WINEQNMR.[21]*

Table 2.3 - *Stability constants calculated from ^{1}H-NMR titrations with $H_2PO_4^-$ and AcO^- in a DMSO-D_6 / 5% deuterium mixture.*

	$H_2PO_4^-$	AcO^-
[Ru(bpy)$_2$(bbib)][PF$_6$]$_2$	pK_1 = 4.39 pβ_2 = 5.50	*pK_1* = 3.81 *pβ_2* = 4.60
[Ru(phen)$_2$(bbib)][PF$_6$]$_2$	pK_1= 5.30 pβ_2 = 8.36	pK_1 = 3.33 pβ_2 = 5.37
Error < ± 5%		

The stability constants calculated for [Ru(bpy)$_2$(bbib)][PF$_6$]$_2$ with AcO$^-$ show a two anion to one cation model with a reasonably sized pK_1 of approximately 3.81 and a pβ_2 value of 4.60. The stability constants calculated for the complex with dihydrogen phosphate also stabilised to a two anion to one cation model with a pK_1 value of around 4.39 and a pβ_2 value of 5.50. The second value was relatively unstable but remained reproducible. The K_2 value was found to be rather small, which may explain the instability of pβ_2 and why the data can also fit well to a one-to-one model. This data implies that the complex is able to bind two anions simultaneously, however the second anion is not bound stably and is removed in situ.

The stability constants calculated for [Ru(phen)$_2$(bbib)][PF$_6$]$_2$ with acetate fit well to a two anion to one cation model with a pK_1 of 3.33 and a pβ_2 of 5.37. There is slight variance from values calculated for the analogous bpy complex but overall, the binding is relatively weak for both complexes. Stability constants calculated for [Ru(phen)$_2$(bbib)][PF$_6$]$_2$ with $H_2PO_4^-$ gave a stable 2:1 model with pK_1 and Pβ_2 values of 5.30 and 8.36, respectively. The data fit the model well, however the values are high and unrealistic for an experiment run in a DMSO/D$_2$O solvent and do not replicate the data provided by [Ru(bpy)$_2$(bbib)][PF$_6$]$_2$. However, the compound does appear to be

binding phosphate albeit potentially in a 1:1 stoichiometric manner in aqueous conditions, assuming the value of pβ_2 is unstable, implying a similar stability of the second anion as with [Ru(bpy)$_2$(bbib)][PF$_6$]$_2$.

2.5 DNA Binding Studies

2.5.1 UV/Vis and Emission Titrations

UV/Vis absorbance and luminescence emission titration studies are both regularly used in the determination of DNA binding modes with ruthenium(II) complexes. Interactions between *ct*-DNA and a luminophore can alter the photophysical properties of the latter in several different ways, depending on the type of binding that is occurring.

Unfortunately *ct*-DNA and Ru(II) polypyridyls both have absorbance peaks between 200 and 300 nm. But changes in the metal to ligand charge transfer (MLCT) can be monitored as these typically occur at longer wavelengths where DNA does not absorb light and therefore comparisons can made between bound and unbound forms of complexes (Section 1.2). There are numerous examples of ruthenium(II) polypyridyls that display a "light-switch" effect upon the introduction to *ct*-DNA, where emission is enhanced from near zero emission to a high level upon change of excited state, usually with groove binding and intercalating agents. The hydrophobic interior of the DNA helix prevents non-radiative decay from the excited state of the metal complex via solvent dissipation resulting in a net increase in emission intensity.

The UV/Vis absorbance and luminescence emission spectra of $[Ru(bpy)_2(bbib)][PF_6]_2$ and $[Ru(phen)_2(bbib)][PF_6]_2$ (10 µM) were recorded in the absence and presence of *ct*-DNA. Concentration of DNA was increased in each sample relative to complex concentration, up to five equivalents of DNA in 90% tris buffer pH 7.2 and 10% DMF. Initial experiments were undertaken in tris buffer alone, however this resulted in precipitation of the complex-DNA adduct out of solution with $[Ru(bpy)_2(bbib)][PF_6]_2$ and $[Ru(phen)_2(bbib)][PF_6]_2$, suggestive of both complexes having a strong DNA binding. The addition of DMF to the solution resulted in no precipitation, but due to possibly hydrophobic (albeit potentially also just electrostatic) interaction between the DMF and the complexes, the results appear to be much weaker than the initial experiments run in tris buffer alone as any changes in emission that are observed are much smaller than in tris buffer.
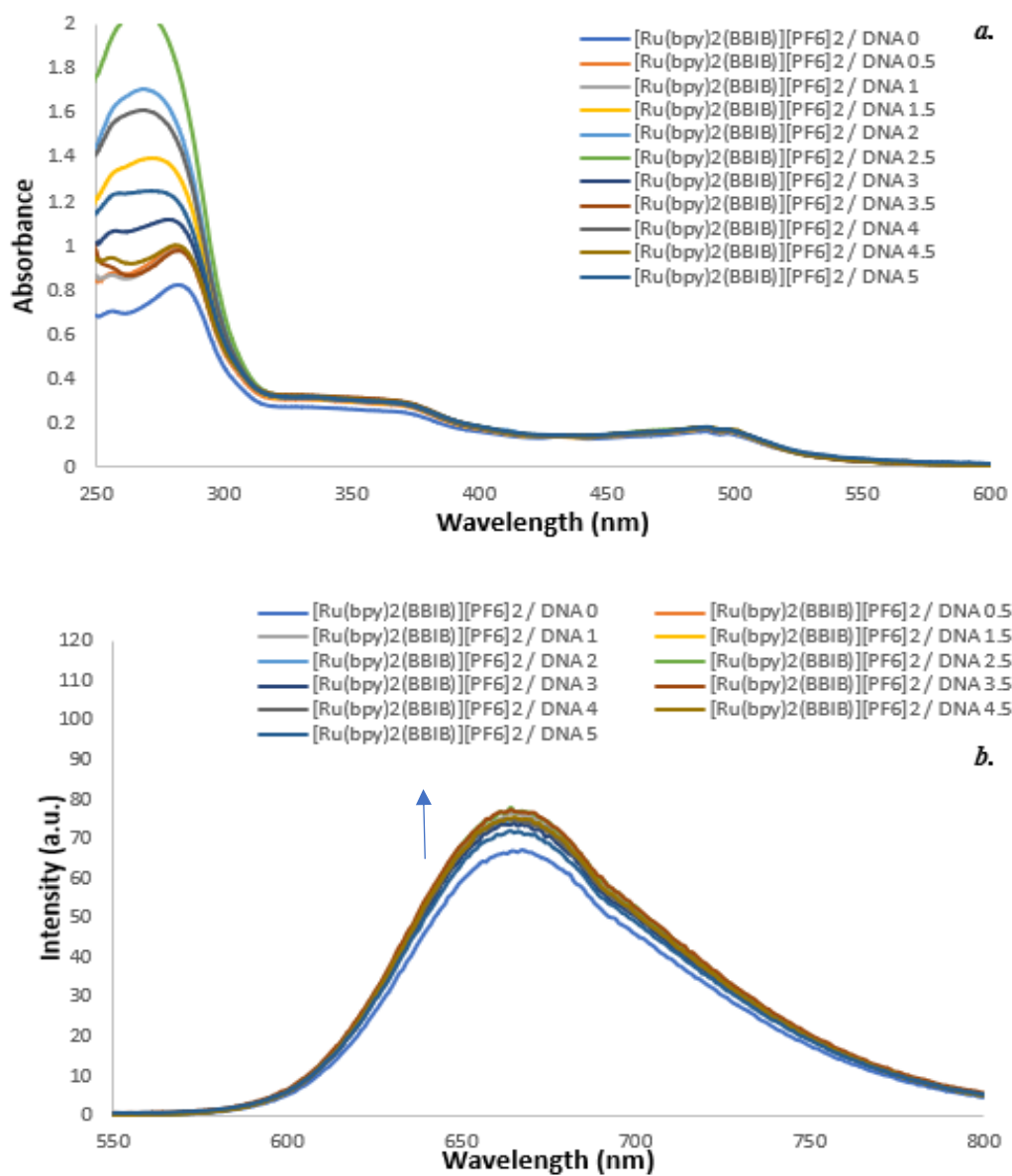
Figure 2.20 *– (a.) UV/Vis absorbance titration and (b) Luminesence emission titration of [Ru(bpy)$_2$(bbib)]2PF$_6$ (25 μM) in the absence and presence of ct-DNA in 9:1 tris buffer and DMF solution.*

In DMF/Tris buffer, the UV/Vis absorbance spectra of [Ru(bpy)$_2$(BBIB)][PF$_6$]$_2$ (Figure 2.20) shows minimal change upon introduction of 0.5 base pair equivalents of *ct*-DNA. This does not change as further amounts of nucleic acid are added. This does not indicate that there is no interaction occurring, but it also does not provide evidence for

interaction. The initial change upon addition of DNA could be caused by a change in the ion pairing of the ruthenium complex.

On initial introduction of 0.5 base pair equivalents of *ct*-DNA into the solution of [Ru(bpy)$_2$(bbib)][PF$_6$]$_2$ (Figure 2.20), a slight increase in emission intensity is observed, from 67 a.u. to 75 a.u.. The emission intensity is constant after 1 to 3.5 base pair equivalents of DNA, after which there is small amount of quenching (Figure 2.21). This decrease in emission is possibly caused by a secondary binding mode occurring. It is hypothesised that this second mode is caused by anion interactions between the phosphate backbone of the DNA strands and the complex. This data appears to relatively insignificant as little overall change occurs. Phosphate binding in aqueous conditions was established in Section 2.4, where the interaction was observed to cause a quenching of emission as it opens new non-emissive decay pathways. However, further UV/vis and emission titrations need to be undertaken between zero and one equivalent of DNA to establish whether there is a trend.
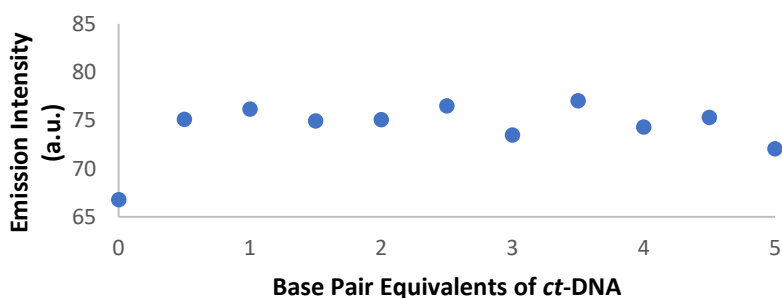
Figure 2.21 *– A plot of λ$_{max}$ for the emission spectra of [Ru(bpy)$_2$(bbib)][PF$_6$]$_2$ with increasing concentration of ct-DNA in 9:1 tris buffer pH 7.2 and DMF. [Ru] = 25 μM.*

UV/Vis and Emission Titrations of [Ru(phen)₂(bbib)][PF₆]₂ with ct-DNA
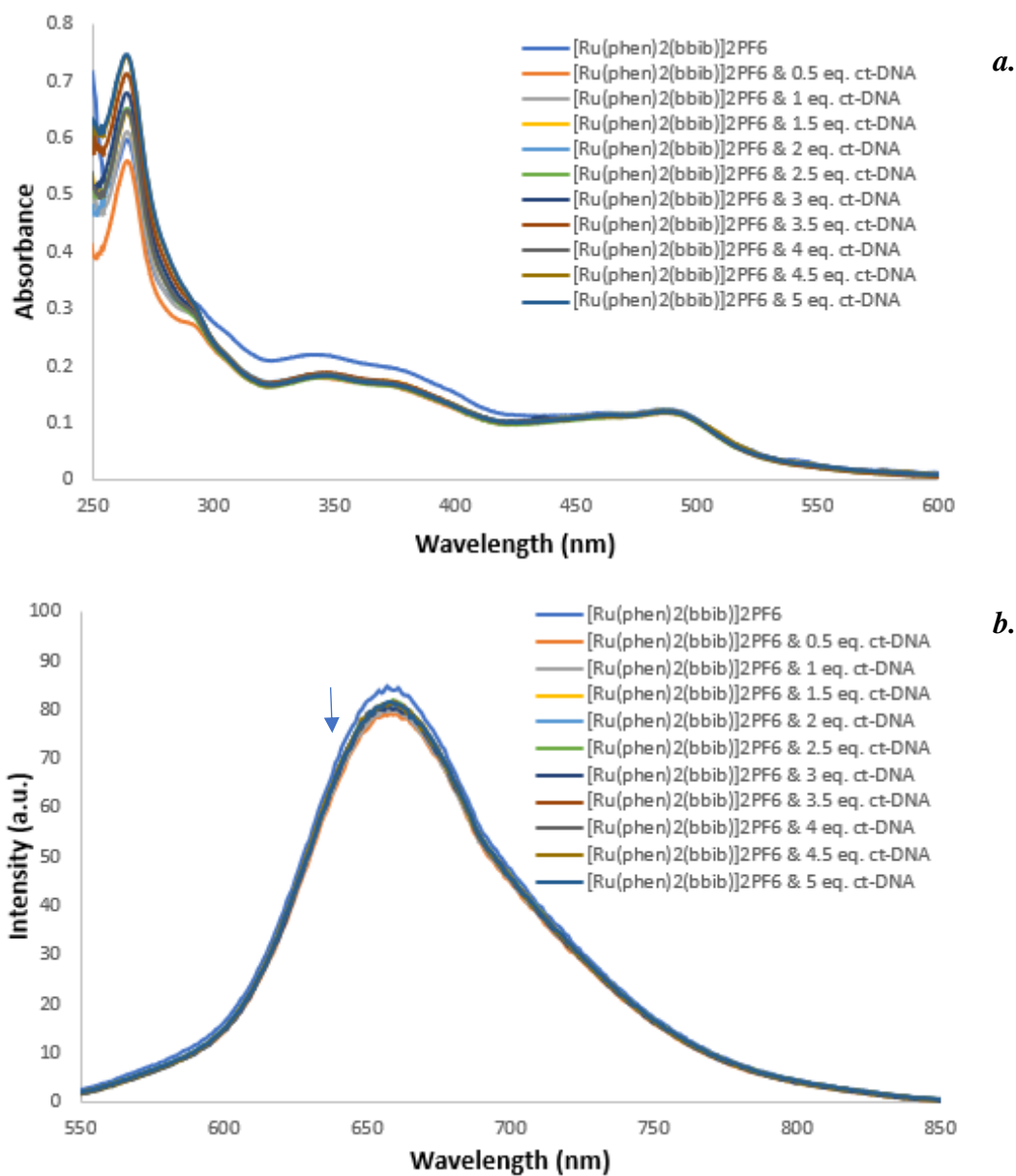
***Figure 2.22** – (a.) UV/Vis absorbance titration and (b) Luminesence emission titration of [Ru(phen)₂(bbib)]2PF₆ (25 µ M) in the absence and presence of ct-DNA in 3:1 tris buffer and DMF solution.*

The UV/Vis absorbance spectra for [Ru(phen)₂(bbib)][PF₆]₂ (Figure 2.22) displays a decrease in absorbance upon addition of 0.5 equivalents of *ct*-DNA, between 450 nm and 300 nm. This is possibly indicative of interaction occurring between the DNA and complex. The difference between the changes in spectra of [Ru((bpy)₂(bbib)][PF₆]₂ and

[Ru(phen)$_2$(bbib)][PF$_6$]$_2$ may be caused by the difference in solvent ratios as there was a much higher amount of DMF added into the samples containing [Ru(phen)$_2$(bbib)][PF$_6$]$_2$ than was added to the [Ru(bpy)$_2$(bbib)][PF$_6$]$_2$ samples. Changing the solvent ratios of a solution can potentially change the UV/Vis absorbance spectrum of a substance due to the change in environment surrounding it causing different stabilisations of the ground and excited state of the solute (solvatochromism).[23]

The emission spectra of [Ru(phen)$_2$(bbib)][PF$_6$]$_2$ (Figure 2.22) shows a small initial decrease in intensity from 84 a.u. to 78 a.u. (Figure 2.23) upon addition of 0.5 base pair equivalents *ct*-DNA. Increasing the DNA concentration further yields no significant change to the spectra. This is counter to the emission increase observed with [Ru(bpy)$_2$(bbib)][PF$_6$]$_2$, thought to be caused by the higher levels of DMF in the solvent causing further change in the solute ground and excited states.[24] There is no obvious change in λ_{max} observed. The data recorded does not indicate that there is interaction occurring in this solvent mixture.
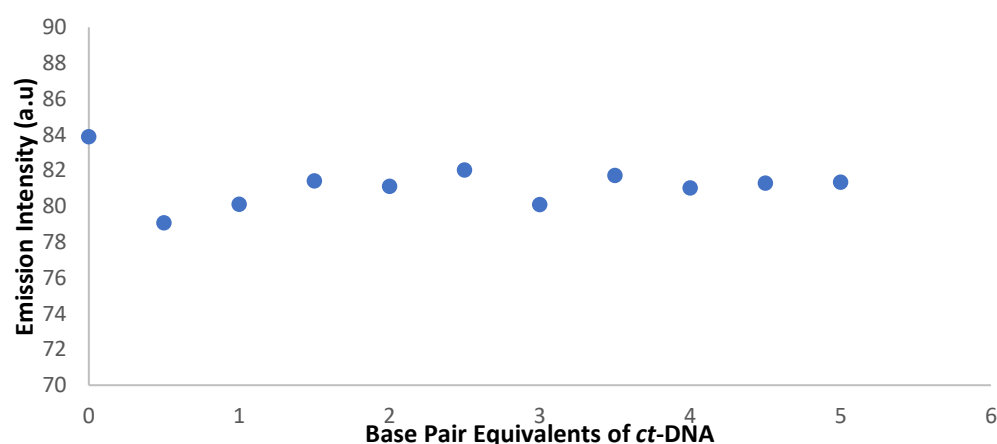
Figure 2.23 - *A plot of λ_{max} for the emission spectra of [Ru(phen)$_2$(bbib)][PF$_6$]$_2$ with increasing concentration of ct-DNA in 9:1 tris buffer pH 7.2 and DMF. [Ru] = 25 μM.*

It is important to recognise with the data gathered in this section that any change to emission with both [Ru(bpy)$_2$(bbib)][PF$_6$]$_2$ and [Ru(phen)$_2$(bbib)][PF$_6$]$_2$ occur with the first addition of 0.5 base pair equivalents of DNA, and then effectively remain at a near constant value. This could indicate that some form of interaction is taking place, however the difference could result from the change in the solution itself, i.e. the ionic strength. This means that it is difficult to make overall conclusions whether there are interactions occurring between complexes and DNA from this data, outside of the formation of precipitate in tris buffer.

2.5.2 Circular Dichroism Spectroscopy.

2.5.2.1 Circular Dichroism Titrations

The CD spectra of [Ru(bpy)$_2$(bbib)][PF$_6$]$_2$ and [Ru(phen)$_2$(bbib)][PF$_6$]$_2$ (25 µM) were taken in the absence and presence of *ct*-DNA up to 2 base pair equivalents. Each solution was made up using 9:1 tris buffer pH 7.2 and DMF and recorded between 300 and 600 nm.
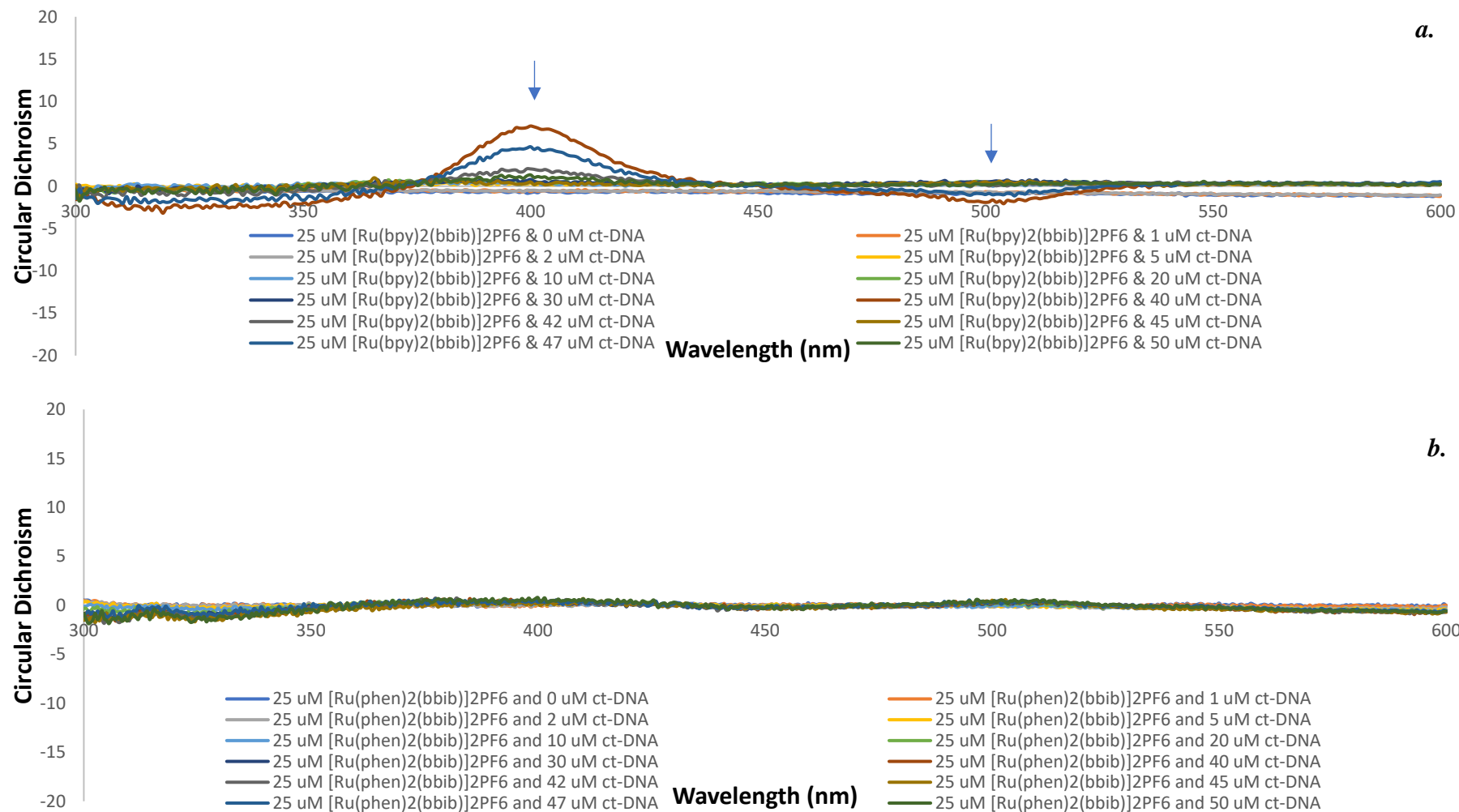
Figure 2.24 *– Circular dichroism spectra of (a.) [Ru(bpy)₂(bbib)][PF₆]₂ and (b.) [Ru(phen)₂(bbib)][PF₆]₂ in the presence and absence of ct-/DNA in 9:1 tris buffer and DMF.*
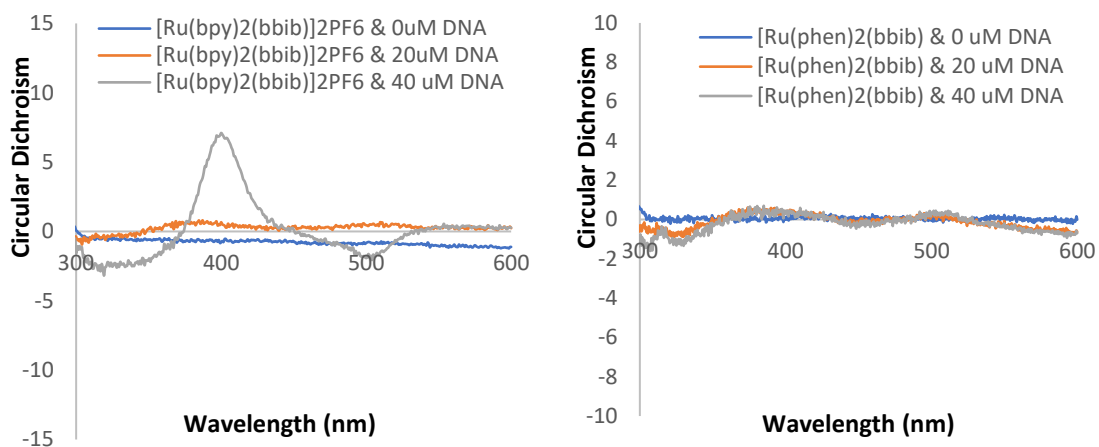
Figure 2.25 *– A comparison of the CD spectra of [Ru(bpy)₂(bbib)][PF₆]₂ and [Ru(phen)₂(bbib)][PF₆]₂ in the presence of 0 μM, 20 μM and 40 μM of ct-DNA in 9:1 tris buffer pH 7.2 and DMF. [Ru] = 25 μM.*

The spectra of racemic [Ru(bpy)₂(bbib)][PF₆]₂ (Figure 2.25) displays two sets of changes on addition of increasing DNA concentration. At a medium concentration (around one base pair equivalent of DNA to complex) small changes are observed in the CD spectra well above the DNA absorption wavelength. This suggests that the complex is adapting a non-racemic concentration or conformation in the presence of DNA. At higher concentrations of DNA, i.e. there is an excess, a second set of changes is observed. An increase of positive absorbance is seen at 400 nm, and a negative absorbance observed at around 500 nm. These differences in the signal are indicative of an enantioselective binding event, where it is possible that one enantiomer has electrostatically bound to the DNA so strongly that the ruthenium enantiomer has precipitated out of the solution, leaving behind the less favoured system. The spectra of [Ru(phen)₂(bbib)][PF₆]₂ (Figure 2.24) shows only one domain. Conformational changes are observed with medium and high concentrations of *ct*-DNA, however unlike [Ru(bpy)₂(bbib)][PF₆]₂, there are no observable enantioselective interactions occurring (Figure 2.25).

2.5.2.2 Thermal Denaturation Studies

The double helical structure of DNA is the dominant form found under physiological conditions, held together by hydrogen bonding between base pairs and π stacking of neighbouring bases. Enzymes called helicases have been evolved to separate the two helices (for DNA replication, etc.) or "unzip" them. This same result can also come about by heating the DNA, forcing the strands apart and denaturing the biopolymer.[24]

Thermal denaturation experiments involve the measurement of absorbance at a constant wavelength with increasing temperature (for DNA, measurements take place around 260 nm arising from $\pi - \pi^*$ base interactions, where a change in hydrogen bonding between base pairs would be observed by a change in absorbance, i.e,, the splitting of a duplex into two strands). The melting temperature (T_m) of the DNA is determined to be the temperature at which half of the double strands have become "unzipped" single strands.

Some ruthenium(II) polypyridyl complexes have been established to affect the T_m of *ct*-DNA.[25] Intercalating species are known to cause a large increase in T_m, resulting from the enhanced stability afforded to the double helix from the increased amount of π-stacking interactions. Groove binders display a smaller change in observed temperature and may cause a decrease, due to the lessening of structural stability by the complex sitting within the groove.

The melting profiles of *ct*-DNA (25 µM) were taken both with and without [Ru(bpy)$_2$(bbib)][PF$_6$]$_2$ and [Ru(phen)$_2$(bbib)][PF$_6$]$_2$ at 10 and 25 µM (Figure 2.26). The

solutions were made up using a 9:1 tris buffer (pH 7.2) and DMF mixture and the spectra were recorded between 20 and 90 °C at 2 °C intervals.

Table 2.4 - *Observed Tm values for ct-DNA.*

Experiment	Melting Temperature (°C)	Error (°C)	ΔT_m (°C)
Calf thymus DNA	79	± 0.6	N/A
$[Ru(bpy)_2(bbib)][PF_6]_2$	75	± 0.4	-4
$[Ru(phen)_2(bbib)][PF_6]_2$	75	± 0.5	-4
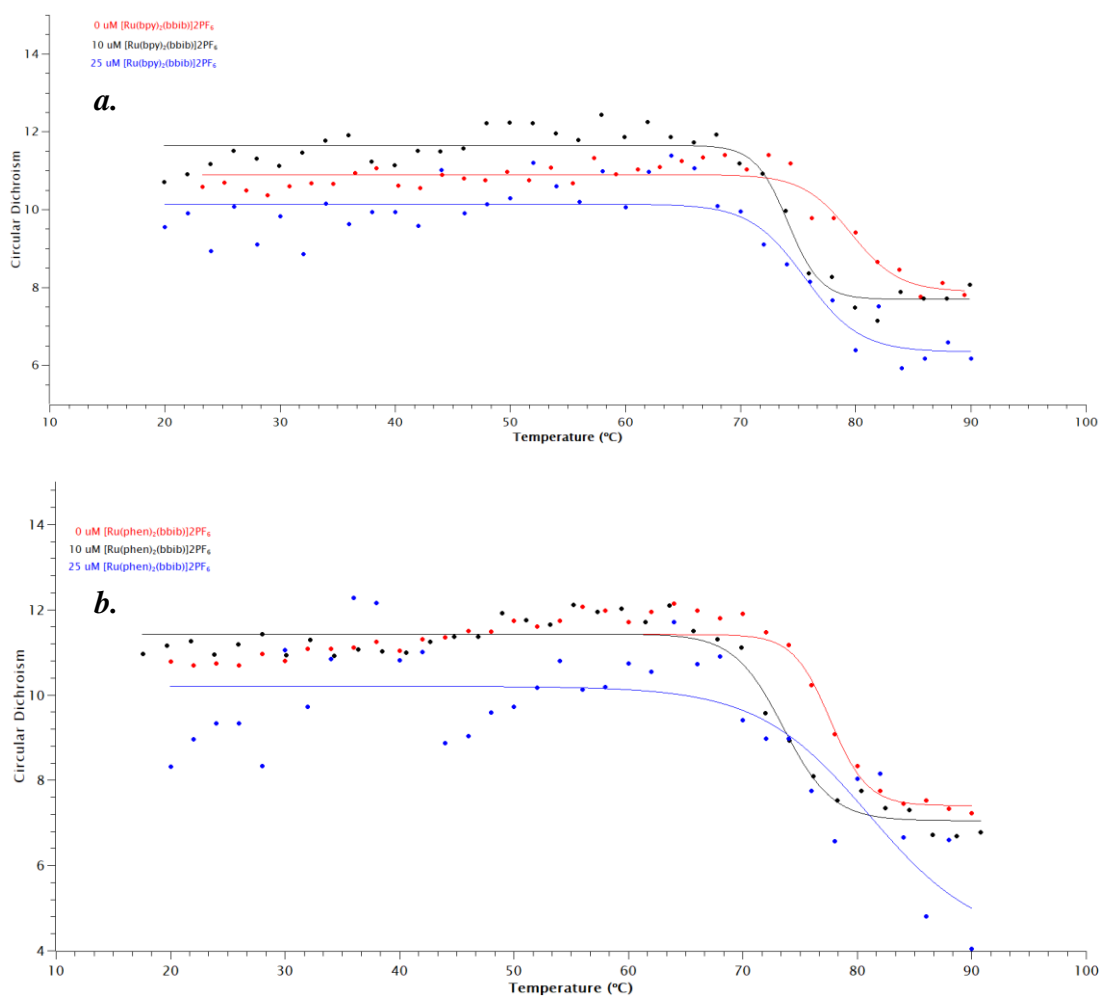
Figure 2.26 – *"Melting curves" of ct-DNA (25 µM) with (a.) $[Ru(bpy)_2(bbib)][PF_6]_2$ and (b.) $[Ru(phen)_2(bbib)][PF_6]_2$ obtained using QTIplot data fitting software.*

The control experiment of *ct*-DNA (25 µM) alone gave a melting temperature of 79 °C. Both [Ru(bpy)$_2$(bbib)][PF$_6$]$_2$ and [Ru(phen)$_2$(bbib)][PF$_6$]$_2$ yielded T$_m$s of 75 °C, resulting in a ΔT$_m$ of -4 °C. This implies that there is interaction between these complexes and *ct*-DNA, destabilising the integrity of the double-stranded structure and causing the net decrease in denaturation temperature. It implies that intercalation is not the binding mode for these complexes. The similarities between both complexes suggests that the ancillary ligands are not the important factor in the binding with DNA, with the functionalised bbib ligands being the main section that interacts. Unfortunately, it is unknown whether there is a difference in DNA interaction between enantiomers as chiral separation was not able to be completed on these compounds. However, the significant change in T$_m$ for both complexes implies that there is an interaction regardless of enantiomeric preference.

2.5.3 Dialysis Equilibrium Studies

There is the potential for one enantiomer of ruthenium polypyridyl complexes to interact with DNA more easily than its counterpart, helped by a complimentary conformation to the double helix. With intercalating ruthenium(II) polypyridyls, the Δ-enantiomer is usually preferred due to the right-handed structure of the DNA double helix.[26]

Dialysis experiments are used in this instance to determine whether there is preferential DNA interaction between enantiomers. Over time, the complex can pass through the porous tubing to interact with the DNA, which cannot pass through the tubing. The CD spectrum of the dialysate can then be recorded to find out whether there is a change in

enantiomeric ratio. Detecting one enantiomer over the other implies that other enantiomer cannot diffuse back across the membrane, as it has bound to the DNA.
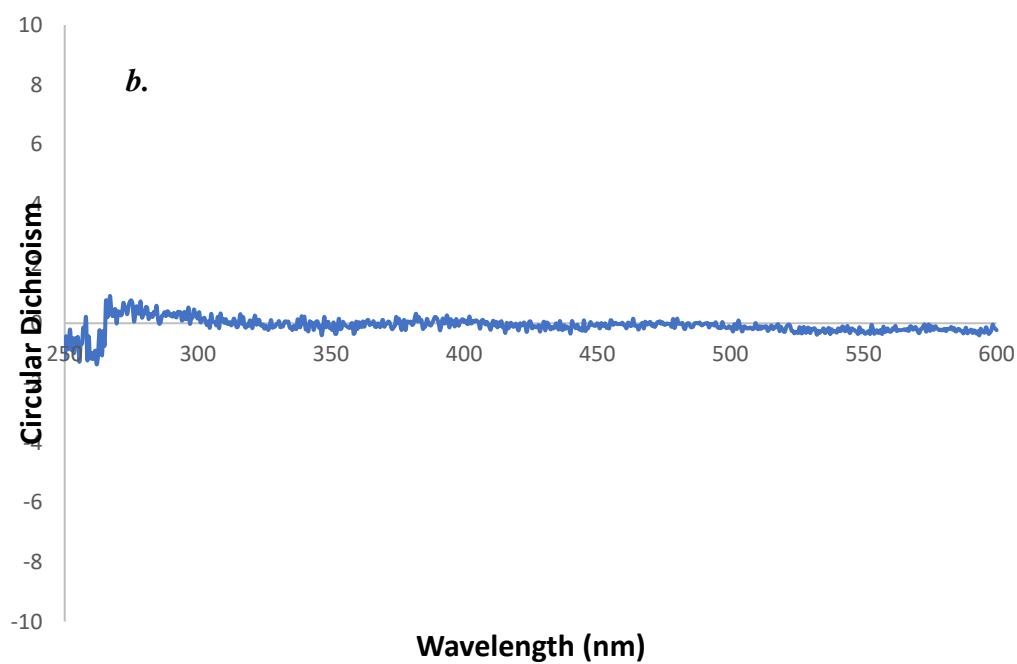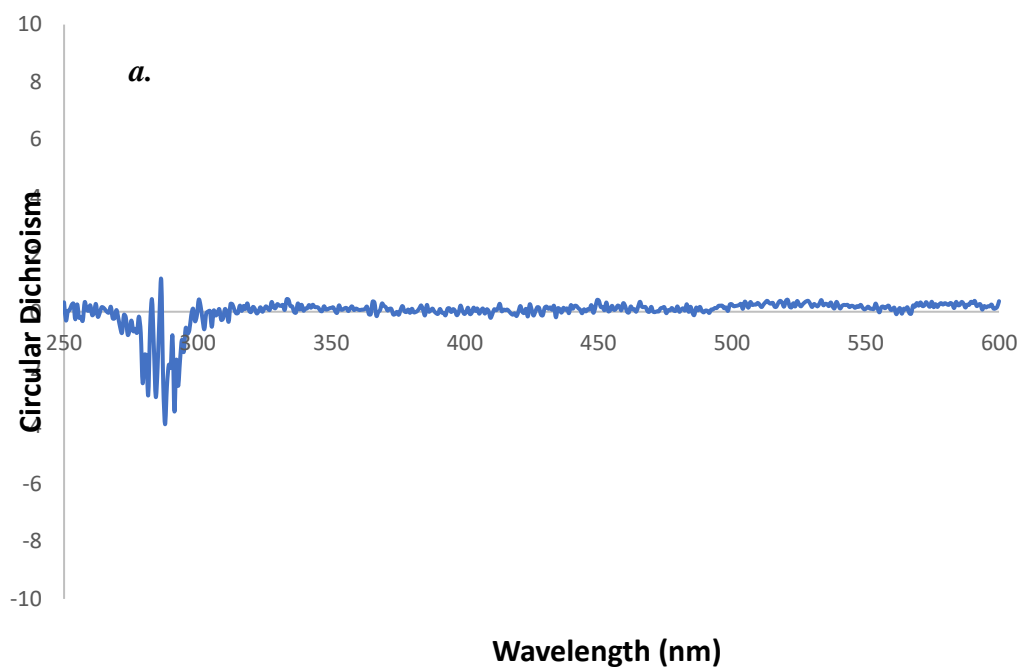
Figure 2.27 – *Circular Dichroism spectra of ct-DNA (25 μM) with (a.) [Ru(bpy)$_2$(bbib)][PF$_6$]$_2$ (60 μM) and (b.) [Ru(phen)$_2$(bbib)][PF$_6$]$_2$ (60 μM).*

[Ru(bpy)$_2$(bbib)][PF$_6$]$_2$ and [Ru(phen)$_2$(bbib)][PF$_6$]$_2$ (60 μM) were investigated to establish whether there is any enantiomeric preference for interaction with DNA (25 μM). The dialysis tubing was steeped in solutions of [Ru(bpy)$_2$(bbib)][PF$_6$]$_2$ and [Ru(phen)$_2$(bbib)][PF$_6$]$_2$ for 24 hours and the CD spectra of the dialysates were recorded (Figure 2.26). It was evident that the complexes had passed through the dialysis tubing as the colour of the DNA solution inside the tube had changed from colourless to pale orange. Analysis of the dialysate provided no information regarding enantiomeric preference in DNA interaction for either complex. CD spectra of the DNA samples from inside the tubing showed no change in the signal, although it was noted that the DNA had precipitated in the presence of both complexes.

2.5.4 Viscosity Studies

Measuring the viscosity of DNA in a buffer solution is method of determining change within the helical structure.[27] When used alongside spectroscopic data, measuring viscosity can indicate the binding mode of a complex with less ambiguity in most cases, aside from crystallographic evidence. The different modes of binding (groove binding, intercalation, etc.) affect the hydrodynamic properties of DNA, by potentially changing the structure. Classical intercalation results in an increase in viscosity, due to insertion of a ligand between the bases, increasing π-stacking therefore stiffening and lengthening the duplex.[28] However, non-classical intercalation results in the opposite effect, decreasing observed viscosity, an effect from bends or "kinks" being introduced into the DNA structure, thus shortening it.[26] Groove binding agents show little to no effect on the viscosity, having a similar but more subtle effect as non-classical intercalation. Common compounds used as a comparison tool for effects on viscosity are ethidium bromide (EtBr) for intercalation and various Hoechst stains for groove binding.[28]
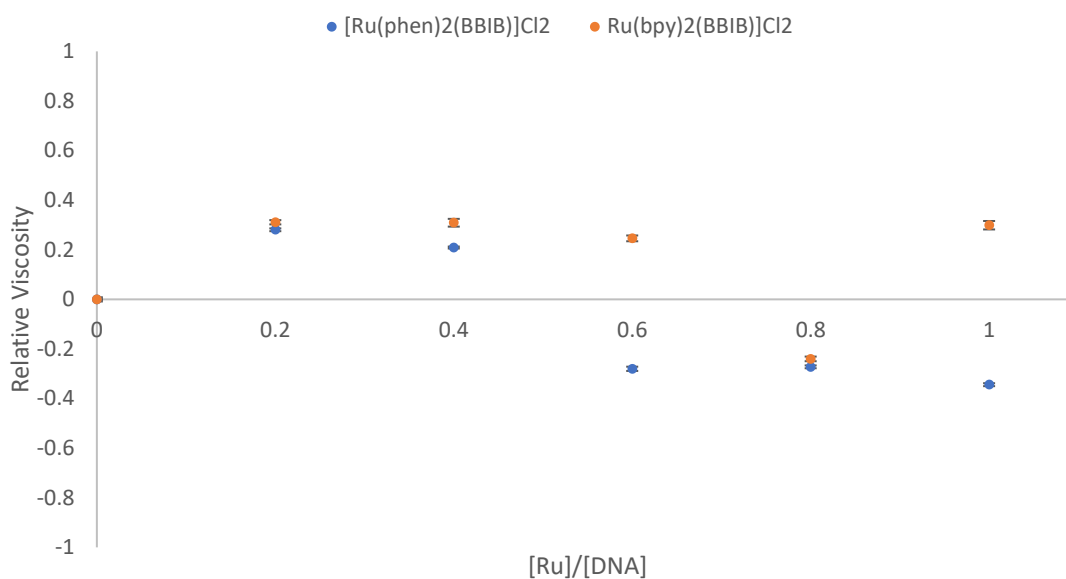
Figure 2.28 – *The observed relative viscosity measurements for [Ru(bpy)$_2$(BBIB)]Cl$_2$ and [Ru(phen)$_2$(BBIB)]Cl$_2$ in tris buffer. [DNA] = 25 μM BP^{-1}.*

The relative viscosities of sonicated *ct*-DNA solutions (25 µM bp^{-1}) were measured without and with the presence of [Ru(bpy)$_2$(bbib)]Cl$_2$ and [Ru(phen)$_2$(bbib)]Cl$_2$ between 5 and 25 µM and made up in tris buffer (5 mM Tris-HCl, 50 mM NaCl, 7.2 pH). An Ubbelohde type kinematic viscometer was used to measure relative flow times at a constant temperature of 30 °C, and each measurement was taken in triplicate with an average taken.

The plot of sample relative viscosities shows no significant change when either [Ru(bpy)$_2$(BBIB)]Cl$_2$ or [Ru(phen)$_2$(BBIB)]Cl$_2$ are introduced (Figure 2.28). This is indicative there is no classical intercalation occurring between the complexes and DNA. This concurs with the results obtained from thermal denaturation studies above (Section

2.5.3). It is not indicative of whether the majority of the binding is groove binding or phosphate binding. As phosphate binding is thought to have not been previously established, there are no results to which ours can be compared. However, it is assumed that an electrostatic interaction should not show any evidence of DNA structural change.

There is a spread of results observed and this could be due to an issue that has arisen within many of the experiments involving DNA:precipitate. Throughout this study, when the complexes have been added to the DNA in aqueous solution (tris buffer), solid particulates precipitate out of solution, assumed to be the complex-bound DNA. This presents two problems in the experiment, that of the solid clogging up the viscometer, which result in a smaller hole for the solutions to flow through thus theoretically increasing the flow time, and the removal of DNA from the solution itself. Lowering the DNA concentration through this means would decrease the viscosity of the solution, and therefore would show a decrease in flow time. In conclusion, these viscosity measurements did not provide any useful indication for the complexes' mode of DNA binding, although the data does suggest that it is not intercalation.

2.6 Conclusion

The successful synthesis of two novel ruthenium(II) complexes with the ability to bind to dihydrogen phosphate and possibly DNA has been accomplished in $[Ru(bpy)_2(bbib)][PF_6]_2$ and $[Ru(phen)_2(bbib)][PF_6]_2$. Initial results indicated that very strong interactions were occurring between these complexes and both $H_2PO_4^-$ and perhaps DNA, but the adducts formed readily precipitate out of aqueous solution, unlike the previously reported complexes $[Ru(bpy)_2(bbob)]^{2+}$ and $[Ru(bpy)_2(bbtb)]^{2+}$.[1,2] Both

complexes were found to have greater emission intensities than $[Ru(bpy)_3][PF_6]_2$. The degree of hydrogen bonding formed by the addition of another proton on the heterocyclic-functionalised ligands appears to have increased, based on higher levels of interaction occurring between complex and DNA/ligand and has potentially opened the pathway to a novel form of DNA interaction where the complex recognises the anionic phosphate backbone, although further studies are required to confirm this.

The data obtained for $[Ru(bpy)_2(bbib)][PF_6]_2$ and $[Ru(phen)_2(bbib)][PF_6]_2$ indicate that they do not intercalate between the base pairs of the strands as there was minimal change to the viscosity of *ct*-DNA. The data suggests that the complexes most likely undergo two forms of competing interactions with DNA, firstly a groove binding interaction into their preferred groove, until the groove is full where the complexes could switch to anion recognition of the phosphate backbone. These complexes have great potential as anion interacting agents as they show visual results when bound to phosphate and acetate ions (i.e. precipitation). Further exploration into the behaviour of the two complexes in the presence of anions in aqueous environments is required. There are currently very few reported complexes that are able to bind to phosphate in water, and this aspect of the results is promising.

2.7 References

1   P. A. Elliott, Bipyridyl Complexes of Ruthenium(II) to Target Nucleic Acid Structures, Queen's University Belfast, 2012.
2   C. B. Spillane, Synthesis of Ruthenium(II) Complexes as Potential Photoactive Minor Groove Binders, Queen's University Belfast, 2005.
3   M. Singh and V. Tandon, *Eur. J. Med. Chem.*, 2011, **46**, 659–669.
4   R. Mocharla, H. Mocharla and M. E. Hodes, *Nucleic Acids Res.*, 1987, **15**, 10589.
5   P. E. Pjura, K. Grzeskowiak and R. E. Dickerson, *J. Mol. Biol.*, 1987, **197**, 257–271.
6   S. C. Yu, X. Gong and W. K. Chan, *Macromolecules*, 1998, **31**, 5639.
7   H. F. M. Nelissen, M. C. Feiters and R. J. M. Nolte, *J. Org. Chem.*, 2002, **67**, 5901–5906.
8   C. Fu, M. Wenzel, E. Treutlein, K. Harms and E. Meggers, *Inorg. Chem.*, 2012, **51**, 10004–10011.
9   X. Hua and A. von Zelewsky, Inorg. Chem, 1995, **34**, 5791 - 5797.
10   C. B. Spillane, M. N. V Dabo, N. C. Fletcher, J. L. Morgan, F. R. Keene, I. Haq and N. J. Buurma, *J. Inorg. Biochem.*, 2008, **102**, 673–683.
11   K. Suzuki, A. Kobayashi, S. Kaneko, K. Takehira, T. Yoshihara, H. Ishida, Y. Shiina, S. Oishi and S. Tobita, *Phys. Chem. Chem. Phys.*, 2009, **11**, 9850.
12   M. H. W. Lam, D. Y. K. Lee, K. W. Man and C. S. W. Lau, *J. Mater. Chem.*, 2000, **10**, 1825.
13   M. Haga, T. Takasugi, A. Tomie, M. Ishizuya, T. Yamada, M. D. Hossain and M. Inoue, *Dalt. Trans.*, 2003, 2069.
14   F. Liu, K. Wang, G. Bai, Y. Zhang and L. Gao, *Inorg. Chem.*, 2004, **43**, 1799.
15   M. J. Han, L. H. Gao, Y. Y. Liu and K. Z. Wang, *J. Phys. Chem. B*, 2006, **110**, 2364.
16   F. Gao, H. Chao, F. Zhou, B. Peng and L.-Z. Ji, *Inorg. Chem. Commun.*, 2007, **10**, 170.
17   M. Pucéat, *Cell. Mol. Life Sci.*, 1999, **55**, 1216.
18   D. Lagadic-Gossmann, L. Huc and V. Lecureur, *Cell Death Differ.*, 2004, **11**, 953–961.
19   H. Behera and N. Madhavan, *J. Am. Chem. Soc.*, 2017, **139**, 12919–12922.
20   X. H. Yu, X. Q. Hong, Q. C. Mao and W. H. Chen, *Eur. J. Med. Chem.*, 2019, **184**, 111782.
21   M. J. Hynes., *J. Chem. Soc. Dalton. Trans.,* 1993, 311.
22   C. Hubler, *Chem. - Methods*, 2022, **2**, 1–20.
23   B. Schmidtgall, A. Kuepper, M. Meng, T. N. Grossmann and C. Ducho, *Chem. - A Eur. J.*, 2018, **24**, 1544–1553.
24   T. Y. Chao and R. T. Raines, *Biochemistry*, 2011, **50**, 8374–8382.
25   F. Naderi and A. Farajtabar, J. Mol. Liq., 2016, 221, 102–107.
26   A. Marchand, F. Rosu, R. Zenobi and V. Gabelica, *J. Am. Chem. Soc.*, 2018, **140**, 12553–12565.
27   L. Perdisatt, S. Moqadasi, L. O'Neill, G. Hessman, A. Ghion, M. Q. M. Warraich, A. Casey and C. O'Connor, *J. Inorg. Biochem.*, 2018, **182**, 71–82.
28   J. K. Barton, A. T. Danishefsky and J. M. Goldberg, *J. Am. Chem. Soc.,* 1984, **106**, 2172 - 2176.
29   Y. Xiong, X. He, X. Zou, J. Wu, X. Chen, L. Ji, R. Li, J. Zhou and K. Yu, *Dalton*, 1999, 19–23.

30   L. S. Lerman, *J. Mol. Biol.*, 1961, **3**, 18 - 30.
31   Y. Kafri, D. Mukamel and L. Peliti, *Phys. Rev. Lett.*, 2000, **85**, 4988.
32   J. K. Barton and S. J. Lippard, *Biochemistry*, 1979, **18**, 2661 - 2668.

Chapter Three

Chapter Three: Synthesis and Binding Studies of Benzimidazole Functionalised Ruthenium(II) Polypyridyl Complexes with Amide Linkages

3.1 Introduction

Many known nucleic acid binders contain amide linkage moieties which are directly involved in the DNA/RNA interactions, such as lexitropsins (polyamide antibiotics with antiviral activities), as discussed in Chapter one.[1]

y' = CH, N
z' = CH, N
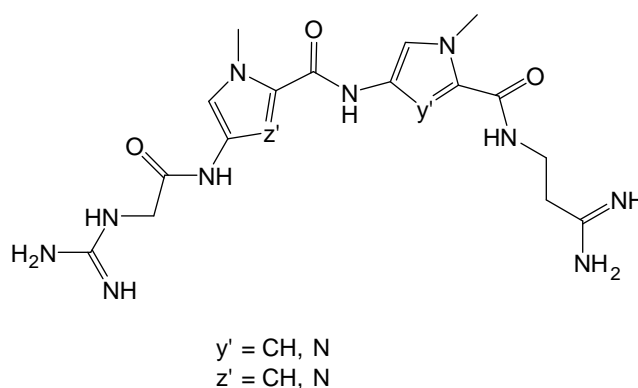
Figure 3.1 – Lexitropsin general structure

The inclusion of amide groups into a functionalised ligand has the potential of increasing the strength of DNA and anion binding interactions by including more hydrogen donors, giving more opportunities for hydrogen bonds to form between anionic groups and the complex. The results from Chapter two, and the previous work of the Fletcher group on benzoxazoles and benzothiazoles, have demonstrated that the introduction of further nitrogen atoms into a functionalised conjugated system

dramatically increases the strength of coordination between the complex and the target.[2,3] Importantly, incorporating amide groups will not disrupt the extended conjugation of the ligand and the complex overall, an essential component in the ability of a molecule to minor groove bind.[4] Thus, two amide-linked benzimidazole-containing ruthenium(II) complexes have been synthesised and investigated for their affinities toward DNA and anionic species with the aim to improve on the results gathered from Chapter two without modifying the benzimidazole rings themselves.
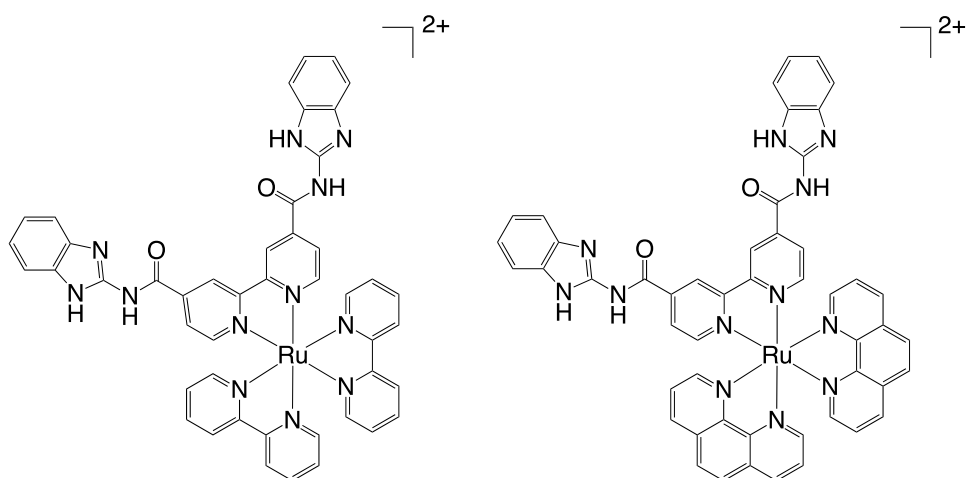
Figure 3.2 - *Target Complexes*

3.2 Synthesis and Characterisation of Benzimidazole Functionalised Ruthenium(II) Polypyridyl Complexes with Amide Linkages

3.2.1 General Synthesis of Ligands and Complexes

3.2.1.1 Synthesis of 4,4'-bis(amidobenzimidazol-2-yl)-2,2'-bipyridine (bbaib)

4,4'-dicarboxylic acid-2,2'-biyridine was converted to the acid chloride derivative by refluxing it with thionyl chloride for 24 hours in a nitrogen atmosphere. Distillation was used to remove the thionyl chloride and the remaining solid was refluxed in dry toluene

with 2-aminobenzimidazole and triethylamine for 48 hours. Once cooled, the resulting precipitate was collected via filtration as a yellow solid and washed with water. bbaib was characterised using mass spectrometry which gave (m/z) 497.15 [M + Na]⁺ and IR spectroscopy, showing a C=O stretch at 1680 cm⁻¹ and a N-H stretch at 3000 cm⁻¹ (Appx. 51).

3.2.1.2 ^{1}H-NMR Characterisation of bbaib

The ^{1}H-NMR spectrum of bbaib was recorded in DMSO-D$_6$. Despite the solubility issues of the ligand, sufficient dissolved. Previous characterisation was reported in CDCl$_3$ with trifluoroacetic acid to protonate the ligand. The ^{1}H-NMR spectrum for bbaib (Figure 3.3) is similar those recorded in Chapter Two. The significant difference is the presence of a peak at 12.65 ppm in the bbaib spectrum and is attributed to the amide NH.
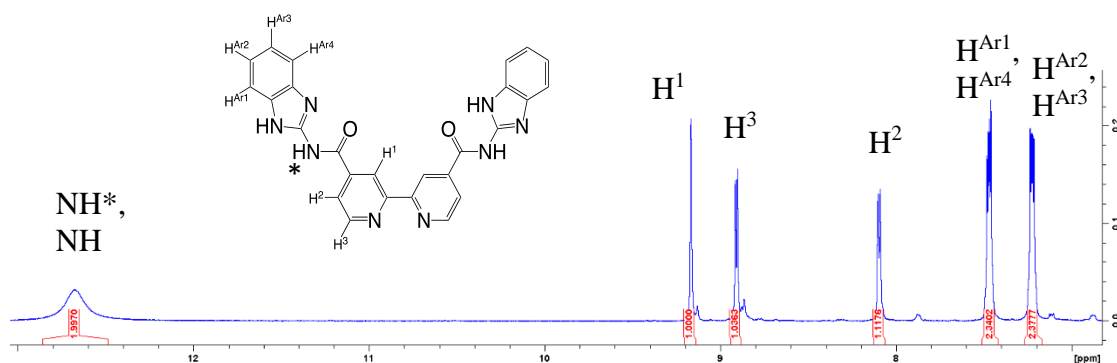
Figure 3.3 - ^{1}H-NMR assignment of BBAIB in DMSO-D$_6$, 400 MHz, 25 °C

3.2.1.3 Synthesis of [Ru(bpy)$_2$(bbaib)]$^{2+}$ and [Ru(phen)$_2$(bbaib)]$^{2+}$

[Ru(bpy)$_2$(bbaib)][PF$_6$]$_2$ was synthesised using 4,4'-bis(amidobenzimidazol-2-yl)-2,2'-bipyridine by heating to 180 °C with [Ru(bpy)$_2$Cl$_2$].2H$_2$O and triflic acid in ethylene glycol in an inert atmosphere for 4 hours, forming a dark red solution. Once cooled, aqueous potassium hexafluorophosphate was added and a dark orange salt precipitated

from the solution, which was isolated by filtration. Impurities were removed via size exclusion chromatography using Sephadex LH20 with a 1 : 1 acetone/methanol eluant. [Ru(phen)$_2$Cl$_2$].2H$_2$O was used to synthesise [Ru(phen)$_2$(BBAIB)][PF$_6$]$_2$ following the same procedure. Both [Ru(bpy)$_2$(bbaib)][PF$_6$]$_2$ and [Ru(phen)$_2$(bbaib)][PF$_6$]$_2$ were characterised by mass spectrometry which gave (m/z) 444.10 [M]$^{2+}$ and (m/z) 468.10 [M]$^{2+}$ respectively. IR spectra for both complexes showed a C=O stretch at 1680 cm^{-1} and a N-H stretch at 3000 cm^{-1} (Appx. 52 and 53).

3.2.1.4 ^{1}H-NMR   Characterisation   of   [Ru(bpy)$_2$(bbaib)][PF$_6$]$_2$ and [Ru(phen)$_2$(bbaib)][PF$_6$]$_2$

^{1}H-NMR spectra of the complexes were carried out in acetone-D$_6$. There are differences between the spectra of [Ru(bpy)$_2$(bbaib)][PF$_6$]$_2$ and [Ru(phen)$_2$(bbaib)][PF$_6$]$_2$ and their bbib analogues. There is a doublet peak present at 8.70 ppm for [Ru(bpy)$_2$(bbaib)][PF$_6$]$_2$ and 8.65 ppm for [Ru(phen)$_2$(bbaib)][PF$_6$]$_2$, representative of the amide proton on the functionalised ligand. The peaks representing the H^6 proton on the functionalised bypyridine is relatively shifted downfield in both bbaib complexes in comparison with with the bbib analogues. This is most likely due to the proximity of the hydrogen atom to the amide group, resulting in a deshielding effect. The doublet of doublets attributed to H^4 and H$^{4'}$ protons of the ancillary ligands appear to have shifted upfield into a similar environment to the H^5 and H$^{5'}$ protons. This is possibly due to the amide acting as an electron donating group. There are several impurities observed within the ^{1}H-NMR spectra for [Ru(bpy)$_2$(bbaib)][PF$_6$]$_2$ and [Ru(phen)$_2$(bbaib)][PF$_6$]$_2$ despite multiple purification attempts via Sephadex LH20. This is potentially caused by impurities passing through the Sephadex at a similar rate as the major product and in the interest of time, it was decided to carry through experiments with the level of purity obtained.
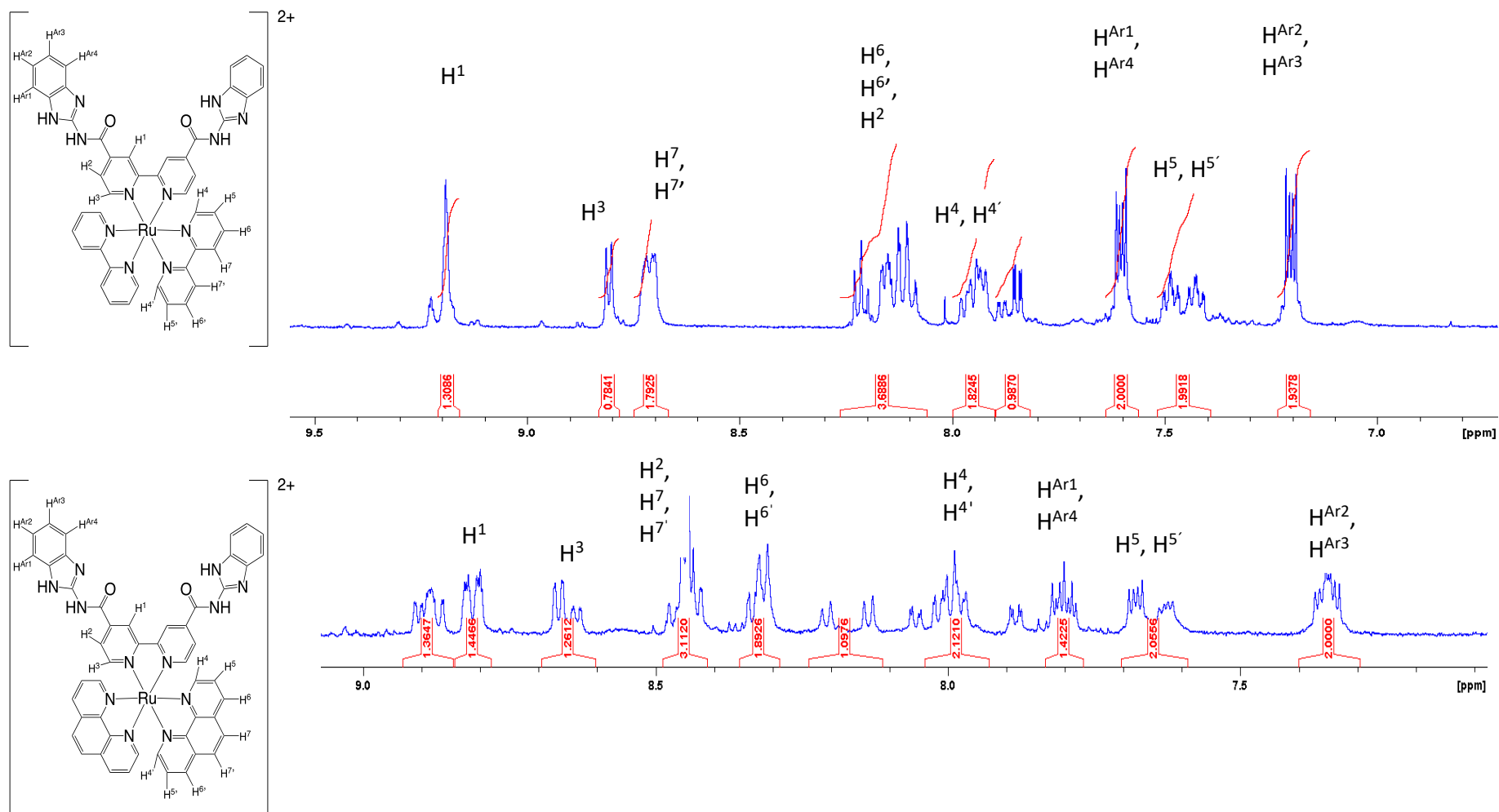
Figure 3.4 - *¹H-NMR Assignment of [Ru(bpy)₂(BBAIB)][PF₆]₂ and [Ru(phen)₂(BBAIB)][PF₆]₂ in Acetone-D6, 400 MHz, 25 °C*
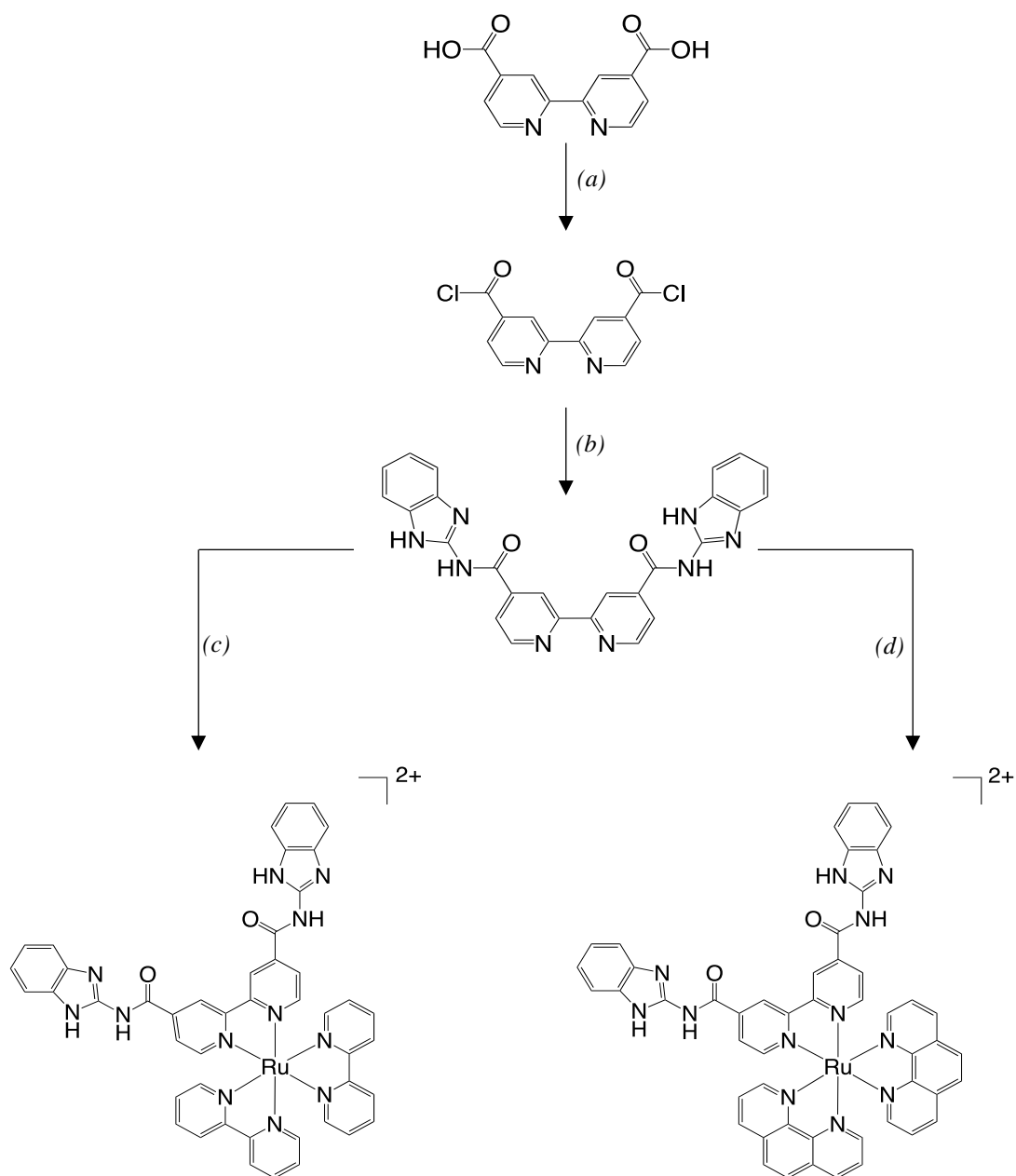
Scheme 3.1 - *Reaction scheme of the general synthesis of ligand and complexes. (a) SOCl₂, reflux; (b) Et₃N, 2-aminobenzimidazole, toluene (dry), reflux; (c) [Ru(bpy)2Cl₂], triflic acid, ethylene gycol, 140 °C; (d) [Ru(phen)₂Cl₂], triflic acid, ethylene glycol, 140 °C.*

3.2.3 Photophysical Properties of [Ru(bpy)$_2$(bbaib)]$^{2+}$ and [Ru(phen)$_2$(bbaib)]$^{2+}$

The absorbance spectrum of [Ru(bpy)$_2$(bbaib)][PF$_6$]$_2$ (Figure 3.5) is made up of four defined peaks between 200 – 600 nm. Bands are observed at 354 and 279 nm are representative of LC excitations, thought to be caused by ancillary $\pi_{bpy} > \pi_{bpy}*$ transitions and bbaib $\pi \rightarrow \pi*$ transitions respectively. The band at 279 nm is approximately twice the intensity of 354 nm, similar to that observed in the spectra of [Ru(bpy)$_2$(bbib)][PF$_6$]$_2$ and [Ru(phen)$_2$(bbib)][PF$_6$]$_2$ and is assigned to an aromatic ligand transition. The bands seen at 231 nm and 491 nm are assigned as MLCT d $\rightarrow \pi*$ transitions. An additional peak is observed at 300 nm that was not present in the spectrum of the bbib complexes and could possibly be attributed to an amide N $- \pi*$ transition. The absorbance spectrum of [Ru(phen)$_2$(bbaib)][PF$_6$]$_2$ (Figure 3.5) has a fifth peak at 265 nm caused by the LC excited state of the ancillary $\pi_{phen} > \pi_{phen}*$ transition.
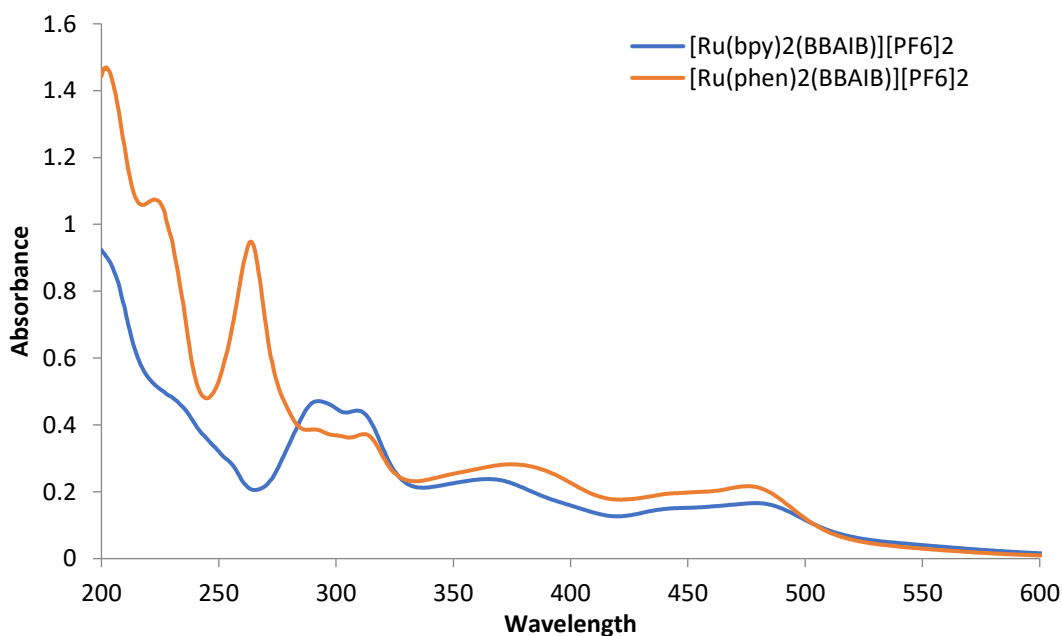
***Figure 3.5** - UV/Vis absorbance spectrum of [Ru(bpy)$_2$(BBAIB)][PF$_6$]$_2$ (blue) and[Ru(phen)$_2$(BBAIB)][PF$_6$]$_2$ (orange) measured in acetonitrile at 25 °C.*

The emission spectra of [Ru(bpy)(bbaib)][PF$_6$]$_2$ and [Ru(phen)$_2$(bbaib)][PF$_6$]$_2$ (Figure 3.6) were recorded from 500 to 900 nm at 25 °C and excited at 450 nm. A strong emission was observed as a result, at 654 nm and 644 nm for the bipyridine and phenanthroline complexes respectively. [Ru(bpy)$_3$]$^{2+}$ was used as the standard luminophore (ϕ = 0.04)[7]. The relative quantum yields of [Ru(bpy)(bbaib)][PF$_6$]$_2$ and [Ru(phen)$_2$(bbaib)][PF$_6$]$_2$ were calculated as ϕ = 0.039 and 0.05 respectively. Both complexes have similar quantum yield values to the literature standard.[7]
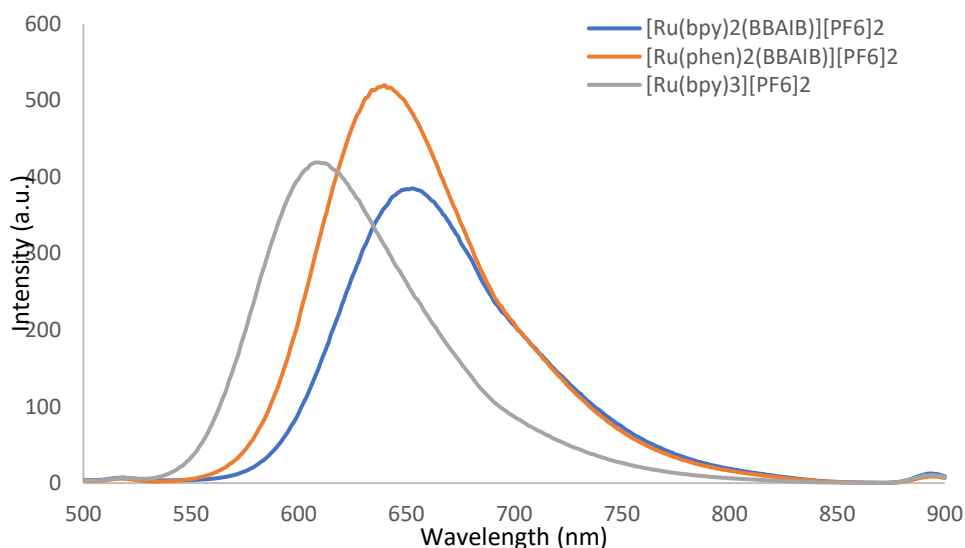
Figure 3.6 - *Emission spectra of [Ru(bpy)$_2$(bbaib)][PF$_6$]$_2$ (blue), [Ru(phen)$_2$(bbaib)][PF$_6$]$_2$ (orange) and [Ru(bpy)$_3$][PF$_6$]$_2$ (grey) excited at 450 nm at 25°C in acetonitrile.*

Table 3.1 - *The photophysical properties of [Ru(bpy)₂(BBAIB)]²⁺ and of [Ru(phen)₂(BBAIB)]²⁺*

	Absorption λ_{max} $\pm$ 1 nm	ε x10⁻³ $(mol^{-1}cm^{-1})$	Emission λ_{max} $\pm$ 1 n	Quantum Yield $(\phi_{em})^*$
[Ru(bpy)₂(BBAIB)]²⁺	292	4714	654	0.039
	311	2275		
	367	4428		
	480	1660		
[Ru(phen)₂(BBAIB)]²⁺	231	9443	638	0.050
	265	10713		
	290	3865		
	374	2825		
	476	2169		

*The spectra of the complexes were recorded as their hexafluorophosphate salts in acetonitrile at 298 K. The quantum yield of each complex was calculated relative to [Ru(bpy)₃](PF₆)₂ as a standard in acetonitrile (0.04).[7] λ_{ex} = 450 nm when absorption = 0.1 at 450 nm.

3.3 pH Titrations

The UV/Vis absorbance spectra of racemic [Ru(bpy)₂(bbaib)]²⁺ and [Ru(phen)₂(bbaib)]²⁺ (10 µM) were recorded over a pH range between pH 2 and 13 in a mixture of 0.1 M NaOH solution and 0.1 M Britton-Robinson buffer. The UV/Vis absorbance spectra of [Ru(bpy)₂(bbaib)]²⁺ (Figure 3.7) and [Ru(phen)₂(bbaib)]²⁺ (Figure 3.8) display several changes as a function of pH. The most significant change for [Ru(bpy)₂(bbaib)]²⁺ occurs between pH ~2.5 and ~4 where a peak can be observed

decreasing in intensity at 486 nm and a new one increasing in intensity at 467 nm for

$[Ru(bpy)_2(bbaib)]^{2+}$ and at 490 and 479 nm for $[Ru(phen)_2(bbaib)]^{2+}$, respectively. This

region is assigned as MLCT $d - \pi^*$ transitions, and the change in peak position suggests

that protonation of the bbaib ligand results in a red shift in the excitation of $d - \pi^*_{bbaib}$

transitions. Acidic conditions cause the functionalised ligand to become protonated,

resulting in a decrease in energy required for electron promotion from the metal d-

orbital to the π^* orbital of the protonated ligand. Increasing the pH causes the ligand to

deprotonate through a neutrally charged ligand to a negative charged one, requiring a

higher energy level for electron promotion to occur, higher than the energy requirement

for $d - \pi^*_{bpy/phen}$ transition (Equation 3.1). This change is visible to the naked eye as the

acidic solution is orange and the basic solution is yellow.

$$[Ru\,(L)_2(bbaib + H_2)]^{4+} \leftrightarrow [Ru\,(L)_2(bbaib)]^{2+} \leftrightarrow [Ru\,(L)_2(bbaib - H_2)]^0$$

Acidic pH   Basic pH
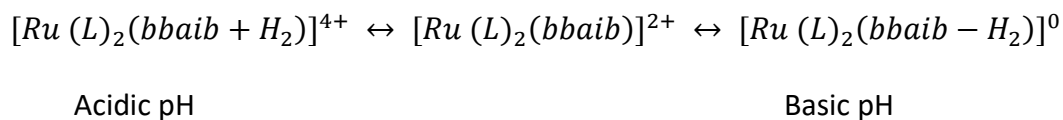
Equation 3.1 – An equation to describe the variation in complex charge as a function of pH.
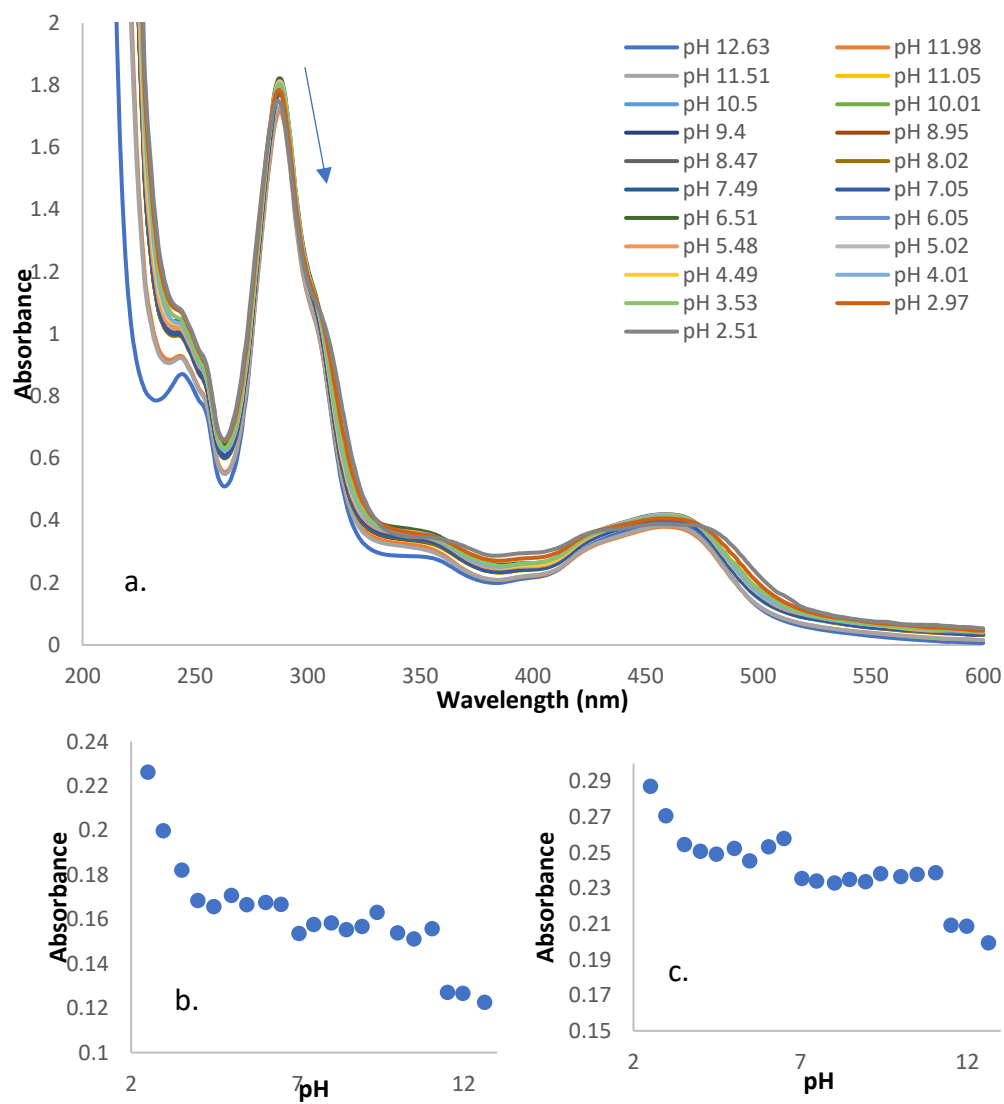
Figure 3.7 *- UV/Vis absorbance spectra of [Ru(bpy)$_2$(BBAIB)]Cl$_2$ at (a). pH ~2.5 to ~12.5 and plotted absorbance values at (b). 385 nm and (c). 486 nm.*
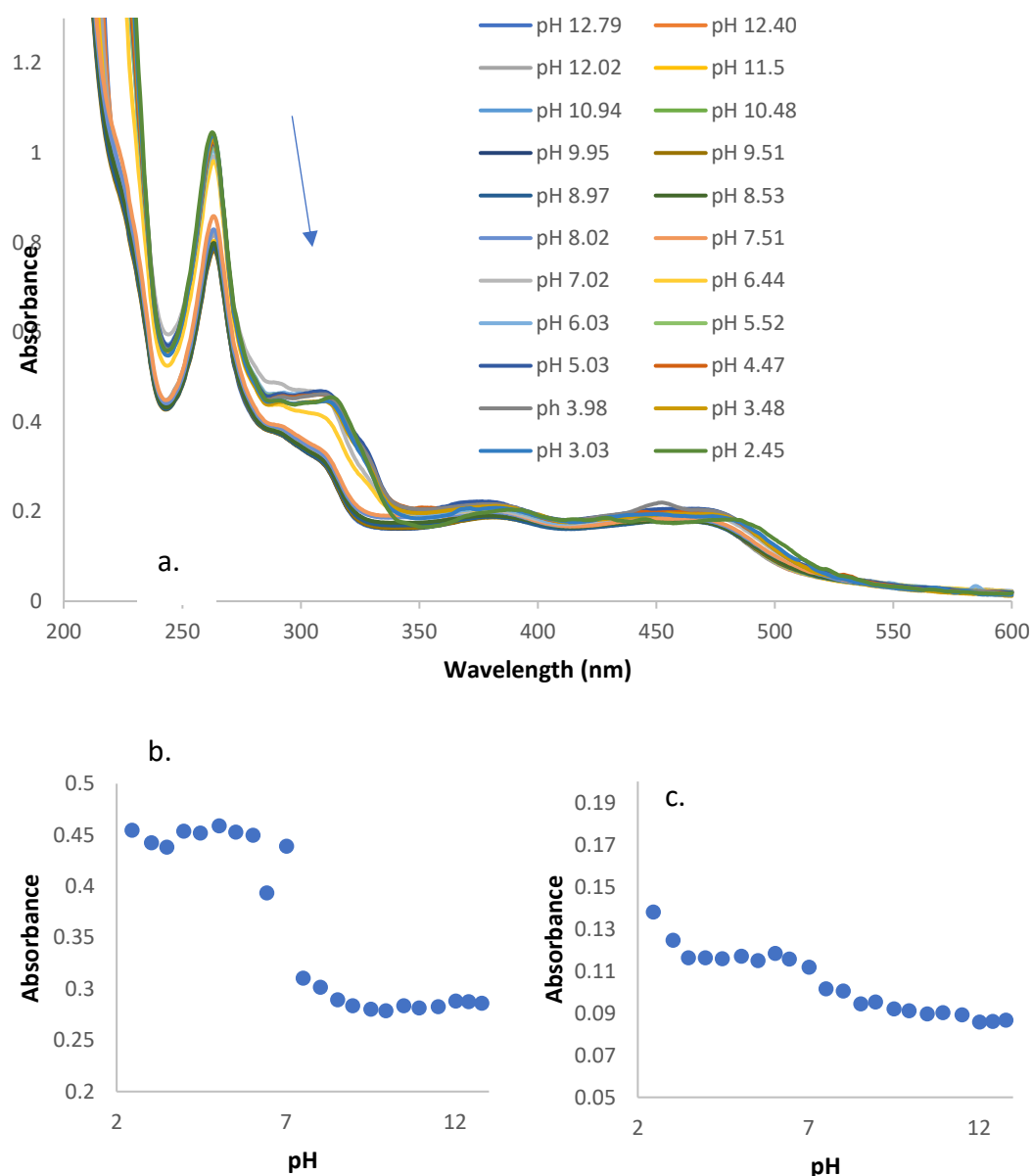
Figure 3.8 - *UV/Vis absorbance spectra of [Ru(phen)₂(BBAIB)]Cl₂ at (a). pH ~2 to ~12.5 and plotted absorbance values at (b). 330 nm and (c). 500 nm.*

The emission spectra of [Ru(bpy)$_2$(bbaib)]Cl$_2$ (Figure 3.9) and [Ru(phen)$_2$(bbaib)]Cl$_2$ (Figure 3.10) were recorded over a range of pH values from ~12.5 to ~2.45, resulting in changes in both emission intensity and maximum wavelength. The maximum wavelength blue shifts from 670 to 641 nm for [Ru(bpy)$_2$(bbaib)]Cl$_2$ and red shifts from 634 to 671 nm for [Ru(phen)$_2$(bbaib)]Cl$_2$. As with the bbib complexes in Chapter Two, these shifts are most likely caused by a switch in emissive regions within the complex

as pH changes from basic to acidic. In acidic environments, the bbaib ligand is protonated which lowers the energy requirement for π^*_{bbaib} - d transitions to occur, therefore emission is almost exclusively coming from the functionalised ligand. The positive charge stabilises the $^3\pi^*_{bbaib}$ excited state, resulting in non-radiative decay pathways being favoured (i.e. solvent dissipation) thus the lowered emission intensity observed. The energy gap law dictates that rate of radiationless decay transitions increase with decrease in energy gap between initial and final states. This is also an explanation for the trend observed of decreasing radiative emission in this data set.*

As the environment becomes less acidic (approximately pH 4), the additional proton is removed from the bbaib ligand, raising the energy requirement for π^*_{bbaib} – d. It is likely that it is then at a similar energy level to the $\pi^*_{bpy/phen}$ - d. At this point, dual emission is likely to be happening, where radiative decay is occurring from both ligand π^* - d transitions. At approximately pH 10, bbaib becomes completely deprotonated and the dominant transition is the $^3\pi^*_{bpy/phen}$ – d transition.
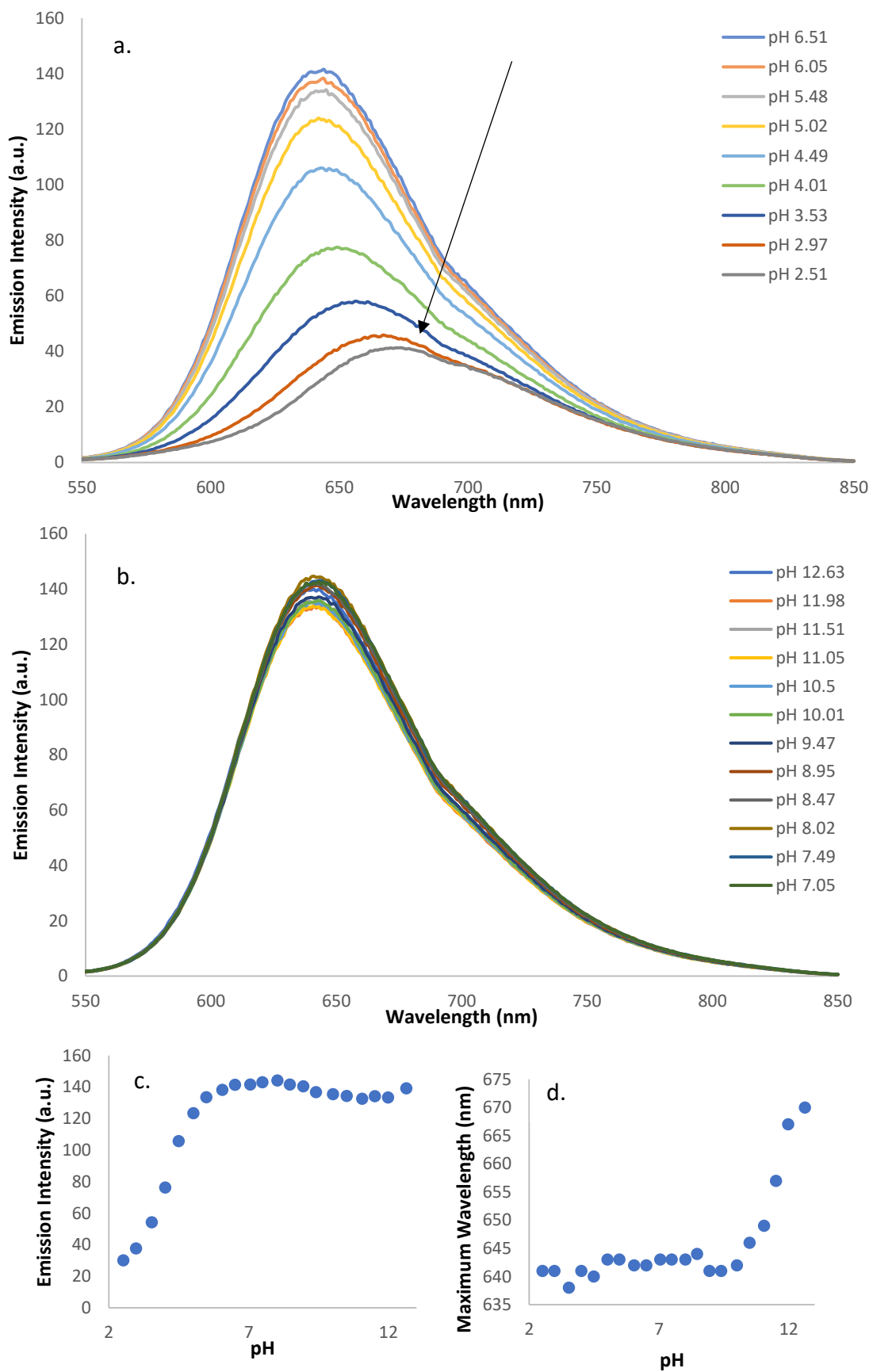
Figure 3.9 – *Emission spectra of [Ru(bpy)$_2$(bbaib)]Cl$_2$ at (a). pH ~2.5 to ~6.5, and (b). pH ~7 to ~12.5, (c). plotted emission intensity values and (d). maximum wavelength.*
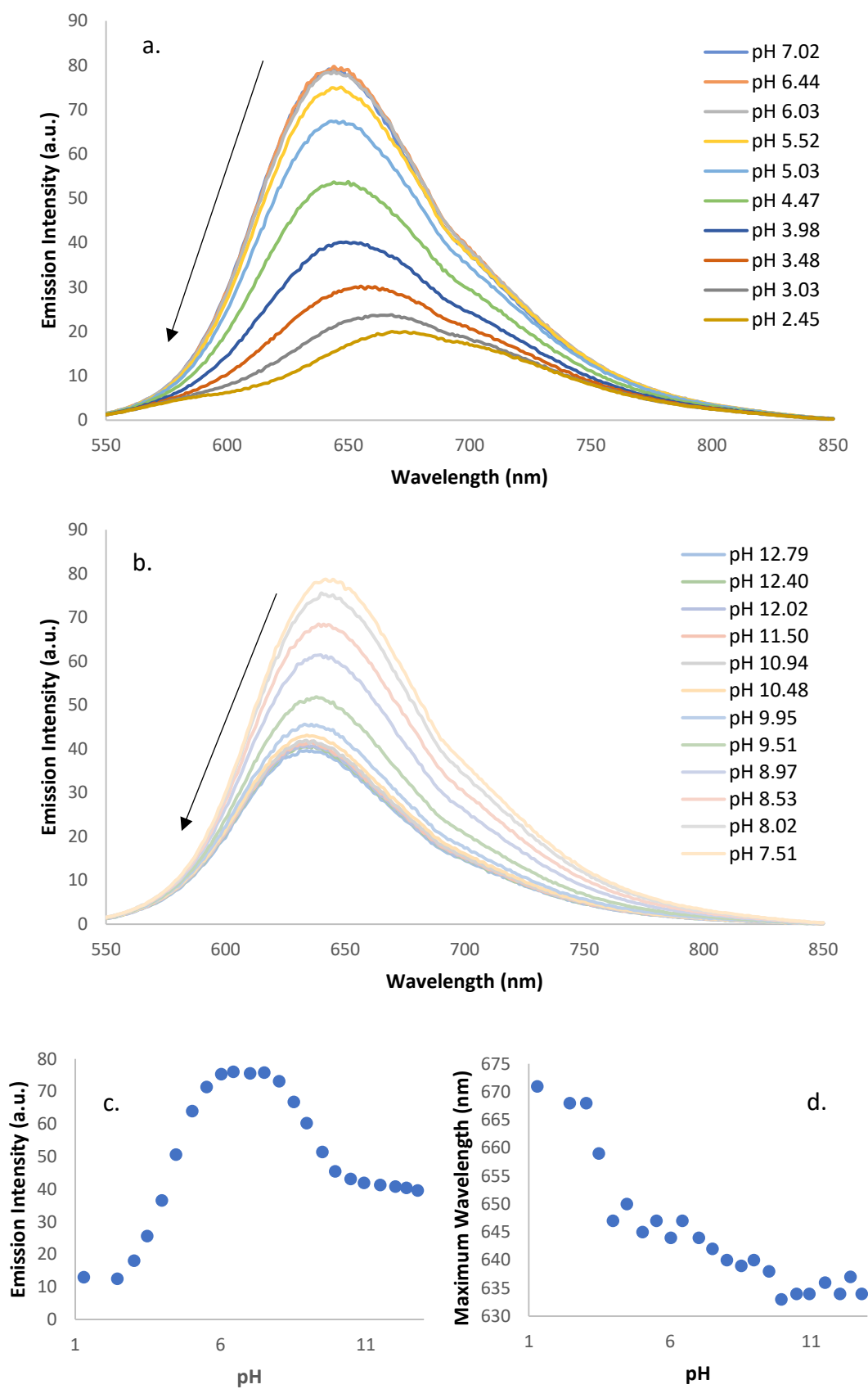
Figure 3.10 – *Emission spectra of [Ru(phen)₂(BBAIB)]Cl₂ at (a). pH ~2.5 to ~6.5, and (b). pH ~7 to ~12.5, (c). plotted emission intensity values and (d). maximum wavelength.*
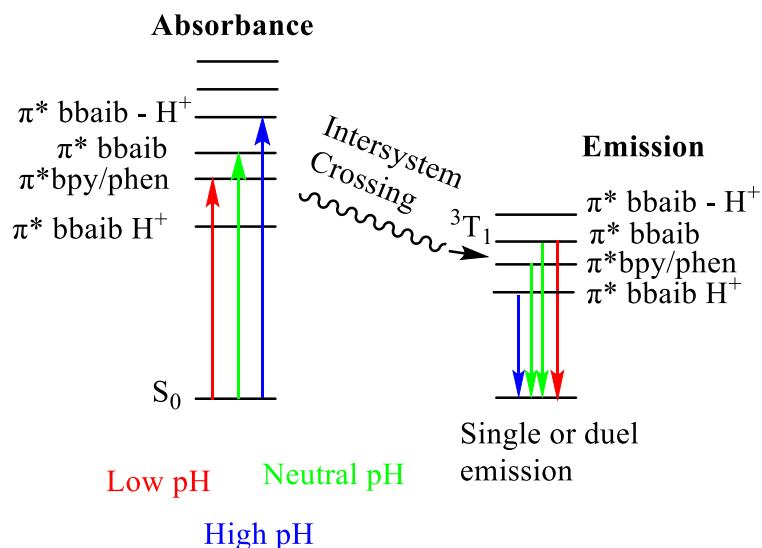
Figure 3.11 – *A Jablonski diagram to describe the changes in transitions for [Ru(bpy)$_2$(bbaib)]$^{2+}$ and [Ru(phen)$_2$(bbaib)]$^{2+}$ as a function of pH.*

Table 3.2 – *Estimated experimental pK$_a$ and pK$_b$ values for [Ru(bpy)$_2$(bbaib}Cl$_2$ and [Ru(phen)$_2$(bbaib)]Cl$_2$, determined via line of best fit using QTIPlot, compare to the literature valuesfor pKa and pKb of benzimidazole.[9]*

	pK$_a$ of Ground State	**pK$_a$ of Excited State**	**pK$_b$ of Ground State**	**pK$_b$ of Excited State**
[Ru(bpy)$_2$(bbaib)]Cl$_2$	~3	~4	~11	~10
[Ru(phen)$_2$(bbaib)]Cl$_2$	~3	~4	~7	~8
Benzimidazole	5.6	-	12.8	-

The ground and excited state pK$_a$ and pK$_b$ of both complexes have been considered (Table 3.2) using mid-point estimation where the absorbance values at a specific wavelength or the maximum emission wavelength were plotted for the ground and excited states respectively against pH, and the pK$_a$ and pK$_b$ values were estimated byt finding the pH at the mid point of a trend of change in absorbance/emission wavelength. The pK$_a$ of [Ru(bpy)$_2$(bbaib)]Cl$_2$ for ground and excited states was found to be approximately 3 and 4 respectively and pK$_b$ values of approximately 11 for the ground

state and 10 for the excited state. The ground and excited pK_a values for [Ru(phen)$_2$(bbaib)]Cl$_2$ was estimated to be around 3 and 4, as with [Ru(bpy)$_2$(bbaib)]Cl$_2$, however the pK_b values differ with a ground state value of ~7 and an excited state value of ~8. These are lower than the values for benzimidazole and bbib complexes in Chapter Two (Section 2.2). The lowering of the pK values is most likely due to presence of the additional electron withdrawing amide groups in the bbaib complexes, but these determinations were carried out in Britton-Robinson buffer, so the presence of bound phosphate, borate or acetate could also be influencing the result.

3.4 Anion Binding Studies

The anion recognition qualities of [Ru(bpy)$_2$(bbaib)][PF$_6$]$_2$ and [Ru(phen)$_2$(bbaib)][PF$_6$]$_2$ have been tested using UV/Vis absorbance, emission and ^{1}H-NMR spectroscopy as described in Chapter Six. All anions (H$_2$PO$_4^-$, Cl$^-$, Ac$^-$ and Br$^-$) were tested as their tetrabutylammonium salts.

3.4.1 UV/Vis and Emission Titrations

A series of sequential addition titrations of [Ru(bpy)$_2$(bbaib)][PF$_6$]$_2$ and [Ru(phen)$_2$(bbaib)][PF$_6$]$_2$ were recorded using UV/Vis absorbance and emission spectroscopy. The experiments were initially attempted using acetonitrile as it is the standard solvent for these types of studies with a complex concentration of 50 µM and a maximum anion concentration of 500 µM. However these attempts resulted in strong precipitation of what is assumed to be a complex:anion adduct. Therefore, solutions were made up of DMSO / 5% distilled water and the relevant anion (H$_2$PO$_4^-$, Br$^-$, Cl$^-$, AcO$^-$) added to a total of 50 µM (10 equivalents). Data has been normalised to account

for dilution effects. In all cases, there is minimal change in the absorbance spectra for both [Ru(bpy)$_2$(bbaib)][PF$_6$]$_2$ and its phenanthroline analogue (Appx. 27 – 34). From this
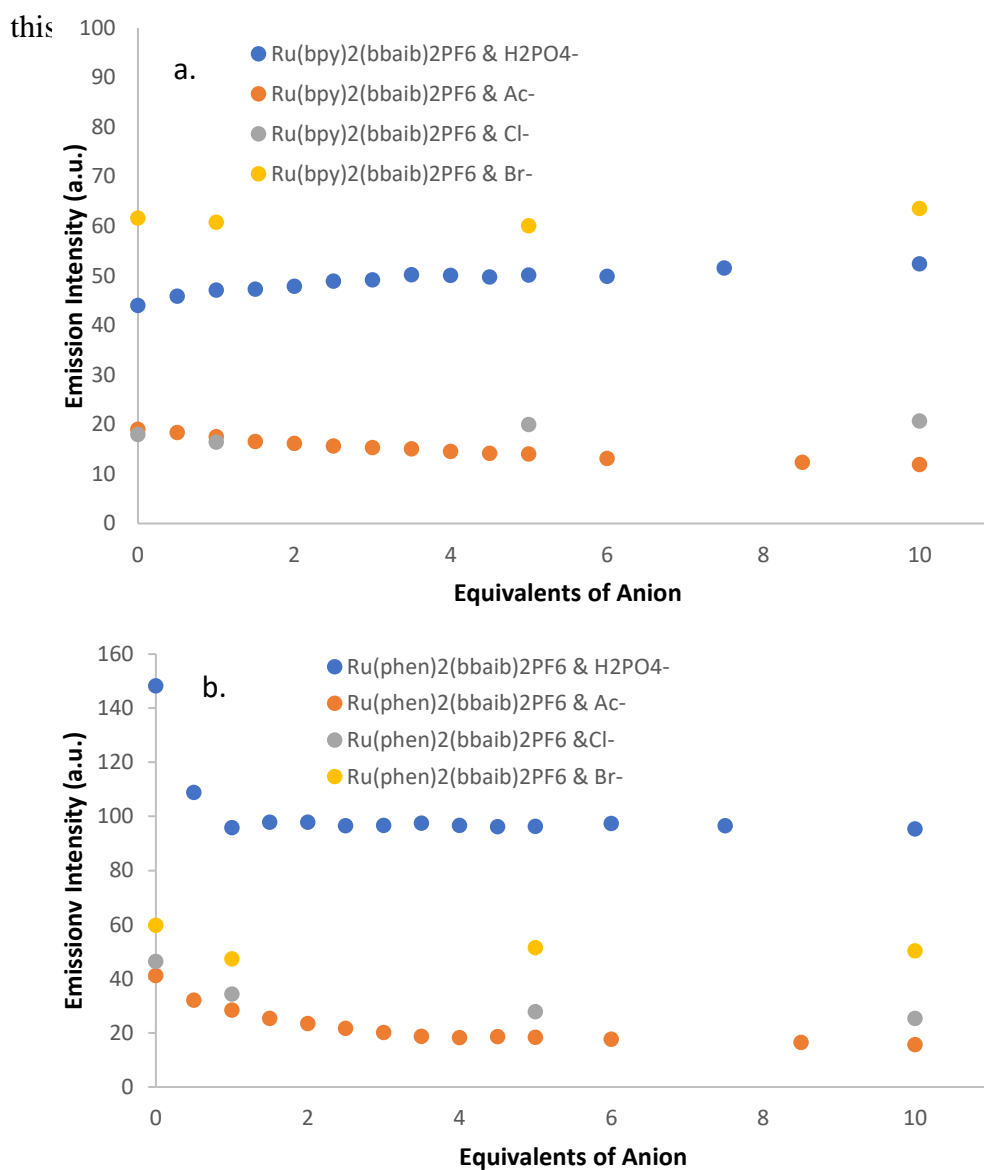
Figure 3.11 – Emission intensity of (a.) [Ru(bpy)$_2$(bbaib)][PF$_6$]$_2$ and (b) [Ru(phen)$_2$(bbaib)][PF$_6$]$_2$ at λ_{max} with increasing anion concentration (Ac$^-$, Br$^-$, Cl$^-$, H$_2$PO$_4^-$). Spectra run at 25 °C in DMSO / 5% deionised water.

The emission intensity of [Ru(bpy)$_2$(bbaib)][PF$_6$]$_2$ (Figure 3.11) showed little change on the addition of dihydrogen phosphate, chloride, bromide and acetate anions (Appx.

35 – 42). It is uncertain whether this is due to the DMSO/water solvent mixture forming a strong hydration sphere around the anions and the complex. Emission intensity was observed to decrease for [Ru(phen)$_2$(bbaib)][PF$_6$]$_2$ on addition of dihydrogen phosphate (Figure 3.11), indicative of an interaction occurring. It can be reasoned that this is strong as it has resulted in significant quenching in an aqueous environment, where there is a competitive hydration sphere surrounding the ruthenium complex. The sequential addition of either acetate, bromide or chloride anions to [Ru(phen)$_2$(bbaib)][PF$_6$]$_2$ resulted in only a minimal change to the emission intensity.

The substantial quenching of emission for [Ru(phen)$_2$(bbaib)][PF$_6$]$_2$ with dihydrogen phosphate, whilst not significantly observed with the other anions shows that there is potentially a high selectivity towards phosphate, even in aqueous environments. This could potentially make the complex a candidate for testing phosphate levels in biological settings.

3.4.2 ^{1}H-NMR Spectroscopy Titrations

[Ru(bpy)$_2$(bbaib)][PF$_6$]$_2$ and [Ru(phen)$_2$(bbaib)][PF$_6$]$_2$ were also investigated for their anion recognition abilities using ^{1}H-NMR spectroscopy, through the sequential addition of the TBA anions (dihydrogen phosphate, acetate and chloride) with up to ten equivalents. ^{1}H-NMR titrations of [Ru(bpy)$_2$(bbaib)][PF$_6$]$_2$ and [Ru(phen)$_2$(bbaib)][PF$_6$]$_2$ (5 mM, 0.5 ml) (Appx. 43 - 47) in a DMSO-D$_6$ /5% D$_2$O solution were undertaken with up to ten equivalents of TBA-Cl and no changes in peak position were observed for either complex in the presence of Cl$^-$, indicative of no significant interaction occurring between complex and anion.

Dihydrogen Phosphate (H₂PO₄⁻) and Acetate (AcO⁻)

The titration of [Ru(bpy)$_2$(bbaib)][PF$_6$]$_2$ and dihydrogen phosphate (Figure 3.12) shows a downfield shift of a peak from 9.28 to 9.45 ppm, characteristic of the H^3 ligand bbaib proton of the benzimidazole, indicating the formation of a hydrogen bond with the anion. There is another peak that shifts downfield from 9.09 to 9.18 ppm. This peak is thought to represent the -NH proton of the amide linker group. This shift implies that the amide group takes part in the recognition of H$_2$PO$_4^-$. There is also upfield movement of a peak from 7.353 to 6.981 ppm, indicative of a compensative effect from the back two protons of the benzimidazole. There is no indication of any interaction between dihydrogen phosphate or acetate anions and the ancillary bpy ligands. The titrations with acetate give similar results as the H$_2$PO$_4^-$ titrations and the anion titrations of [Ru(phen)$_2$(bbaib)][PF$_6$]$_2$ showed comparable results to the bipyridine analogue.
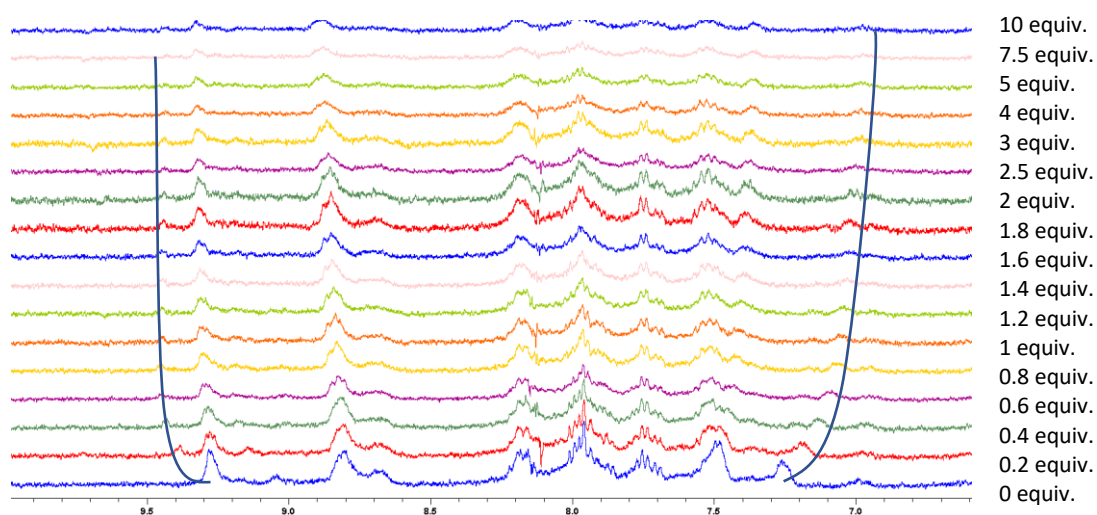
Figure 3.12 – *^{1}H-NMR titration of [Ru(bpy)$_2$(bbaib)][PF$_6$]$_2$ and H$_2$PO$_4^-$ in DMSO/5% deuterated water.*

Stability Constants

Stability constants for the ^{1}H-NMR titrations with dihydrogen phosphate and acetate were calculated by Dr. Fletcher using WINEQNMR[6] (Table 3.3) with a two anion to one complex binding ratio, as described in Section 2.4. This model was chosen to best represent the interpretation of the data gathered from the UV/Vis absorbance, emission and ^{1}H-NMR titrations.

Table 3.3 - *Stability constants calculated from the ^{1}H-NMR titrations with H2PO4[-] and AcO[-] in a DMSO-d_6: % deuterium mixture.*

	$H_2PO_4^-$	AcO^-
[Ru(bpy)₂(bbaib)][PF₆]₂	$pK_1 = 3.64$	$pK_1 = $ n/a
	$p\beta_2 = $ n/a	$p\beta_2 = 4.59$
[Ru(phen)₂(bbaib)][PF₆]₂	$pK_1 = 3.64$	$pK_1 = 2.51$
	$p\beta_2 = $ n/a	$p\beta_2 = 4.51$
Error < ± 5.9%		

The stability constants calculated for [Ru(bpy)₂(bbaib)][PF₆]₂ with the addition of acetate show a reasonably large value for the second stability constant but could not readily stabilise a value for *pK₁*. It is approximated to be 1.54, which would be indicative of a complicated binding behaviour occurring. Constants calculated for interactions between this complex and dihydrogen phosphate resulted in a p*K₁* of 3.64 and an unstable value for p*β₂*. This is most likely due to the complex effectively only binding one $H_2PO_4^-$ ion, with an extremely weak interaction occurring with a second (residual) anion, subsequently destabilising the second stability constant. However, the r factor (a measure goodness of fit to data in order to estimate error) was determined to

be approximately 5.89% which is too high to have confidence in the output values. Overall, all that can be said is that [Ru(bpy)$_2$(bbaib)][PF$_6$]$_2$ does have an interaction with dihydrogen phosphate but it is not currently possible to ascertain the relative strength with confidence for this data set.

The stability constants calculated for [Ru(phen)$_2$(bbaib)][PF$_6$]$_2$ showed a similar result to the bipyridine analogue, with a pK_1 of 2.51 and a pβ_2 of 4.51 with acetate, showing a two anion to one cation fit. The stability results for this complex with dihydrogen phosphate replicate the values obtained with [Ru(bpy)$_2$(bbaib)][PF$_6$]$_2$, with a pK_1 of 3.64 and an unstable value for the pβ_2 constant.

It is noted that while the stability constants for both [Ru(bpy)$_2$(bbaib)][PF$_6$]$_2$ and [Ru(phen)$_2$(bbaib)][PF$_6$]$_2$ effectively fit to a one to one stoichiometry for dihydrogen phosphate, the fitted data show the same systematic error where the modelled data crosses the experimental data at approximated one equivalent, rather than passing through at random. This could indicate that the model is not fitting correctly to the data, and that the values reported are potentially on the lower side. Essentially, due to these systematic errors, it cannot be validated whether these complexes will stably bind two dihydrogen phosphate anions or only one without repetition of the experiment.

The ^{1}H-NMR spectroscopy titrations and the subsequently calculated stability constants of [Ru(bpy)$_2$(bbaib)][PF$_6$]$_2$ and [Ru(phen)$_2$(bbaib)][PF$_6$]$_2$ has provided evidence that the anion interaction occurs on the functionalised ligand and does not include the ancillary ligands. However, due to the limitations of [1]H-HMR titrations and potential human error in calculating concentrations, it cannot be confirmed with this data set whether these

values are truly representative of the strength of binding and should have been repeated, but this was not possible due to limited access to the spectrometer during the pandemic lockdown.

3.5 DNA Binding Studies

3.5.1 UV/Vis and Emission Titrations

The UV/Vis absorbance and emission spectra of $[Ru(bpy)_2(bbaib)]Cl_2$ and $[Ru(phen)_2(bbaib)]Cl_2$ (50 µM) were recorded with and without the presence of *ct*-DNA (up to 400 µM). The samples were made up using tris buffer (pH 7.2). The absorbance spectra of $[Ru(bpy)_2(bbaib)]Cl_2$ (Figure 3.13) does not show any change upon adding increasing concentrations of *ct*-DNA, apart from the region that responds to the increasing DNA concentration. This does not indicate whether an interaction is present, but provides evidence that if there is one, it is not a deprotonation event, which has been established in Section 3.2.
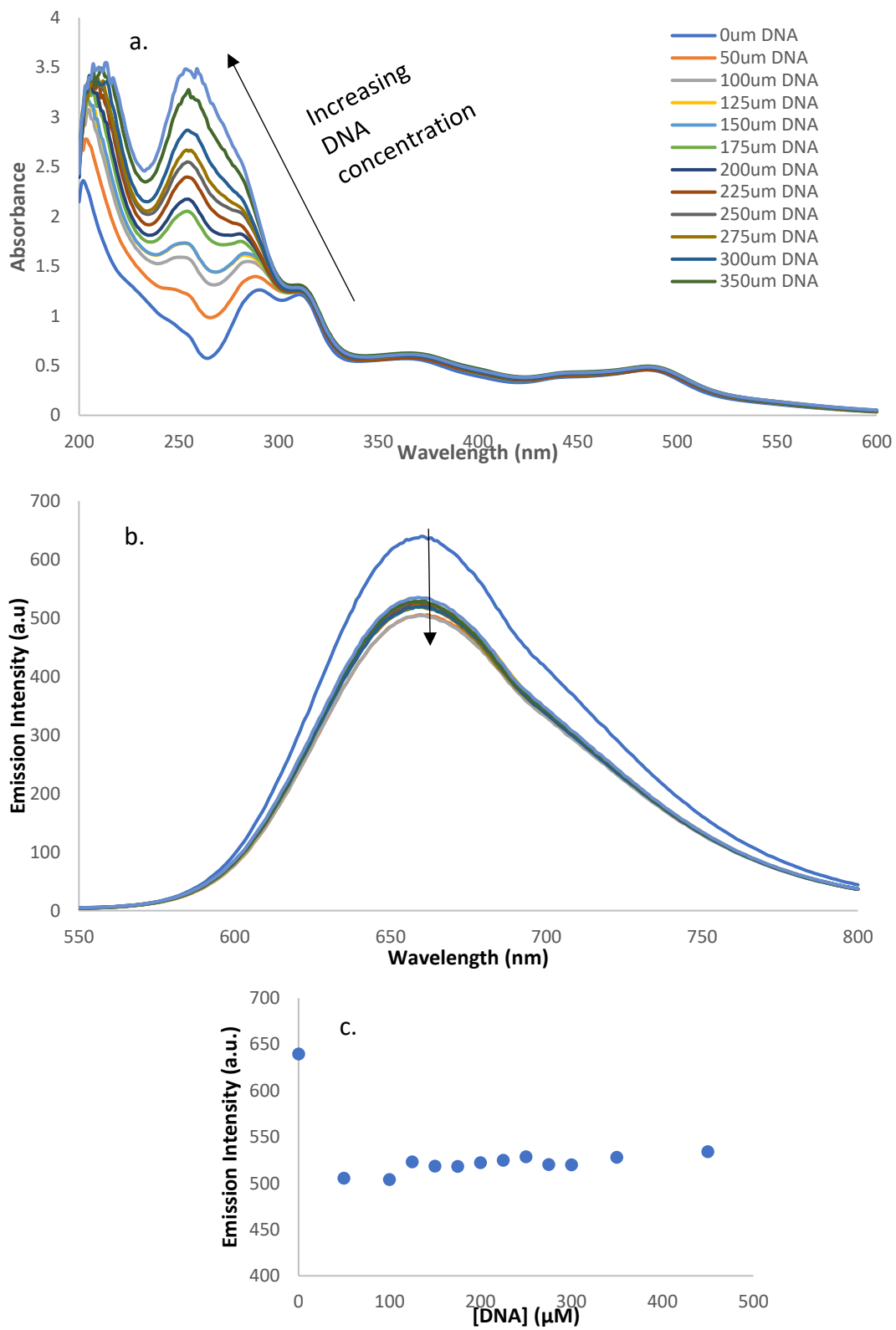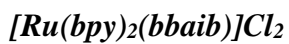
[Ru(bpy)₂(bbaib)]Cl₂

Figure 3.13 – *(a.) UV/Vis absorbance titration, (b) Luminescence emission titration of [Ru(bpy)₂(bbaib)]Cl₂ (50 μM) in the absence and presence of ct-DNA in tris buffer solution and (c.) the emission intensity values at 662 nm.*

The emission spectra of [Ru(bpy)$_2$(bbaib)]Cl$_2$ (Figure 3.13) shows a small decrease in intensity upon introduction of 50 µM of *ct*-DNA from 639 to 505 a.u.. Increasing the concentration of DNA further, from 100 to 400 µM gives a constant emission intensity. The quenching of emission could stem from an interaction between complex and phosphate, which was established in Section 3.4. However the majority of the change in emission occurs between the presence of 0 µM and 50 µM *ct*-DNA, which is insufficient evidence to be able to say whether this is a result of an interaction, or if there is another reason. Further experiments need to be undertaken between 0 and 50 µM of *ct*-DNA to observe the behaviour of the complex.

[Ru(phen)$_2$(bbaib)]Cl$_2$
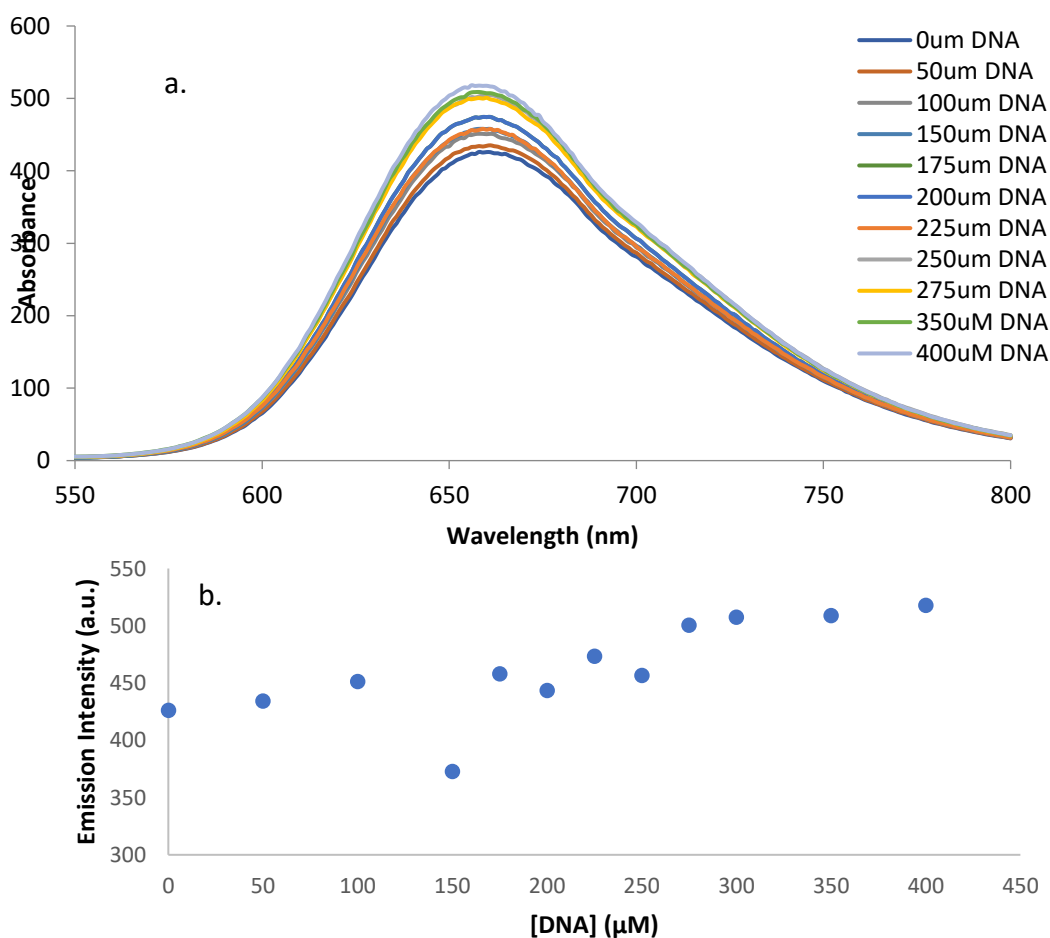
Figure 3.14 – (a.) Luminescence emission titration of [Ru(phen)$_2$(bbaib)]Cl$_2$ (50 µM) in the absence and presence of ct-DNA in tris buffer solution and (b.) the emission intensity values at 662 nm.

132

Unfortunately, the absorbance spectra of [Ru(phen)$_2$(bbaib)]Cl$_2$ were lost and the data was unable to be replicated due to the pandemic, however the data was considered to be consistent with the data obtained from [Ru(bpy)$_2$(bbaib)]Cl$_2$.

The emission spectra of [Ru(phen)$_2$(bbaib)][PF$_6$]$_2$ demonstrate a small enhancement in intensity with increasing concentration of *ct*-DNA (426 a.u. without DNA to 517 a.u. with 400 µM *ct*-DNA) (Figure 3.14). This increase in emission could possibly be due to interactions between the complex and the minor groove as the data appears to show a very weak increase in emission, which is not seen with the bbib complexes (Section 2.5). There is no observable difference in maximum wavelength, indicating that there is no deprotonation of the functionalised ligand (established in Section 3.3) or an indication of an intercalation.

3.5.2 Circular Dichroism Titration

The CD spectra of *ct*-DNA (25 µM) were recorded in the absence and presence of varying concentrations of racemic [Ru(bpy)$_2$(bbaib)][PF$_6$]$_2$ and [Ru(phen)$_2$(bbaib)][PF$_6$]$_2$ (up to 50 µM) (Figure 3.15). The titrations were recorded in a solution of 90% tris buffer (7.2 pH) and 10% DMF between 250 and 600 nm. The *ct*-DNA CD spectra display a change on addition of 30 µM [Ru(bpy)$_2$(bbaib)][PF$_6$]$_2$ at ~283 nm. The measurement of circular dichroism is observed to shift to a negative value at a complex concentration of 40 µM, which is intensified at a ruthenium concentration of 50 µM. This transformation is below 300 nm, in the region of a DNA absorption, so it is potentially a change to the DNA structure, but it is also in the overlap region where the complex can also absorb light. 283 nm is the wavelength that represents the bbaib π

– π^* transition, therefore could potentially indicate a change in the behaviour of the functionalised ligand. The *ct*-DNA spectra with [Ru(phen)$_2$(bbaib)][PF$_6$]$_2$ (Figure 3.15) shows comparable results to the bipyridine analogue. There is a change in the measurement of circular dichroism from a positive value to a negative value at 283 nm between 30 µM and 40 µM complex concentrations but this result is not as significant as with [Ru(bpy)$_2$(bbaib)][PF$_6$]$_2$. The similar outcomes of the experiments indicate that if there is an interaction occurring, it is irrespective of the ancillary ligands.
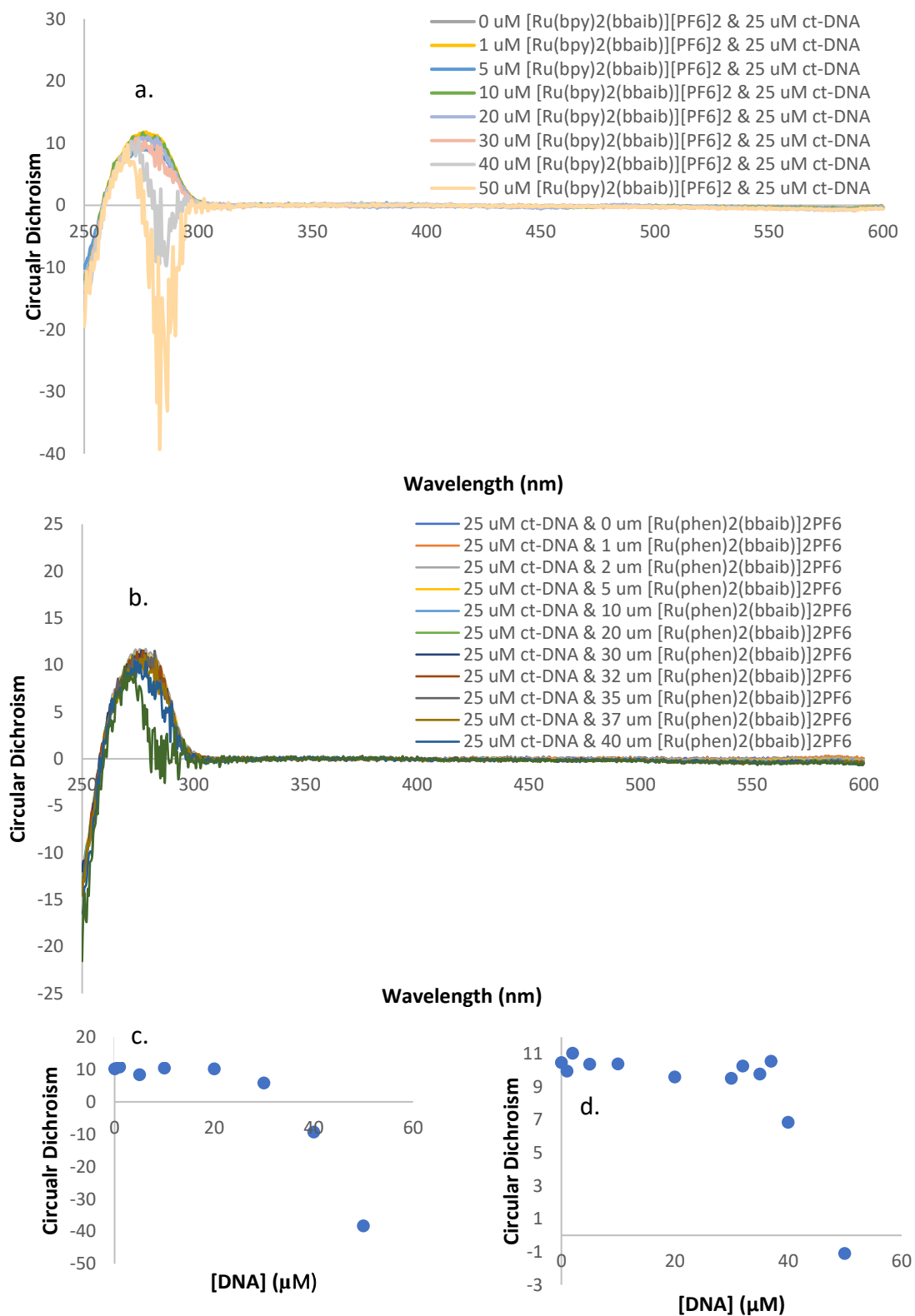
Figure 3.15 - *Circular dichroism spectra of (a.) [Ru(bpy)₂(bbaib)][PF₆]₂ and (b.)*
[Ru(phen)₂(bbaib)][PF₆]₂ in the presence and absence of ct-DNA in 9:1 tris buffer and DMF and
the circular dichroism values of (c.) [Ru(bpy)₂(bbaib)][PF₆]₂ and (d). [Ru(phen)₂(bbaib)][PF₆]₂
at 283 nm.

3.5.3 Thermal Denaturation Studies

The thermal denaturation profiles of *ct*-DNA (25 µM) with and without racemic [Ru(bpy)$_2$(bbaib)][PF$_6$]$_2$ and [Ru(phen)$_2$(bbaib)][PF$_6$]$_2$ (at concentrations of 10 µM and 25 µM) were determined using CD spectroscopy. Solutions were made up of a 90:10 tris buffer (5 mM Tris-HCl, 50 mM NaCl, pH 7.2) and DMF and recordings were taken as described in Chapter Six. "Melt curves" were calculated using QTI plot software and denaturation temperature was estimated from the mid-point analysis.

Table 3.4 - *Observed Tm Values for ct-DNA at 10 µM.*

Experiment	Melting Temperature (°C)	ΔT_m (°C)
Calf thymus DNA	79	N/A
[Ru(bpy)$_2$(bbaib)][PF$_6$]$_2$	76	-3
[Ru(phen)$_2$(bbaib)] [PF$_6$]$_2$	75	-4
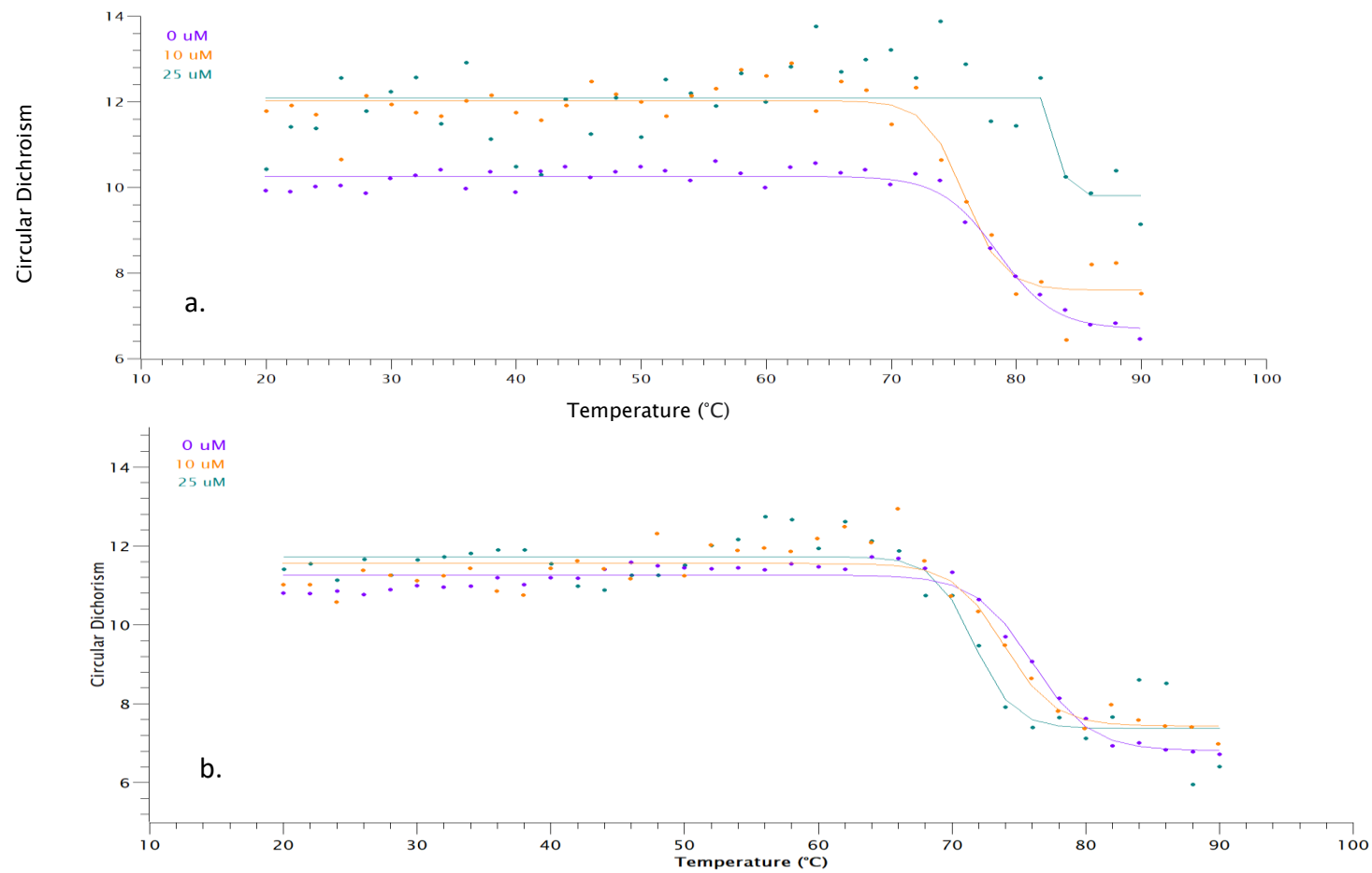
Figure 3.16 – *Melting curves of (a.) [Ru(bpy)$_2$(bbaib)][PF$_6$]$_2$ and (b.) [Ru(phen)$_2$(bbaib)][PF$_6$]$_2$ obtained using QTIplot data fitting software.*

ct-DNA (25 µM) control experiments showed an approximate denaturation temperature of 79 °C in each case. The addition of [Ru(bpy)$_2$(bbaib)][PF$_6$]$_2$ and [Ru(phen)$_2$(bbaib)][PF$_6$]$_2$ to the solutions resulted in a lower melt temperature, -3 °C and -4 °C respectively. This outcome is very similar to the outcome of this experiment described in Chapter Two, possibly indicative that the bbaib complexes are interacting with DNA to a comparable degree with the bbib variants. The similar decrease in denaturation temperatures of the bipyridine and phenanthroline analogues once again suggests that the ancillary ligands do not take part in the interaction with nucleic acids, and the functionalised ligand is the location that recognises DNA. Although this data is evidence that there is an interaction occurring, it confirms that the complexes are most likely not intercalating as the denaturation temperature is decreasing.

3.5.4 Dialysis Equilibrium Studies

Dialysis equilibrium studies were undertaken using [Ru(bpy)$_2$(bbaib)][PF$_6$]$_2$ and [Ru(phen)$_2$(bbaib)][PF$_6$]$_2$ (60 µM) as described in Chapter Two and the dialysate was tested using CD spectroscopy after 24 hours (Figure 3.17). The CD spectra of the dialysate containing racemic [Ru(bpy)$_2$(bbaib)][PF$_6$]$_2$ shows a positive change at 297 nm, potentially signifying a slight enantiomeric preference, albeit without confirmation of which enantiomer is preferred. The CD spectra of the dialysate [Ru(phen)$_2$(bbaib)][PF$_6$]$_2$ showed no change, indicating that there is no enantiomeric preference between the Δ- and Λ- forms. However, in both experiments, the dialysis tubing used to contain the DNA solutions turned from colourless to a pale orange, suggesting that some complex had dialysed across the membrane. The Ru(II) concentration of the dialysate was calculated from the UV/Vis absorbance spectrum to

be 18 µM, confirming that complex had moved through the porous membrane into the DNA solution.
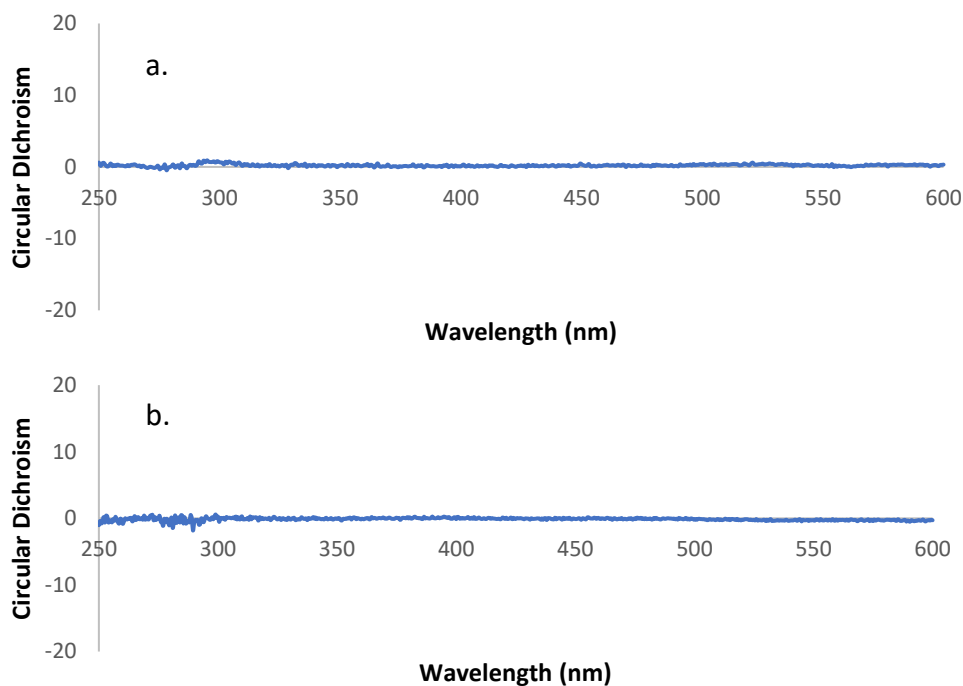
Figure 3.17 – *Circular Dichroism spectra of ct-DNA (25 µM) with (a.) [Ru(bpy)$_2$(bbaib)][PF$_6$]$_2$ (60 µM) and (b.) [Ru(phen)$_2$(bbaib)][PF$_6$]$_2$ (60 µM).*

3.5.5 DNA Viscosity Studies

The relative viscosities of *ct*-DNA solutions (25 µM bp^{-1}) were measured in the absences and presences of racemic [Ru(bpy)$_2$(bbaib)]Cl$_2$ and [Ru(phen)$_2$(bbaib)]Cl$_2$ between 5 and 25 µM in tris buffer (5 mM Tris-HCl, 50 mM NaCl, pH 7.2) (Figure 3.18). Relative viscosity was measured as described in Chapter Six. There was little change observed in relative viscosities of solutions upon introduction of [Ru(bpy)$_2$(bbaib)][PF$_6$]$_2$ and [Ru(phen)$_2$(bbaib)]Cl$_2$, and any variation was most likely caused by human error given the nature of the experiment. The former appears to have caused no increase and the latter shows a small decrease in relative viscosity. These

results suggest that if there is an interaction between DNA and complexes, it is not intercalative.

An issue that was raised in Chapter Two also arises with $[Ru(bpy)_2(bbaib)][PF_6]_2$ and $[Ru(phen)_2(bbaib)][PF_6]_2$. Throughout the study, solid particles precipitate out when complexes are added with DNA in tris buffer, not only clogging the viscometer but reducing the concentration of DNA in solution, which would decrease the solution viscosity. Overall, the viscosity studies gave no obvious indication of DNA binding mode, just that it most likely not intercalation.
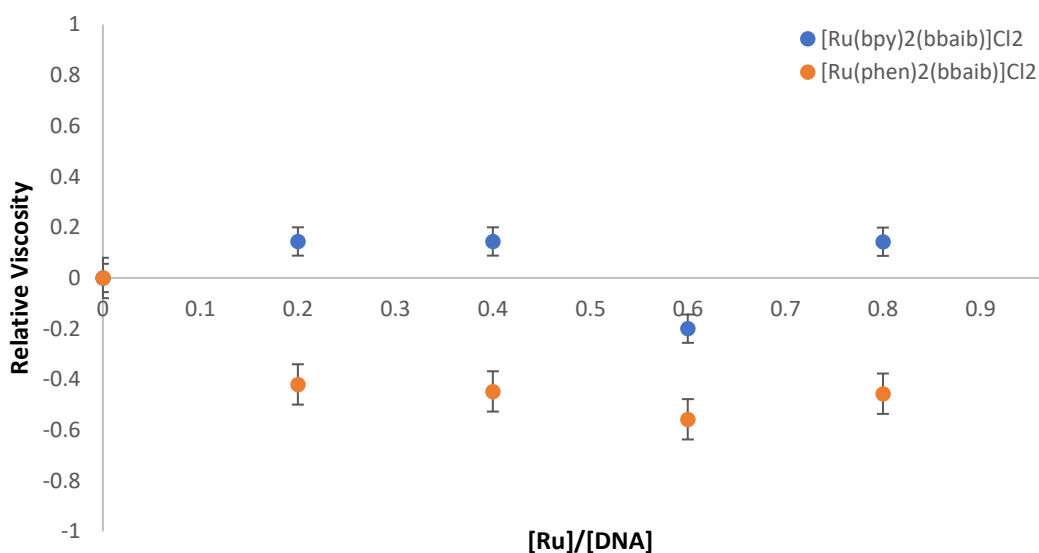
Figure 3.18 *– The observed relative viscosity for [Ru(bpy)₂(bbaib)][PF₆]₂ and [Ru(phen)₂(bbaib)][PF₆]₂ in tris buffer. [DNA] = 25 μM BP.*

3.6 Conclusion

Two novel ruthenium(II) complexes have been successfully synthesised and characterised, namely $[Ru(bpy)_2(bbaib)][PF_6]_2$ and $[Ru(phen)_2(bbaib)][PF_6]_2$. Both complexes were found to have a similar emission and quantum yield as

[Ru(bpy)$_3$][PF$_6$]$_2$. It has been established that these complexes are capable of anion recognition, especially with dihydrogen phosphate, even in aqueous environments. Although the addition of an amide linker group hypothetically should increase the ability for the complexes to recognise anions, calculated stability constants indicate that the bbaib complexes interact with dihydrogen phosphate to a lower extent than the bbib complexes of Chapter Two. Data was also obtained which suggests that these complexes interact with DNA in a non-intercalative manner, however further testing is required to determine whether this is the case or not.

3.7 References

1   H. Y. Alniss, I. Witzel, M. H. Semreen, P. K. Panda, Y. K. Mishra, A. Ahuja and J. A. Parkinson, *J. Med. Chem.*, 2019, **62**, 10423–10440.
2   C. B. Spillane, PhD Thesis, Queen's University Belfast, 2005.
3   P. A. Elliott, PhD Thesis, Queen's University Belfast, 2012.
4   A. I. Khalaf, N. Anthony, D. Breen, G. Donoghue, S. P. Mackay, F. J. Scott and C. J. Suckling, *Eur. J. Med. Chem.*, 2011, 5343–5355.
5   S. C. Yu, X. Gong and W. K. Chan, *Macromolecules*, 1998, **31**, 5639.
6   H. F. M. Nelissen, M. C. Feiters and R. J. M. Nolte, *J. Org. Chem.*, 2002, **67**, 5901–5906
7   K. Suzuki, A. Kobayashi, S. Kaneko, K. Takehira, T. Yoshihara, H. Ishida, Y. Shiina, S. Oishi and S. Tobita, *Phys. Chem. Chem. Phys.*, 2009, **11**, 9850 - 9860.
8   D. Escudero, B. Happ, A. Winter, M. D. Hager, U. S. Schubert and G. L., *Chem. Asian J.*, 2012, **7**, 667–671.
9   M. J. Hynes., *J. Chem. Soc. Dalton. Trans.,* 1993, 311 - 312.

Chapter Four

Chapter Four: Synthesis and Binding Studies of Benzimidazole Functionalised Ruthenium(II) Polypyridyl Complexes with Methyl or Carbonyl Linkages

4.1 Introduction

Previously within the Fletcher group benzimidazole-functionalised ruthenium(II) complexes with methylene groups had been synthesised.[1] The original hypothesis was based on the hopes that by inserting a methyl linking group in the original benzothiazole based complexes ($[Ru(bpy)_2(bbtmb)]^{2+}$) (Figure 4.1), the fluorescence properties would improve by removing the extended conjugated system. This system would have prevented delocalisation onto the additional heterocycle, resulting in an enhancement of radiationless decay of the excited state, making the system more like $[Ru(bpy)_3]^{2+}$. It was also thought that disruption of the π-system would increase solubility of the ligand and make the synthesis and preparation of the metal complex easier.
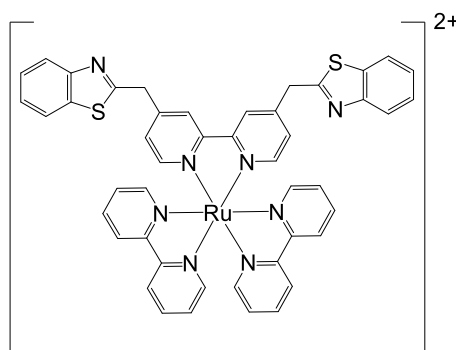
Figure 4.1 – The structure of $[Ru(bpy)_2(bbtmb)]^{2+}$.[1]

The Fletcher group then discovered that a structural change was occurring when a benzothiazole based ligand was affixed to the metal centre, although it is not fully understood what that change was. It was found that exposing these molecules to air and water in acidic media, the methyl linkage is surprisingly oxidised to a ketone (Figure 4.2). The aim of this chapter is to see if a similar reaction occurs with the imidazole analogue and to determine whether a change in linking group makes a difference in anion recognition and the DNA interaction of the complex.
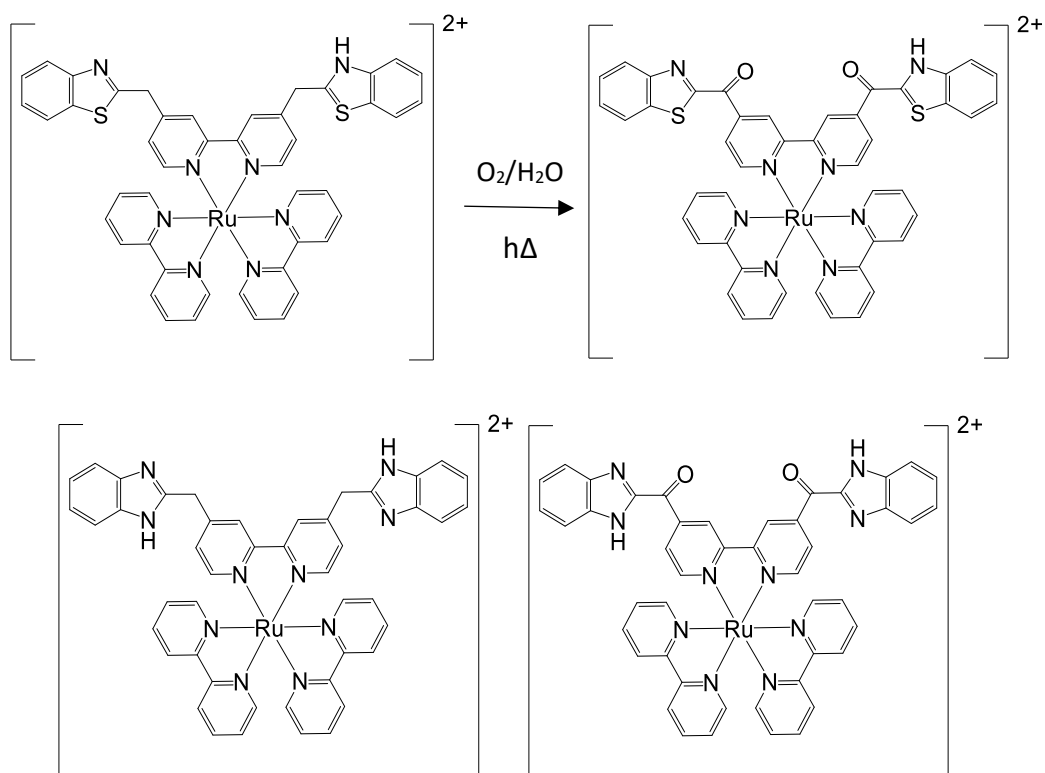
Figure 4.2 *– The oxidation of [Ru(bpy)$_2$(bbtmb)]$^{2+}$ to [Ru(bpy)$_2$(bbtmbo)]$^{2+}$ and the target complexes of [Ru(bpy)$_2$(bbimb)]$^{2+}$ and [Ru(bpy)$_2$(bbimbo)]$^{2+}$.*

4.2 Synthesis and Characterisation of Benzimidazole Functionalised Ruthenium(II) Polypyridyl Complexes with Methyl Linkages
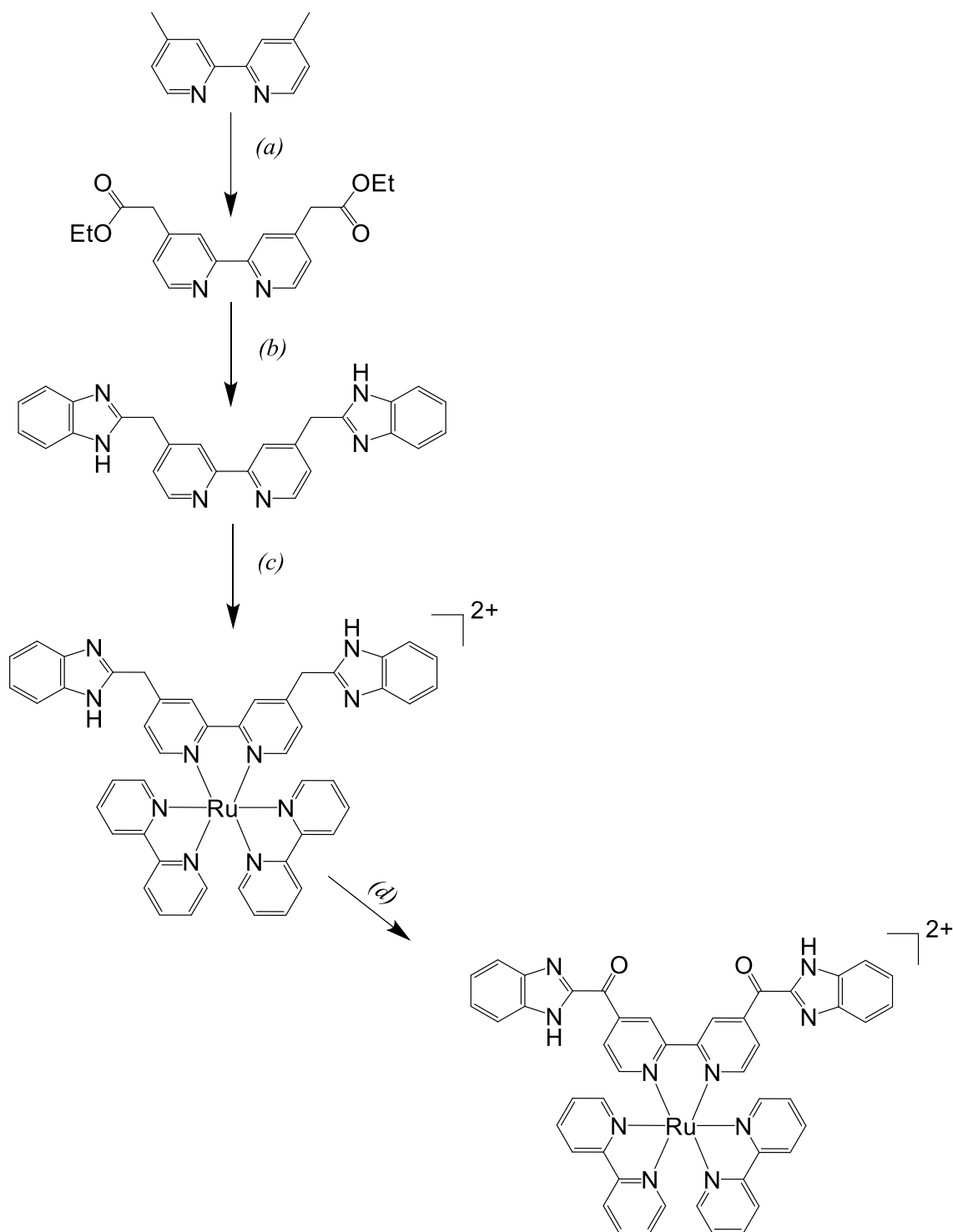
Scheme 4.1 – *Reaction scheme for the general synthesis of ligand and complexes. (a)(i) THF, N₂, LDA, -78 ˚C (ii) in situ (EtO)₂CO; (b) 1,2-phenylenediamine, PPA, 200 ˚C; (c) Ru(bpy)₂Cl₂, EtOH, N₂, 90 ˚C; (d) exposure to air and light.*

4.2.1 Synthesis of Ligands and Complexes

4.2.1.1 Synthesis of 4,4′-*bis*(benzimidazole-2-yl-methyl)-2,2′-bipyridine (bbimb)[1]

4,4′-Dimethyl-2,2′-bipyridine was lithiated at the methyl groups using lithiumdiisopropylamide (LDA) in dry tetrahydrofuran (THF) under Schlenk line conditions. This was then converted to 4,4′-bis(ethylester-methyl)-2,2′-bipyridine by reacting with diethyl carbonate and used without further purification in good yield. This was then heated with 1,2-phenylenediamine in polyphosphoric acid at 200°C under a nitrogen atmosphere for 24 hours. After cooling, the solution was neutralised using aqueous 1 M sodium bicarbonate solution, which precipitated out a light brown solid which was collected and used without further purification. The ligand was characterised using ^{1}H- and ^{13}C-NMR spectroscopy, IR and mass spectrometry.

The spectrum for bbimb (Figure 4.3) appears to be very similar to that of bbib with three major differences. A large singlet peak is present with bbimb at approximately 4.4 ppm, corresponding to the two protons of the methylene group. The -NH proton peak is much further downfield than is observed with bbib, most likely an effect of the extended conjugation being broken in the bbimb ligand. The H^2 proton of bbimb is shifted upfield compared to its location in the bbib spectra. It is assumed that this is caused by the addition of the methyl linking group increasing the distance between the -NH proton and H^2 meaning that the electron withdrawing effects of the amine group are smaller.

The ^{1}H-NMR spectrum of bbimb also shows the effect that changing heteroatom has on the ligand when compared with the spectra of bbomb and bbtmb.[1] The chemical shift of the H^2 proton on the 2,2′-bipyridine moiety is downfield in the bbimb spectrum than the spectra of the analogue ligands (bbimb = ~7.4 ppm, bbomb and bbtmb = ~7.3 ppm).

4.2.1.2 Synthesis of [Ru(bpy)$_2$(bbimb)]$^{2+}$ and [Ru(bpy)$_2$(bbimbo)]$^{2+}$

The complex [Ru(bpy)$_2$(bbimb)][PF$_6$]$_2$ was prepared by refluxing bbimb and [Ru(bpy)$_2$Cl$_2$].xH$_2$O in EtOH under a nitrogen atmosphere for ~24 hours. After cooling the resulting orange-brown complex was precipitated out of solution using potassium hexafluorophosphate (KPF$_6$) which was isolated by filtration. Size exclusion chromatography (Sephadex™ LH20) was used with a 1:1 acetone/methanol eluant to purify. The complexes were characterised using ^{1}H-NMR, UV/Vis absorbance and emission spectroscopy and IR. It was not possible to obtain a conclusive mass spectrometry result as of the time of writing.

To convert [Ru(bpy)$_2$(bbimb)][PF$_6$]$_2$ to [Ru(bpy)$_2$(bbimbo)][PF$_6$]$_2$, a sample of complex was left in a solution of deionised water and acetone in a closed vial in direct sunlight and the transformation was monitored via ^{1}H-NMR spectroscopy. A colour change of the solution was observed from orange-brown to brown. Conversion of the complexes to the chloride salt was undertaken using Amberlite IRA-410 ion exchange resin. The conversion from [Ru(bpy)$_2$(bbimb)][PF$_6$]$_2$ to [Ru(bpy)$_2$(bbimbo)][PF$_6$]$_2$ was also confirmed by the presence of an IR peak at 1656.8 cm^{-1} (C=O stretch) which is not present in the IR spectrum of [Ru(bpy)$_2$(bbimb)][PF$_6$]$_2$.

The ^{1}H-NMR spectrum of [Ru(bpy)(bbimb)][PF$_6$]$_2$ (Figure 4.4) is similar to the spectrum of [Ru(bpy)$_2$(bbib)][PF$_6$]$_2$. The peak for H^1 proton of the bbimb complex is shifted downfield from approximately 8.35 ppm for the bbib complex to approximately 8.6 ppm. This deshielding is most likely caused by the lack of an extended conjugation

system by the insertion of the methyl linking group. The methylene protons present as one distinct peak around 4 ppm.

The ^{1}H-NMR spectrum of [Ru(bpy)(bbimbo)][PF$_6$]$_2$ (Figure 4.4) shows several differences to the spectrum of its unoxidized form. The most significant of these is the lack of methylene peaks. The H^1 proton has dramatically shifted downfield from ~8.4 to ~9.8 ppm, due to the proximity of the proton to the electron withdrawing carbonyl group.
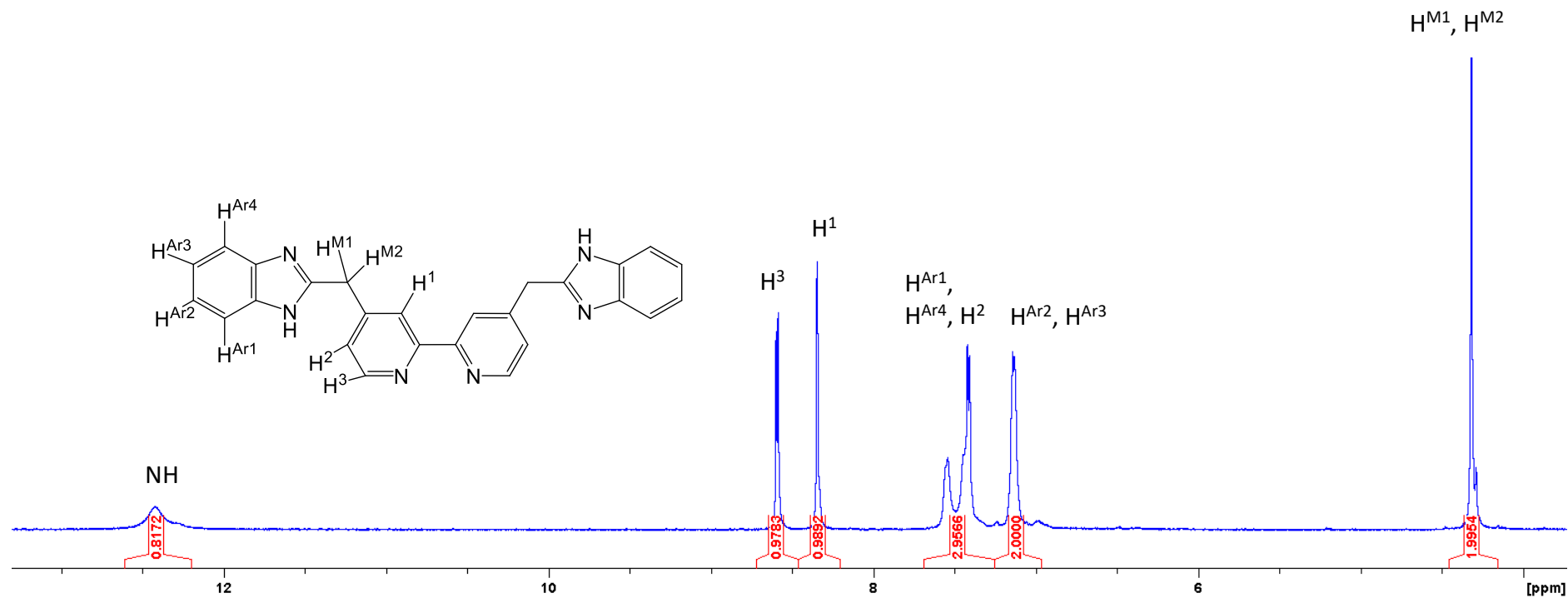
***Figure 4.3** – The ¹H-NMR spectrum of bbimb in DMSO-D₆ at 25 °C.*
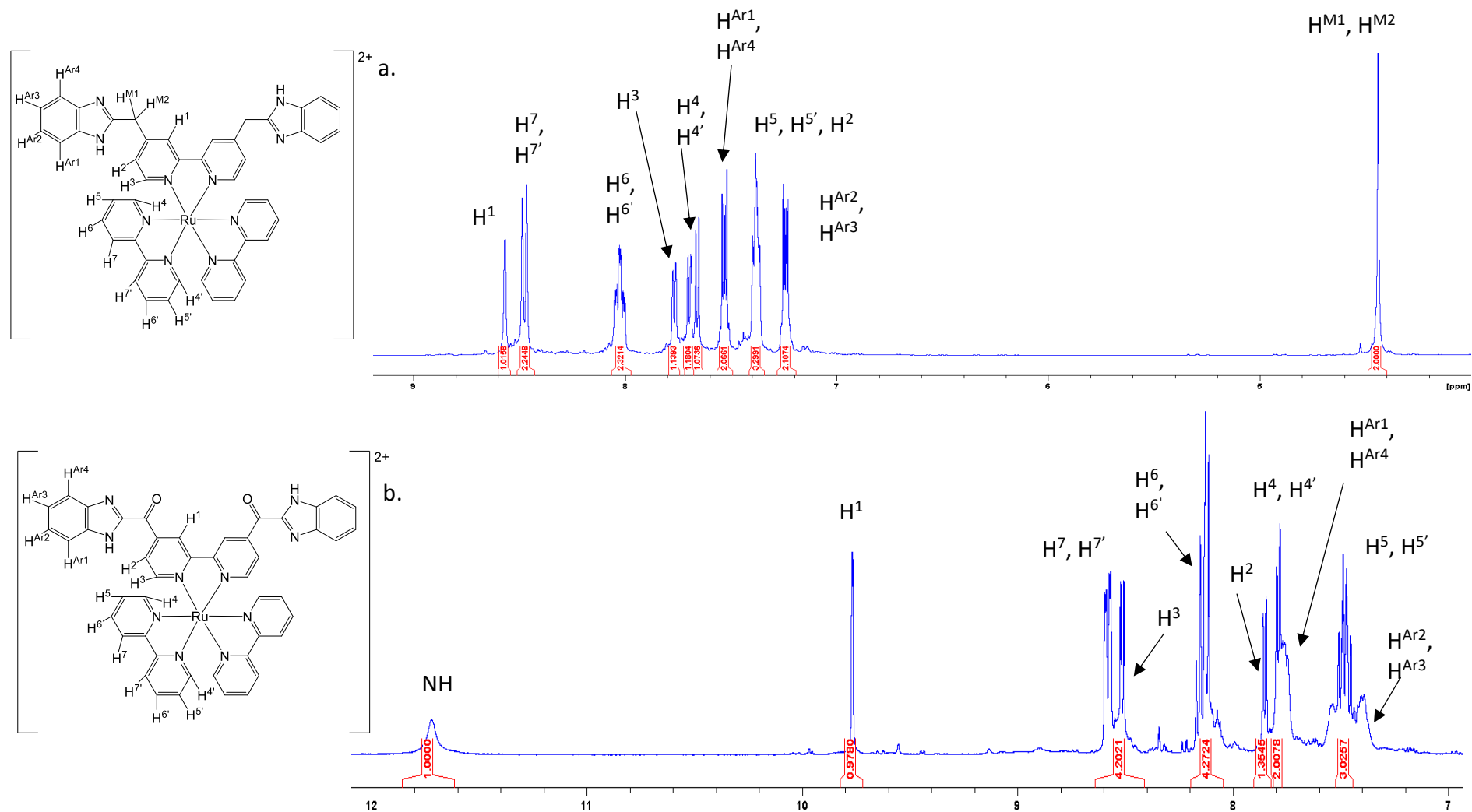
Figure 4.4 *– The ^{1}H-NMR spectra of (a.) [Ru(bpy)$_2$(bbimb)][PF$_6$]$_2$ and (b.) [Ru(bpy)$_2$(bbimbo)][PF$_6$]$_2$ in Acetone-D$_6$ at 25 °C.*

4.2.3 Photophysical Properties of [Ru(bpy)$_2$(bbimb)]$^{2+}$ and [Ru(bpy)$_2$(bbimbo)]$^{2+}$

Table 4.1 - *A table to summarise the photophysical properties of [Ru(bpy)2(bbimb)]$^{2+}$ and of [Ru(bpy)$_2$(bbimbo)]$^{2+}$*

	Absorption λ_{max} ± 1 (nm)	ε x10^{-3} (mol^{-1}cm^{-1})	Emission λ_{max} ± 1 (nm)	Quantum Yield (ϕ_{em})^2
[Ru(bpy)$_2$(bbimb)]$^{2+}$	245 286 455	75400 78260 13100	616	0.035
[Ru(bpy)$_2$(bbimbo)]$^{2+}$	285 329 427 494	73000 36230 13100 17910	729	0.00132

*The spectra of the complexes were recorded as their hexafluorophosphate salts in acetonitrile at 298 K between 200 and 600 nm. The quantum yield of each complex was calculated relative to [Ru(bpy)$_3$](PF$_6$)$_2$ as a standard in acetonitrile (0.04).[2] λ_{ex} = 450 nm when absorption = 0.1 at 450 nm.

The UV/Vis absorbance spectrum of [Ru(bpy)$_2$(bbimb)][PF$_6$]$_2$ (Figure 4.5) consists of three distinct regions. A peak at 286 nm is most likely to be representative of an overlap between $\pi_{bpy} - \pi^*_{bpy}$ and $\pi_{bbimb} - \pi^*_{bbimb}$. The spectrum is surprisingly similar to the spectrum of [Ru(bpy)$_3$]$^{2+}$.[3] Therefore this large peak is representative of another $\pi_{bpy} - \pi^*_{bpy}$ transition. Absorption also occurs at 455 nm, which corresponds to MLCT d $- \pi^*$ transitions for both bpy and bbimb.

The UV/Vis absorbance spectrum of $[Ru(bpy)_2(bbimbo)][PF_6]_2$ (Figure 4.5) is made up of four distinct regions of absorption. A LC peak is observed at 285 nm, standing for the $\pi_{bpy} - \pi^*_{bpy.}$ This region has lower energy than the analogous region of $[Ru(bpy_2(bbimb)][PF_6]_2$, potentially because this system contains additional conjugation from the sp^2 carbon of the carbonyl group. A peak is present at 329 nm, representing the $\pi_{bbimbo} - \pi^*_{bbimbo}$ transition, again displaying the changes in photophysical properties that can be caused by differences in conjugation in similar species. Further bands occur at 427 and 494 nm, relating to the MLCT $d - \pi^*_{bpy}$ and d $- \pi^*_{bbimbo}$ respectively.
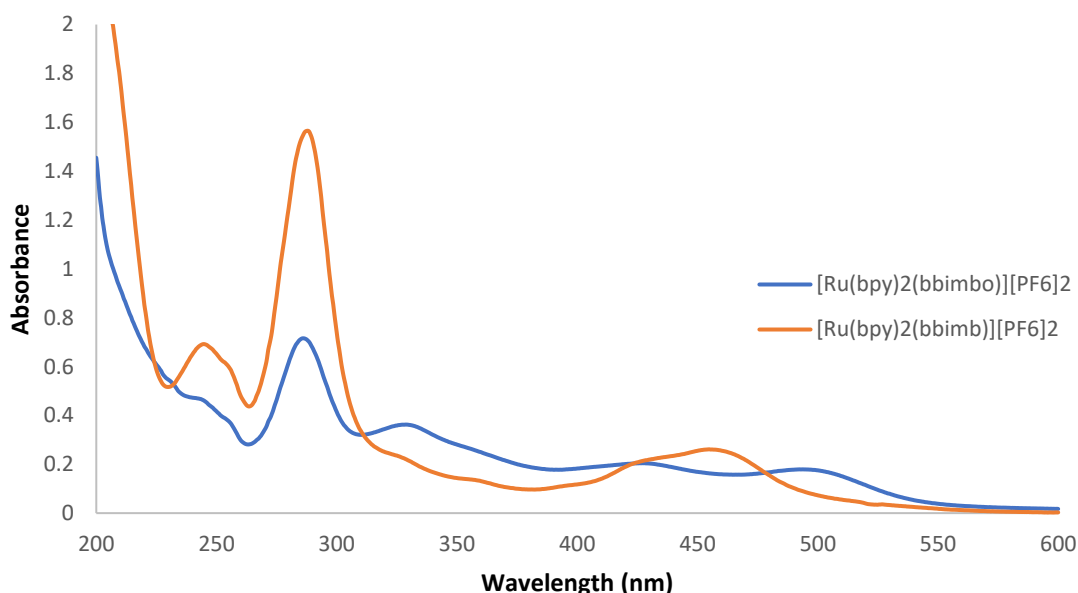
Figure 4.5 - *UV/Vis absorbance spectrum of $[Ru(bpy)_2(bbimb)][PF_6]_2$ and $[Ru(bpy)_2(bbimbo)][PF_6]_2$ measured at 25°C in MeCN.*

The emission spectra for $[Ru(bpy)_2(bbimb)][PF_6]_2$ and $[Ru(bpy)_2(bbimbo)][PF_6]_2$ were recorded between a range of 550 – 850 nm at 25 ˚C in MeCN and excited at 450 nm. Relatively strong emission is observed from $[Ru(bpy)_2(bbimb)][PF_6]_2$ with a λ_{max} of 616 nm. Weak emission is seen with $[Ru(bpy)_2(bbimbo)][PF_6]_2$ with a λ_{max} of 729 nm. This is considerably red-shifted compared to the bbimb analogue, due to the oxidation

of the ligand introducing conjugation into the system. $[Ru(bpy)_3]^{2+}$ was used as a standard luminophore (ϕ = 0.04)[2]. The relative emission quantum yield of $[Ru(bpy)_2(bbimb)][PF_6]_2$ was found to be ϕ = 0.035 and the relative emission quantum yield of $[Ru(bpy)_2(bbimbo)][PF_6]_2$ was calculated as ϕ = 0.0013. The unoxidized complex has comparable relative quantum yield values to the standard of $[Ru(bpy)_3]^{2+}$ however, the conversion to the ketone reduces the relative quantum yield considerably. This could be caused by a formation of an intramolecular hydrogen bond between the carbonyl and the NH of the benzimidazole moiety.
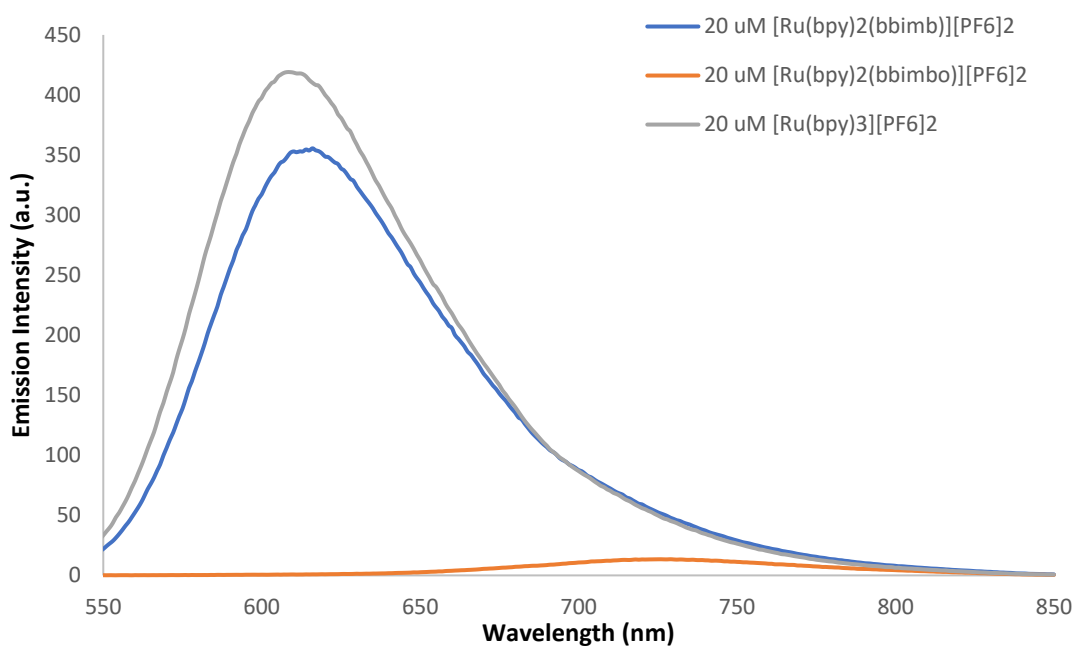
Figure 4.6 – *The comparison of emission spectra of $[Ru(bpy)_2(bbimb)][PF_6]_2$ and $[Ru(bpy)2(bbimbo)][PF_6]_2$, excited at 450 nm and recorded at 25 °C in MeCN between 550 and 850 nm.*

4.3 pH Titrations

The UV/Vis absorbance and emission spectra of racemic $[Ru(bpy)_2(bbimb)]^{2+}$ and $[Ru(bpy)_2(bbimbo)]^{2+}$ (10 µM) were recorded over a pH range of approximately 3 – 12.5 (Section 6.5). The UV/Vis absorbance spectra of $[Ru(bpy)_2(bbimb)]^{2+}$ (Figure 4.7) show several changes as a function of pH. The methyl group adds a break between the conjugated system of the metal centre and bipyridine ligands and the benzimidazole groups. Therefore, the complex can be considered as two separate systems. A slight decrease in absorbance is observed (0.89 - 0.72) from approximately pH 3 – 7 at 243.5 nm, after which no further change is seen. This peak represents an overlap of the MLCT $d – \pi^*_{bbimb}$ and MLCT $d – \pi^*_{bpy}$ transitions. The ligand is most likely protonated in acidic pH, which lowers the energy requirement for the promotion of electrons from the d orbital of the metal centre to the π^* orbital of the functionalised ligand. Around pH 6, the ligand becomes deprotonated, however, as this is also a region of light where phosphate anions absorb, this could also be the reason for the change in acidic environments where phosphate concentrations are higher. As pH is increased, there is a simultaneous peak increase and decrease in intensity at 462 and 474 nm, respectively. Both peaks are in the region of the MLCT $d – \pi^*_{bbimb}$ transition, indicative of a deprotonation of the benzimidazoles resulting in a peak that undergoes a redshift.
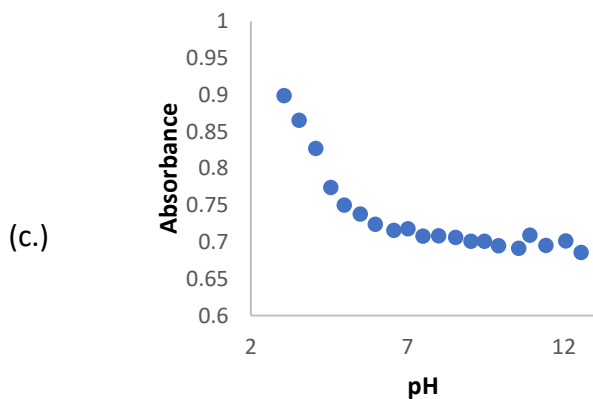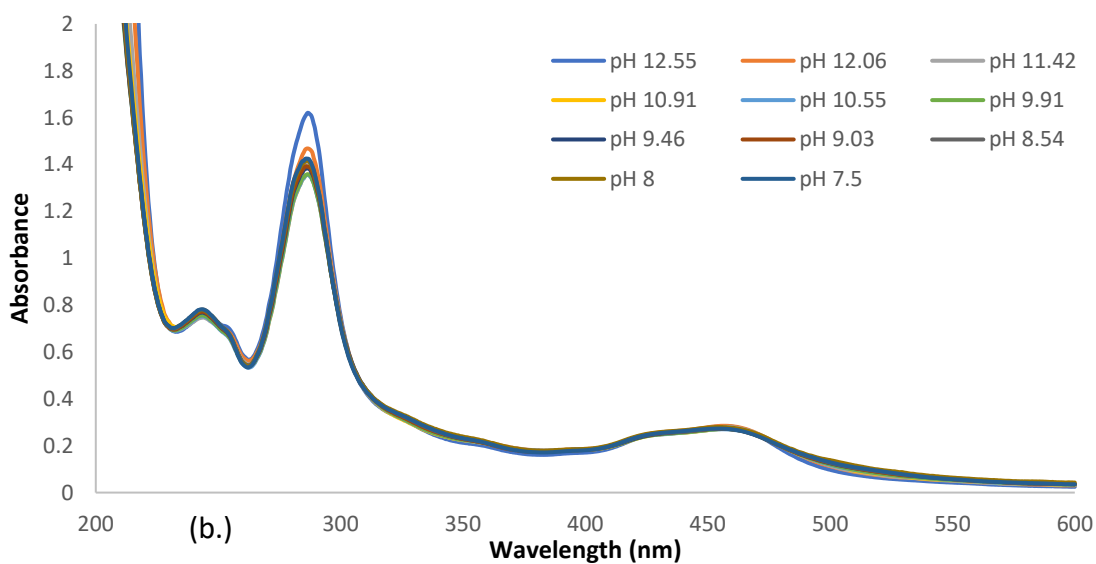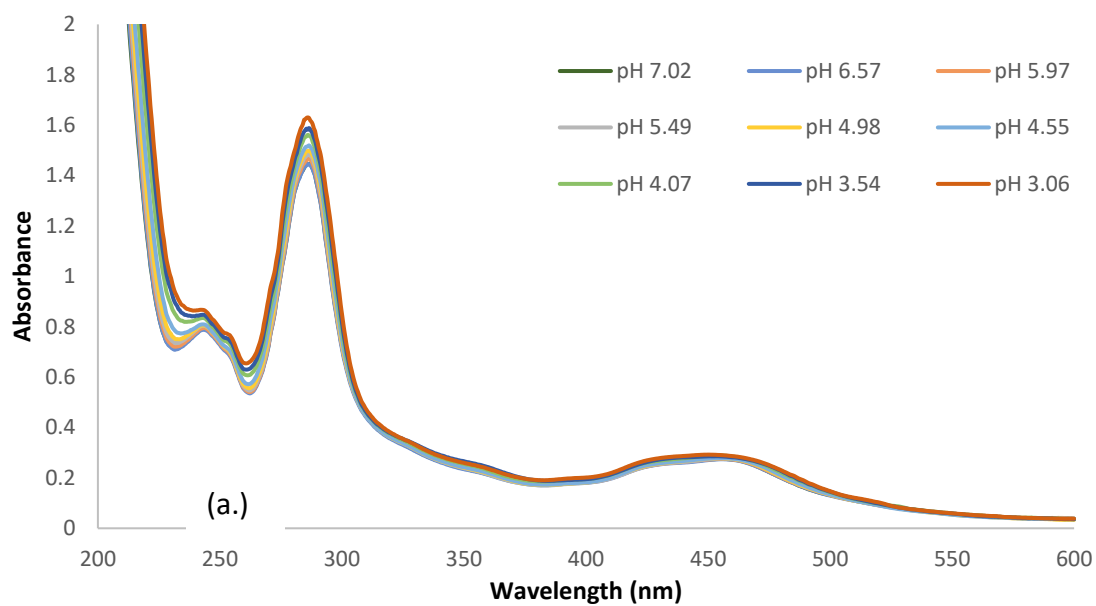
Figure 4.7 – *(a.) UV/Vis absorbance spectra between pH of approximately 3 – 7 and (b.) UV/Vis absorbance spectra between pH of approximately 7.5 – 12.5 of [Ru(bpy)₂(bbimb)]²⁺ between 200 – 600 nm recorded at 25 °C. (c.) Plot of absorbance values at 243.5 nm.*

The emission spectra of $[Ru(bpy)_2(bbimb)]^{2+}$ varies significantly with pH (Figure 4.8). Three main areas of change can be seen, the first one between pH 3 and pH 6.5, the second between pH 7 and pH 10 and the third between pH 10 and pH 12.5. In the first section at an acidic pH range, a large emission intensity is observed (50.5 – 89.9 a.u.) while the λ_{max} decreases from 640 to 621 nm. In this pH range, the bbimb ligand is presumed to be protonated, here the energy gap between the ground state and $\pi^*_{bbimbH+}$ is greater than the energy gap between the ground state and π^*_{bpy}, therefore the emission is mainly coming from the π^*_{bpy} – d transition due electrons being excited to the lower energy level of π^*_{bpy}.

Between pH 6.5 and pH 10, there is minimal change in both emission intensity and maximum wavelength. The bbimb ligand is no longer protonated and is neutrally charged. As there are no variations across this pH range, it is possible that dual emission is occurring in this range as the energy levels of π^*_{bpy} and π^*_{bbimb} are in similar positions, and therefore the energy is decaying from both.

The third area, at high pH (pH 10 and above), shows a further increase in emission intensity (78 – 105 a.u.) and decrease in maximum wavelength (621 – 614 nm). In this pH range, the bbimb ligand is deprotonated on the benzimidazole moieties. The negative change on the functionalised ligand has increased the energy gap between the excited state on the bbimb ligand and the ground state.
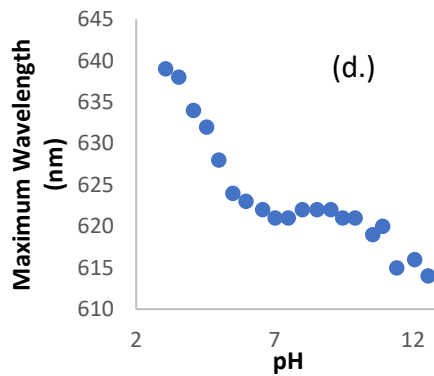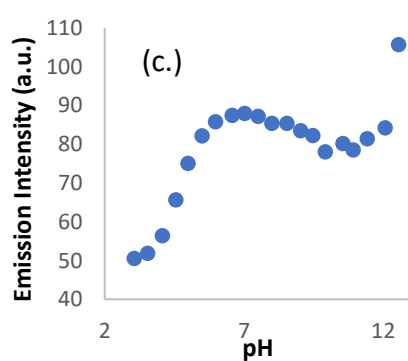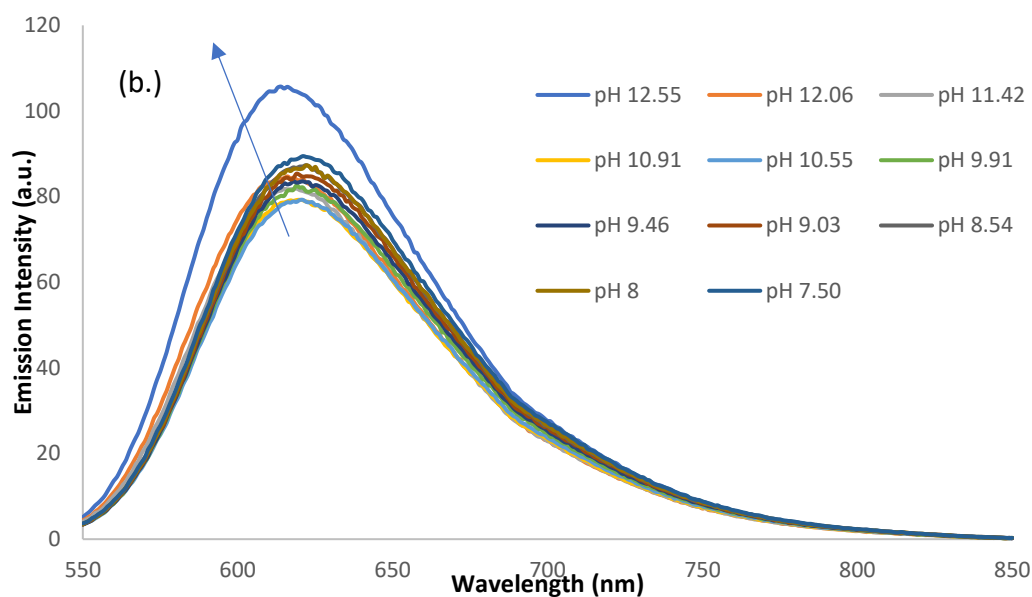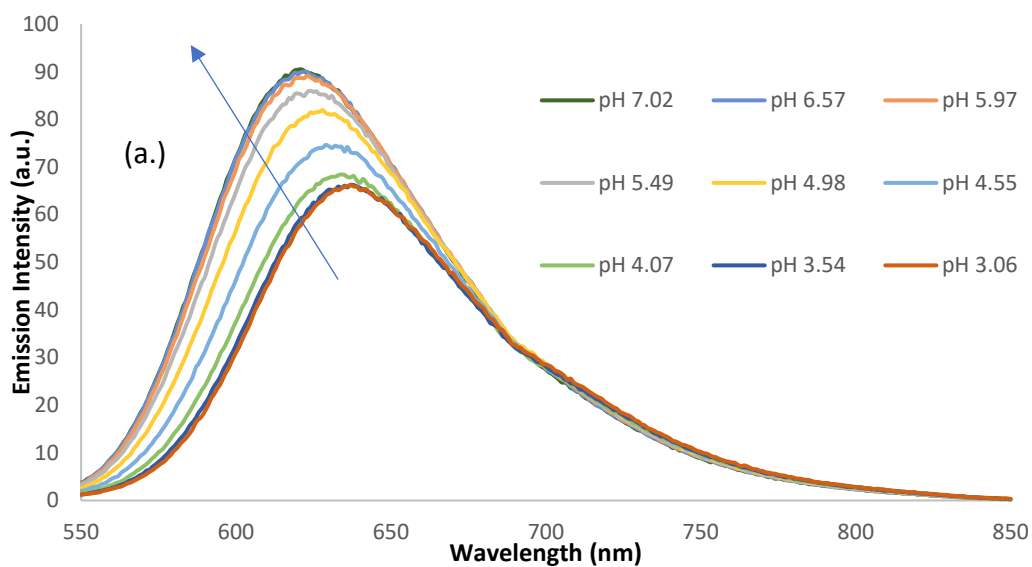
Figure 4.8 *– Emission spectra of [Ru(bpy)₂(bbimb)]²⁺ at (a). pH ~3 to ~7, and (b).*
pH ~7.5 to ~12.5, (c). plotted emission intensity values and (d). maximum wavelength.
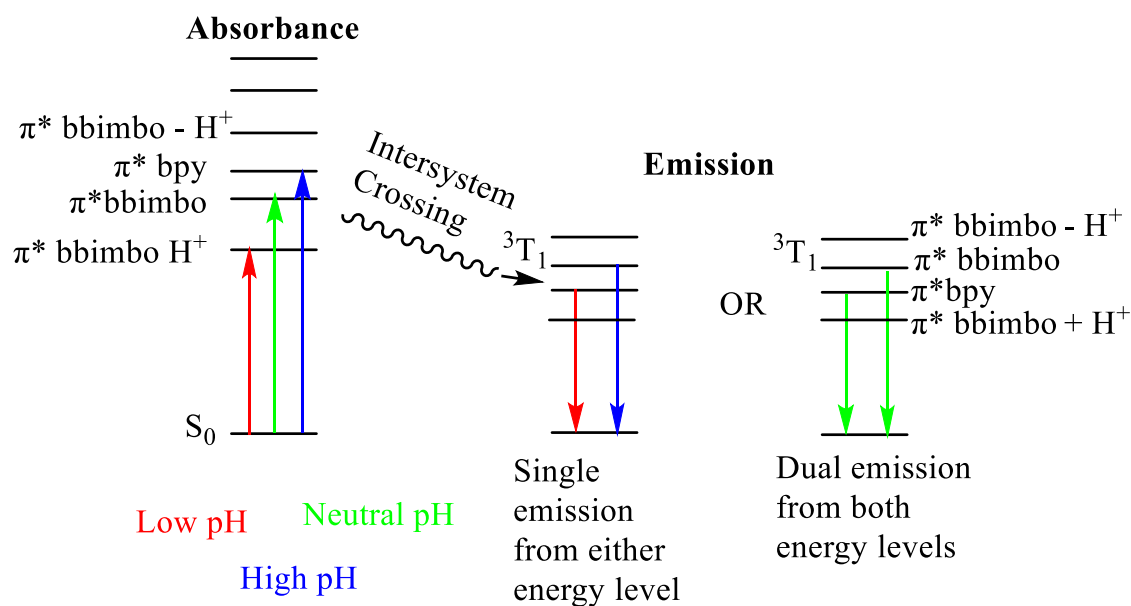
Figure 4.9 – *A Jablonski diagram to describe the changes in transitions for [Ru(bpy)$_2$(bbimbo)]$^{2+}$ as a function of pH.*

The UV/Vis absorbance spectra of [Ru(bpy)$_2$(bbimbo)]$^{2+}$ (Figure 4.10) displays considerable changes with variation in pH. An initial peak is present at approximately 512 nm between pH 3 and pH 7. This peak represents the MLCT d – $\pi^*_{\text{bbimboH+}}$ transition. The absorbance intensity decreases between pH 7.5 and pH 12.5, whilst simultaneously another peak is increasing in intensity at approximately 499 nm. This blue shift in the MLCT position results from the removal of protons from the benzimidazole by the basic environment. There is further change in peak intensity at 395 nm in basic environments, characteristic of the d – π^*_{bbimbo} transition. There is no observable change between pH 3 and pH 8.5, where the bbimbo ligand is neutrally charged. At pH 9, the functionalised ligand becomes deprotonated, therefore negatively charged. This suggests that the energy gap between d orbital of the metal and the π^* orbital of the deprotonated bbimbo species has increased (Figure 4.9). The absorbance of light at low and neutral pH levels would be mainly from d – π^*_{bbimbo}. Once the pH is

basic and the ligand has been deprotonated, the dominant transition switches to $d - \pi^*_{bpy}$ due to the smaller distance between energy levels.
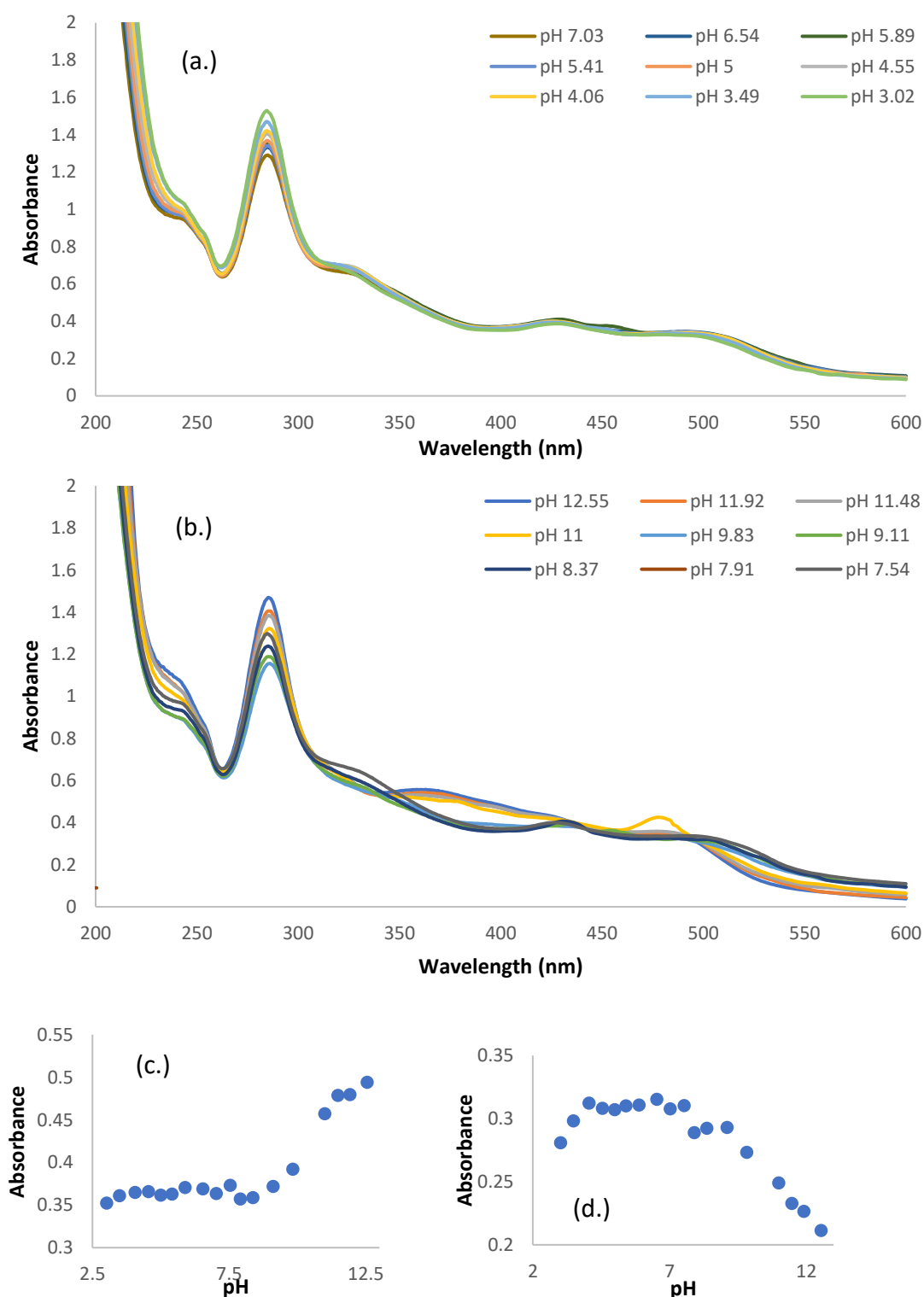
Figure 4.10 *– (a.) UV/Vis absorbance spectra between pH of approximately 3 – 7 and (b.) UV/Vis absorbance spectra between pH of approximately 7.5 – 12.5 of [Ru(bpy)₂(bbimbo)]²⁺ between 200 – 600 nm recorded at 25 °C. (c.) Plot of absorbance values at 395 nm and (d.) 511.5 nm.*

The emission spectra of $[Ru(bpy)_2(bbimbo)]^{2+}$ display change as a function of pH (Figure 4.11). The complex itself is barely emissive, therefore the change in emission intensity is difficult to quantify. However, a definite blue shift is observed between pH 5 and pH 10 (641 – 634 nm). There is no movement in maximum wavelength between pH 3 and pH 5, when the bbimbo ligand would be protonated in the acidic environment. It is most likely that the complex is emitting from the π^*_{bpy} - d transition. At the higher pH range (pH 10 – 12.5) the functionalised ligand is a negatively charged, causing the dominant transition to swap to π^*_{bbimbo} – d. This is caused by the negative charge on the bbimbo increasing the energy gap from the electrons to return to the ground state from the excited state. Between pH 5 and pH 10, a shoulder is visible in the emission spectra at approximately 715 nm. This is potentially caused by dual emission from both π^*_{bbimbo} – d and π^*_{bpy} – d transitions. The emission is very weak however, and it must be considered that there could be some contamination of unoxidized $[Ru(bpy)_2(bbimb)]^{2+}$ present potentially.
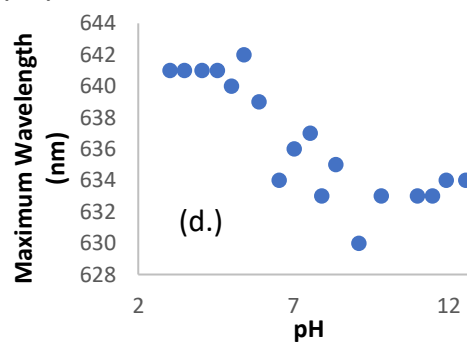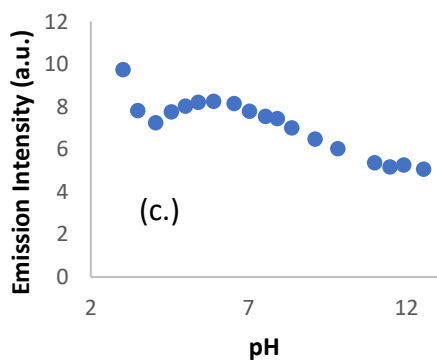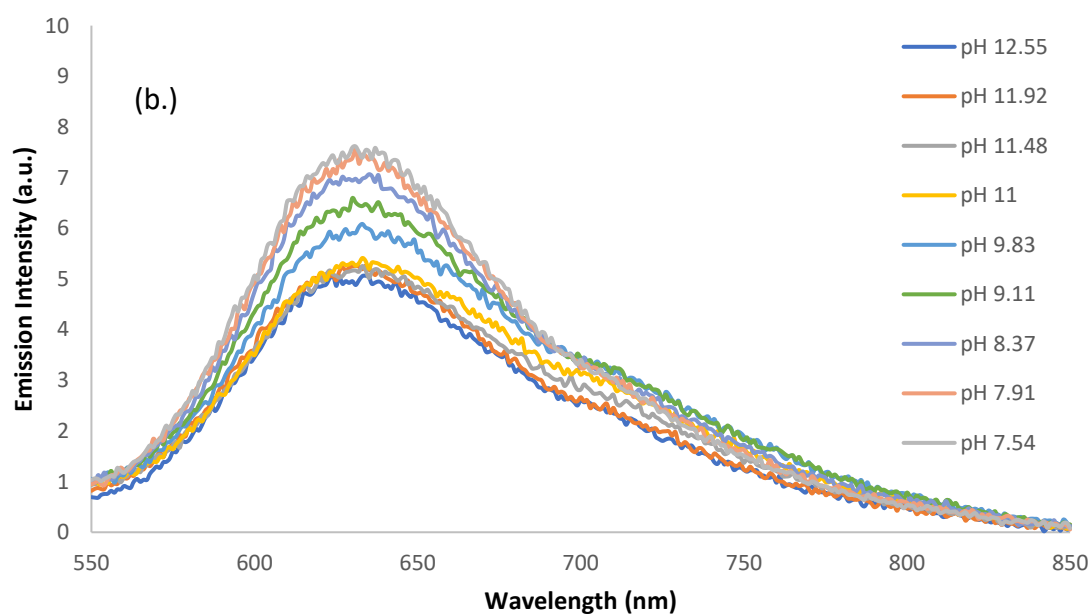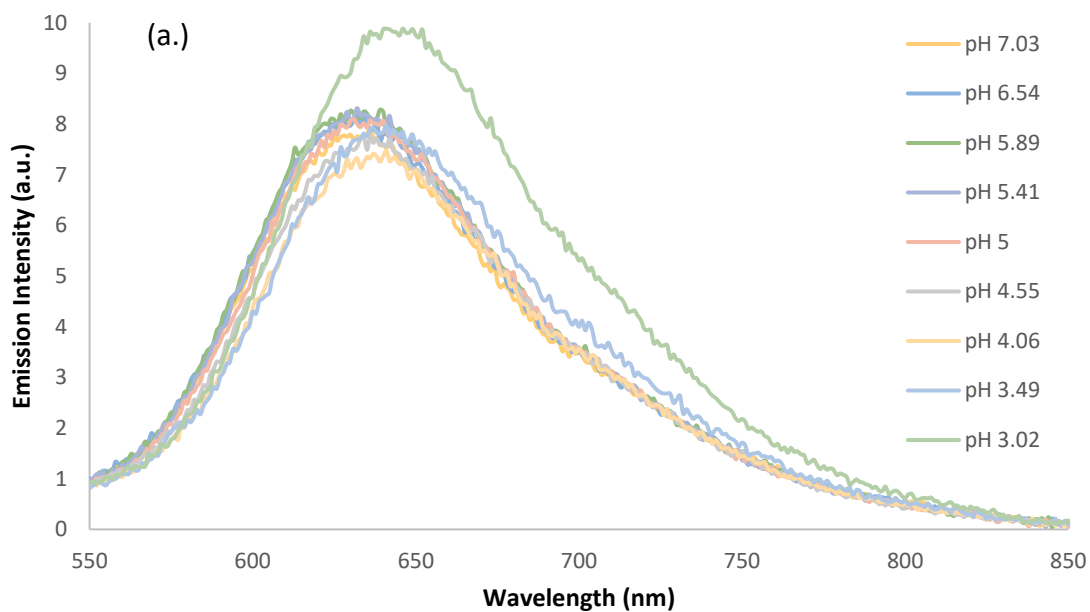
Figure 4.11 - *Emission spectra of [Ru(bpy)₂(bbimbo)]²⁺ at (a). pH ~3 to ~7, and (b). pH ~7.5 to ~12.5, (c). plotted emission intensity values and (d). maximum wavelength.*

Table 4.2 - *Estimated experimental pK$_a$ and pK$_b$ values for [Ru(bpy)$_2$(bbaib]$^{2+}$ and [Ru(phen)$_2$(bbaib)]$^{2+}$, determined via line of best fit using QTIPlot, compare to the literature values for pK$_a$ and pK$_b$ of benzimidazole.*[3]

	pK$_a$ of ground state	pK$_a$ of excited state	pK$_b$ of ground state	pK$_b$ of excited state
[Ru(bpy)$_2$(bbimb)]Cl$_2$	~4.5	~5.5	~10	~10
[Ru(bpy)$_2$(bbimbo)]Cl$_2$	~4.5	~5	~10	~10.5
Benzimidazole	5.6	-	12.8	-

The ground and excited state pK$_a$ and pK$_b$ of [Ru(bpy)$_2$(bbimb)]$^{2+}$ and [Ru(bpy)$_2$(bbimbo)]$^{2+}$ have been considered using mid-point estimation (Table 4.2). The ground state pK$_a$ of [Ru(bpy)$_2$(bbimb)]$^{2+}$ was estimated to be 4.5 with a pK$_b$ of around 10. [Ru(bpy)$_2$(bbimbo)]$^{2+}$ had an estimated ground state pK$_a$ and pK$_b$ of 4.5 and 9, respectively. The excited state pK$_a$ and pK$_b$ for [Ru(bpy)$_2$(bbimb)]$^{2+}$ were approximated to be 5.5 and 10, while the values were found to be around 5 and 10.5 for [Ru(bpy)$_2$(bbimbo)]$^{2+}$. The determined pK$_a$ and pK$_b$ data was found to be lower than the literature values found for benzimidazole.[3] These experiments were run in Robinson-Britton buffer, and so the lower pK values may be due to the influence of bound phosphate, acetate and borate in the solution.

4.4 Anion Binding Studies

The anion recognition capabilities of [Ru(bpy)$_2$(bbimb)][PF$_6$]$_2$ and [Ru(bpy)$_2$(bbimbo)][PF$_6$]$_2$ were studied via the means of UV/Vis absorbance, emission and ^{1}H-NMR spectroscopy titrations (Appx. 57 – 63, Appx. 64 – 70, Appx. 71 – 75, respectively). In the case of UV/Vis and emission titrations, the solutions were comprised of 95% DMSO / 5% distilled water and anion (H$_2$PO$_4^-$, Br$^-$, Cl$^-$, Ac$^-$) was

sequentially added up to 250 µM (Ten equivalents) with a $[Ru(bpy)_2(bbimb)][PF_6]_2$ and $[Ru(bpy)_2(bbimbo)][PF_6]_2$ concentration of 25 µM. The experiments were undertaken as described in Section 6.6.

^{1}H-NMR titrations of $[Ru(bpy)_2(bbimb)][PF_6]_2$ and $[Ru(bpy)_2(bbimbo)][PF_6]_2$ (5 mM, 0.5 ml) with $H_2PO_4^-$, Cl^- and Ac^- added sequentially up to Ten equivalents (50 mM, 1.5 ml added overall). All samples were made up in DMSO-D_6 / 95% D_2O.

4.4.1 UV/Vis and Emission Titrations

A series of sequential addition titrations were recorded using $[Ru(bpy)_2(bbimb)][PF_6]_2$ and $[Ru(bpy)_2(bbimbo)][PF_6]_2$ and the data has been normalised to account for dilution effects in all cases ($H_2PO_4^-$, Cl^- and Ac^-) there is no observable change in the absorbance spectra with both $[Ru(bpy)_2(bbimb)][PF_6]_2$ and $[Ru(bpy)_2(bbimbo)][PF_6]_2$ (Appx. 54 – 60).

The sequential addition of TBA Cl to $[Ru(bpy)_2(bbimb)][PF_6]_2$ similarly showed no change in emission (Figure 4.12). It is not possible to determine if interaction is occurring from this data alone. The data for the emission titration of $[Ru(bpy)_2(bbimbo)][PF_6]_2$ was lost and therefore it is unknown whether any change in emission occurred upon adding Cl^-.

Upon sequential addition of Ac^- (up to ten equivalents) to $[Ru(bpy)_2(bbimb)][PF_6]_2$ there was no change observed in either the emission intensity or the maximum wavelength (Figure 4.12). This implies that there are no hydrogen bonds forming

163

between the anion and complex in this medium, therefore no interaction is occurring. The lack of apparent hydrogen bond formation could be due to the removal of extended conjugation in the bbimb ligand by the addition of the methyl group. This removal could cause the loss of resonance-assisted hydrogen bonding, where hydrogen bonding is strengthened by the π-conjugation of one or both of the participating molecules.[4] However, it is still possible that there is an interaction with acetate, but with the lack of conjugation, it is not affecting the emissive component.

However, addition of dihydrogen phosphate to $[Ru(bpy)_2(bbimb)][PF_6]_2$ (Figure 4.12) results in a quenching of emission from 60 to 12 a.u. between 0 and 1 equivalents, thereafter there is no further change in emission intensity. It can be inferred from this data that $H_2PO_4^-$ interacts with the complex in 1:1 stoichiometry. The quenching of emission is most likely caused by the opening of radiationless decay pathways by the formation of hydrogen bonds between the anion and complex.

The sequential titration of dihydrogen phosphate with $[Ru(bpy)_2(bbimbo)][PF_6]_2$ also resulted in a quenching to a similar degree as with $[Ru(bpy)_2(bbimb)][PF_6]_2$. The plot of emission intensity versus equivalents of anion added are similar enough to posit the hypothesis that the dihydrogen phosphate is potentially causing or increasing the rate of oxidation of $[Ru(bpy)_2(bbimb)][PF_6]_2$ to $[Ru(bpy)_2(bbimbo)][PF_6]_2$. Further experiments are required in order to determine whether this is the case, such as ^{1}H-NMR studies to observe whether there is removal of the methyl protons over time in the presence of $H_2PO_4^-$. This could be caused by the formation of phosphoric acid resulting in a slight acidity of the solution, which has been observed to increase the rate of oxidation.

The emission intensity observed with $[Ru(bpy)_2(bbimbo)][PF_6]_2$ (Figure 4.12) decreases upon introduction of Ac^-, unlike the unoxidized counterpart. The complex is possibly able to interact by the formation of hydrogen bonds between the carbonyl oxygen of the bbimbo ligand and the protonated oxygen of the acetate and the -NH proton of the benzimidazole and the carbonyl oxygen of the acetate (Figure 4.13). The decrease in emission intensity ceases at approximately two equivalents of acetate added, implying that a 2:1 stoichiometry between anion and complex is happening.
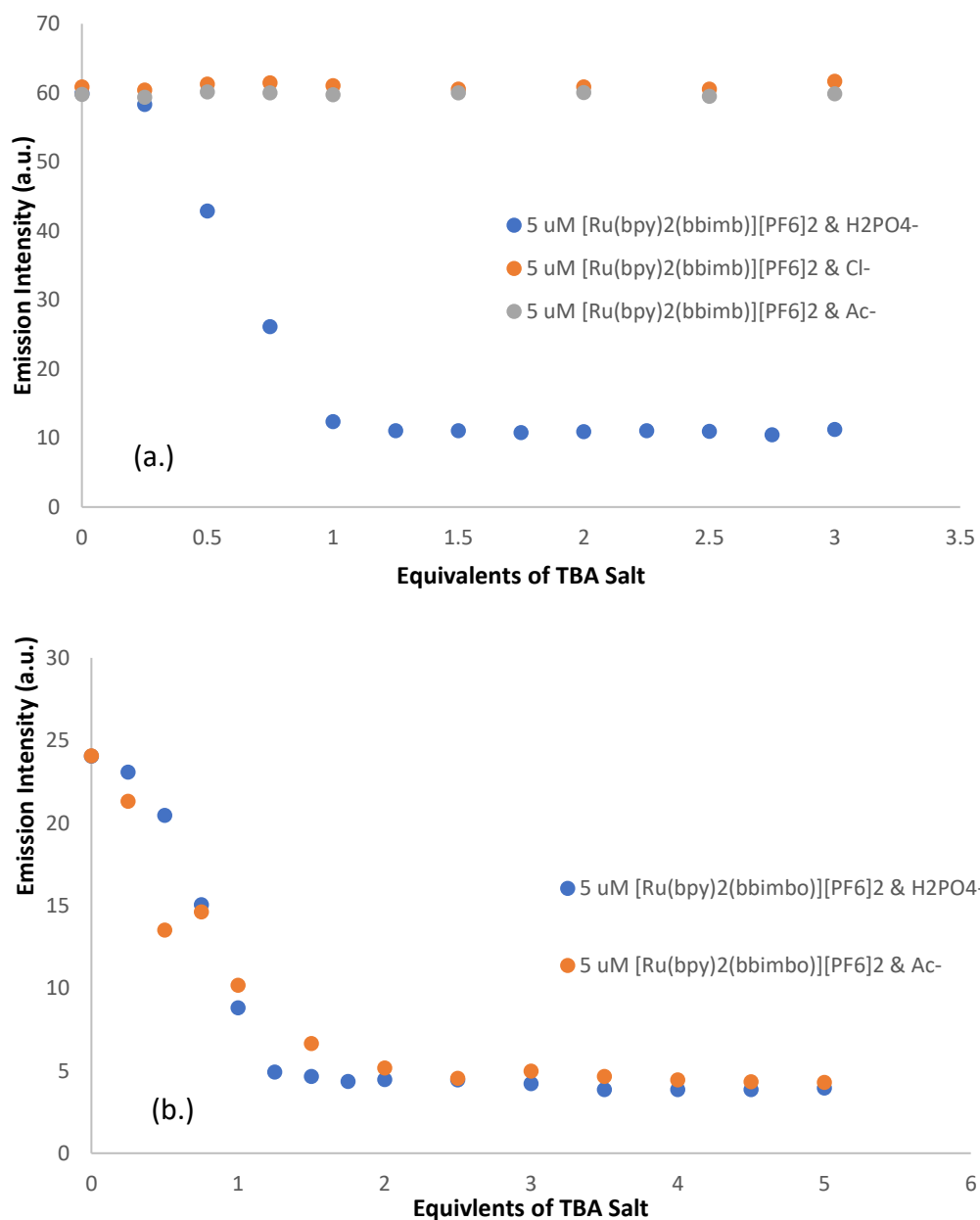
Figure 4.12 - *Maximum emissive wavelengths of (a.) $[Ru(bpy)_2(bbimb)][PF_6]_2$ and (b) $[Ru(bpy)_2(bbimbo)][PF_6]_2$ with increasing anion concentration (Ac^-, Cl^-, $H_2PO_4^-$). Spectra run at 25 °C in DMSO / 5% deionised water.*
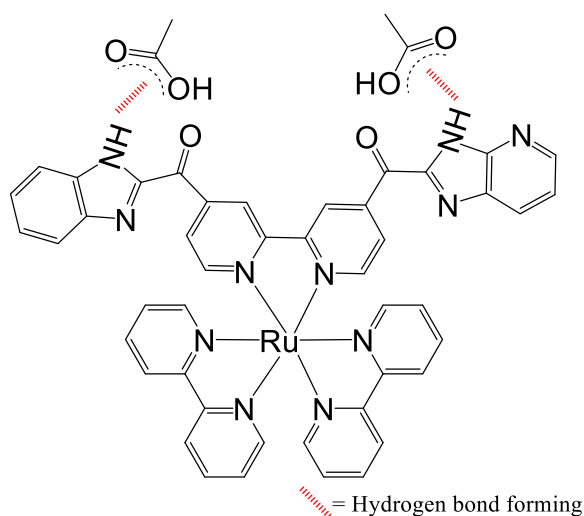
Figure 4.13 – *A diagram illustrating how acetate anions can potentially interact with bbimbo.*

4.4.2 ^{1}H-NMR Spectroscopy Titrations

^{1}H-NMR titrations of [Ru(bpy)$_2$(bbimb)][PF$_6$]$_2$ and [Ru(bpy)$_2$(bbimbo)][PF$_6$]$_2$ (10 µM) (Appx. 68 – 72) were undertaken with TBA Cl up to ten equivalents (100 µM). There were no observable shifts in any peak positions, implying that no interaction is taking place, which is in agreement with the UV/Vis absorbance and emission titrations above. Sequential addition of TBA acetate into a sample of [Ru(bpy)$_2$(bbimb)][PF$_6$]$_2$ results in no change in peak positions, implying that there is no interaction occurring between the complex and anion. This corroborates with the data gathered from the emission sequential addition titrations.

The titration of [Ru(bpy)$_2$(bbimb)][PF$_6$]$_2$ and dihydrogen phosphate (Figure 4.14) shows a loss of one peak at 4.2 ppm. This peak is representative of one of the protons on the bbimb methyl group. This proton is most likely either lost to the phosphate anion or is undergoing solvent exchange. A downfield shift is observed between 8.79 and 9.18

ppm. This peak is indicative of the H^3 proton on the bbimb 2,2'-bipyridine ring which is being deshielded by the presence of the phosphate anion, by moving electron density from the ring to the methyl group in order to compensate for the loss of a methyl proton.

The ^{1}H-NMR titration spectra of [Ru(bpy)$_2$(bbimbo)][PF$_6$]$_2$ with acetate and dihydrogen phosphate show minimal change upon introduction of either anion. This does not mean that there is no interaction occurring, but it is not visible using ^{1}H-NMR spectroscopy, especially as hydrogen bond formation has been previously established in this thesis using emission spectroscopy (Section 4.4.1).
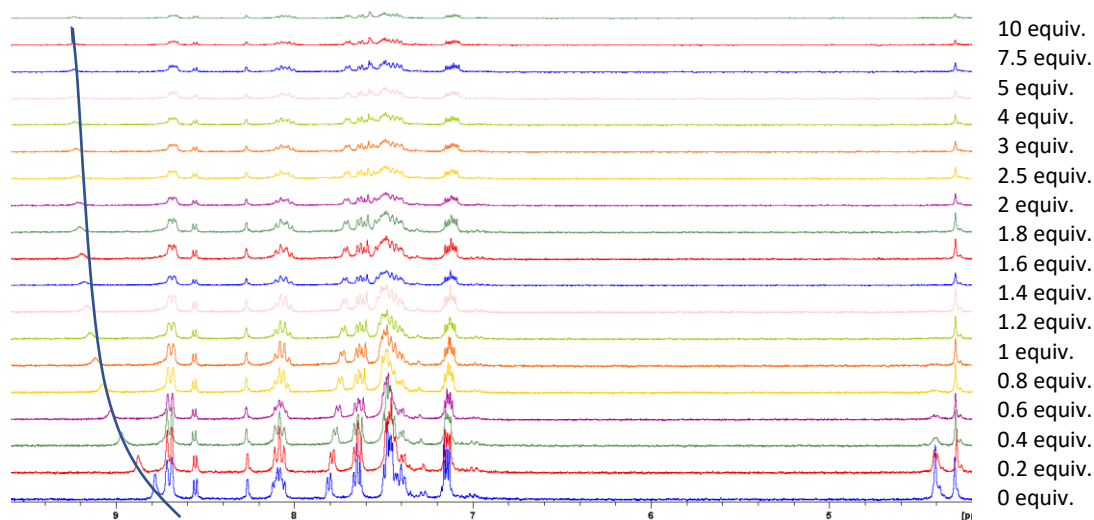
Figure 4.14 *– ^{1}H-NMR titration of [Ru(bpy)$_2$(bbimb][PF$_6$]$_2$ and H$_2$PO$_4^-$ in DMSO/5% deuterated water.*

4.4.3.1 Notes on ^{1}H-NMR Spectroscopy Titrations

A frequent problem that occurred within these experiments was that with increasing additions of the anion solution, resolution was lost in the spectra and the signal to noise ratio decreased due to dilution effects or the formation of precipitate. This meant it was not possible to completely identify if peaks were shifting within the spectra, therefore some crucial data could have been missed.

4.5 DNA Binding Studies

4.5.1 UV/Vis and Emission Titrations

The UV/Vis absorbance and emission spectra of [Ru(bpy)$_2$(bbimb)][PF$_6$]$_2$ (10 µM) and [Ru(bpy)$_2$(bbimbo)][PF$_6$]$_2$ (10 µM) were recorded in the presence and absence of *ct*-DNA (up to 50 µM) between a range of 325 – 600 nm for the UV/Vis absorbance and 550 – 850 nm for the emission spectra. The samples were made up in tris buffer (pH 7.2) with 5% DMF solution. Upon addition of 5 µM (0.5 equivalents) of DNA the absorbance spectra of [Ru(bpy)$_2$(bbimb)][PF$_6$]$_2$ exhibits a small decrease in absorbance This could potentially indicate that there is an interaction, however the change is very slight and could be accounted for by scattering from the sample. The result is not consistent with a deprotonation (as determined in Section 4.3). DMF was added to the solvent to prevent precipitation of *ct*-DNA that was observed in 100% tris buffer with [Ru(bpy)$_2$(bbimb)][PF$_6$]$_2$ and [Ru(bpy)$_2$(bbimbo)][PF$_6$]$_2$.

The emission spectra of [Ru(bpy)$_2$(bbimb)][PF$_6$]$_2$ (Figure 4.15) similarly show no change upon initial addition of *ct*-DNA, or with increasing concentration in a DMF and tris buffer mixture. There is no obvious change in the λ_{max}, further indicative that the
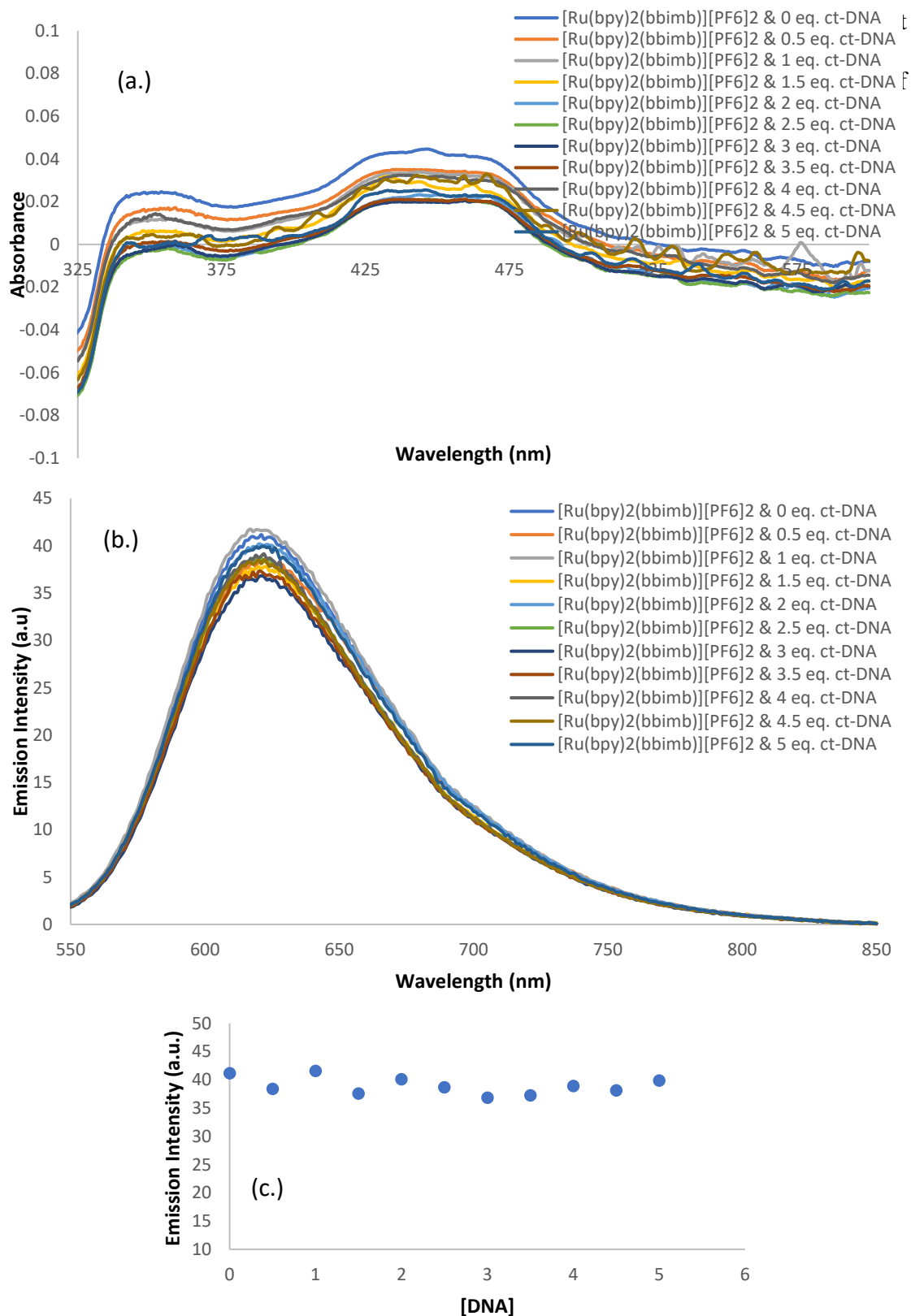
Figure 4.15 – *(a.) UV/Vis absorbance titration, (b) Luminescence emission titration of [Ru(bpy)₂(bbimb)][PF₆]₂ (10 µM) in the absence and presence of ct-DNA in tris buffer/5% DMF and (c.) the emission intensity values at 620 nm.*

Upon addition of 5 µM of *ct*-DNA, the UV/Vis spectra of [Ru(bpy)(bbimbo)][PF$_6$]$_2$ (Figure 4.16) displays an initial decrease in absorbance across the spectrum from 0.08 to approximately 0.04 at 345 nm. This decrease does not change upon further additions of DNA. There is scattering seen in some of the recorded spectra, most likely due to air bubbles in the cell. However, the difference in chromophore absorbance suggests that the oxidation of [Ru(bpy)$_2$(bbimb)][PF$_6$]$_2$ results in a change in interaction, most likely due to the planarity that the carbonyl group instils into the molecule. The only potential evidence that [Ru(bpy)$_2$(bbimb)][PF$_6$]$_2$ interacts with DNA is the formation of precipitate when DMF is not present in the solvent. The experiment should be repeated to ensure that the initial spectrum collected is not erroneous.

The emission spectra of [Ru(bpy)(bbimbo)][PF$_6$]$_2$ (Figure 4.16) exhibits enhancement of emission intensity upon initial introduction of 5 µM of *ct*-DNA, from 8.83 to 13.99 a.u at λ_{max}. There is no change in λ_{max}, signifying that the compound is not being deprotonated. This is a relatively large increase in intensity considering that the complex alone has very weak emission resulting from the entry of the complex into the hydrophobic region of the DNA strand. This result suggests that an interaction is occurring between complex and nucleic acid but does not indicate what the mode of binding is, or how strong it is.
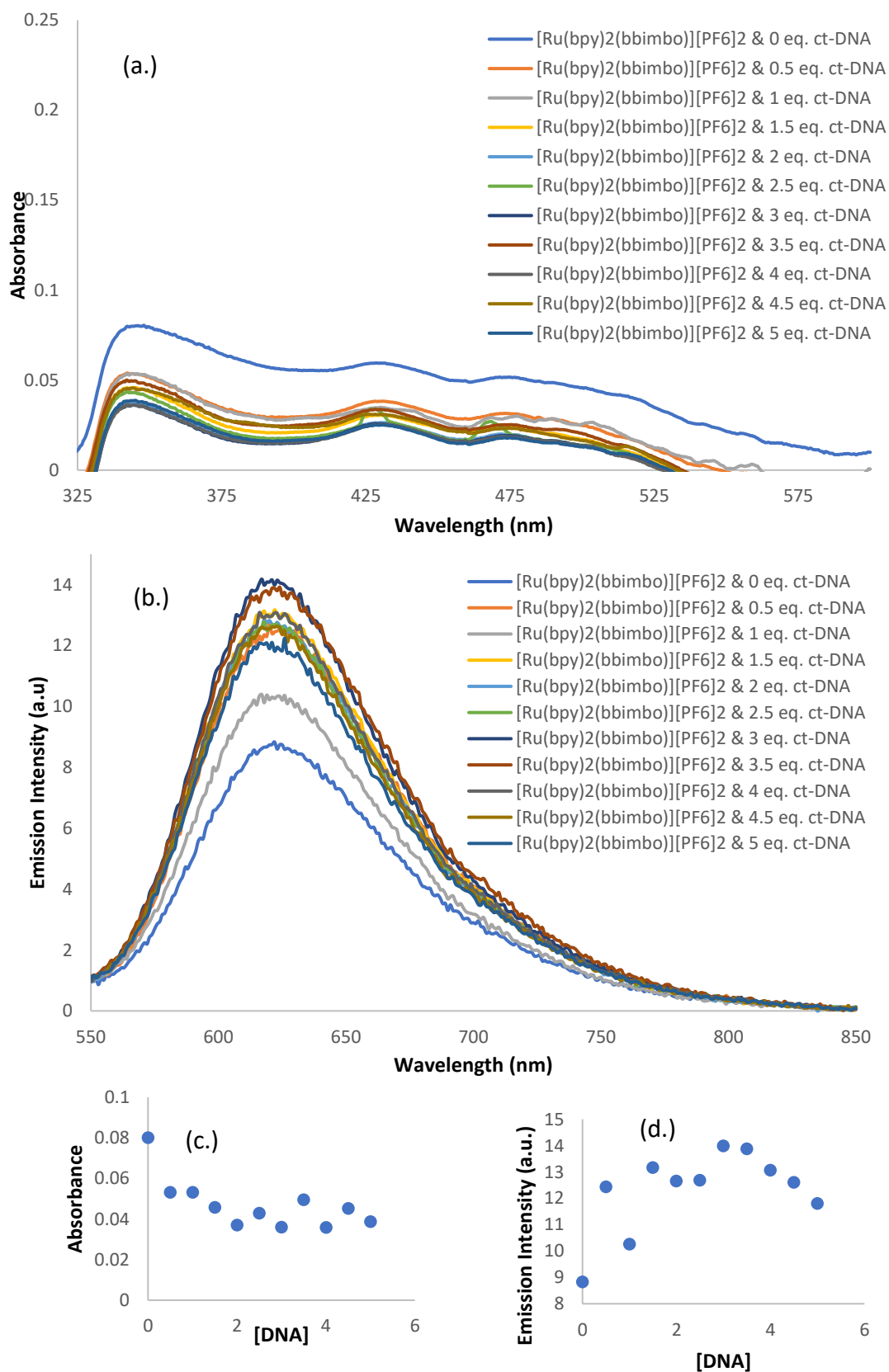
Figure 4.16 *– (a.) UV/Vis absorbance titration, (b) Luminescence emission titration of [Ru(bpy)₂(bbimbo)][PF₆]₂ (10 µM) in the absence and presence of ct-DNA in tris buffer/5% DMF and (c.) the emission intensity values at 624 nm.*

4.5.3 Thermal Denaturation Studies

The thermal denaturation profiles of *ct*-DNA (25 µM) in the absence and presence of 10 and 25 µM of racemic [Ru(bpy)$_2$(bbimb)][PF$_6$]$_2$ and [Ru(bpy)$_2$(bbimbo)][PF$_6$]$_2$ were determined using CD spectroscopy. Samples were made up of 90:10 tris buffer (5 mM Tris-HCl, 50 mM NaCl, pH 7.2) and DMF (Chapter Six). Denaturation temperatures were estimated via the calculation and midpoint analysis of "melt curves" using QTI plot (Figure 4.17, Table 4.3).

The *ct*-DNA control experiments show two different denaturation temperatures (Table 4.3). The control experiment for [Ru(bpy)$_2$(bbimb)][PF$_6$]$_2$ gave an approximate denaturation temperature of 78 °C, which is a similar result to the control experiments in previous chapters. However, the *ct*-DNA control experiment for [Ru(bpy)$_2$(bbimbo)][PF$_6$]$_2$ offered an approximate denaturation temperature of around 89 °C, which is much higher than the temperature expected. This may be caused by the concentrated DNA solution being left in a cold environment for a long period of time, and some of the B-DNA has converted to another form. This may also explain the increase in signal strength between 250 and 300 nm as temperature increases between 20 and 30 °C.

The observed denaturation temperature for *ct*-DNA with [Ru(bpy)$_2$(bbimb)][PF$_6$]$_2$ was 74 °C (Table 4.3), giving an overall decrease in temperature of around 4 °C. This is comparable to the results given with the bbib and bbaib complexes of Chapters Two and Three, suggesting that the bbimb complexes interact with DNA in a similar manner. Once again, the data only confirms that some form of interaction is occurring between

DNA and complex, but not what type. It is probably not intercalation as the denaturation temperature does not increase but decreases, potentially indicating groove binding.

Table 4.3 - *Observed Tm Values for ct-DNA with 10 μM of complex.*

Experiment	Melting Temperature (°C)	ΔT_m (°C)
Calf thymus DNA	78	N/A
[Ru(bpy)$_2$(bbimb)][PF$_6$]$_2$	74	-4
Calf thymus DNA	88	N/A
[Ru(bpy)$_2$(bbimbo)][PF$_6$]$_2$	88	0
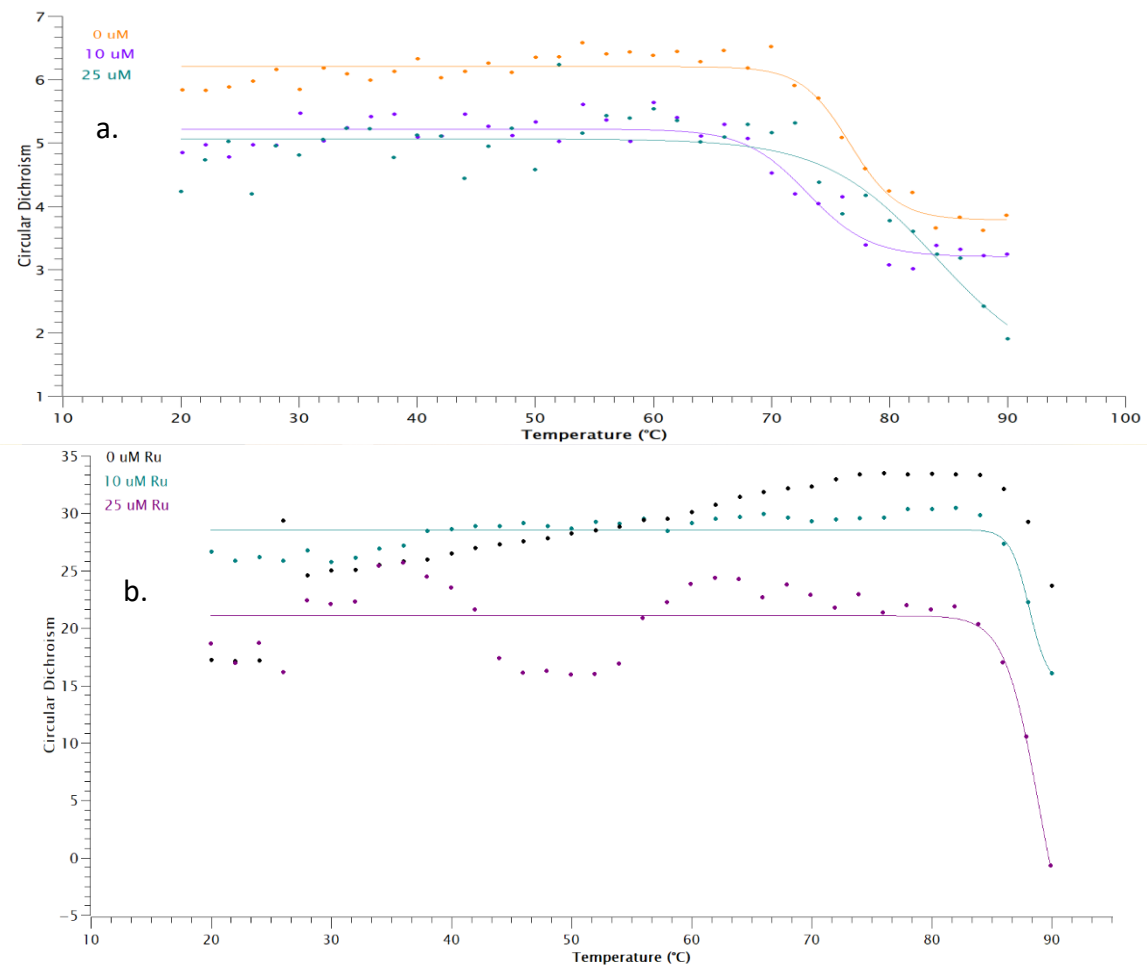
Figure 4.17 - *Melting curves of (a.) [Ru(bpy)₂(bbimb)][PF₆]₂ and (b.) [Ru(bpy)₂(bbimbo)][PF₆]₂ obtained using QTIplot data fitting software.*

4.6 Conclusion

A novel ruthenium(II) complex was successfully synthesised and an oxidised analogue was successfully isolated and both characterised. $[Ru(bpy)_2(bbimb)][PF_6]_2$ was found to have a similar emission quantum yield as $[Ru(bpy)_3]^{2+}$, however $[Ru(bpy)_2(bbimbo)][PF_6]_2$ had very low emissive qualities. There is very limited evidence that $[Ru(bpy)_2(bbimb)][PF_6]_2$ can interact with DNA, with only a change in thermal denaturation temperature and slight perturbations in UV/Vis and emission spectra. There is even less evidence gathered for $[Ru(bpy)_2(bbimbo)][PF_6]_2$ with only some evidence of a change within the emission titration. There is however evidence that both complexes can recognise phosphate over a variety of anions in aqueous environments, such as chlorides and acetates. Specifically, the unoxidised complex only gave a clear change with dihydrogen phosphate and not with the other tested anions. To further determine the phosphate recognition of these complexes in a biological setting, experiments with phosphate containing biological molecules should be considered.

4.6.1 Footnote to the Conclusion

All the data within this chapter was collected during the COVID-19 global pandemic, where access to labs and instruments was highly restricted. Although the utmost effort was taken to make sure that the results are accurate, many experiments require repeating to confirm that the data is reproducible and correct.

4.7 References

1   P. A. Elliott, *Bipyridyl Complexes of Ruthenium(II) to Target Nucleic Acid Structures*, Queen's University Belfast, 2012.
2   K. Suzuki, A. Kobayashi, S. Kaneko, K. Takehira, T. Yoshihara, H. Ishida, Y. Shiina, S. Oishi and S. Tobita, *Phys. Chem. Chem. Phys.*, 2009, **11**, 9850.
3   A. Juris, V. Balzani, F. Barigelletti, P. Belser and A. Von Zelewsky, *Coord. Chem. Rev.,* 1988*,* **84**, 85–277.
4
5   H. Walba and R. W. Isensee, *J. Org. Chem.*, 1961, **26**, 2789–2791.

Chapter Five

Chapter Five: Thesis Conclusions

The synthesis of drug analogues is common in medicinal chemistry research to find improved treatments with, for example, fewer side effects.[1] Small changes to a molecule have the potential to make substantial differences in the capability of interaction with biological species, e.g., DNA. There are multiple factors that determine the DNA binding abilities of metal complexes. These factors include the chirality, molecular shape and the planarity and conjugation of ligands. Another significant influence is the inclusion of hydrogen bond donors and acceptors into a functionalised ligand that are complimentary to the DNA structure. These factors can also impact the ability of a cationic species to interact with anions.

This thesis describes a series of benzimidazole complexes of ruthenium(II) based on previously reported series of complexes.[2-5] It was found that complexes with the 4,4'-functionalisation on 2,2'-bipyridine interacted with DNA to a higher degree than the 5,5'-ligand and that the inclusion of a CH_2 spacer group increased the luminescence properties over the analogous complexes without. None of the previous series of complexes had been tested for their anion recognition abilities or whether the ancillary ligands affect the DNA binding affinity. Three series of benzimidazole based complexes have been synthesised, one excluding "a spacer group" in the functionalised ligand, two with "a spacer group" that does not change the conjugation of the molecule and one that does.

The inclusion of benzimidazole was postulated to potentially increase the DNA binding capabilities over the previously reported benzothiazole and benzoxazole complexes due to the increased capability of hydrogen bond formation from the additional -NH. Changing the ancillary ligand from 2,2'-bipyridine to the bulkier 1,10-phenanthroline does not seem to influence the ability of the complexes to interact with anionic species or with DNA. Extending the length of the functionalised ligand using an amide spacer group allowed for an increase in the number of hydrogen bond donors and acceptors to be included in the functionalised ligand without disrupting the conjugation of the molecule. The extended conjugation of the 4,4'-bis-functionalised ruthenium(II) complexes was hypothesised to be the reason for the weak luminescence observed experimentally, which limits their potential as DNA probes. The inclusion of a methylene spacer group was tested previously but needed further work due to what is now known to be oxidation of the CH_2 group to a ketone in air and the presence of H^+, reinstating the conjugation. The complex which exhibited the highest φ was $[Ru(bpy)_2(bbib)]^{2+}$ and the lowest was $[Ru(bpy)_2(bbimbo)]^{2+}$, which is essentially non-emissive.

UV/Vis absorbance and emission pH titrations of $[Ru(bpy)_2(bbib)]^{2+}$, $[Ru(phen)_2(bbib)]^{2+}$, $[Ru(bpy)_2(bbaib)]^{2+}$, $[Ru(phen)_2(bbaib)]^{2+}$ and $[Ru(bpy)_2(bbimbo)]^{2+}$ all showed similar results where it is implied that either the deprotonation of the functionalised ligand results in an increase in the size of the energy gap for promotion of the electron, with no change in the dominant MLCT or that there is a

change in the dominant fluorophore between the functionalised ligand and the ancillary ligands, which can be observed in the change in the MLCT peak for the benzimidazole

moiety. However, the titrations for $[Ru(bpy)_2(bbimb)]^{2+}$ displayed very little change in this area of absorbance, most likely due to the break in conjugation provided by the methylene link meaning that the benzimidazole is not conjugated to the chromaphore.

By comparing the anion recognition data obtained for $[Ru(bpy)_2(bbib)]^{2+}$, $[Ru(phen)_2(bbib)]^{2+}$, $[Ru(bpy)_2(bbaib)]^{2+}$, $[Ru(phen)_2(bbaib)]^{2+}$, $[Ru(bpy)_2(bbimb)]^{2+}$ and $[Ru(bpy)_2(bbimbo)]^{2+}$, the following conclusions can be drawn:

- $[Ru(bpy)_2(bbimb)]^{2+}$ showed the most significant change in luminescence upon introduction of dihydrogen phosphate, where the emission was effectively quenched. However, it must be considered that the complex is potentially being oxidised to $[Ru(bpy)_2(bbimbo)]^{2+}$.

- $[Ru(bpy)_2(bbib)]^{2+}$ presented the greatest quenching of emission with acetate from approximately 160 to 117 a.u. in an aqueous environment.

- Stability constants were calculated for $[Ru(bpy)_2(bbib)]^{2+}$, $[Ru(phen)_2(bbib)]^{2+}$, $[Ru(bpy)_2(bbaib)]^{2+}$ and $[Ru(phen)_2(bbaib)]^{2+}$ from the ^{1}H-NMR spectroscopy titrations, and all stabilised to fit a two anion-to-one cation model with both acetate and dihydrogen phosphate. However, for phosphate, an unusually low second binding constant was observed, and a one-to-one model would also fit.

- None of the complexes gave any evidence for an interaction with chloride and bromide anions.

The experiments investigating interactions between DNA and $[Ru(bpy)_2(bbib)]^{2+}$, $[Ru(phen)_2(bbib)]^{2+}$, $[Ru(bpy)_2(bbaib)]^{2+}$, $[Ru(phen)_2(bbaib)]^{2+}$, $[Ru(bpy)_2(bbimb)]^{2+}$ and $[Ru(bpy)_2(bbimbo)]^{2+}$ gave the following:

- UV/Vis absorbance and emission titrations with *ct*-DNA showed no significant change upon introduction of DNA into any of the complexes. However, this may be due to the choice of solvent used in the experiments, which requires optimisation.

- CD titrations of $[Ru(bpy)_2(bbib)]^{2+}$ and $[Ru(phen)_2(bbib)]^{2+}$ with *ct*-DNA showed several changes in the spectra above 300 nm. These changes suggest that there is an enantioselective binding event occurring. However, as the spectra for the separate enantiomers have not been established, which enantiomer is selectively binding is ambiguous.

- CD titrations of $[Ru(bpy)_2(bbaib)]^{2+}$ and $[Ru(phen)_2(bbaib)]^{2+}$ showed a decrease in the signal around 283 nm upon introduction of DNA. This could be potentially caused by a change in DNA behaviour or a change in the behaviour of the bbaib ligand. There is no significant change in the spectra above 300 nm, therefore there is no evidence for enantioselectivity.

- Thermal denaturation studies showed that the melting temperature (T_m) of *ct*-DNA was destabilised considerably in the presence of $[Ru(bpy)_2(bbib)]^{2+}$, $[Ru(phen)_2(bbib)]^{2+}$, $[Ru(bpy)_2(bbaib)]^{2+}$, $[Ru(phen)_2(bbaib)]^{2+}$, $[Ru(bpy)_2(bbimb)]^{2+}$ and $[Ru(bpy)_2(bbimbo)]^{2+}$.

ΔT_m was recorded as -4, -4, -3, -4, -4 and 0, respectively. These results suggest that if interaction is occurring, it is not by intercalation.

- Viscosity studies of $[Ru(bpy)_2(bbib)]^{2+}$, $[Ru(phen)_2(bbib)]^{2+}$, $[Ru(bpy)_2(bbaib)]^{2+}$ and $[Ru(phen)_2(bbaib)]^{2+}$ showed that the relative viscosity of *ct*-DNA in the presence of each complex did not change to a significant degree. This suggests that any interaction between the complexes and DNA is not intercalation.

- Dialysis equilibrium studies of $[Ru(bpy)_2(bbib)]^{2+}$, $[Ru(phen)_2(bbib)]^{2+}$, $[Ru(bpy)_2(bbaib)]^{2+}$ and $[Ru(phen)_2(bbaib)]^{2+}$ did not show significant change in the CD spectrum of the dialysate, implying that there are no enantioselective interactions between the complexes and DNA.

All of the experiments which included *ct*-DNA suffered from several issues. When DNA was added to $[Ru(bpy)_2(bbib)]^{2+}$, $[Ru(phen)_2(bbib)]^{2+}$, $[Ru(bpy)_2(bbaib)]^{2+}$, $[Ru(phen)_2(bbaib)]^{2+}$, $[Ru(bpy)_2(bbimb)]^{2+}$ and $[Ru(bpy)_2(bbimbo)]^{2+}$ in tris buffer, a precipitate was formed, resulting in discrepancy in any results obtained. A small amount of DMF was added in order to prevent the solid from forming, however this caused more problems in that it potentially is acting as a competitive interactor with DNA therefore, the complex cannot bind to the nucleic acid.

The key results from this project are that the synthesised series of bis-benzimidazole functionalised ruthenium(II) complexes have the potential to be potent anion recognisers in aqueous media, especially $[Ru(bpy)_2(bbib)]^{2+}$ for acetate and

$[Ru(bpy)_2(bbimb)]^{2+}$ for dihydrogen phosphate. The loss of a conjugated system by including "a spacer group" increases the luminescence properties and this may be of value in the design of future complexes, although the choice of group used must be strongly considered to prevent inclusion of conjugation via oxidation, although the exact mechanism of this is still under investigation. There is only weak evidence that any of these complexes interact with DNA due to problems with the formation of precipitate, so further testing must be done to fully establish whether there is an interaction occurring, where the solvent must be carefully chosen.

1. Patrick, G. L. *An Introduction to Medicinal Chemistry, 3rd Edition* **2005**.
2. Spillane, C. B.; Morgan, J. L.; Fletcher, N. C.; Collins, J. G.; Keene, F. R. *Dalton Trans.* **2006**, 3122-3133.
3. Spillane, C. B.; Fletcher, N. C.; Rountree, S. M.; van den Berg, H.; Chanduloy, S.; Morgan, J. L.; Keene, F. R. *J. Biol. Inorg. Chem.* **2007**, *12*, 797-807.
4. Spillane, C. B.; Dabo, M. N. V.; Fletcher, N. C.; Morgan, J. L.; Keene, F. R.; Haq, I.; Buurma, N. J. *J. Inorg. Biochem.* **2008**, *102*, 673-683.
5. P. A. Elliott, PhD Thesis, Queen's University Belfast, 2012.

Chapter Six

Chapter Six: Experimental of Bis-benzimidazole Ruthenium (II) Polypyridyl Complexes

6.1 Materials

Tris(hydroxymethyl)-aminomethane (Tris), polyphosphoric acid, 1,2-phenylenediamine, 2-aminobenzimidazole and trifluoromethanesulfonic acid were obtained from Merck and used as is. Potassium hexafluorophosphate was obtained from Fluorochem. Acetonitrile and ethylene glycol were purchased from Fisher, and the acetonitrile was dried over 3 Å molecular sieves. Sephadex LH20 and Sephadex C-25 (Sigma Aldrich) were used for chromatographic purification of metal complexes. Tetrabutylammonium (TBA) hydrogenphosphate, TBA chloride, TBA acetate, TBA sulfate, TBA nitrate were purchased from Sigma Aldrich for use in anion binding studies.

Acetone-D_6, D_2O, acetonitrile-D_3, and DMSO-D_6 were obtained from Fluorochem for use as solvents in NMR spectroscopy.

Calf thymus DNA (*ct*-DNA) (lyophilised) was purchased from Sigma Aldrich (now Merck) for use in DNA binding studies.

6.2 Physical Measurements

NMR spectra were recorded on a Bruker Fourier 300 or a Bruker Avance III 400 at 298K and referenced to TMS. Absorbance spectra were recorded using a 1 cm path

length quartz cuvette on an Agilent Carey 60 UV vis spectrometer. Emission spectra were recorded using a clear quartz cuvette on a Agilent Carey Eclipse spectrophotometer, quantum yields were determined by normalization against $[Ru(bpy)_3]^{2+}$ in water (0.028) and acetonitrile (0.040).[1] Circular Dichroism (CD) spectra were recorded in either acetonitrile or tris buffer (5 mM Tris-HCl, 50 mM NaCl, 7.2 pH) at concentrations of *ca.* 5 x 10^{-5} M in a 1 cm cell, using an Applied Photophysics Chirascan-plus CD Spectrometer. *ct*-DNA concentrations were determined from UV absorbance at 260 nm using an extinction coefficient of 6600 M^{-1} cm^{-1} per nucleotide.[1] E.S.I. mass spectroscopy was recorded using a Shimadzu LCMS-IT-TOF mass spectrometer at 298K. Elemental analysis data was recorded using a Vario MICRO Cube. Conversion to Cl^- salts was done using Amberlite IRA-410 beads, stirred in water overnight.

6.2.1 Sources of Error

There are many sources of error that can possibly affect the results presented in this thesis. Given that the significance of this thesis relies heavily on measurements, it is important to highlight these. A major source of error within this thesis is human error. It is possible that interpretation of the data could potentially be incorrect. Other sources of error include impurities contained within samples. It was not possible to completely purify some of the complexes synthesised within this project, especially the complexes in Chapter Four, where, although the utmost care was taken to prevent contact with air and water, $[Ru(bpy)_2(bbimb)][[PF_6]_2$ was oxidising in situ. This meant that the correct mass of product was an unknown and could not be accounted for during the studies. A similar source of error came from the precipitation of assumed bound complex as this would reduce the concentration of the sample to an unknown value too.

6.3 Ligand Synthesis
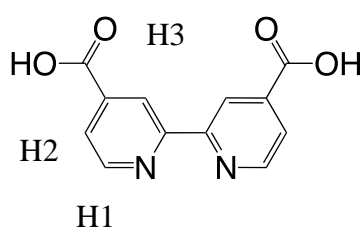
Synthesis of 4,4´-dicarboxylic acid-2,2´-bipyridine

4,4´-Dicarboxylic acid-2,2´-bipyridine was synthesised according to literature procedure.[2] Yield = 0.55 g, 14%.

^{1}H NMR (400MHz, DMSO-D$_6$): δ 8.96 (1H, H3, d, J = 4.9 Hz), 8.91 (1H, H2, dd, J = 1.0, 1.5 Hz), 7.96 (1H, H1, dd, J = 1.2, 4.9 Hz)

Synthesis of 4,4′-bis(benzimidazol-2-yl)-2,2′-bipyridine (4,4'-bbib)
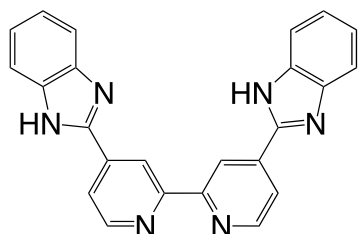
4,4´-Dicarboxylic acid-2,2´-bipyridine[2] (2.00 g, 8.19 mmol), phenylenediamine (1.77 g, 16.38 mmol) and polyphosphoric acid (5 ml) were heated to 200 °C and stirred for 24h in a nitrogen atmosphere. After cooling, the solution was poured into saturated NaHCO$_3$ (aq.) and stirred. The resulting grey/brown precipitate was collected via gravity filtration, washed with water (3 x 30 ml) and dried. Yield = 1.72 g, 76%.

^{1}H NMR (400MHz, DMSO-D$_6$): δ 9.26 (1H, s), 8.96 (1H, d, J = 5.1Hz), 8.25 (2H, dd, J = 1.7, 5.1Hz) 7.70 (2H, dd, J = 3.2, 5.8Hz) 7.30 (2H, dd, J = 3.1, 6.0Hz)

^{13}C-NMR – Unable to acquire due to solubility issues

ESI Mass Spec – (e/z) 389.15 [M + H]$^+$

IR (KBr disc) – 3050 cm^{-1} (N-H stretch)
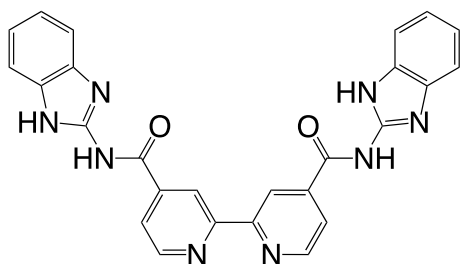
Synthesis of 4,4′-bis(amidobenzimidazol-2-yl)-2,2′- bipyridine (4,4´-bbaib)

4,4´-Dicarboxylic acid-2,2´-bipyridine[2] (0.10 g, 0.41 mmol) was refluxed in $SOCl_2$ (10 ml) for 24h in a nitrogen atmosphere. The $SOCl_2$ was removed by distillation and dried *in vacuo*. Dry toluene (30 ml), 2-aminobenzimidazole (109.18 mg, 0.82 mmol) and triethylamine (5 ml) were added, and the solution was refluxed under nitrogen for 48h. The resulting precipitate was filtered and washed with dry toluene (3 x 30 ml) and air dried. Yield = 0.080 g, 27%.

^{1}H NMR (400MHz, DMSO-D6): δ 12.68 (2H, s) 9.17 (1H, s), 8.91 (1H, d, *J* = 4.9 Hz), 8.10 (1H, dd, *J* = 1, 4.8 Hz), 7.47 (2H, dd, *J* = 3.1, 5.8 Hz), 7.24 (2H, dd, *J* = 3.1, 5.8 Hz)

^{13}C-NMR (400MHz, DMSO-D6): δ 171.14, 156.29, 154.50, 152.67, 150.47, 146.18, 131.18, 123.21, 120.87, 119.90, 112.65, 111.82

ESI Mass Spec – (m/z) 497.15 [M + Na]$^+$

IR (KBr disc) – 1680 cm^{-1} (C=O stretch), 3000 cm (N-H stretch)
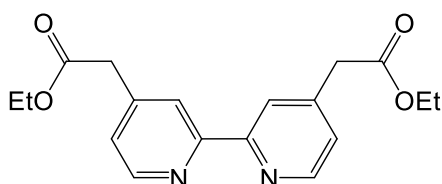
Synthesis of 4,4´-acetic acid-2,2´ bipyridine ethyl ester[3]

4,4'-dimethyl-2,2´-bipyridine (0.999 g, 5.42 mmol) was dissolved in anhydrous THF (40 ml) in nitrogen. The solution was cooled

to -78 °C and LDA (14 ml) was added dropwise over 5 minutes. The solution was stirred for 2 hours. Diethylcarbonate (3.3 ml, 27.24 mmol) was added and the solution was stirred for 12 hours. The resulting red/brown precipitate that formed was dissolved in THF (35 ml) and the product was extracted with H_2O (3 x 30 ml). The combined aqueous layers were extracted with further THF (50 ml) and the combined organic layers were dried with $MgSO_4$ and filtered under gravity. The filtrate was concentrated to an oil *in vacuo* and purified via column chromatography. Yield = 0.60 g, 34 %.

^{1}H-NMR (400 MHz, DMSO-D$_6$): δ 8.67 (1H, d, J = 5.0 Hz), 8.43 (1H, s), 7.36 (1H, dd, J = 5.0, 5.0 Hz), 4.20 (2H, q, J = 7.0, 7.1 Hz), 3.76 (2H, s), 1.29 (3H, t, J = 7.1 Hz)
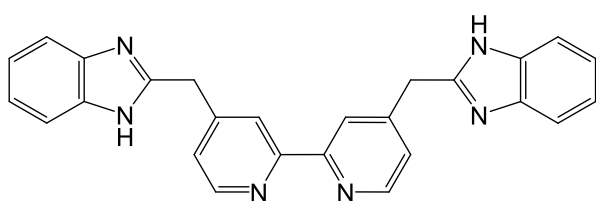
Synthesis of 4,4'-bis(benzimidazole-2yl-methyl)-2,2'-bipyridine (4,4'-bbimb)

4,4'-bis(benzimidazole-2yl-methyl)-2,2'-bipyridine (4,4'-bbimb) was synthesised using 4,4'-acetic acid-2,2'-bipyridine ethyl ester (0.26 g, 0.79 mmol), polyphosphoric acid (~5 ml) and 1,2-phenylenediamine (0.220g, 2.03 mmol) in a manner analogous to 4,4'-bis(benzimidazole-2-yl)-2,2'-bipyridine (4,4'-bbib). Yield = 0.445 g.

^{1}H-NMR (400 MHz, DMSO-D$_6$): δ 8.60 (1H, d, J = 5.0 Hz), 8.35 (1H, s), 7.50 (2H, dd, J = 3.3, 5.8 Hz), 7.42 (1H, dd, J = 1.5, 5.0 Hz), 4.32 (2H, s)

^{13}C-NMR (400MHz, DMSO-d$_6$): δ 155.70, 152.57, 149.87, 148.10, 125.04, 122.27, 121.34, 34.70

6.4 Synthesis of Ruthenium(II) Complexes
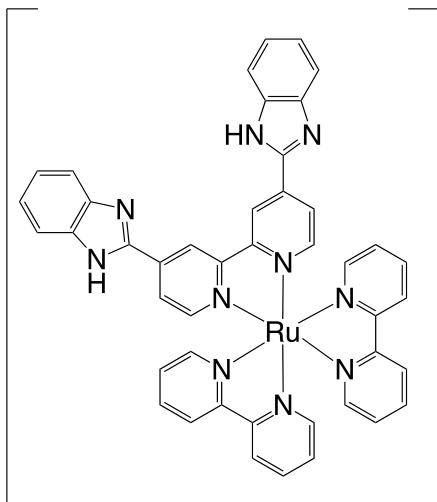
2+   **Synthesis of [Ru(bpy)$_2$(4,4'-bbib)]$^{2+}$**

[Ru(bpy)$_2$Cl$_2$] (0.140 g, 0.29 mmol), 4,4'-bbib (0.112 g, 0.29 mmol) and trifluoromethanesulfonic acid (0.5 ml) in ethylene glycol (30 ml) was heated to 140 °C and stirred in a nitrogen atmosphere for 4h. After cooling, KPF$_6$ (aq.) was added and resulting precipitate was filtered, washed with water (3 x 30 ml) and dried. Product appeared as a red/brown solid. Size exclusion chromatography using Sephadex LH20 and eluting 1 : 1 ethanol and acetone was used to purify. Yield = 0.220 g, 78.5%.

^{1}H NMR (400MHz, Acetone-D6) : δ 12.77 (1H, s) 9.67 (1H, s) 8.877 (2H, dd, J = 8.0, 2.7Hz) 8.35 – 8.20 (5H, m) 8.13 (1H, d, J = 5.2Hz) 7.80 (1H, d, J = 7.5Hz) 7.70 (1H, d, J = 7.5Hz) 7.63 (2H, m) 7.35 (2H, dd, J = 9.1, 8.4Hz)

ESI Mass Spec – (m/z) 401.10 [M]$^{2+}$

IR (KBr disc) – 2950 cm^{-1} (N-H stretch)
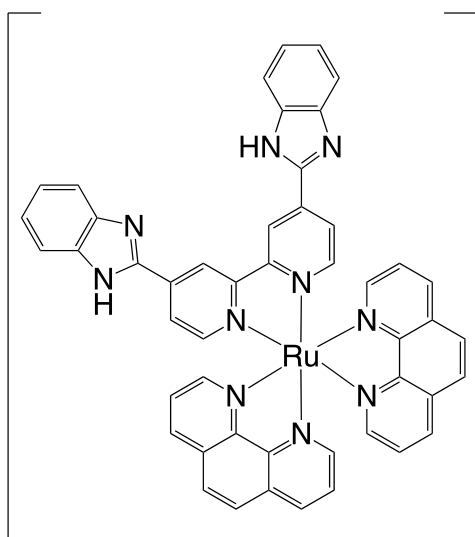
2+ **Synthesis of [Ru(phen)₂(4,4'-bbib)]²⁺**

Procedure analogous to [Ru(bpy)₂(4,4'-bbib)]²⁺ using [Ru(phen)₂Cl₂] (0.140 g, 0.26 mmol) as starting material. Product appeared as a red/brown solid. Size exclusion chromatography using Sephadex LH20 and eluting 1 : 1 ethanol and acetone was used to purify. Yield = 0.13 g, 43%.

¹H NMR (400MHz, Acetone-D6) : δ 13.54 (1H, s) 9.91 (1H, s) 8.87 (1H, dd, *J* = 7.4, 0.9 Hz) 8.82 (2H, dd, *J* = 5.9, 5.5 Hz) 8.44 (2H, d, *J* = 2.5 Hz) 8.34 (1H, dd, *J* = 5.2, 4.2 Hz) 8.24 (1H, dd, *J* = 5.9, 4.6 Hz) 8.00 (2H, dd, *J* = 8.2, 5.3 Hz) 7.81 (1H, dd, *J* = 8.3, 5.2Hz) 7.67 (2H, dd, *J* = 7.8, 5.1 Hz) 7.27 (2H, dd, *J* = 9.3, 9.0 Hz)

ESI Mass Spec – (m/z) 425.10 [M]²⁺

IR (KBr disc) – 2950 cm⁻¹ (N-H stretch)
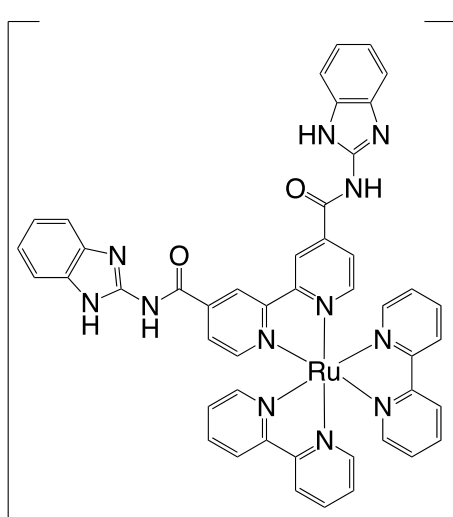
Synthesis of [Ru(bpy)₂(4,4'-bbaib)]²⁺

Procedure analogous to [Ru(bpy)₂(4,4´-bbib)]²⁺ using 4,4´-bbaib (0.137 g, 0.29 mmol) as starting material. Product appeared as a red/orange solid. Size exclusion chromatography using Sephadex LH20 and eluting 1 : 1 ethanol and acetone was used to purify. Yield = 0.107 g, 22%.

^{1}H NMR (400MHz, Acetone-D6) : δ 9.33 (1H, s), 8.95 (1H, d, J = 4.97 Hz), 8.85 (2H, dd, J = 5.06 Hz, 7.28 Hz), 8.36 (1H, dd, J = 5.26 Hz, 5.91 Hz), 8.26 (3H, m), 8.05 (3H, m), 7.74 (2H, dd, J = 2.88 Hz, 6.06 Hz), 7.60 (2H, m), 7.34 (2H, dd, J = 3.13 Hz, 6.06 Hz)

ESI Mass Spec – (m/z) 444.10 [M]²⁺

IR (KBr disc) – 1680 cm^{-1} (C=O stretch), 3000 cm (N-H stretch)
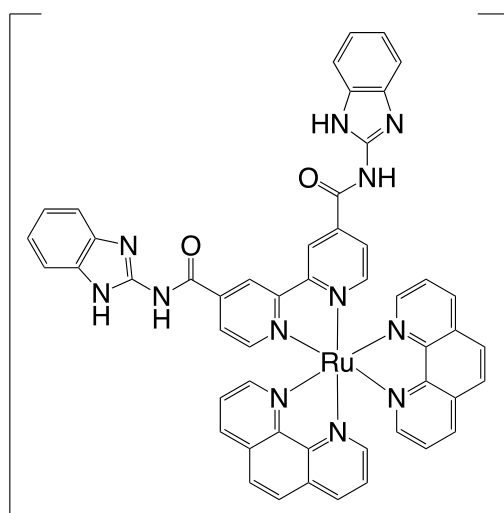
Synthesis of [Ru(phen)₂(4,4´-BBAIB)]²⁺

Procedure analogous to [Ru(bpy)₂(4,4´-BBIB)]²⁺ using [Ru(phen)₂Cl₂] (0.140 g, 0.26 mmol) and 4,4´-BBAIB (0.124 g, 0.26 mmol) as starting material. Product appeared as a red/orange solid. Size exclusion chromatography using Sephadex LH20 and eluting 1 : 1 ethanol and acetone was used to purify. Yield = 0.214 g, 69 %.

^{1}H NMR (400MHz, Acetone-D₆) : δ 9.32 (1H, s), 8.85 (2H, dd, J = 1.10 Hz, 5.28 Hz), 8.65 (1H, dd, J = 1.10 Hz, 5.28 Hz), 8.40 (2H, d, J = 2.83 Hz), 8.30 (1H, dd, J = 1.15, 5.27 Hz), 8.19 (2H, d, J = 5.76 Hz), 8.00 (2H, m), 7.80 (1H, dd, J = 5.20, 8.20 Hz), 7.60 (2H, dd, J = 3.10, 6.1 Hz), 7.37 (2H, dd, J = 3.10, 5.20 Hz)

ESI Mass Spec – (m/z) 468.1 [M]²⁺

IR (KBr disc) – 1680 cm⁻¹ (C=O stretch), 3000 cm (N-H stretch)
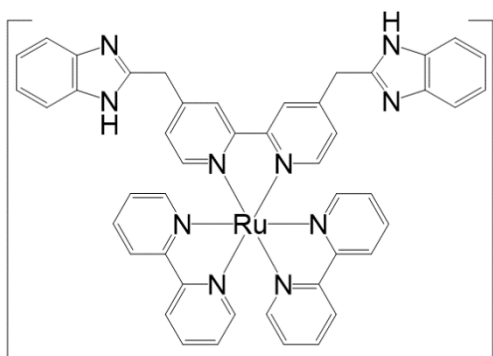
Synthesis of [Ru(bpy)₂(4,4´-BBIMB)]²⁺

[Ru(bpy)₂Cl₂] (280 mg, 0.577 mmol) and 4,4´-BBIMB (240 mg, 0.577 mmol) were dissolved in ethanol (25 ml) and refluxed under nitrogen at 90 °C for 24 hours, with a colour change from dark purple/black to deep red. Reaction was cooled to RT and

shielded from light. The solution was filtered under gravity and excess solvent was removed from the filtrate. KPF$_6$ (aq) was added and a red/orange precipitate was formed. Solid was collected via vacuum filtration and washed with deionised water (~ 5 ml) and diethyl ether (~ 5 ml), recrystallised in water and stored under nitrogen and in darkness. Yield = 313.6 mg, 48.6 %.

^{1}H NMR (400MHz, CD$_3$CN) : δ 8.57 (2H, s), 8.48 (4H, d, J = 8.2 Hz), 8.03 (4H, ddd, J = 7.9 Hz, 3.0 Hz, 1.5 Hz), 7.77 (2H, d, J = 5.5Hz), 7.70 (2H, d, J = 5.5 Hz), 7.66 (2H, d, J = 5.8 Hz,) 7.53 (4H, dd, J = 3.2, 2.9Hz),7.38 (6H, m), 7.24 (4H, dd, J = 3.2Hz, 2.8Hz,), 4.44 (4H, s,)

IR (KBr disc) – 2922.2 cm^{-1} (N-H stretch)

No mass spec. data was able to be acquired at time of writing.
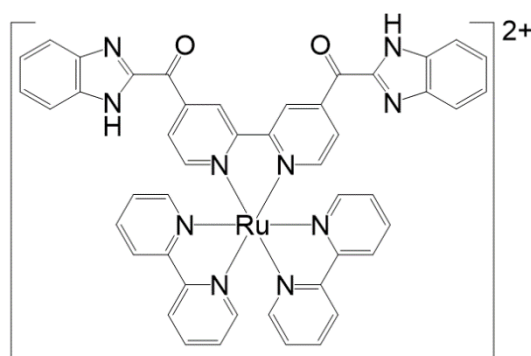
Synthesis of [Ru(bpy)$_2$(4,4'-BBIMBO)]$^{2+}$

[Ru(bpy)$_2$(BBIMB)][PF$_6$]$_2$ was synthesised as above. 100 mg (0.089 mmol) was dissolved in acetone and left in direct light for 120 hours. Solid was collected via removal of solvent *in vacuo*.

^{1}H NMR (400MHz, CD$_3$CN) : δ 11.72 (1H, s,), 9.77 (1H, d, J = 1.28 Hz), 8.58 (2H, dd, J, = 2.8, 8.1 Hz), 8.51 (1H, dd, J = 1,7, 5.9 Hz), 8.13 (3H, m), 7.85 (1H, d, J = 5.9 Hz), 7.79 (1H, d, J = 5.6 Hz), 7.76 (2H, m), 7.54 (1H, m), 7.49 (2H, m), 7.40 (1H, m)

IR (KBr disc) – 2929.7 cm^{-1} (N-H stretch), 1656.8 cm^{-1} (C=O stretch)

No mass spec. data was able to be aquired at time of writing.

6.5 UV/Vis Absorbance and Emission pH Titrations of Ru(II) Complexes

NaOH and Britton-Robinson buffer were purchased from Sigma and used without further purification. NaOH and Britton-Robinson buffer solutions (0.1 M) were made and used to produce complex (as a chloride salt) solutions (100 μM). pH was measured using a Mettler Toledo FiveEasy FE20 Benchtop pH meter which was calibrated using 2 points of reference (4.0 and 9.2 pH). Each titration was performed with a constant complex concentration (50 μM) between ca. 2 – 12 pH. The absorbance spectra were analysed between 200 – 600 nm. The fluorescence intensity of complexes was measured in 1 cm quartz cell between 550 – 800 nm, with an excitation wavelength of λ_{ex}= 450 nm. pKa and pKb of complexes were determined using QTI plot applying a non-liner curve fit to achieve a curve of best fit to assign acid and base disassociation constants and error.

6.6 Binding of Ru(II) Complexes to Anions

6.6.1 Absorption and Emission Titrations

TBA salts were diluted in acetonitrile or 95:5 DMSO/water solution. Stock solutions of all reagents were prepared (TBA hydrogen phosphate monobasic, TBA chloride, TBA bromide, TBA acetate, TBA nitrate and TBA hydrogen sulphate at 2 mM) and the spectroscopic experiments were performed as series of titrations. Each titration was performed with a constant complex (as a hexafluorophosphate salt) concentration (50 μM in acetonitrile, 5 μM in DMSO/water solution) and an anion concentration varying between 0 and 450 μM. The absorbance spectra were analysed between 200 – 600 nm. The fluorescence intensity of complexes was measured in 1 cm quartz cell between 550 – 800 nm, with an excitation wavelength of λ_{ex}= 450 nm.

6.6.2 ^{1}H-NMR Spectroscopy Titrations

TBA salts (TBA hydrogen phosphate monobasic, TBA chloride and TBA acetate) were diluted in 5:95 D_2O/DMSO-D_6 solution. Stock solutions of all reagents were prepared to 5 M, and the spectroscopic experiments were performed as series of titrations. Each titration was performed with a constant complex (as a hexafluorophosphate salt) concentration (5 mM) with anion concentration varying between 0 – 50 mM. Stability constants were calculated using WINEQNMR2.[3]

6.7 Binding of Ru(II) Complexes to Calf Thymus DNA

6.7.1 Absorption, Emission and Circular Dichroism Titrations

Lyophilised calf thymus DNA (*ct*-DNA) was purchased from Sigma and used without further purification. *Ct*-DNA was diluted in Tris Buffer (5 mM Tris-HCl, 50 mM NaCl, pH 7.2) and allowed to equilibrate at 4 °C overnight. Concentration of *ct*-DNA per base pair was determined spectroscopically using the extinction coefficient of 6600 molar base^{-1}cm^{-1}dm^3 at 260 nm. Solutions of calf thymus DNA in the buffer gave a ratio of UV absorbance at 260 and 280 nm of *ca.* 1.9 : 1, indicating that the DNA was sufficiently free of protein.[5] Stock solutions of all reagents were prepared, and the spectroscopic experiments were performed as series of titrations.

Each titration was performed with a constant complex concentration (50 μM) and a DNA concentration expressed in base pairs varying between 0 and 450 μM. The absorbance spectra were analysed between 200 – 600 nm (however DNA has an absorbance of *ca*. 300 nm). The fluorescence intensity of complexes was measured in 1 cm quartz cell between 550 – 800 nm, with an excitation wavelength of λ_{ex}= 450 nm. Circular dichroism spectra of the racemic complexes were recorded between 200 – 600 nm. All experiments were performed at room temperature. Emission quantum yields of the complexes were determined in aerated aqueous solutions at room temperature and relative to an aqueous solution of [Ru(bpy)$_3$]$^{2+}$ (ϕ_{em} = 0.04) using Equation (1).[6]

$$\phi = \phi_{std}(A_{std} / A)(I / I_{std}) \ (1)$$

6.7.2 Thermal Denaturation Experiments

Melting temperatures of ct-DNA (50 μM) were recorded with and without the presence of racemic complexes (25 – 50 μM) between 20 and 90 °C using an Applied Photophysics Chirascan-plus CD Spectrometer. Data was processed using Microsoft Excel and QTI Plot by applying a non-liner curve fit so as to achieve a curve of best fit to assign denaturation temperature and error.

6.7.3 Viscosity Measurements

Viscosity measurements of ct-DNA with and without racemic complexes were taken using an Ubbeholde type kinematic viscometer at a constant temperature of 30 °C. Sonicated ct-DNA with an average BP length of ca. 200 so as to minimise contributions to viscosity due to changes in DNA length.[7] Triplicate measurements were taken per sample and an average flow time was calculated. Data is offered as $(\eta-\eta_0)^{1/3}$ against DNA/complex ratios, were η is DNA viscosity with complex present, and η_0 is viscosity of DNA only.[8] Relative viscosities were obtained using $\eta = (t - t_0)/t_0$, where t = observed flow time and t_0 = flow time of buffer only.

6.7.4 Equilibrium Dialysis Experiments

Equilibrium dialysis experiments were undertaken using ct-DNA (2 ml, 0.025 mM) sealed in dialysis tubing. The tubing was soaked in racemic complexes (10 ml, 60 μM). After $ca.$ 24hrs, a CD spectrum of the dialysate was recorded.[9,10]

6.8 References

1. J. M. Carnerero, A. Jiminez-Ruiz, E. M. Grueso and R. Prado-Gotor, *Phys. Chem. Chem. Phys.*, 2017,**19**, 16113-16123

2. Y. Miyake, Y. Itoh, A. Hatanaka, Y. Suzuma, M. Suzuki, H. Kodama, Y. Arai and T. Suzuki, *Bioorganic Med. Chem.*, 2019, **27**, 1119–1129.

3. P. A. Elliott, Queen's University Belfast, 2012.

4. J. Van Houten and R. J. Watts, *J. Am. Chem. Soc.*, 1976, **98**, 4853.

5. W. Li, Y. Y. Ji, J. W. Wang and Y. M. Zhu, *DNA Cell Biol.,* 2012, **6**, 1046 – 1053.

6. M. J. Hynes, J. Chem. Soc., *Dalton Trans*., 1993, 311–312.

7. Haq, I.; Lincoln, P.; Suh, D. C.; Norden, B.; Chowdhry, B. Z.; Chaires, J. B. *J. Am. Chem. Soc.* **1995**, *117*, 4788-4796.

8. Cohen, G.; Eisenberg, H. *Biopolymers* **1968**, *6*, 1077-100.

9. Kumar, C. V.; Barton, J. K.; Turro, N. J. *J. Am. Chem. Soc.* **1985**, *107*, 5518-5523.

10. Barton, J. K.; Danishefsky, A. T.; Goldberg, J. M. *J. Am. Chem. Soc.* **1984**, *106*, 2172-2176.

7.0 – Appendix

7.1 Data Obtained for [Ru(bpy)₂(bbib)]²⁺ and [Ru(phen)₂(bbib)]²⁺ (Chapter Two)

7.1.1 Data for the Crystal Structure of bbib

Chemical Formula	$2(C_2H_6OS).C_{24}H_{16}N_6$
Molecular Weight	544.68
Crystal system	Triclinic
Space Group	P1
Temperature (K)	100
Unit cell dimensions	$a = 4.7998\ (1)$ Å $\alpha = 92.168\ (2)°$ $b = 9.4816\ (2)$ Å $\beta = 94.662\ (3)°$ $c = 14.1642\ (5)$ Å $\gamma = 93.809\ (2)°$
Volume	$640.45\ (3)$ Å^3
Z	1
Density (calculated)	1.412 mg m^{-3}
Absorption Coefficient	2.21
F(000)	286
Crystal Size	$0.1 \times 0.06 \times 0.04$ mm^3
Theta range for data collection	$4.6 – 76.2$
Index Ranges	$h = -6<=0<=6$, $k = -11<=0<=11$, $l = -17<=0<=17$
Reflections collected	4900
Independent reflections	4900
Max. and Min. Transmission	1.000, 0.756
Refinement method	Full-matrix least-squares on F^2

| Data/restraints/parameters	4900 / 0 / 229
Final R indices [I>2sigma(I)]	0.048
Largest diff. peak and hole	0.36, -0.44 e.$\mathring{A}^3$

7.1.2 UV/Vis Absorbance Spectra
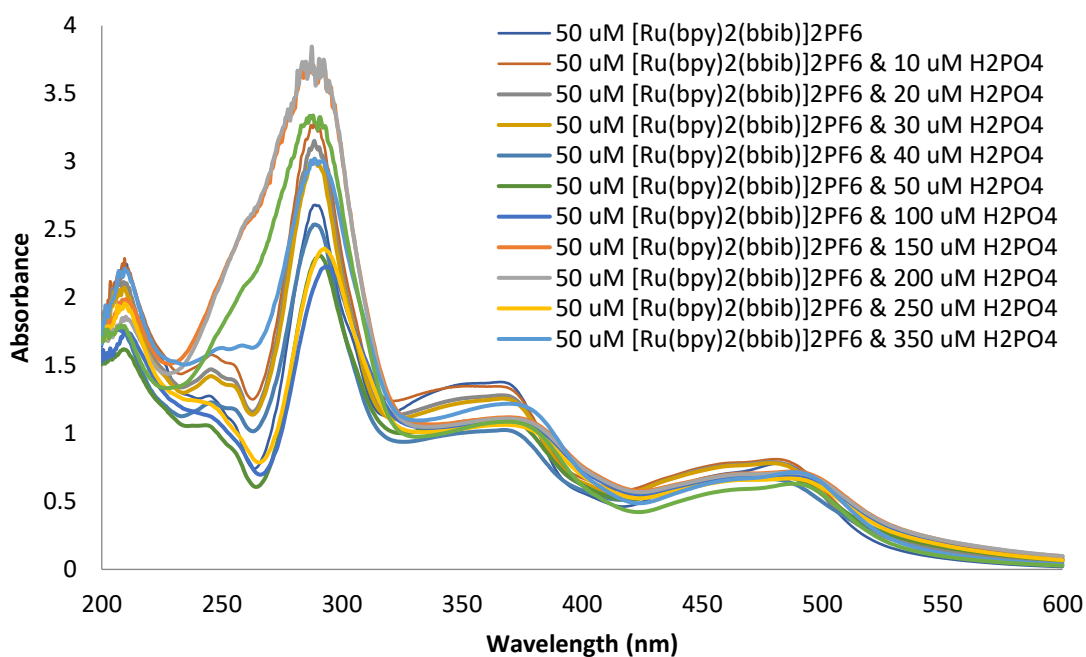
Appx. 1 *– UV/Vis absorbance spectra of [Ru(bpy)$_2$(bbib][PF$_6$]$_2$ (50 μM) with increasing concentration of TBA H$_2$PO$_4$. Spectra recorded in acetonitrile at 25˚C.*
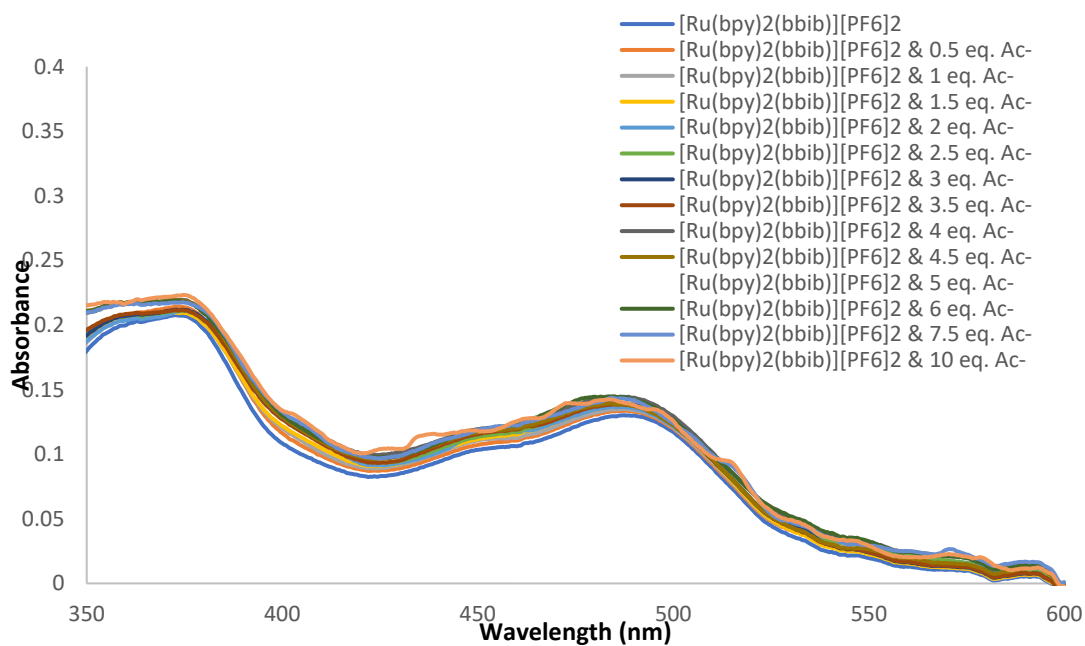
Appx. 2 - *UV/Vis absorbance spectra of [Ru(bpy)₂(bbib][PF₆]₂ (50 µM) with increasing concentration of TBA AcO. Spectra recorded in DMSO/ 5% deionised water at 25 C.*
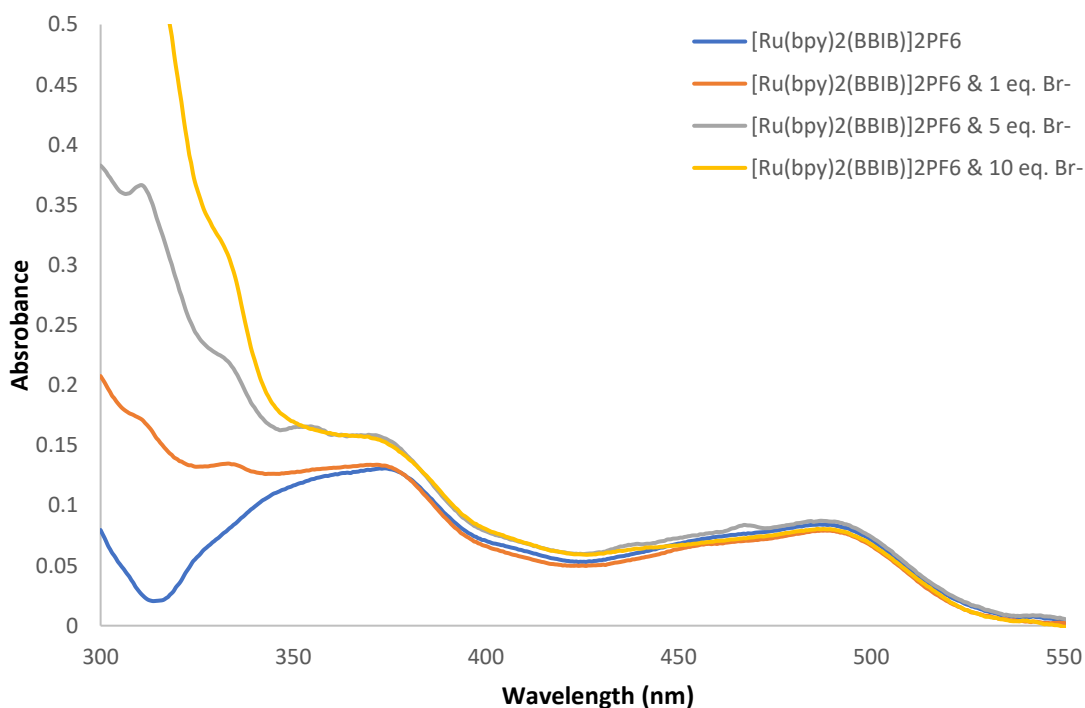
Appx. 3 - *UV/Vis absorbance spectra of [Ru(bpy)₂(bbib][PF₆]₂ (5 µM) with increasing concentration of TBA Br. Spectra recorded in DMSO/ 5% deionised water at 25 C.*
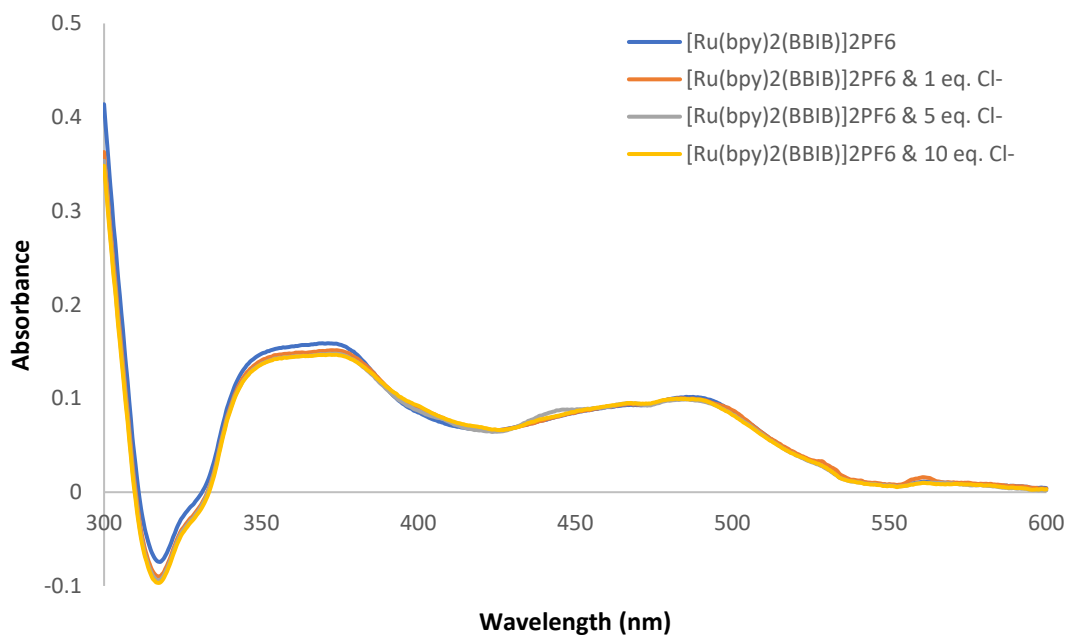
Appx. 4 - *UV/Vis absorbance spectra of [Ru(bpy)₂(bbib][PF₆]₂ (5 μM) with increasing concentration of TBA Cl. Spectra recorded in DMSO/ 5% deionised water at 25 C.*
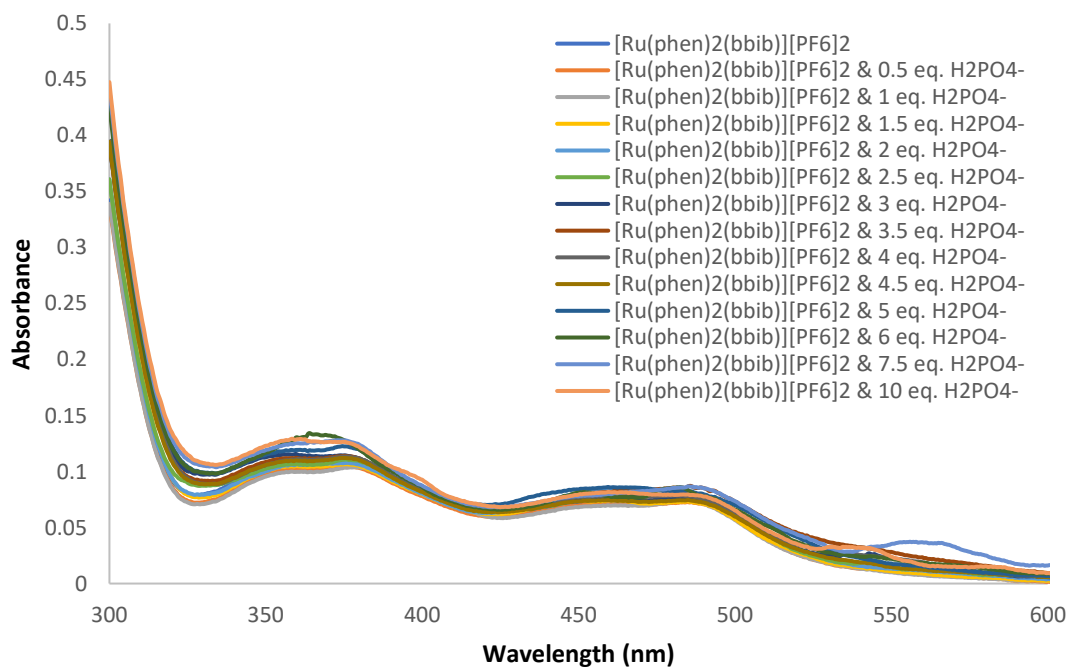
Appx. 5 - *UV/Vis absorbance spectra of [Ru(phen)₂(bbib][PF₆]₂ (5 μM) with increasing concentration of TBA H₂PO₄. Spectra recorded in DMSO/ 5% deionised water at 25 C.*
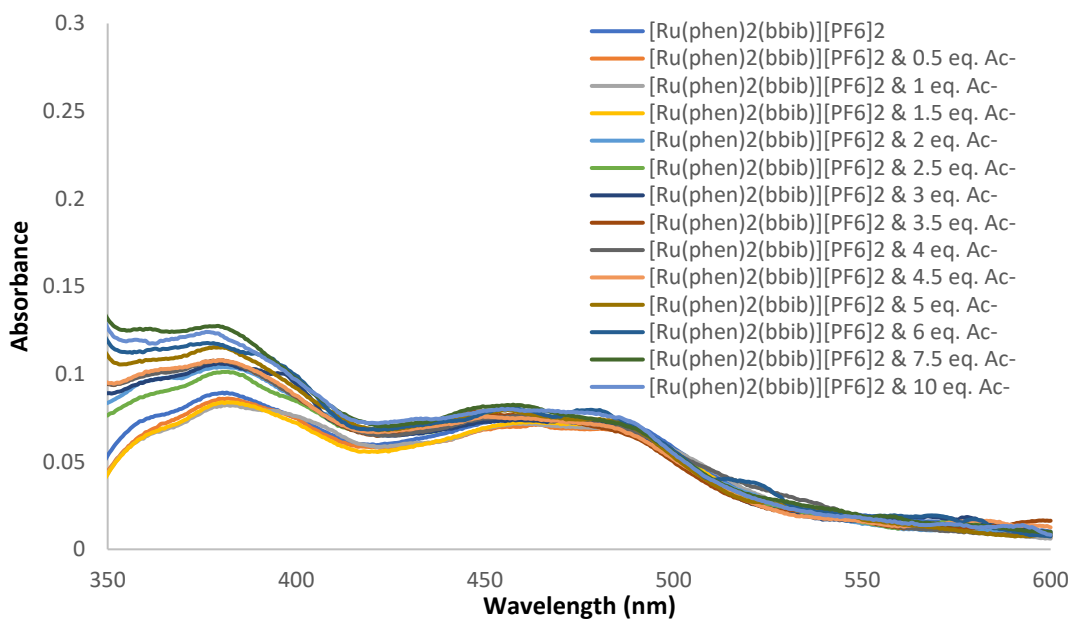
Appx. 6 - *UV/Vis absorbance spectra of [Ru(phen)₂(bbib][PF₆]₂ (5 μM) with increasing concentration of TBA H₂PO₄. Spectra recorded in DMSO/ 5% deionised water at 25 C.*
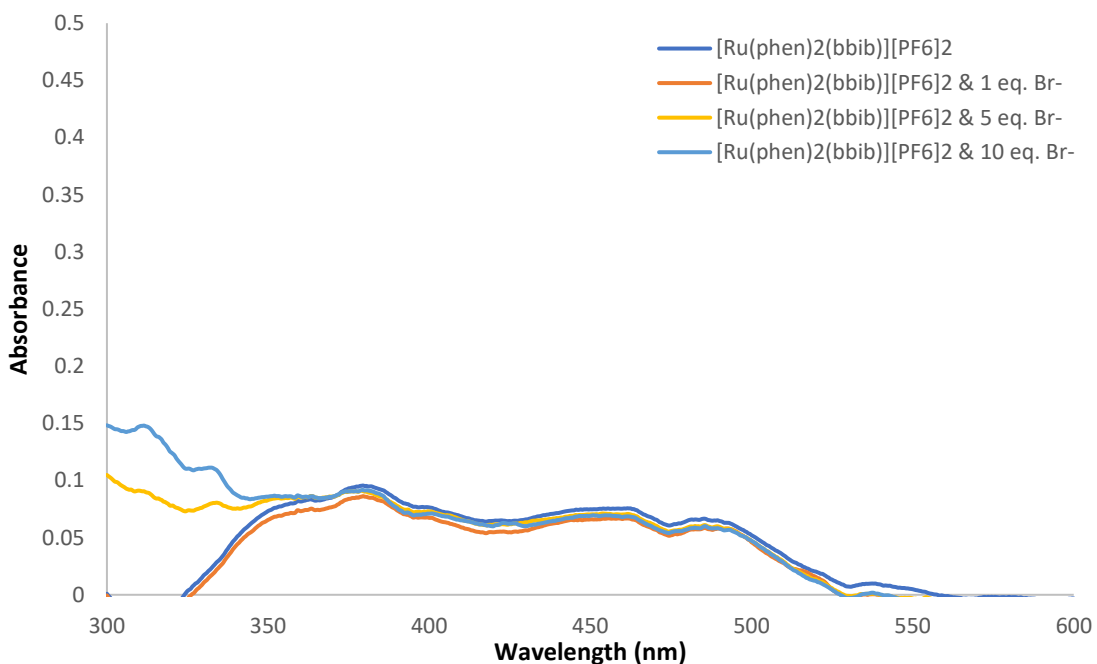
Appx.7 - *UV/Vis absorbance spectra of [Ru(phen)₂(bbib][PF₆]₂ (5 μM) with increasing concentration of TBA Br. Spectra recorded in DMSO/ 5% deionised water at 25 C.*
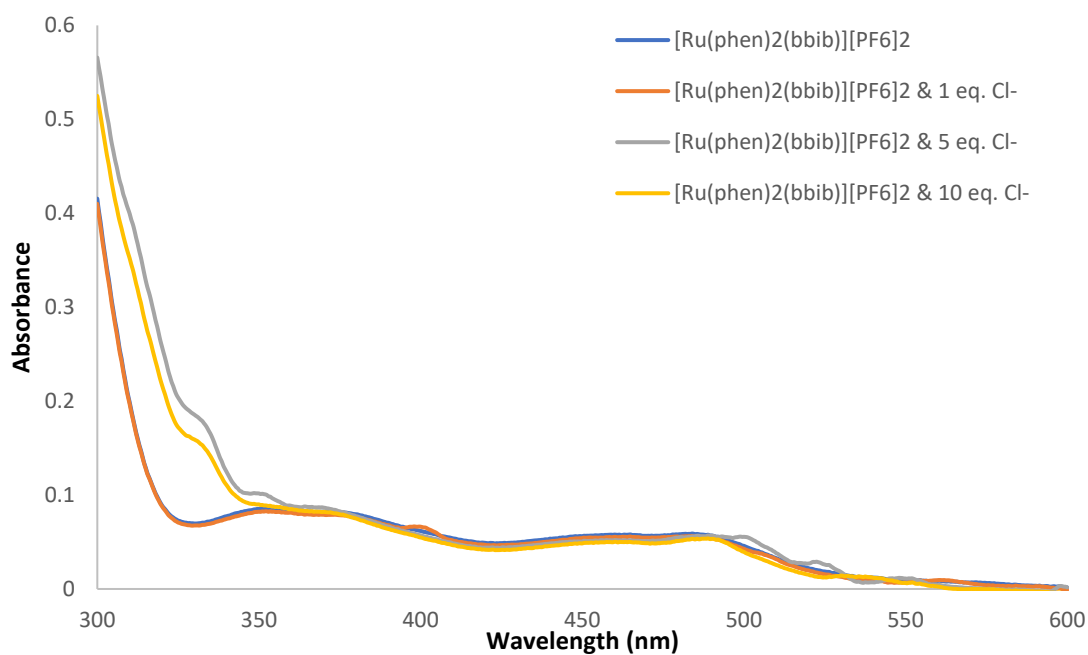
Appx. 8 - *UV/Vis absorbance spectra of [Ru(phen)₂(bbib][PF₆]₂ (5 µM) with increasing concentration of TBA Cl. Spectra recorded in DMSO/ 5% deionised water at 25 C.*

7.1.3 Emission Spectra
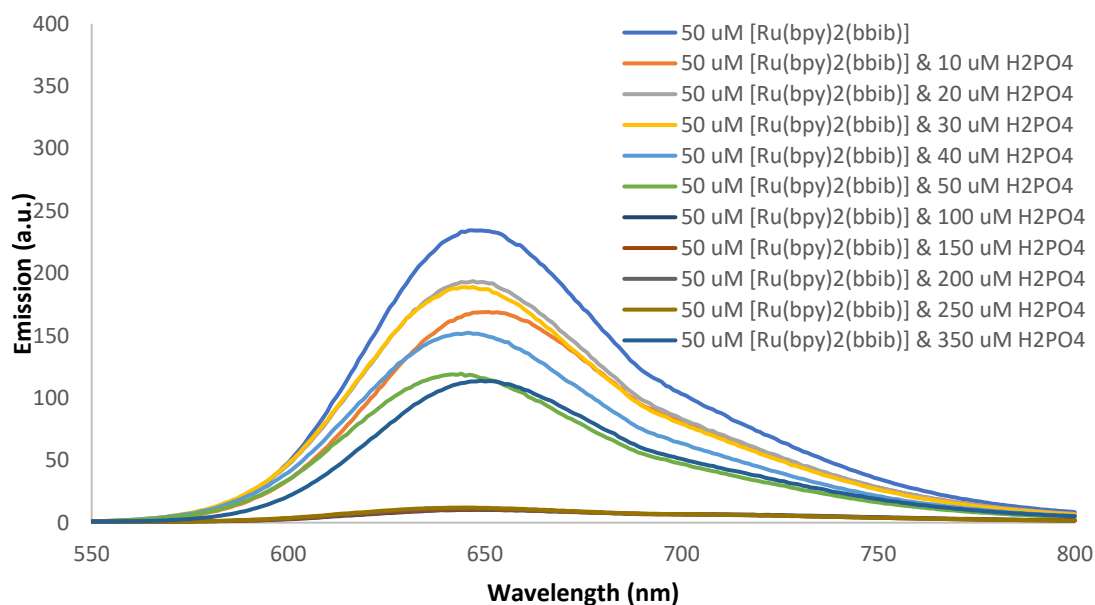
Appx. 9 - *Luminescence emission titration of [Ru(bpy)₂(bbib)][PF₆]₂ (50 µM) with increasing concentration of TBA H₂PO₄. Spectra recorded in acetonitrile at 25 C.*
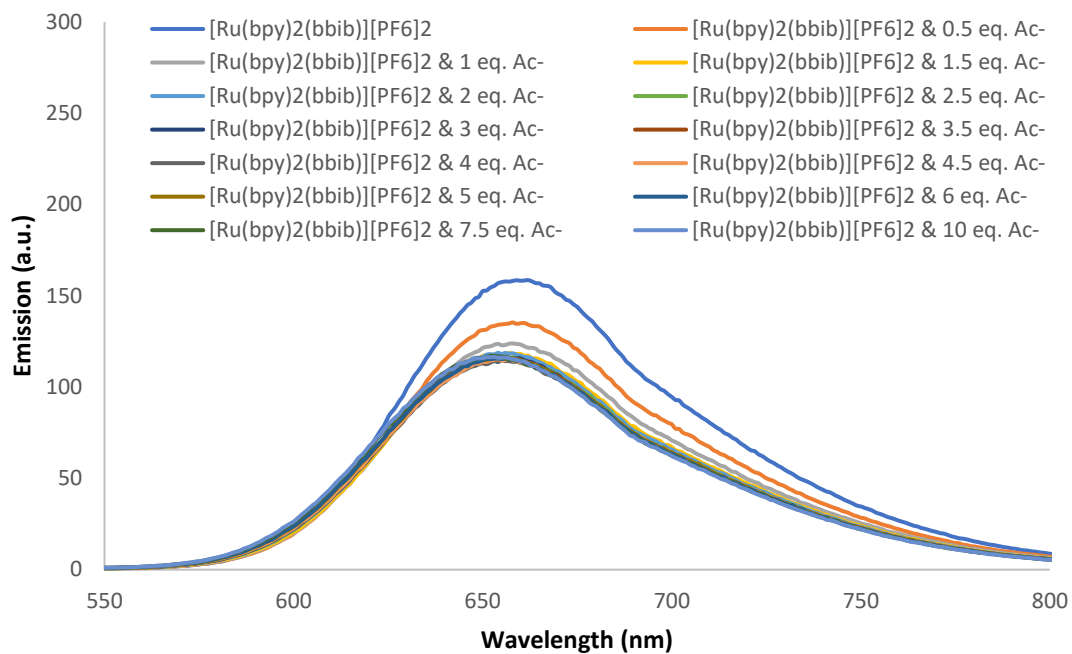
Appx. 10 - *Luminescence emission titration of [Ru(bpy)₂(bbib][PF₆]₂ (5 µM) with increasing concentration of TBA AcO. Spectra recorded in DMSO/ 5% deionised water at 25 C.*
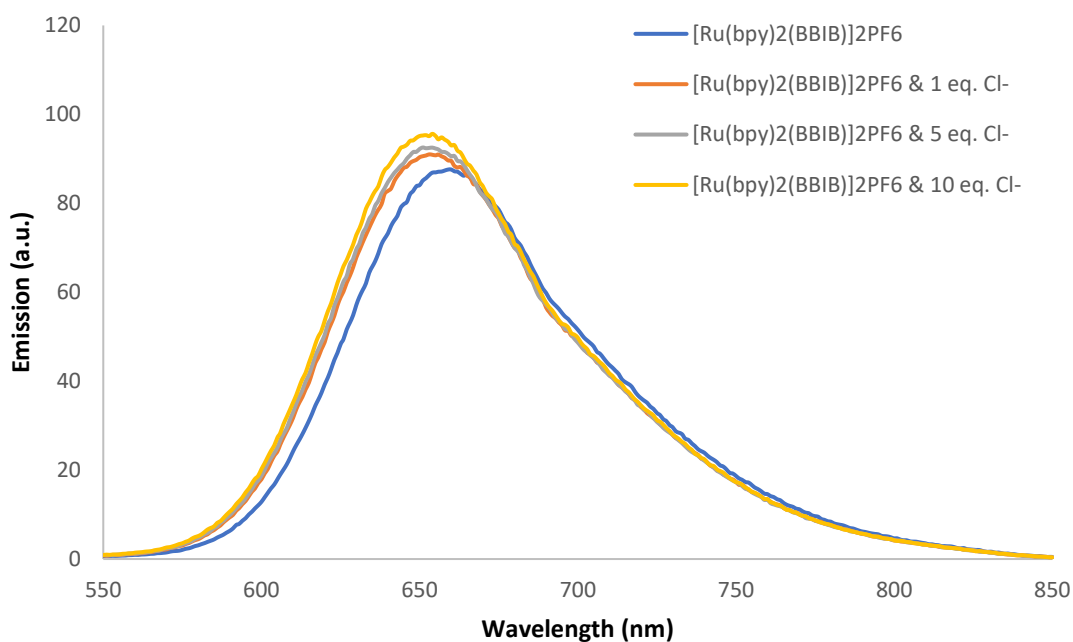
Appx. 11 - *Luminescence emission titration of [Ru(bpy)₂(bbib][PF₆]₂ (5 µM) with increasing concentration of TBA Cl. Spectra recorded in DMSO/ 5% deionised water at 25 C.*
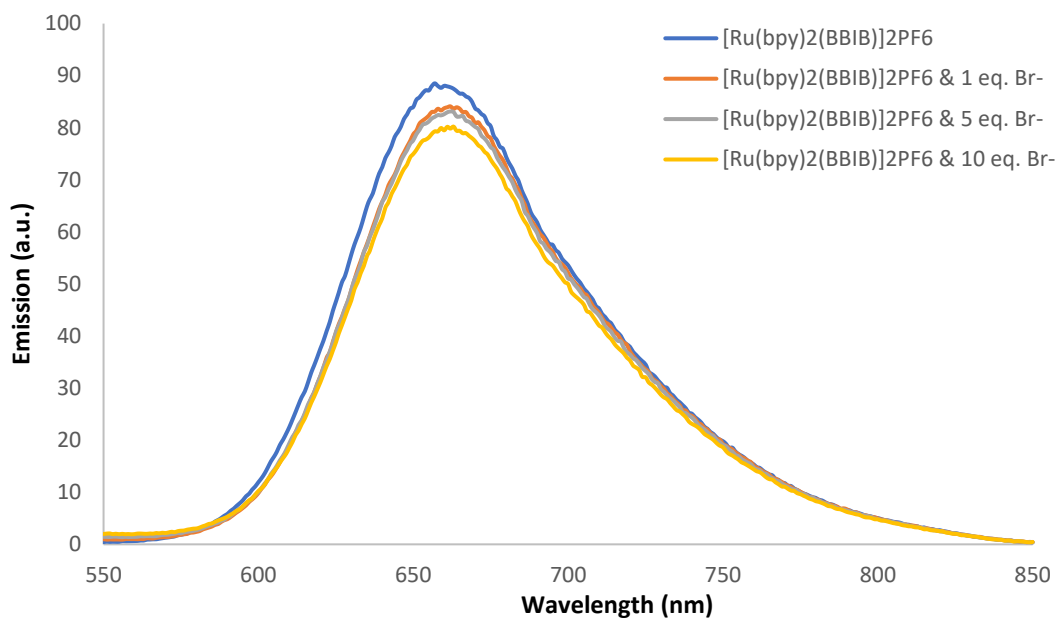
Appx. 12 - *Luminescence emission titration of [Ru(bpy)₂(bbib][PF₆]₂ (5 µM) with increasing concentration of TBA Br. Spectra recorded in DMSO/ 5% deionised water at 25 C.*
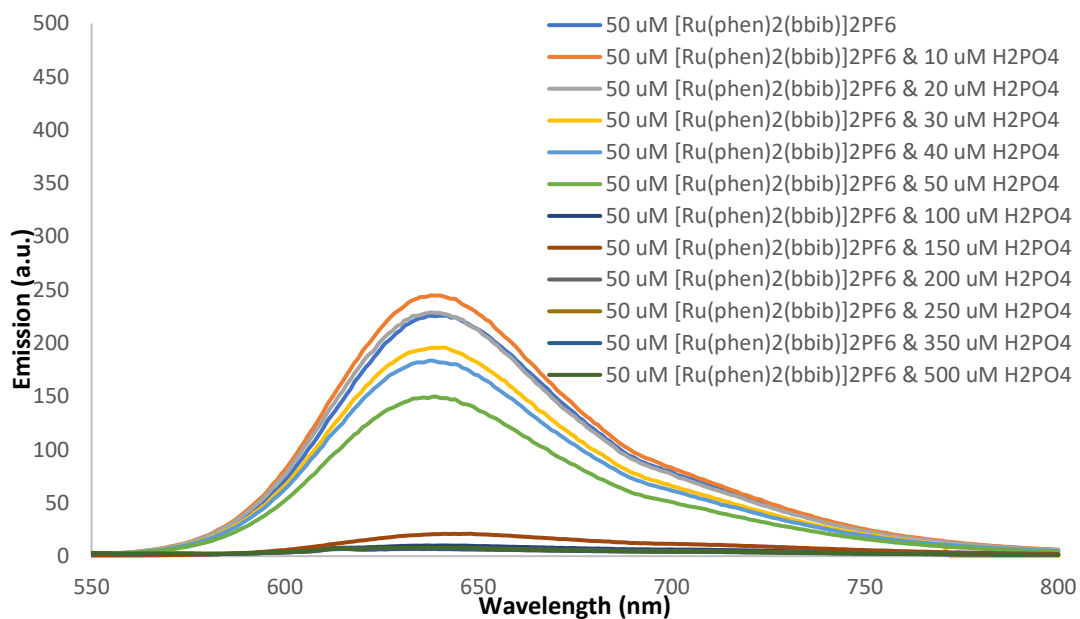
Appx. 13 - *Luminescence emission titration of [Ru(phen)₂(bbib][PF₆]₂ (50 µM) with increasing concentration of TBA H₂PO₄. Spectra recorded in acetonitrile at 25 C.*
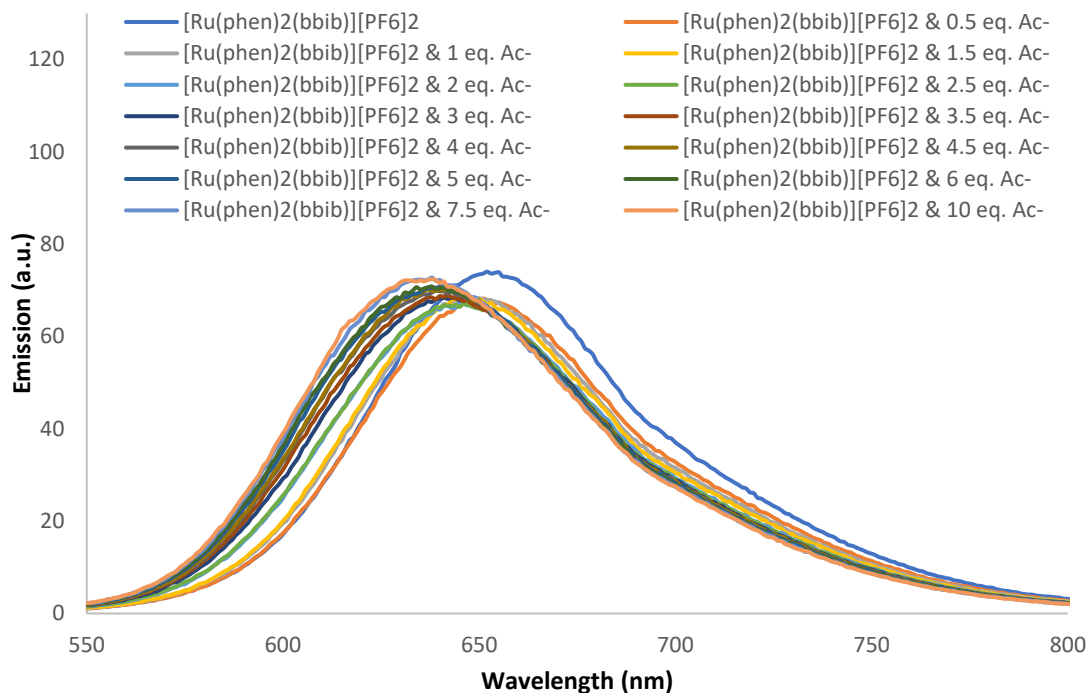
Appx. 14 - *Luminescence emission titration of [Ru(phen)₂(bbib][PF₆]₂ (5 µM) with increasing concentration of TBA AcO. Spectra recorded in DMSO/ 5% deionised water at 25 C.*
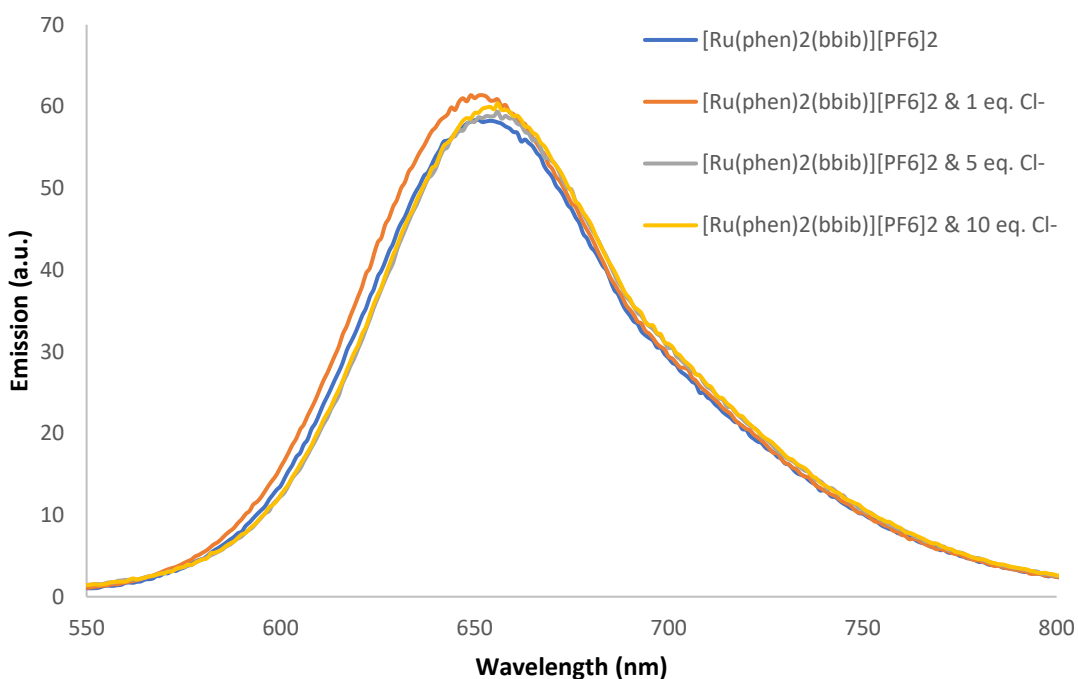
Appx. 15 - *Luminescence emission titration of [Ru(phen)₂(bbib][PF₆]₂ (5 µM) with increasing concentration of TBA Cl. Spectra recorded DMSO/ 5% deionised water at 25 C.*
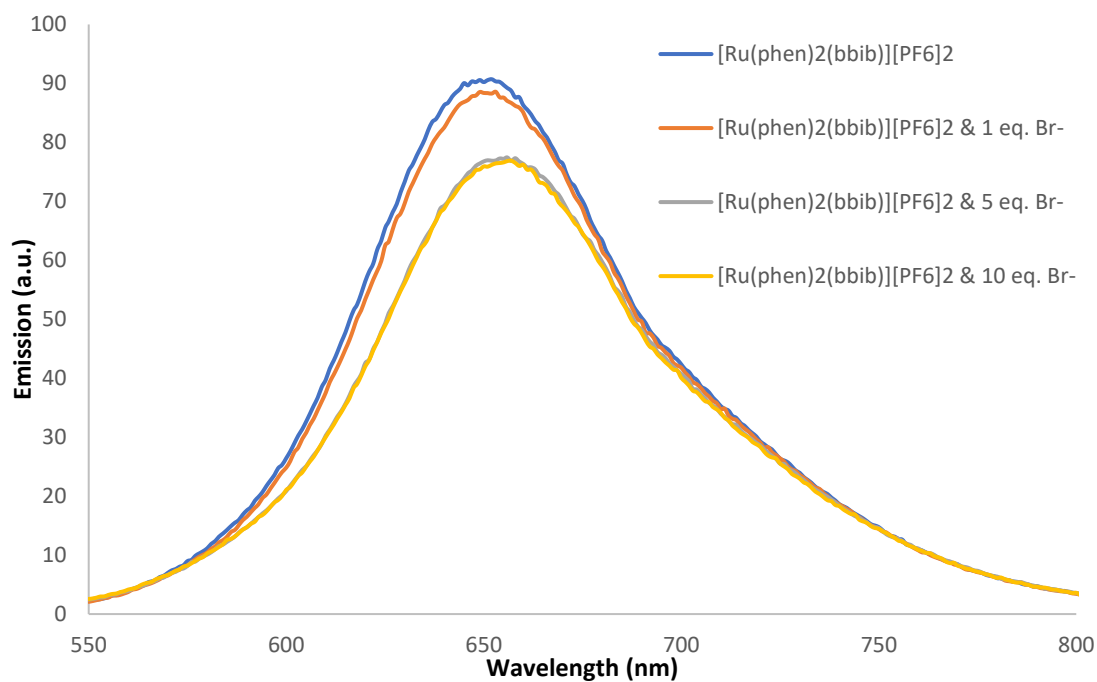
Appx. 16 - *Luminescence emission titration of [Ru(phen)₂(bbib][PF₆]₂ (5 μM) with increasing concentration of TBA Br. Spectra recorded DMSO/ 5% deionised water at 25°C.*

7.1.4 ¹H-NMR Titration Spectra
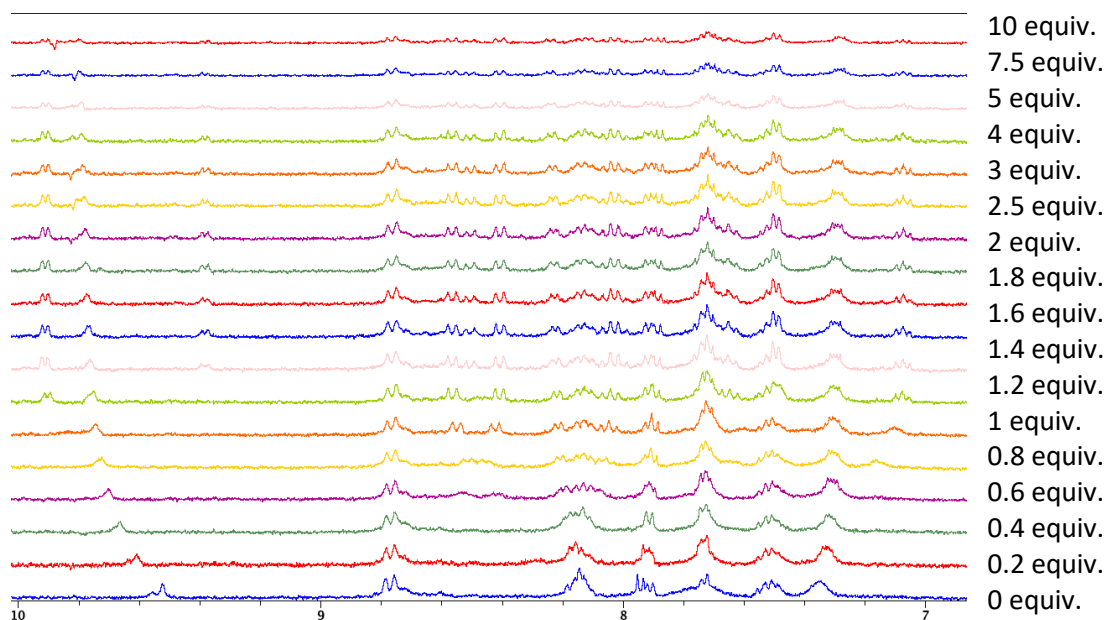
Appx. 17 – *¹H-NMR titration of [Ru(bpy)₂(bbib][PF₆]₂ and AcO⁻ in DMSO/5% deuterated water.*
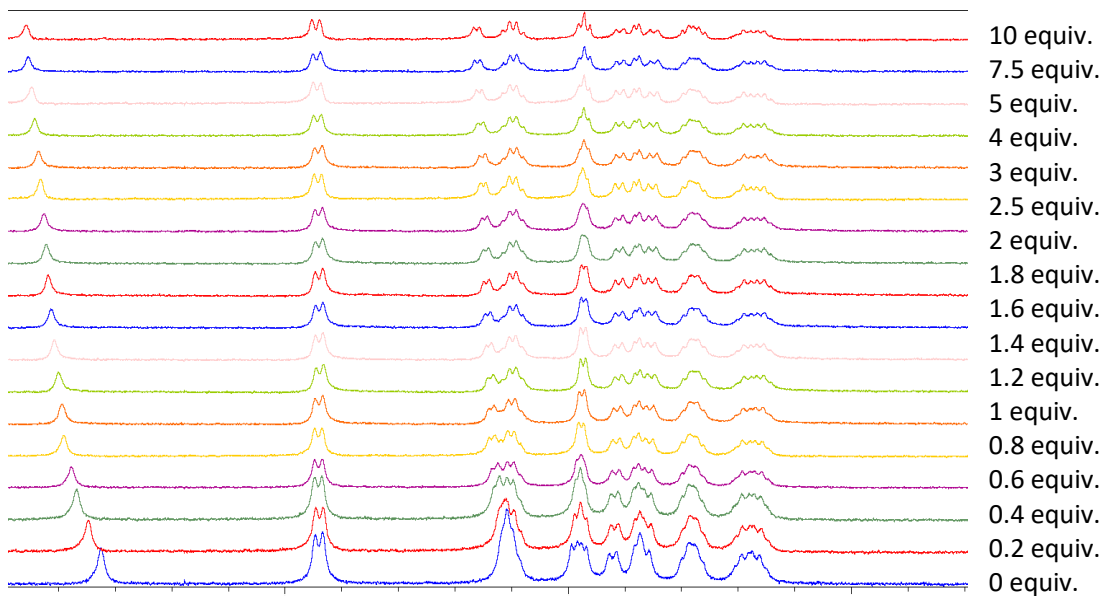
Appx. 18 – *^{1}H-NMR titration of [Ru(bpy)$_2$(bbib)][PF$_6$]$_2$ and Cl$^-$ in DMSO/5% deuterated water.*
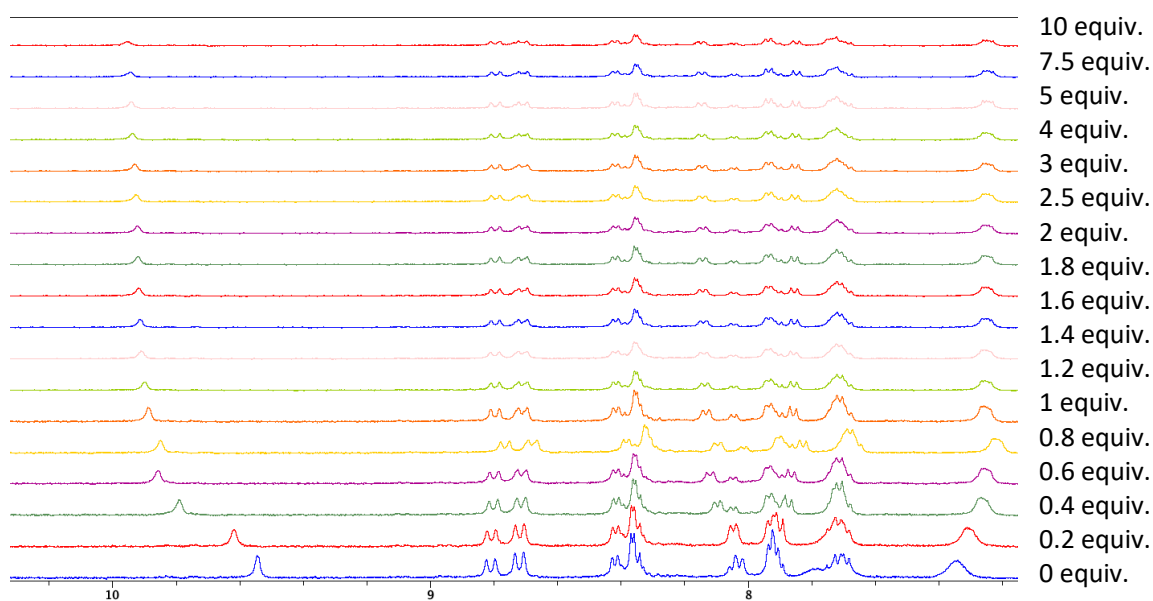
Appx. 19 – *^{1}H-NMR titration of [Ru(phen)$_2$(bbib)][PF$_6$]$_2$ and H$_2$PO$_4$$^-$ in DMSO/5% deuterated water.*
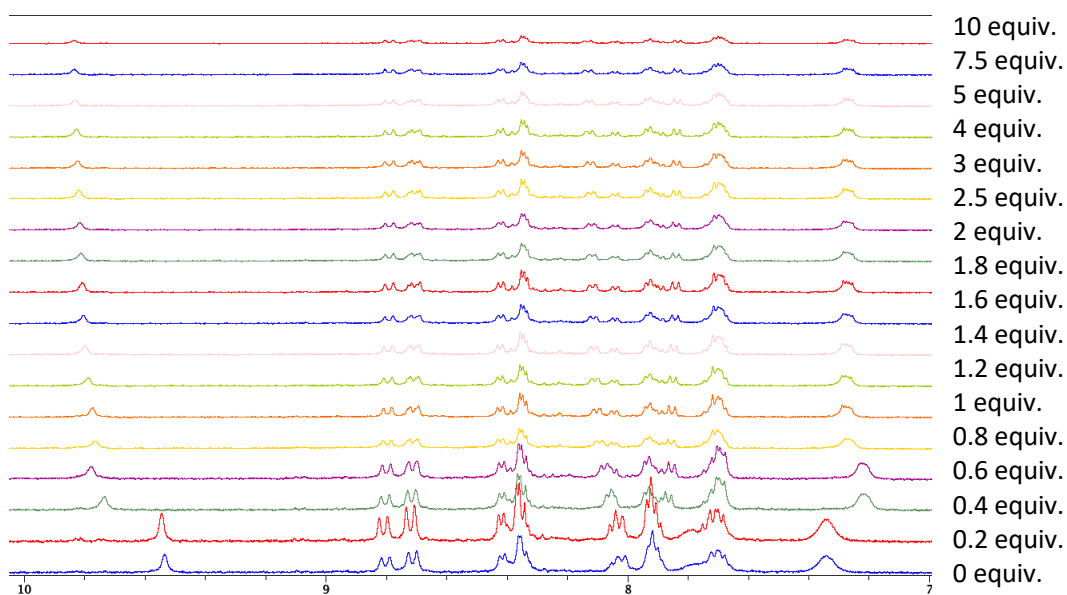
Appx. 20 - *¹H-NMR titration of [Ru(phen)₂(bbib][PF₆]₂ and AcO⁻ in DMSO/5% deuterated water.*
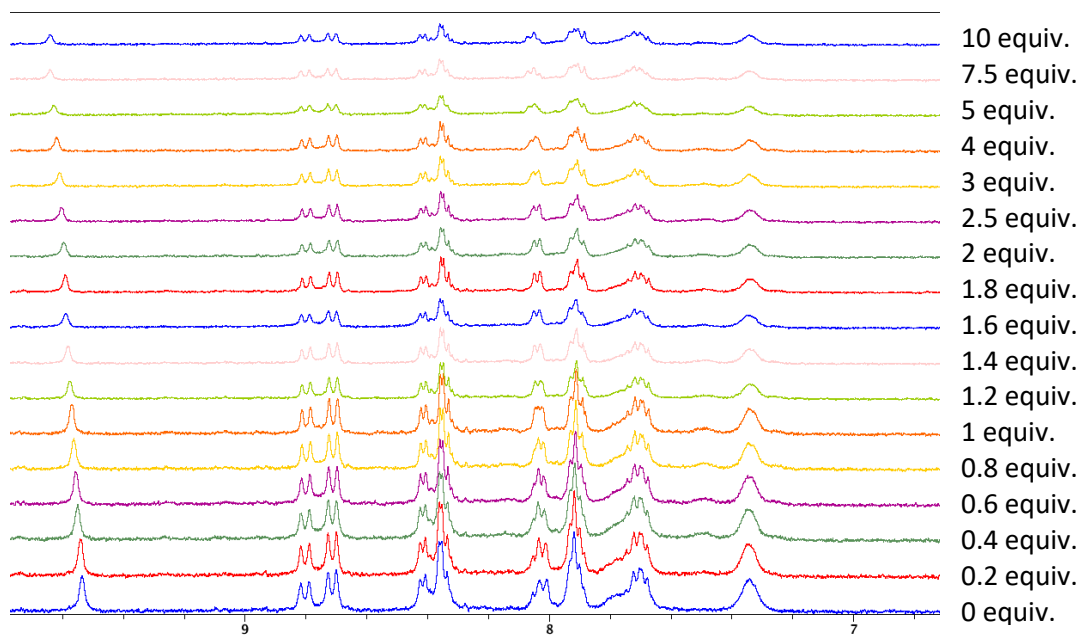
Appx. 21 – *¹H-NMR titration of [Ru(phen)₂(bbib][PF₆]₂ and Cl⁻ in DMSO/5% deuterated water.*

7.1.5 IR Spectra
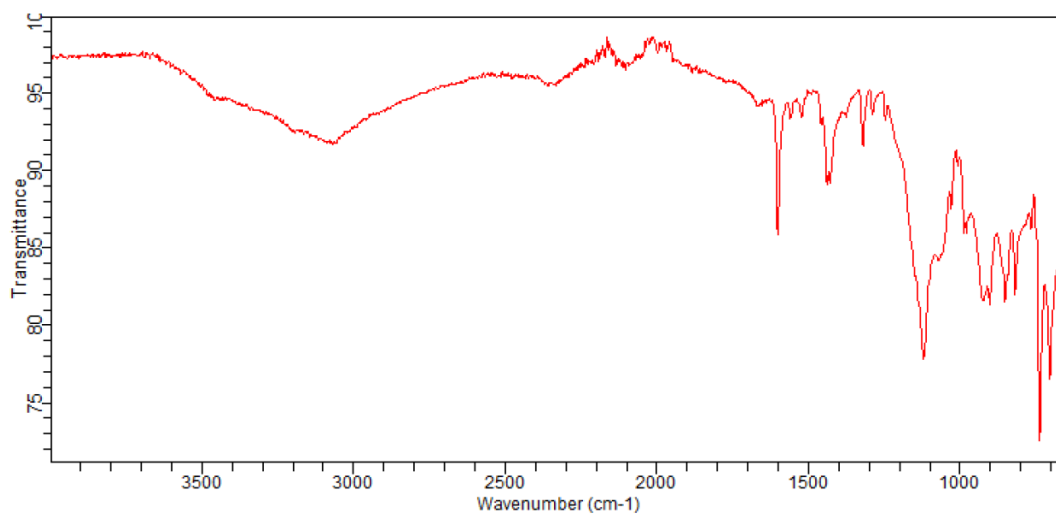
***Appx. 22** – IR spectrum of bbib (KBr Disc) recorded at 25°C.*
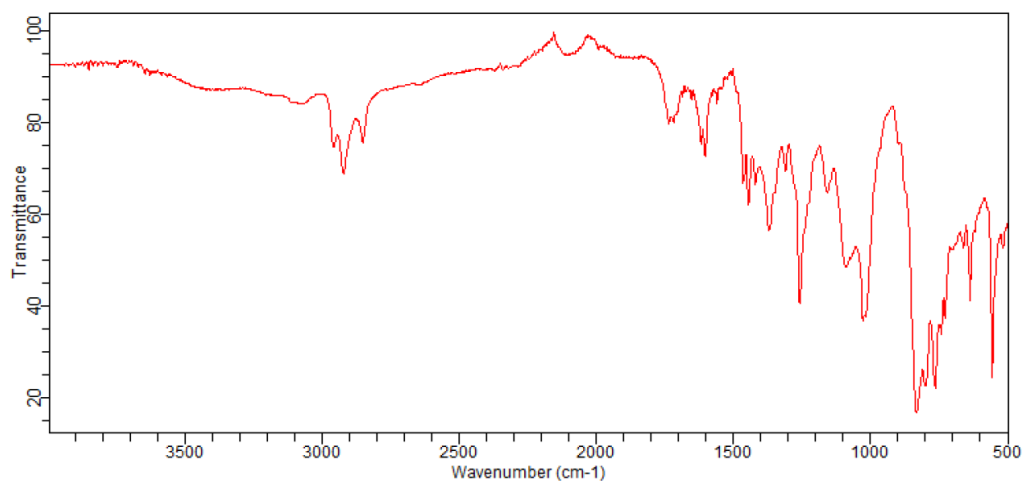
***Appx. 23** – IR spectrum of [Ru(bpy)$_2$(bbib)][PF$_6$]$_2$ (KBr Disc) recorded at 25°C.*
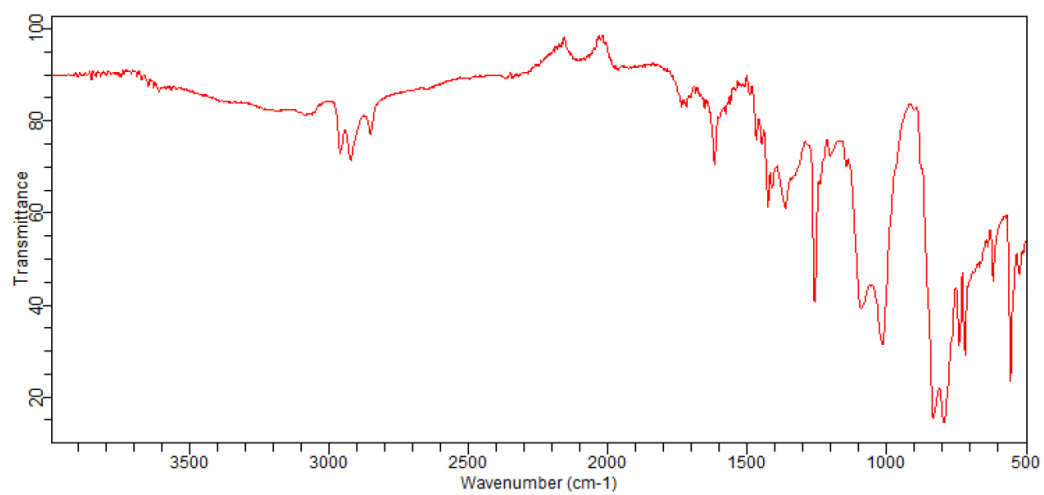
***Appx. 24** – IR spectrum of [Ru(phen)$_2$(bbib)][PF$_6$]$_2$ (KBr Disc) recorded at 25°C.*

7.1.6 COSY Spectra
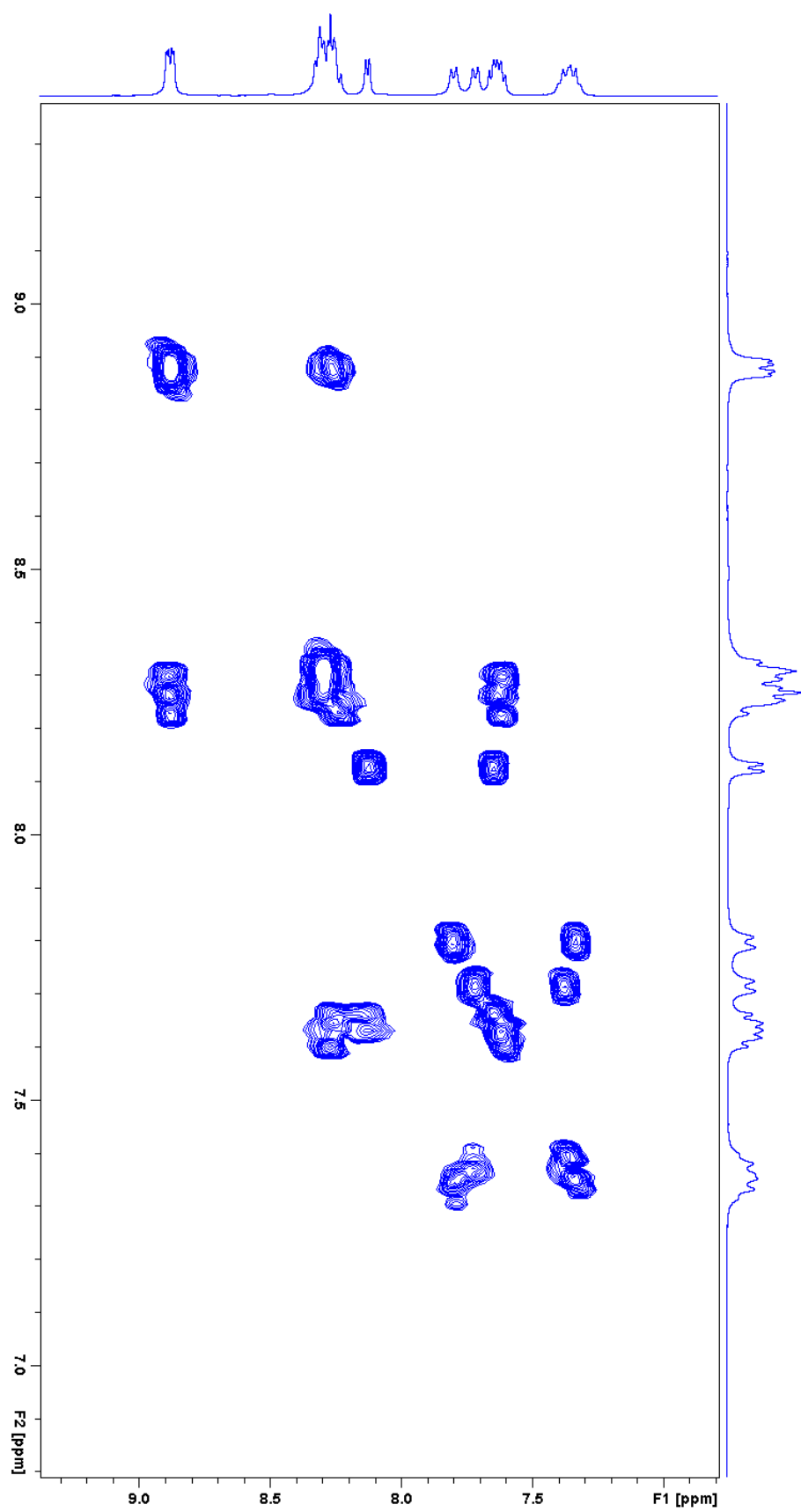
Appx. 25 – *COSY spectrum recorded for [Ru(bpy)$_2$(bbib)][PF$_6$]$_2$ in Acetone-d$_6$ at 25°C.*
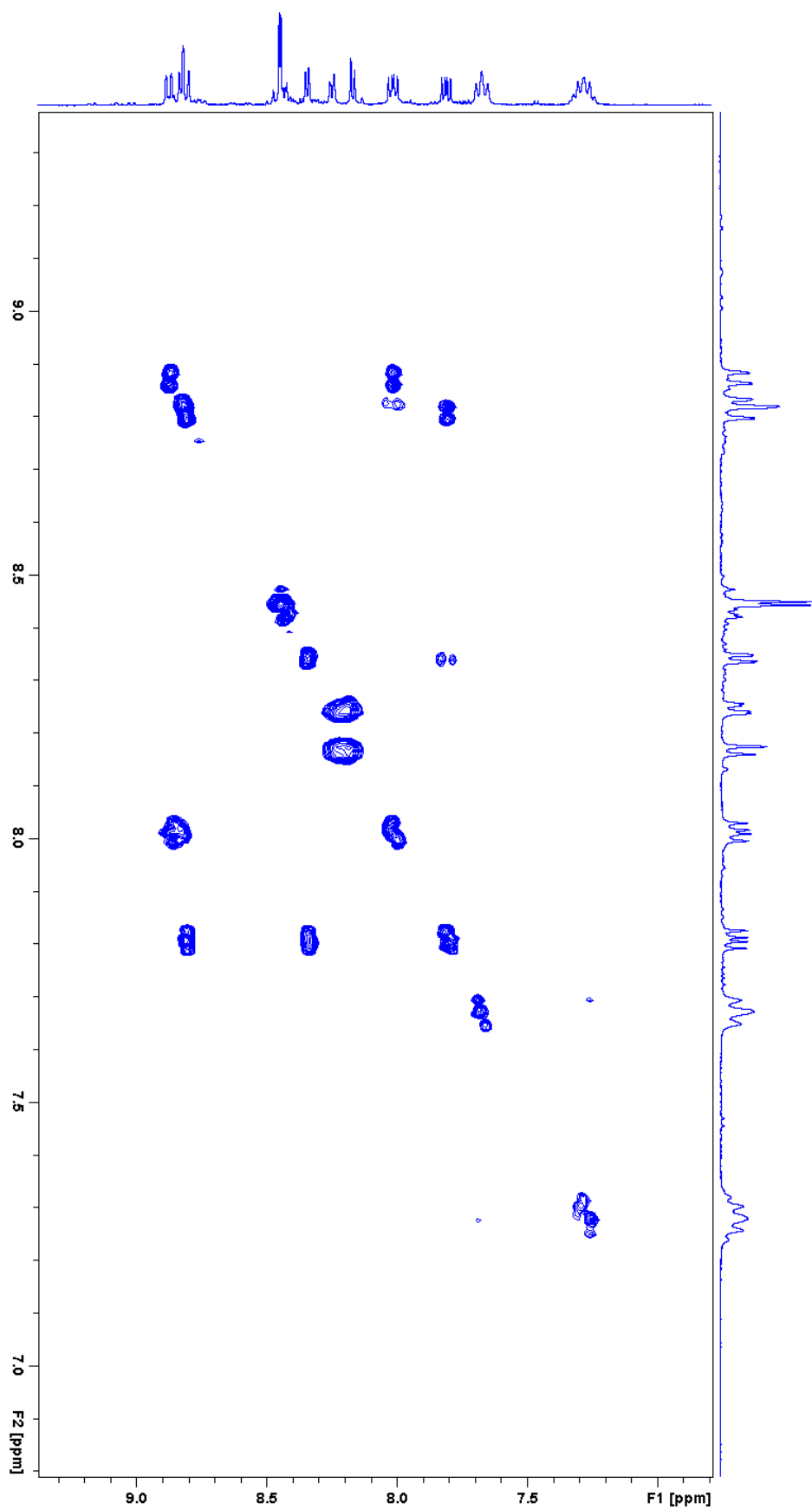
Appx. 26 – *COSY spectrum recorded for [Ru(phen)₂(bbib)][PF₆]₂ in Acetone-d₆ at 25°C.*

7.2 Data Obtained for [Ru(bpy)₂(bbaib)]²⁺ and [Ru(phen)₂(bbaib)]²⁺ (Chapter Three)

7.2.1 UV/Vis Absorbance Spectra
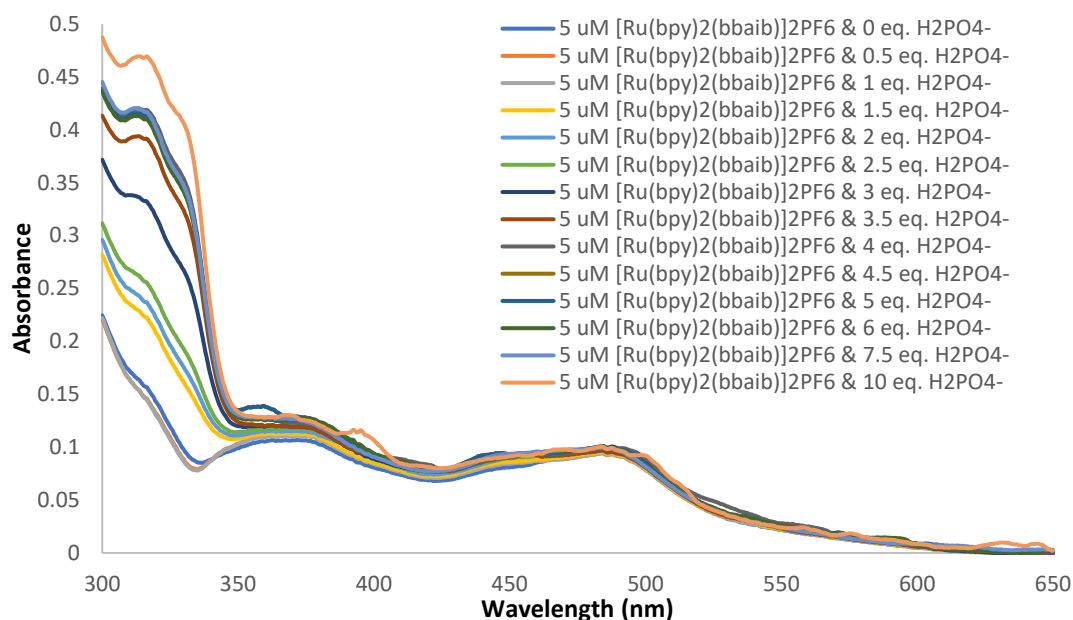
Appx. 27 - *UV/Vis absorbance spectra of [Ru(bpy)₂(bbaib)][PF₆]₂ (50 µM) with increasing concentration of TBA H₂PO₄. Spectra recorded in DMSO/ 5% deionised water at 25 C.*
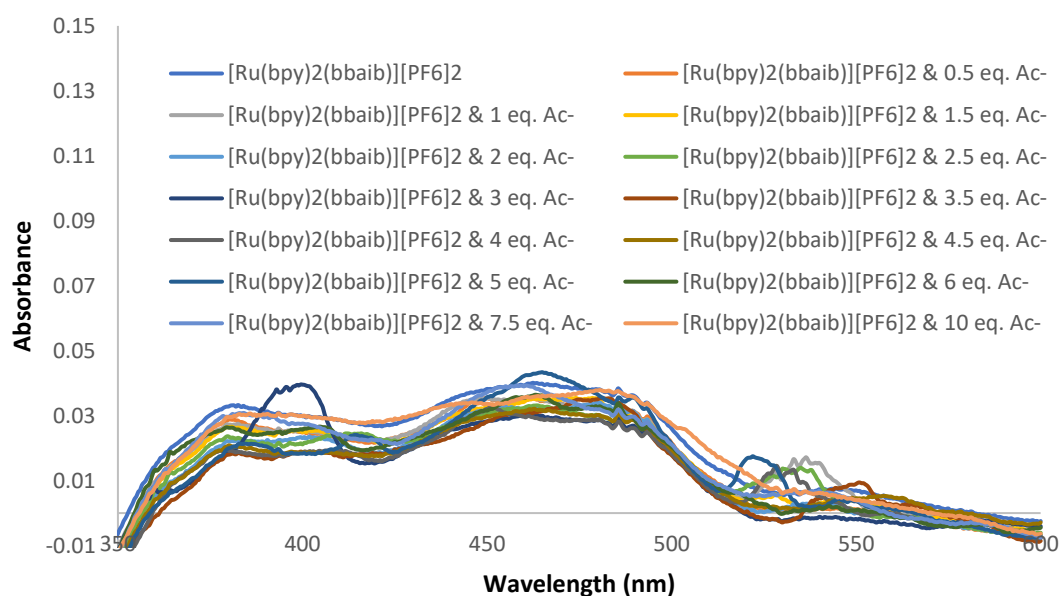
Appx. 28 - *UV/Vis absorbance spectra of [Ru(bpy)₂(bbaib)][PF₆]₂ (5 µM) with increasing concentration of TBA AcO. Spectra recorded in DMSO/ 5% deionised water at 25 C.*
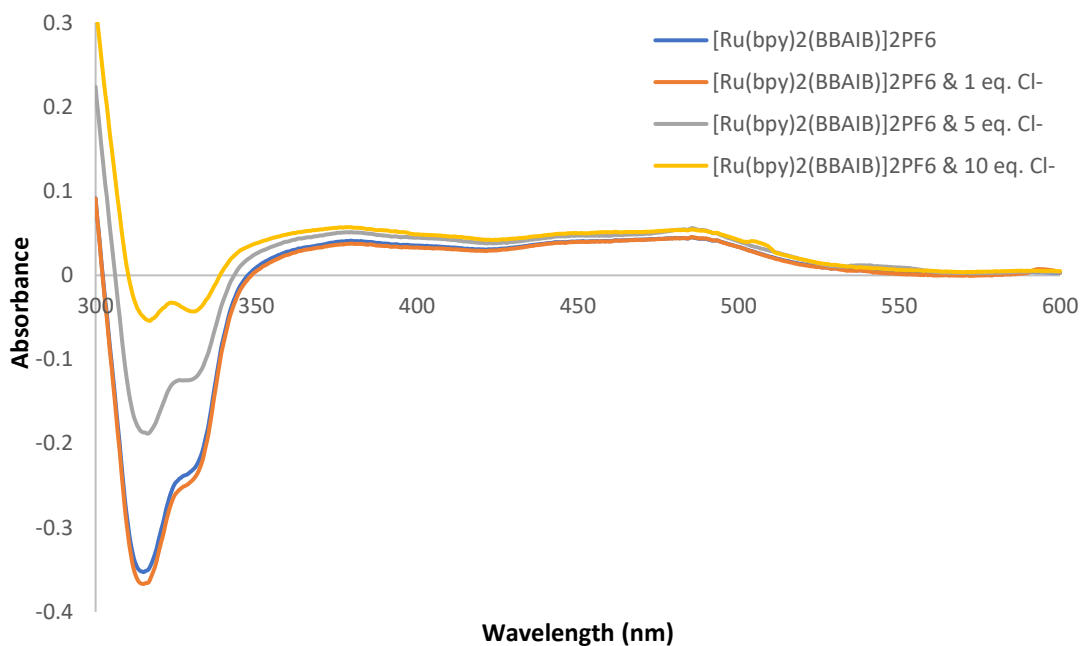
Appx. 29 - *UV/Vis absorbance spectra of [Ru(bpy)₂(bbaib][PF₆]₂ (5 µM) with increasing concentration of TBA Cl. Spectra recorded in DMSO/ 5% deionised water at 25˚C.*
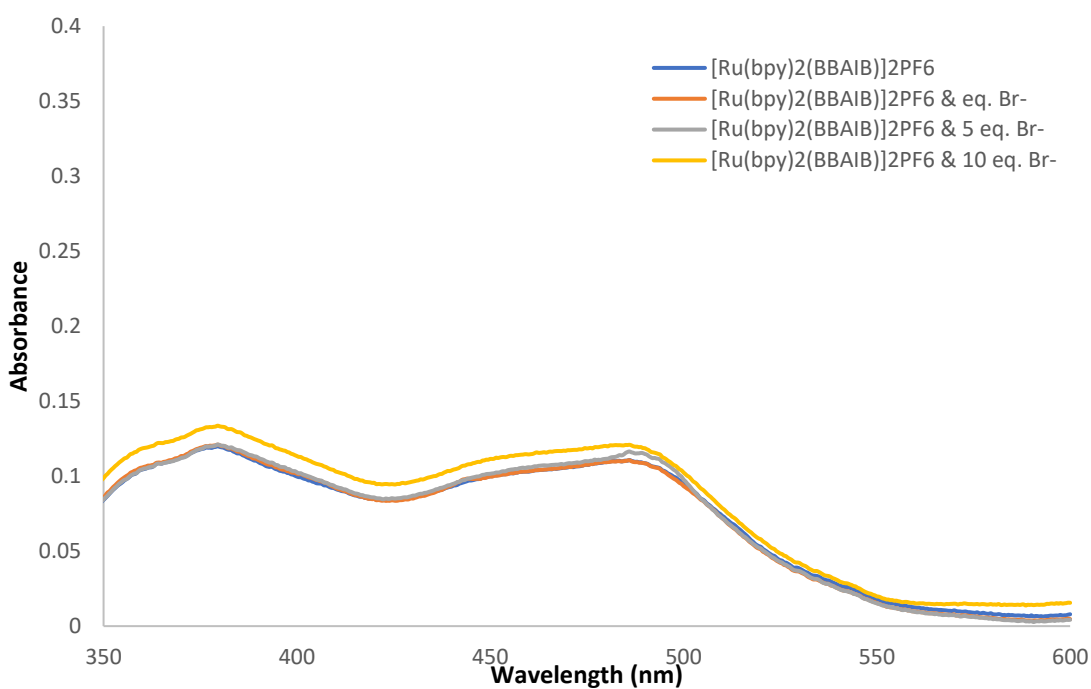
Appx. 30 - *UV/Vis absorbance spectra of [Ru(bpy)₂(bbaib][PF₆]₂ (5 µM) with increasing concentration of TBA Br. Spectra recorded in DMSO/ 5% deionised water at 25˚C.*
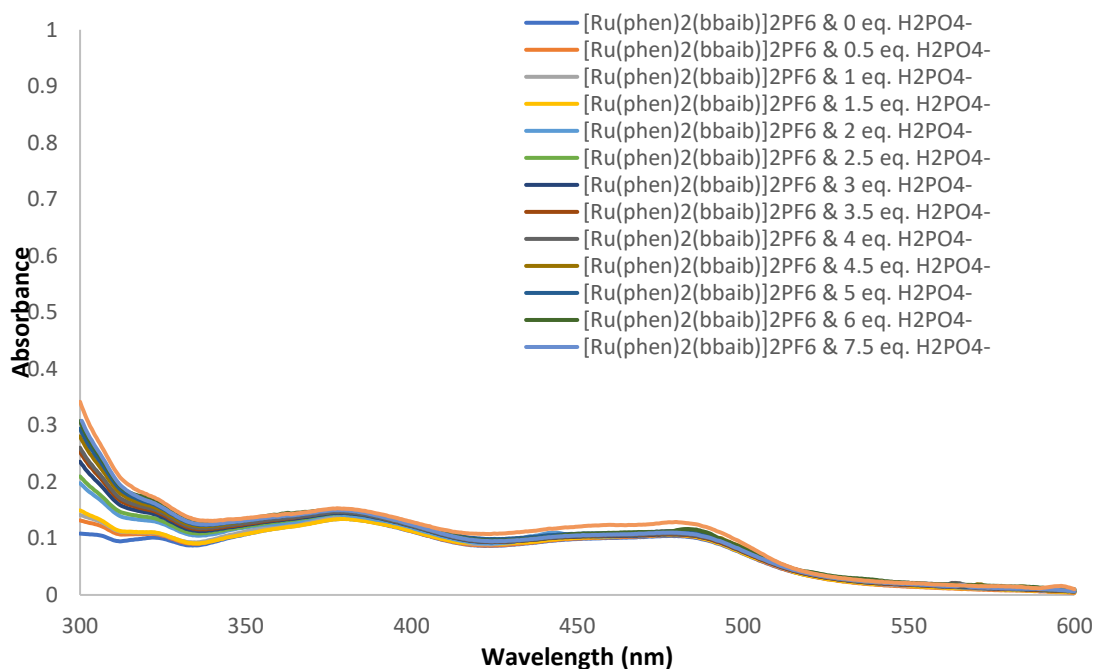
Appx. 31 - *UV/Vis absorbance spectra of [Ru(phen)₂(bbaib][PF₆]₂ (5 μM) with increasing concentration of TBA H₂PO₄. Spectra recorded in DMSO/ 5% deionised water at 25°C.*
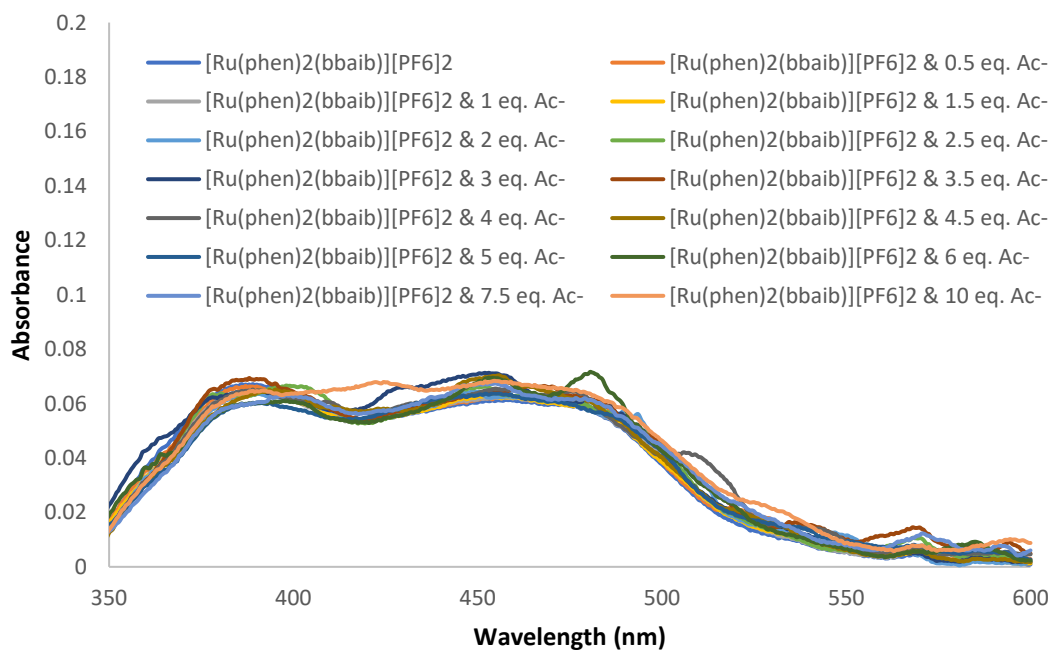
Appx. 32 - *UV/Vis absorbance spectra of [Ru(phen)₂(bbaib][PF₆]₂ (5 μM) with increasing concentration of TBA AcO. Spectra recorded in DMSO/ 5% deionised water at 25°C.*
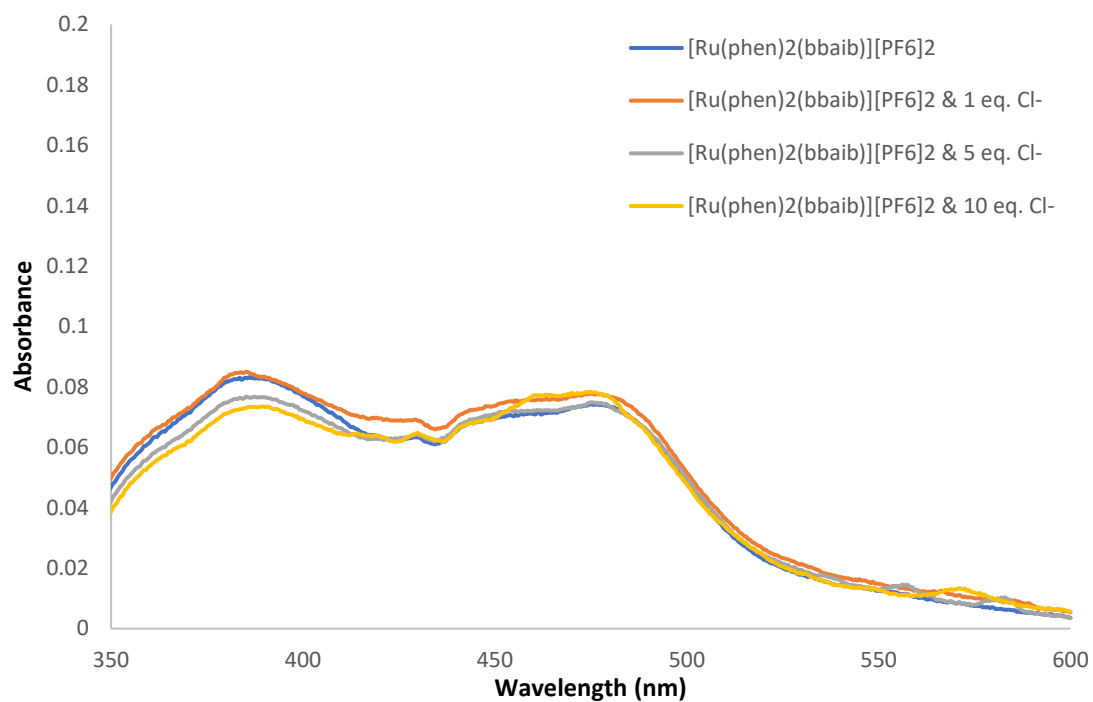
Appx. 33 - *UV/Vis absorbance spectra of [Ru(phen)₂(bbaib][PF₆]₂ (5 μM) with increasing concentration of TBA Cl. Spectra recorded in DMSO/ 5% deionised water at 25°C.*
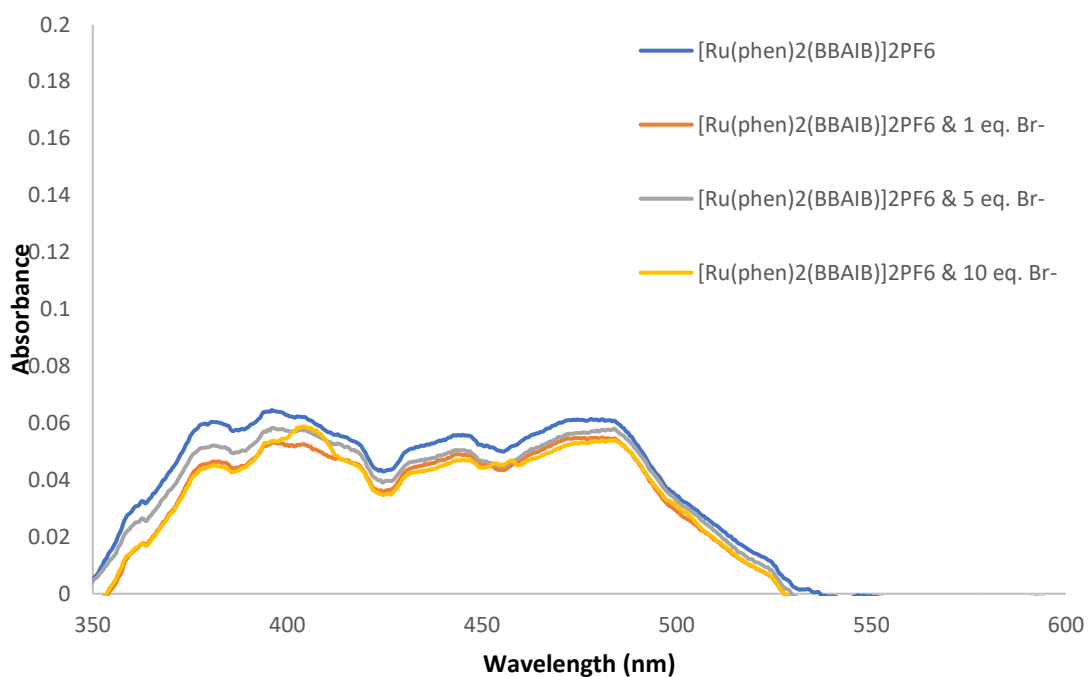
Appx. 34 - *UV/Vis absorbance spectra of [Ru(phen)₂(bbaib][PF₆]₂ (5 μM) with increasing concentration of TBA Br. Spectra recorded in DMSO/ 5% deionised water at 25°C.*

220

7.2.2 Emission Spectra
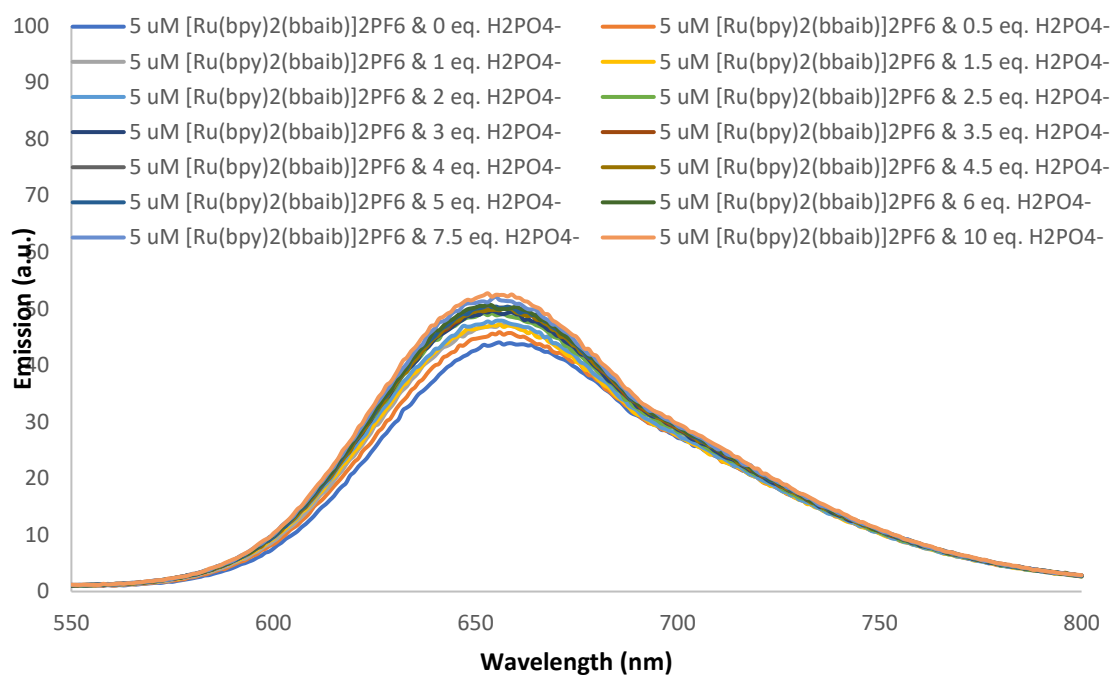
Appx. 35 -
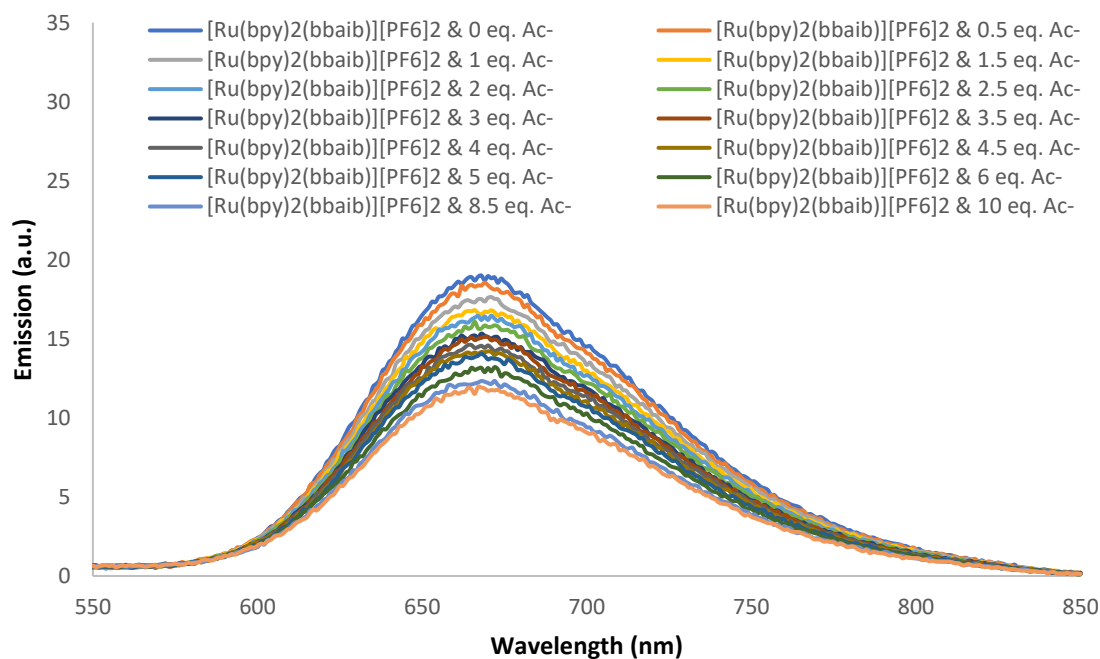
Appx. 36 -
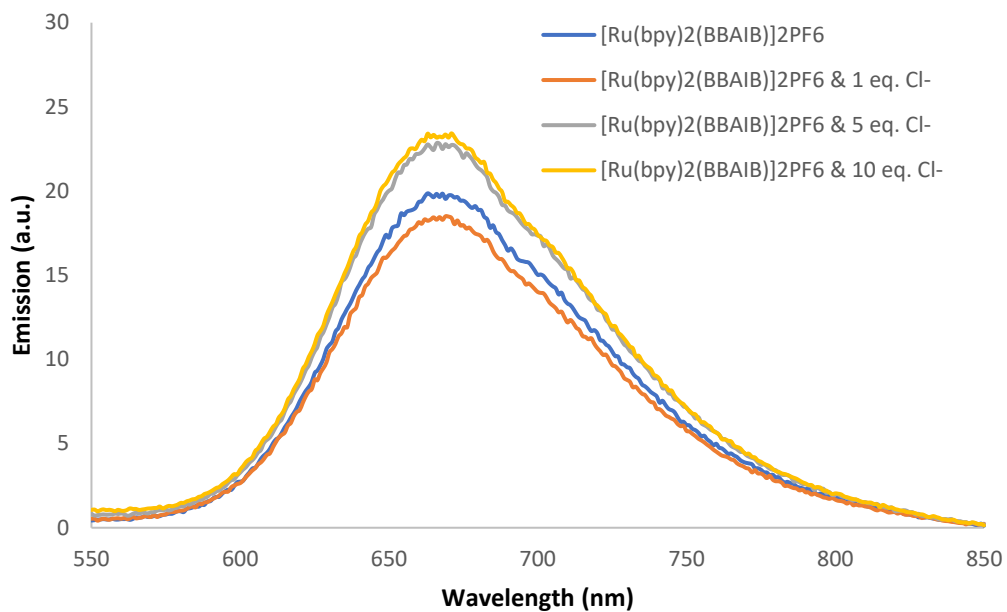
Appx. 37 -
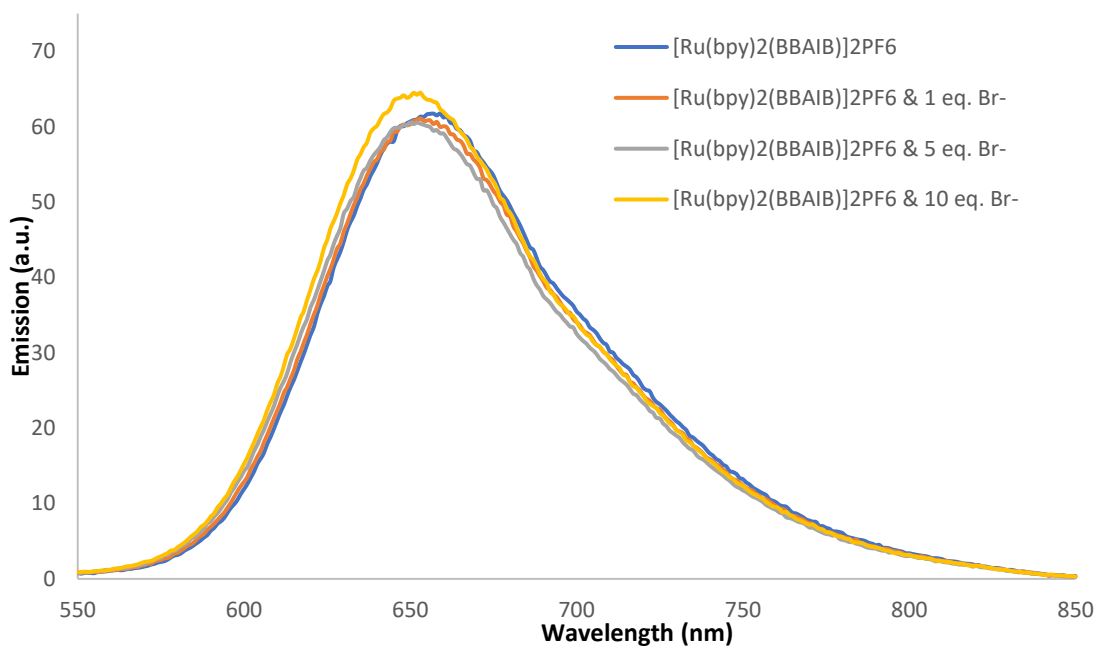
Appx. 38 -
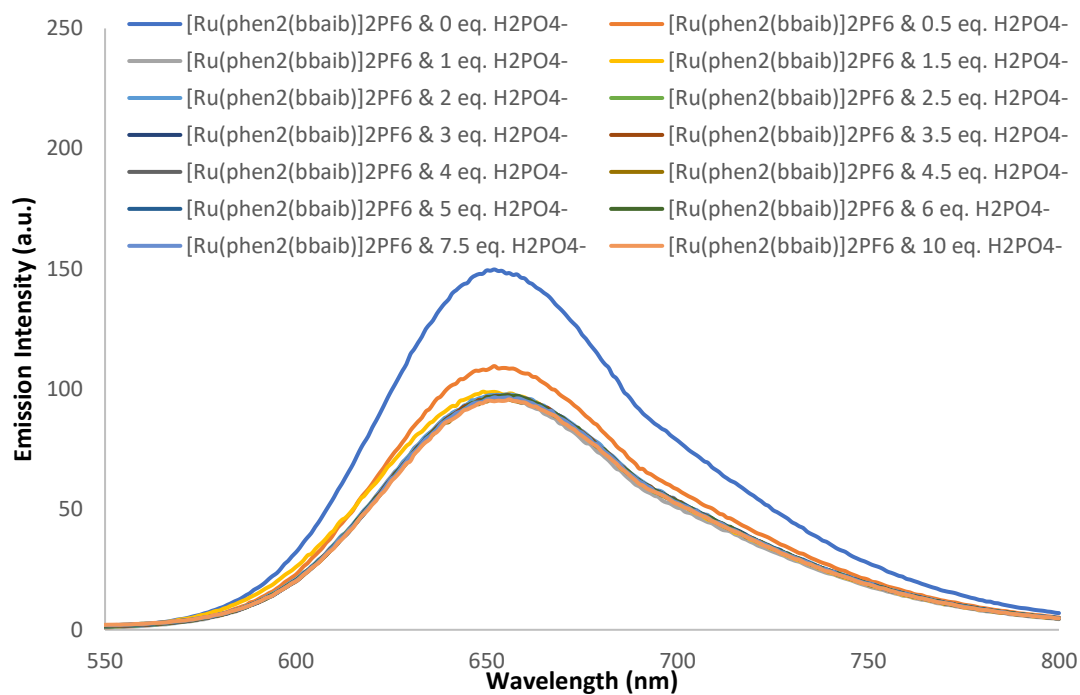
Appx. 39 -
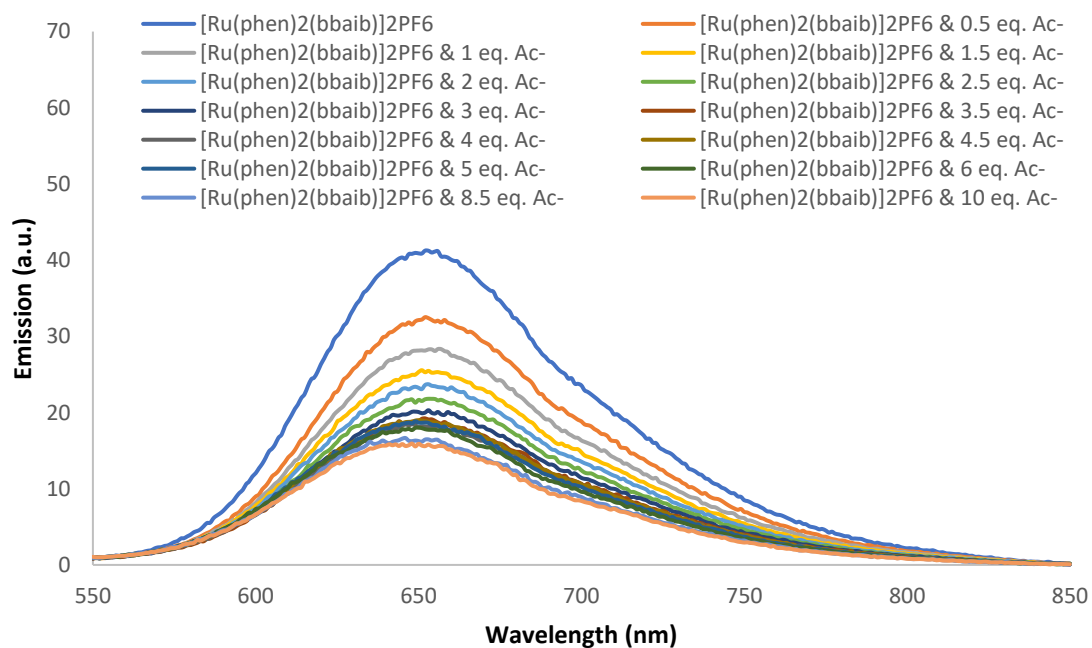
Appx. 40 -
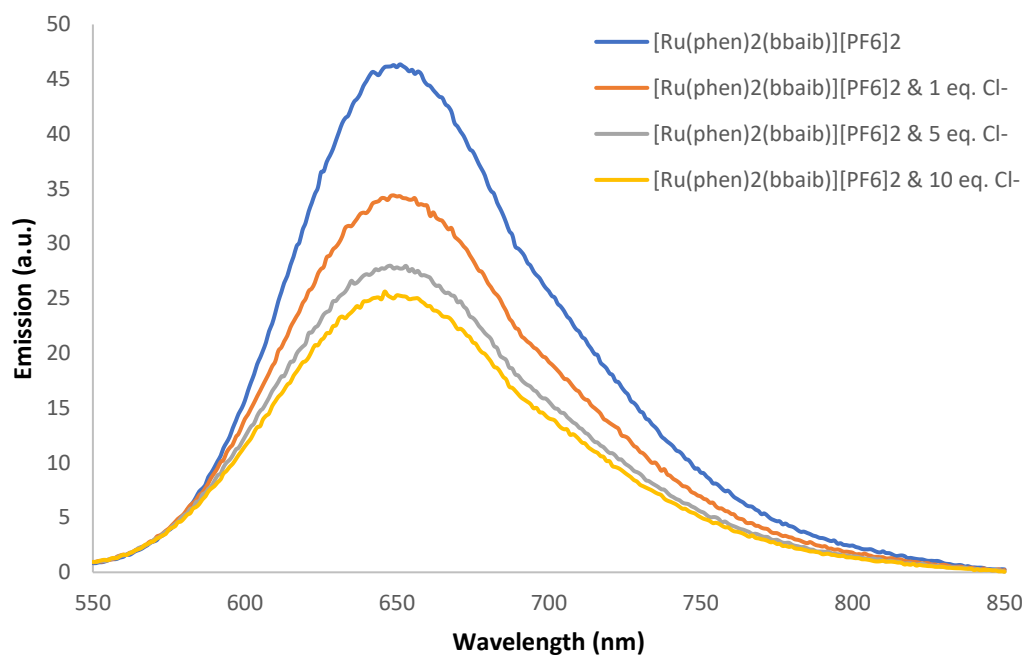
Appx. 41 -
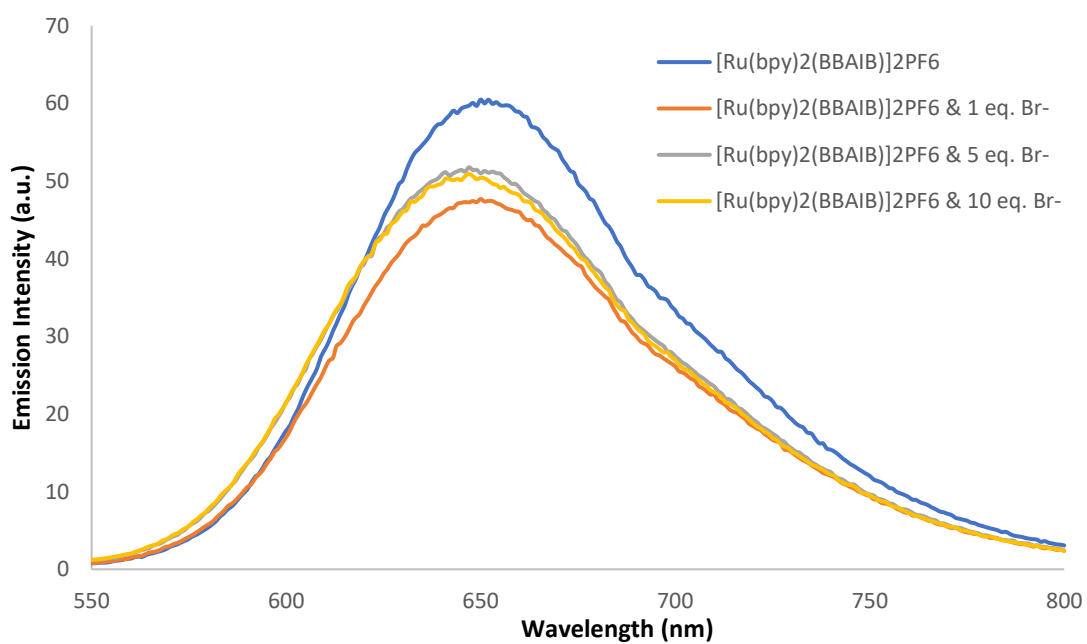
Appx. 42 -

7.2.3 ¹H-NMR Titration Spectra
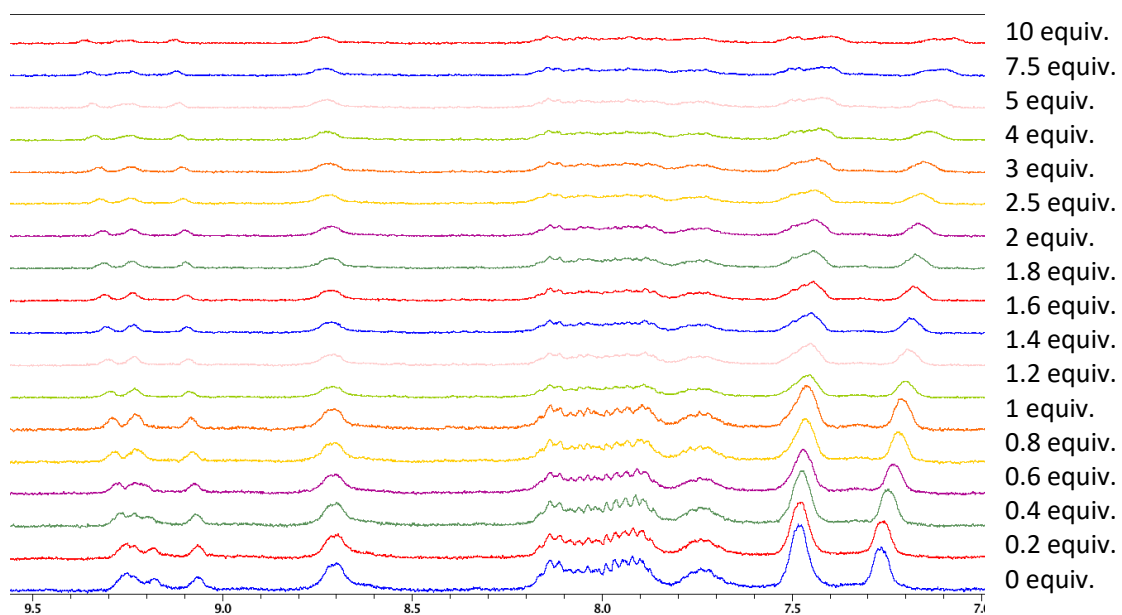
Appx. 43 – bpy ac
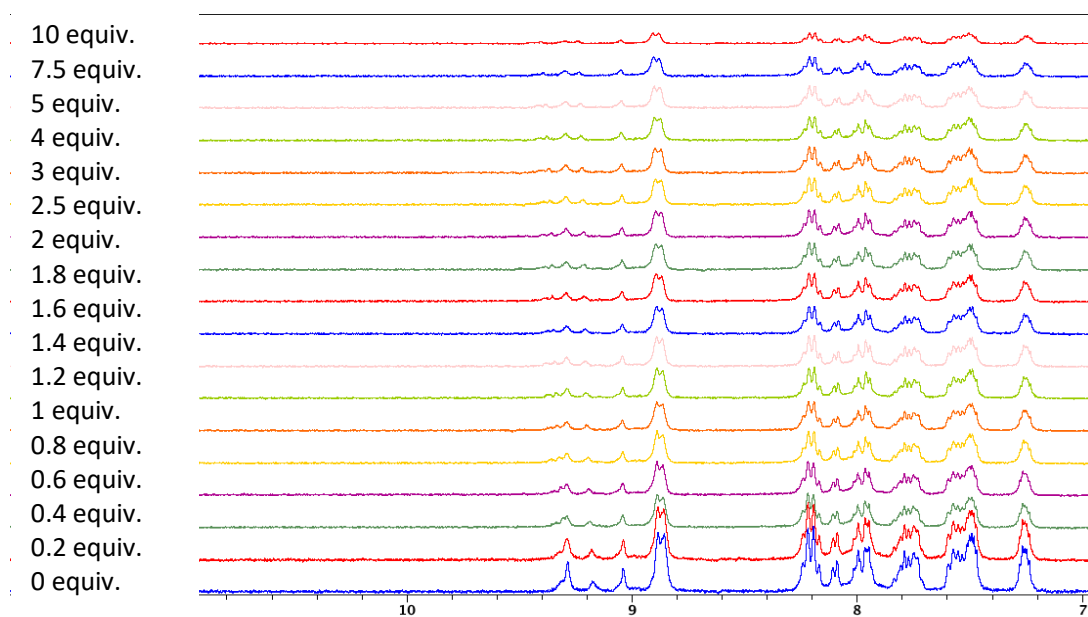
Appx. 44 – bpy cl
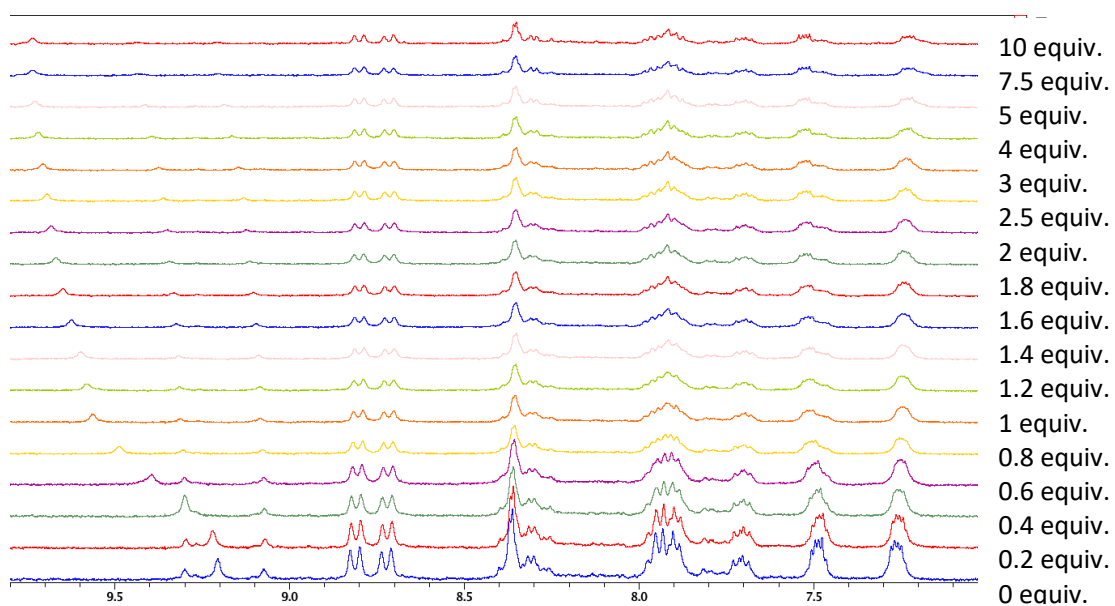
Appx. 45 – phen phos
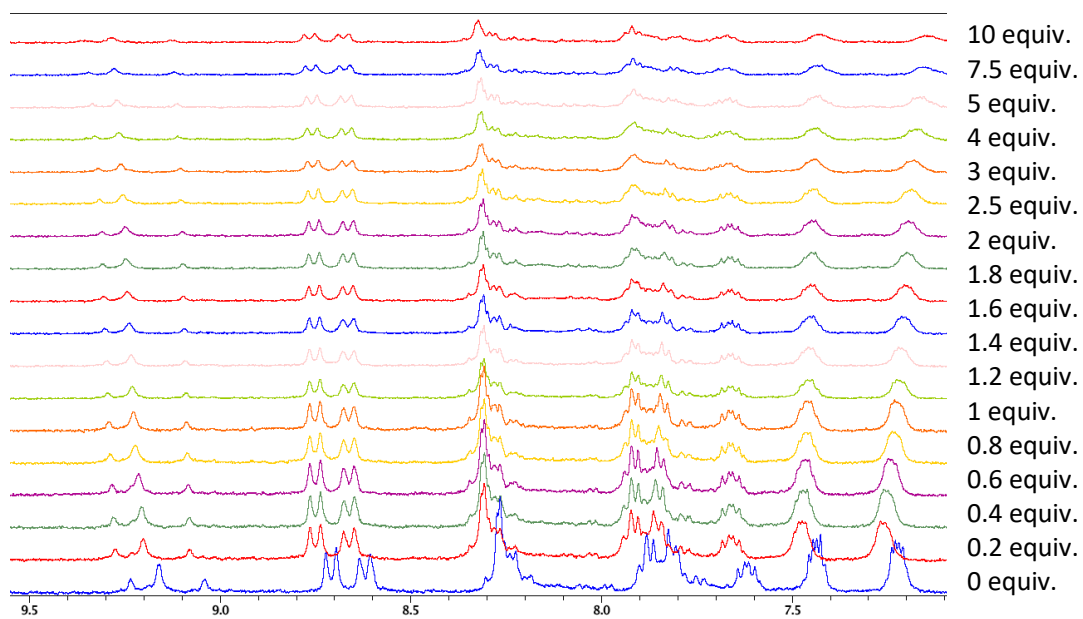
Appx. 46 – phen ac
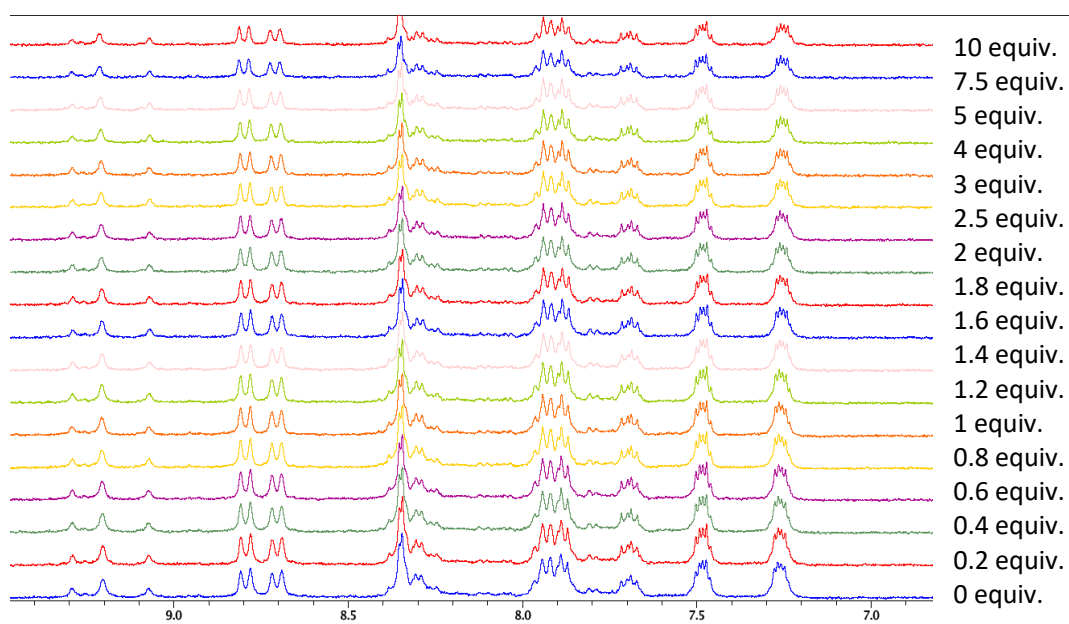
Appx. 47 – phen cl

IR
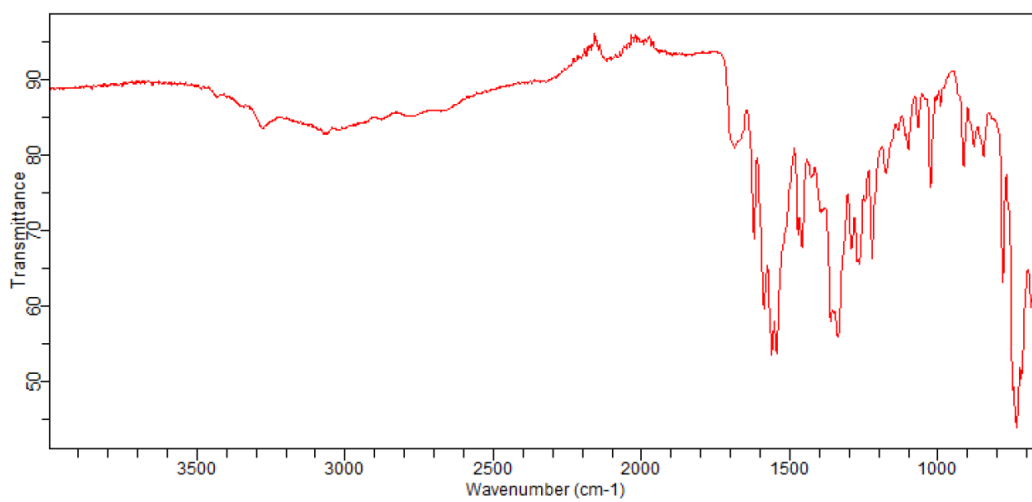
Appx. 48 – bbaib ligand
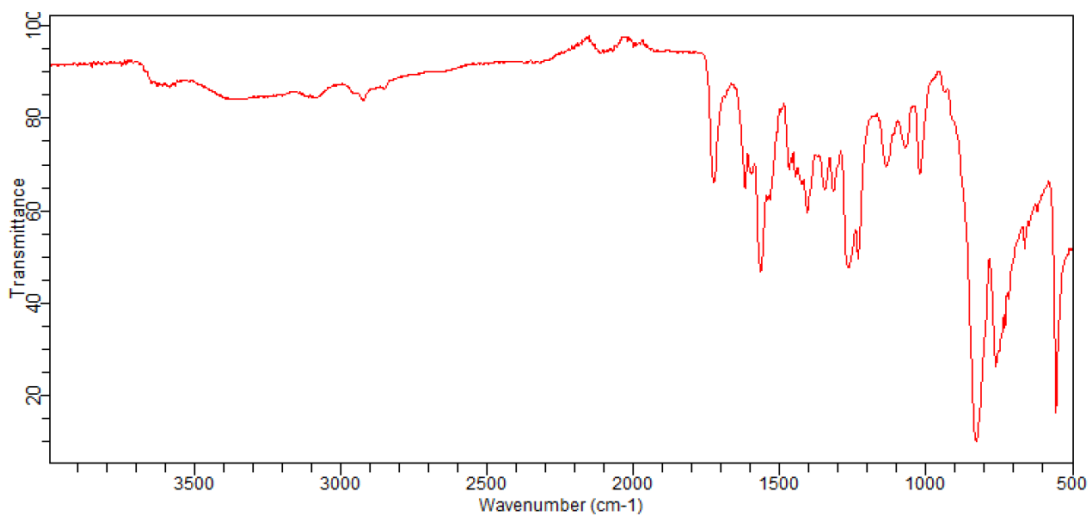
Appx. 49 – bpy bbaib
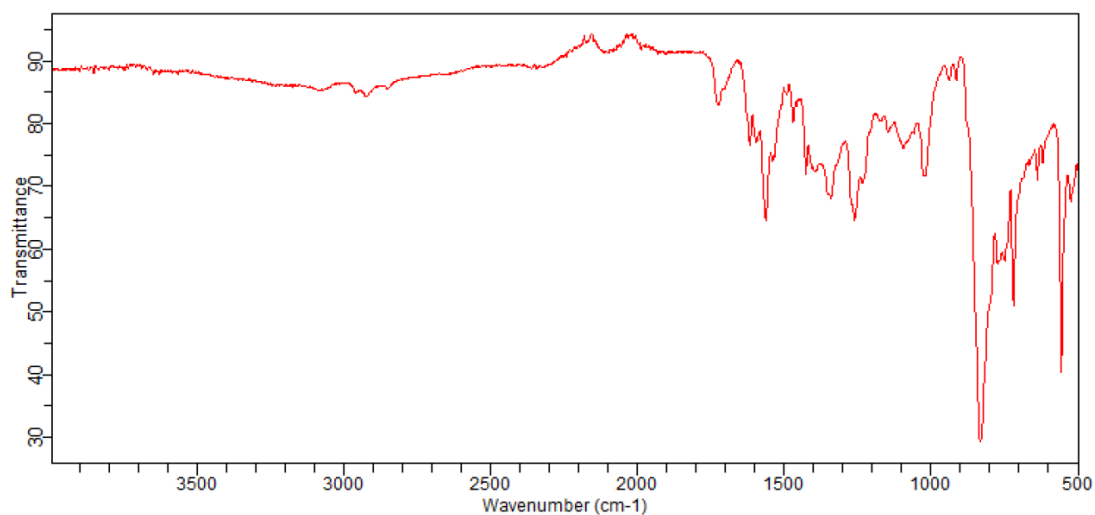
Appx. 50 – phen bbaib

7.2.4 ^{13}C-NMR Spectra
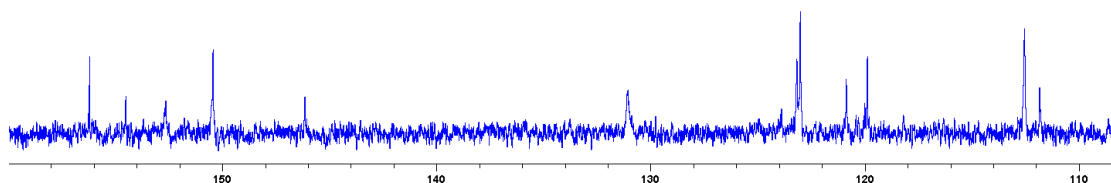
Appx. 51 - bbaib

7.2.5 ¹H-NMR Spectra
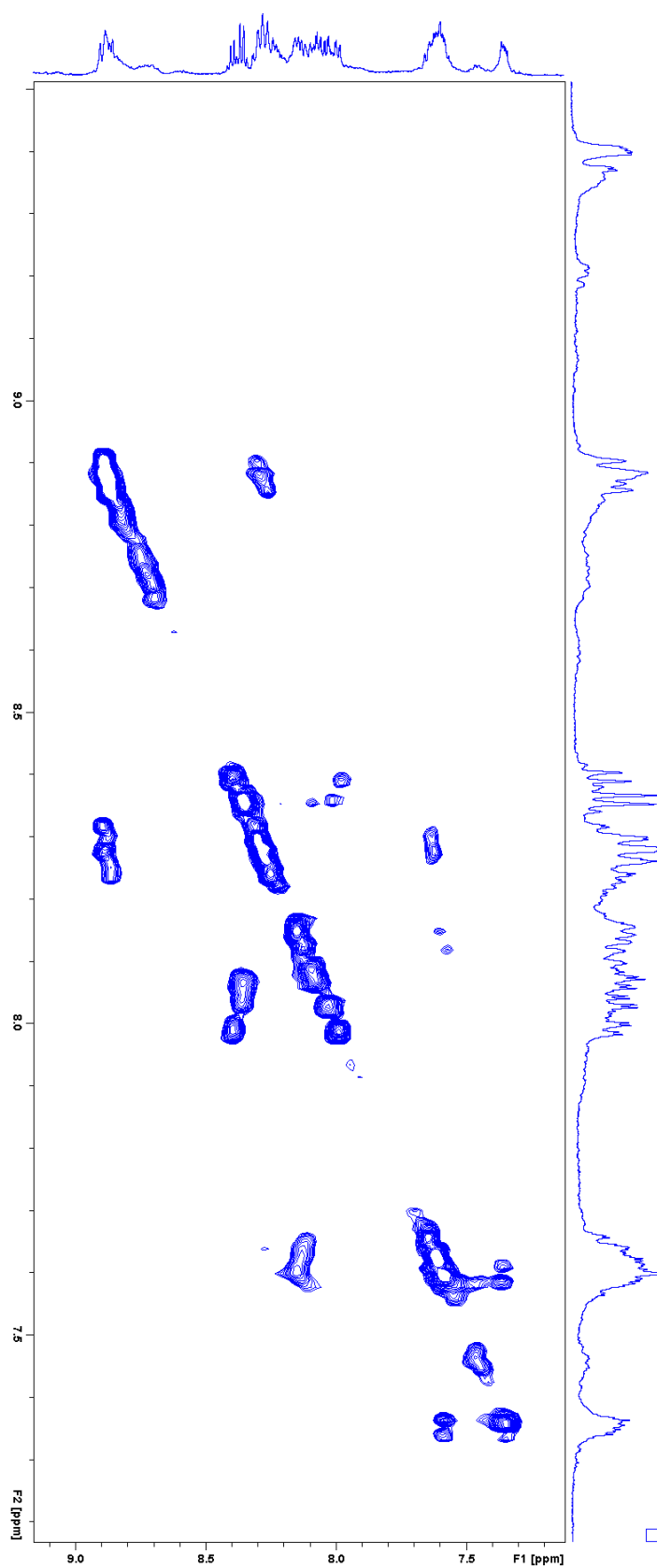
Appx. 52 – bpy bbaib
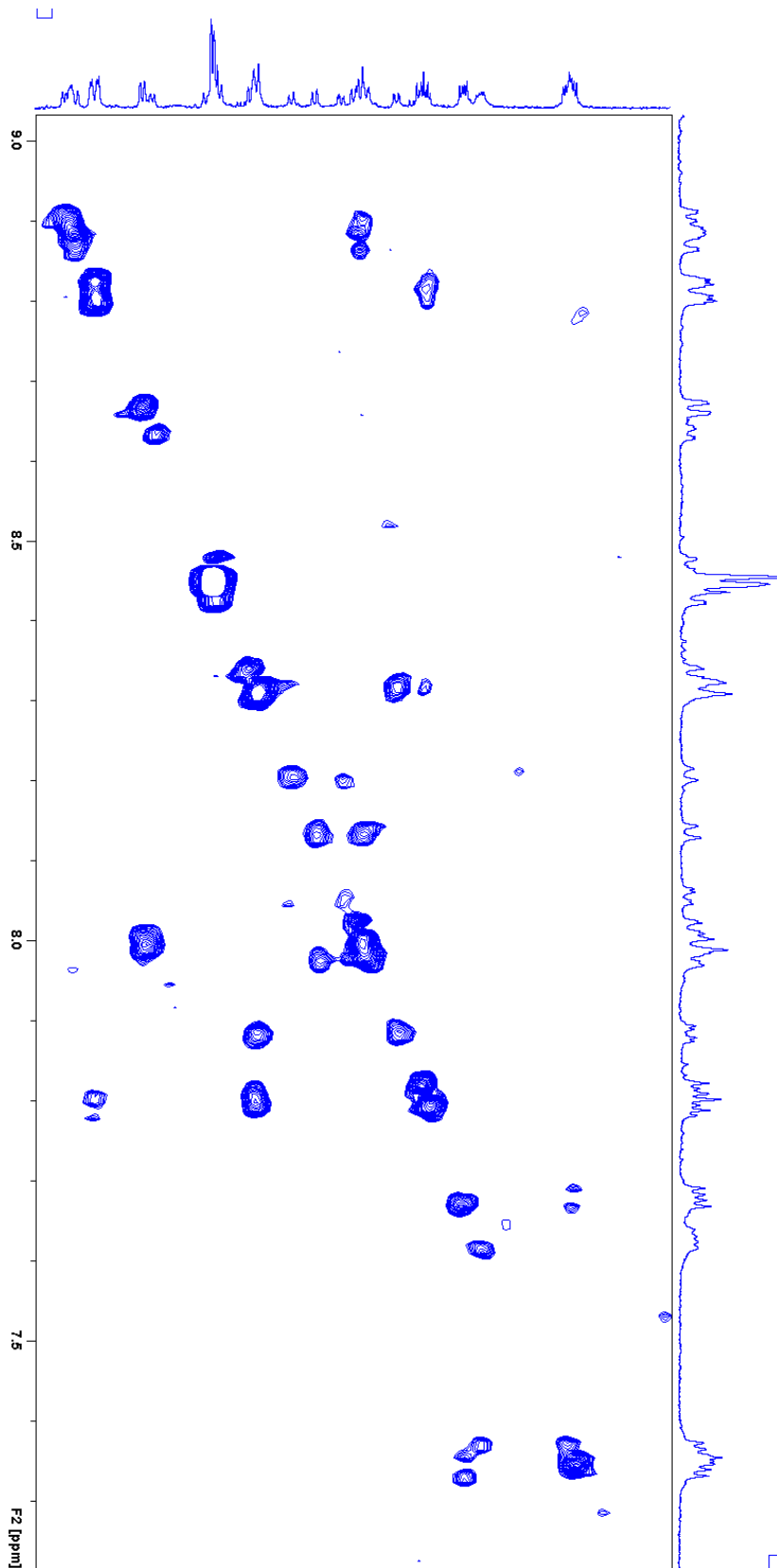
Appx. 53 – phen bbaib

7.3 Data Obtained for [Ru(bpy)$_2$(bbimb)]$^{2+}$ and [Ru(bpy)$_2$(bbimbo)]$^{2+}$ (Chapter Four)

7.3.1 UV/Vis Absorbance Spectra
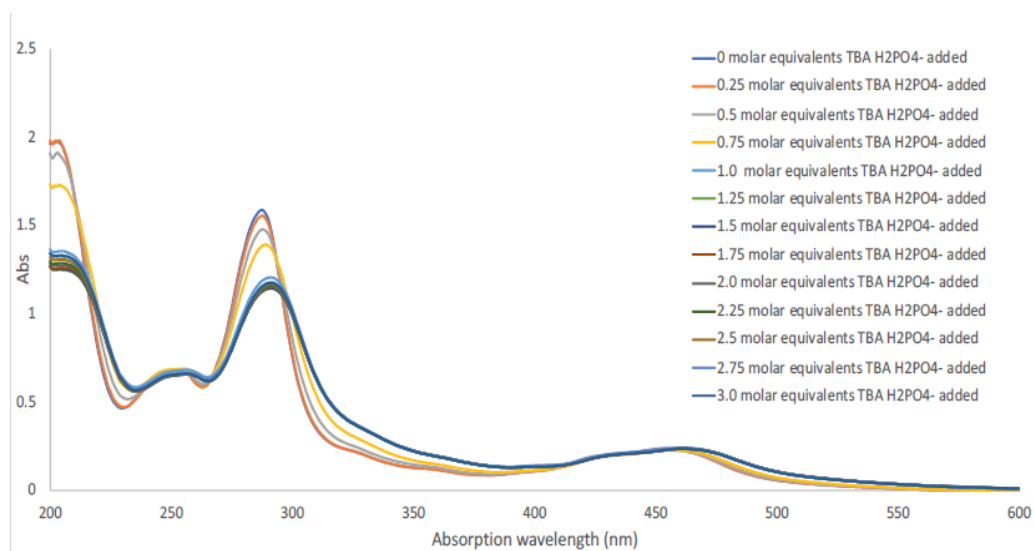
Appx. 54 -
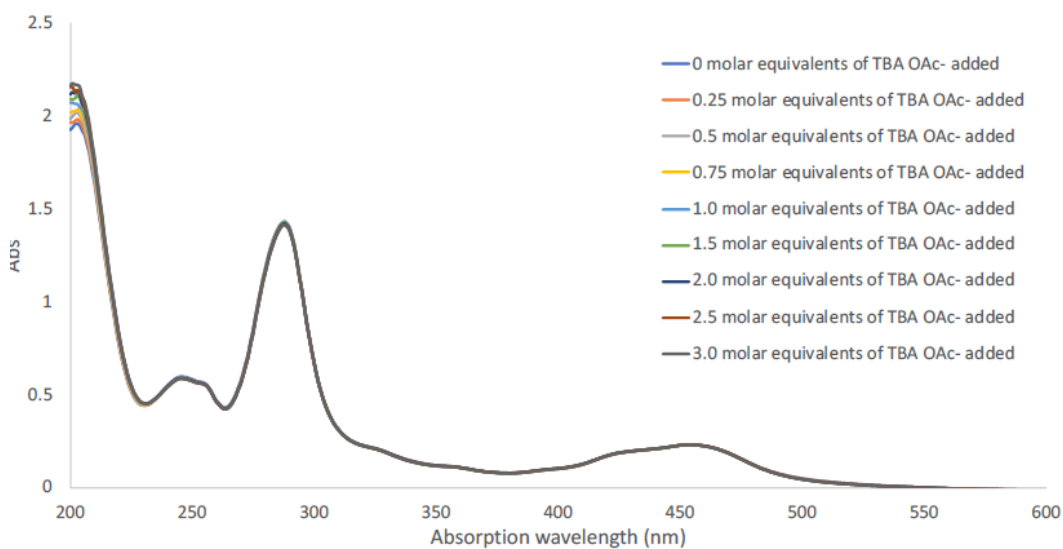
Appx. 55 -
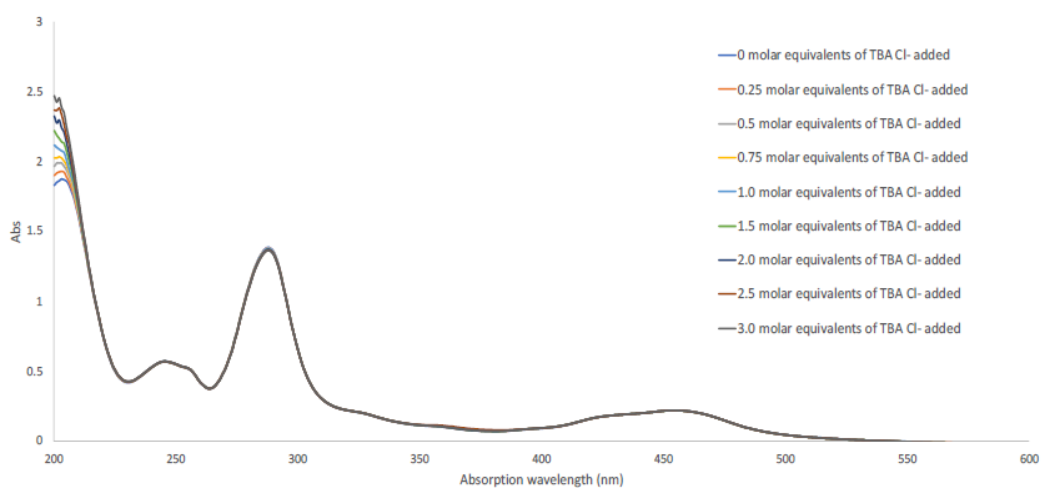
Appx. 56 -
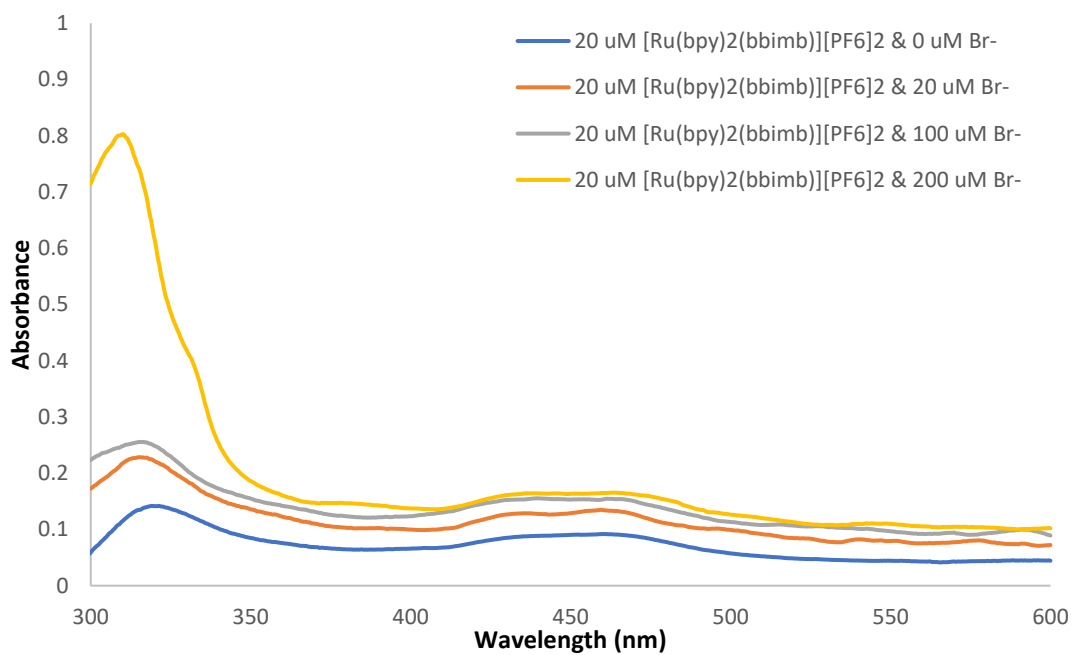
Appx. 57 -
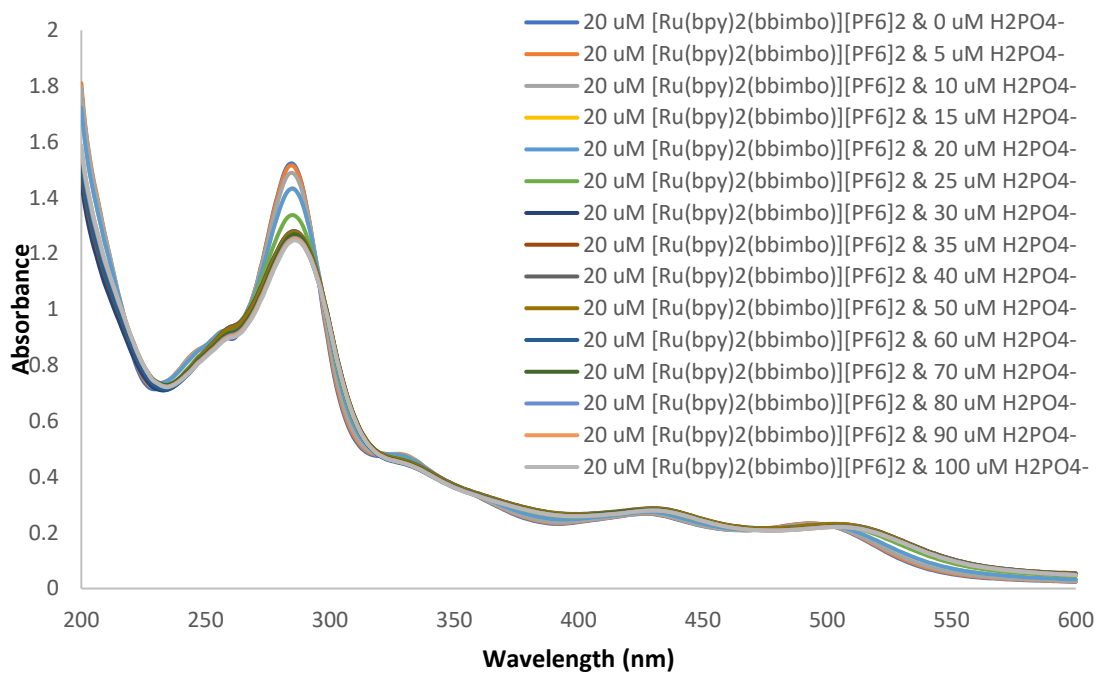
Appx. 58 -
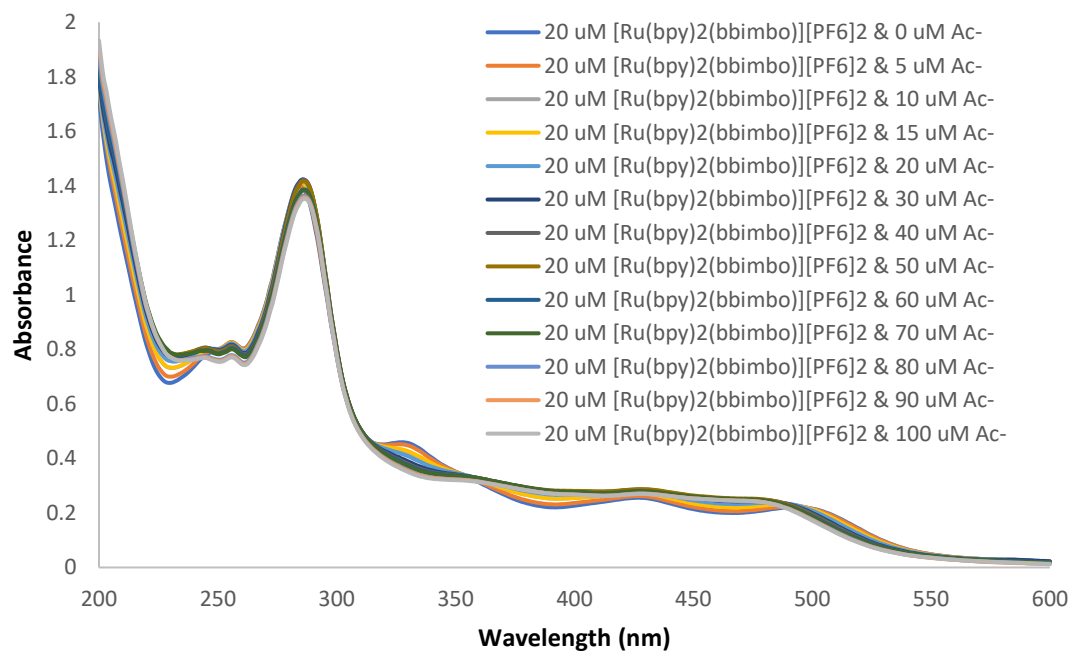
Appx. 59 -
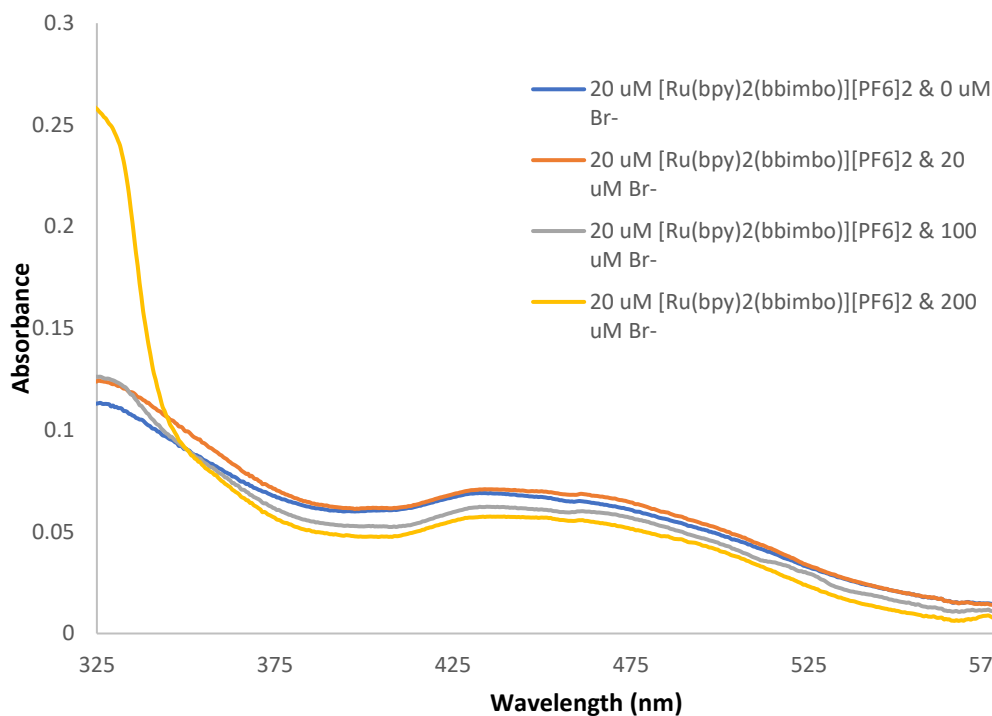
Appx. 60 -

7.3.2 Emission Spectra
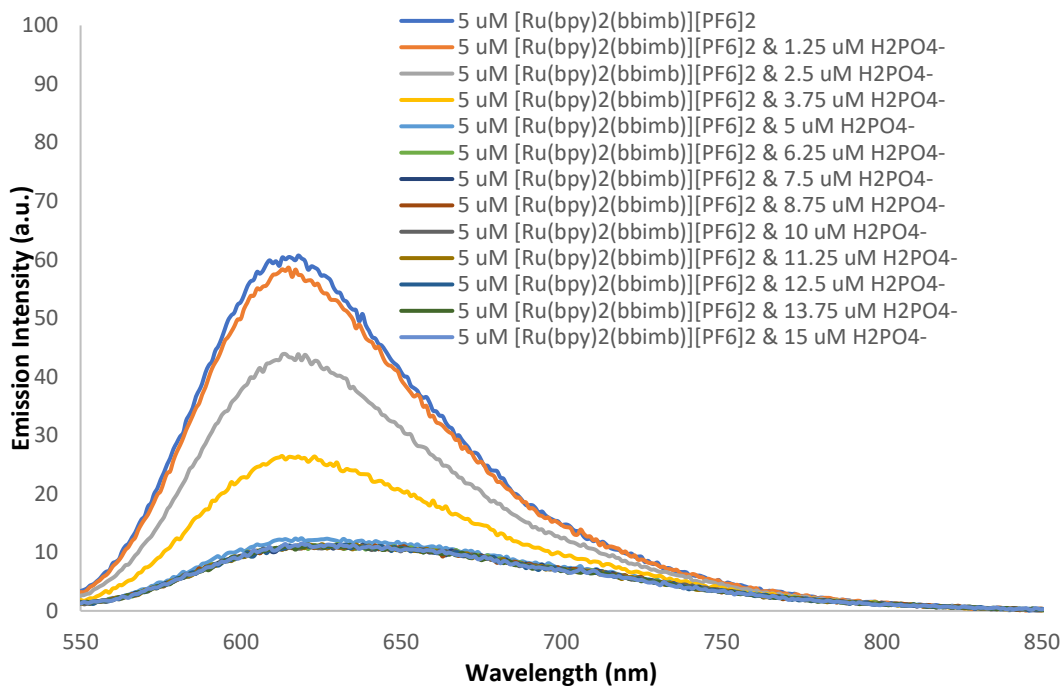
Appx. 61 -
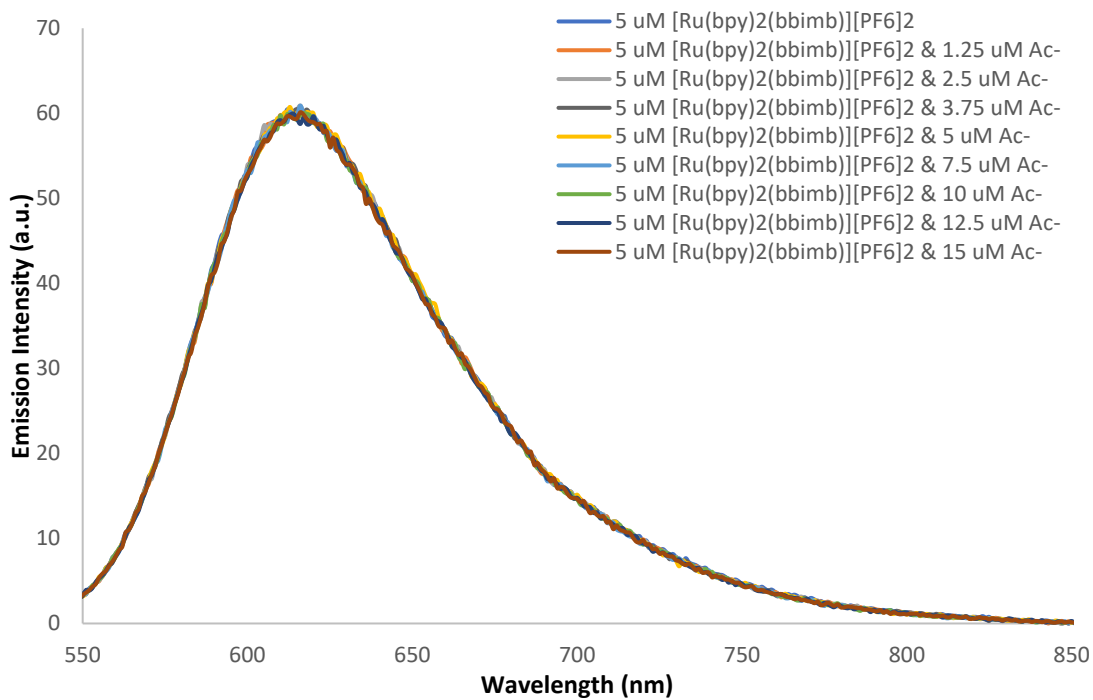
Appx. 62 -
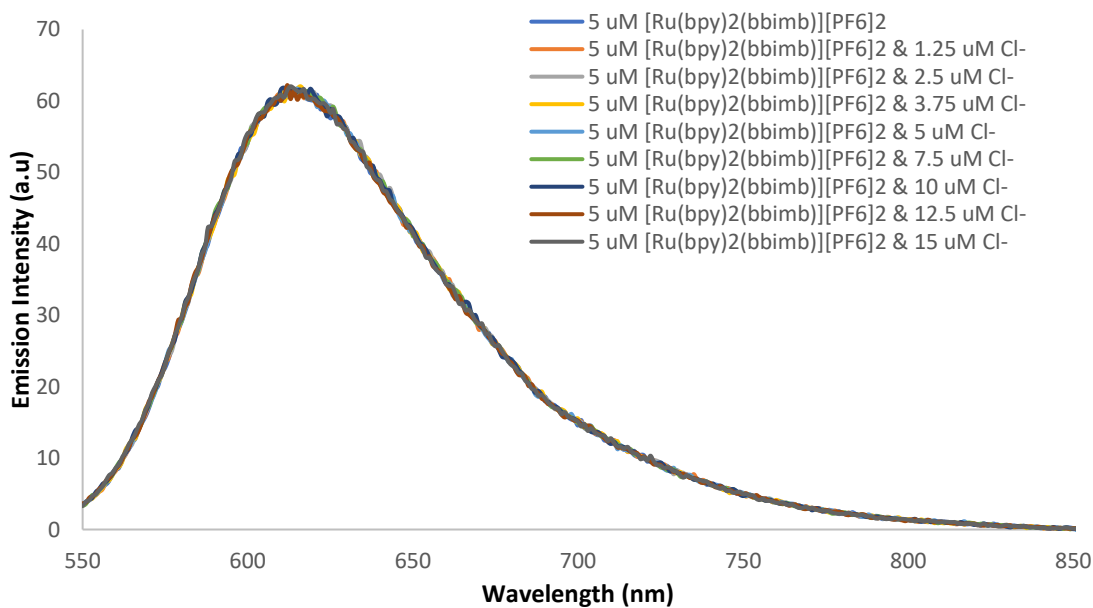
Appx. 63 -
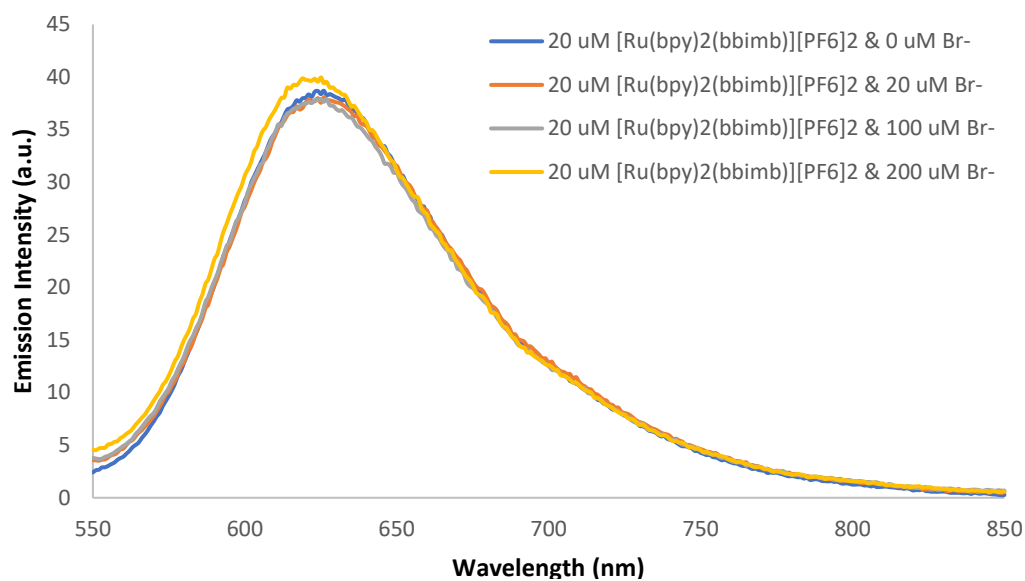
Appx. 64 -
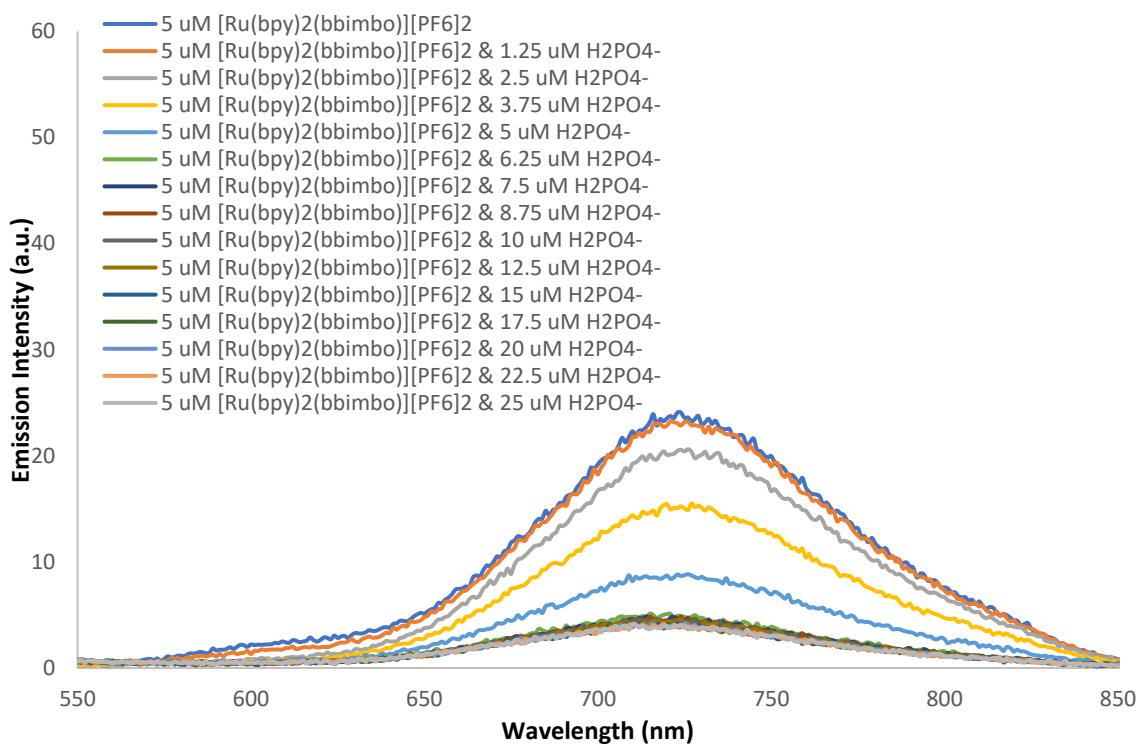
Appx. 65 -
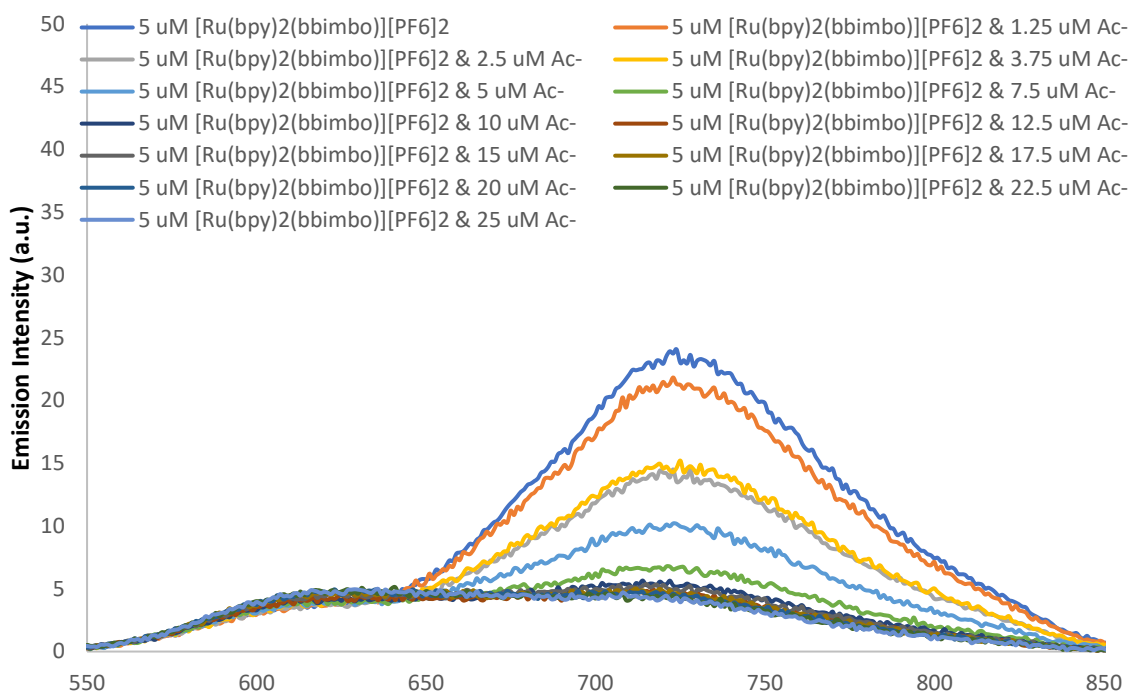
Appx. 66 -
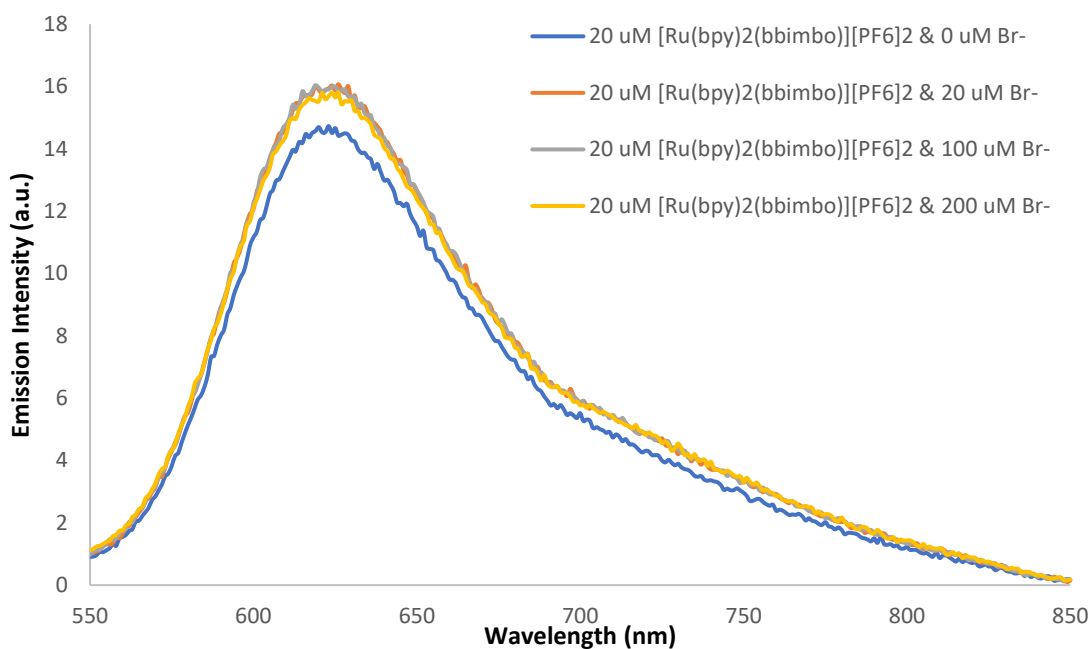
Appx. 67 -

7.3.3 ^{1}H-NMR Titration Spectra
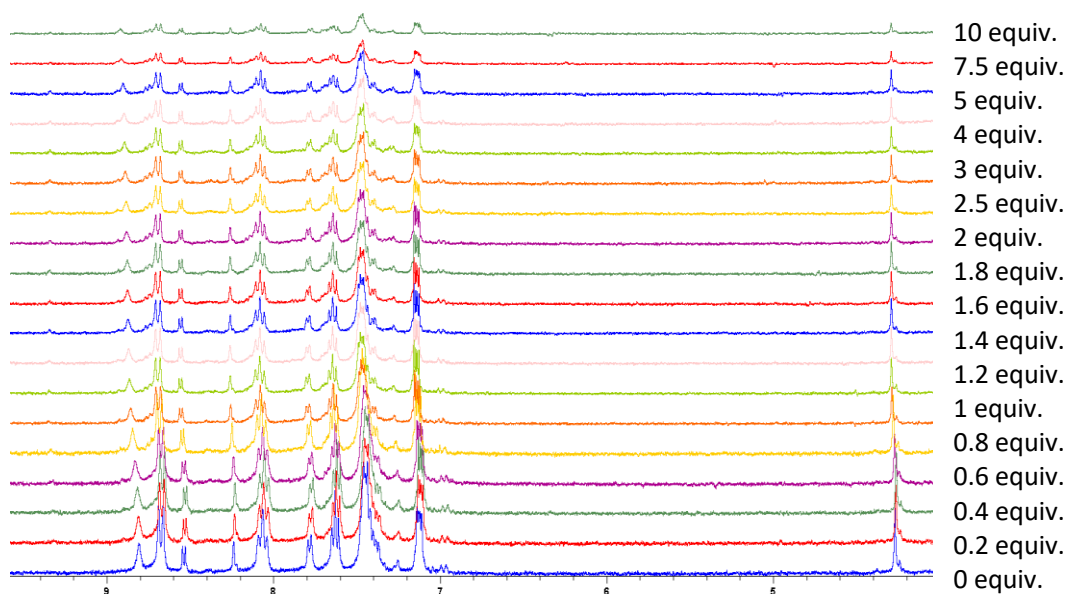
Appx. 68 – bbimb ac
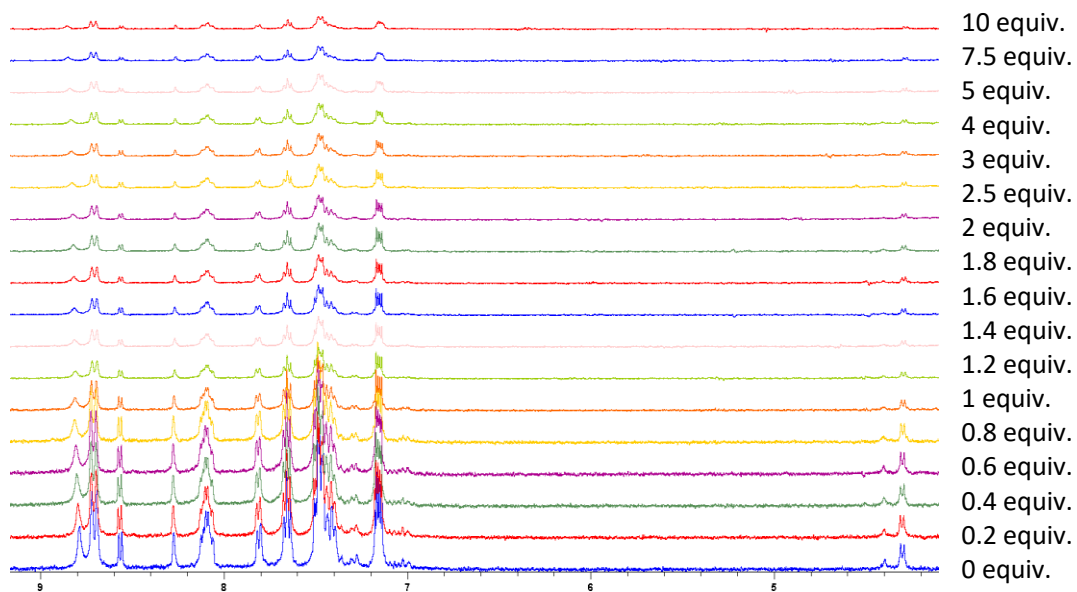
Appx. 69 – bbimb cl
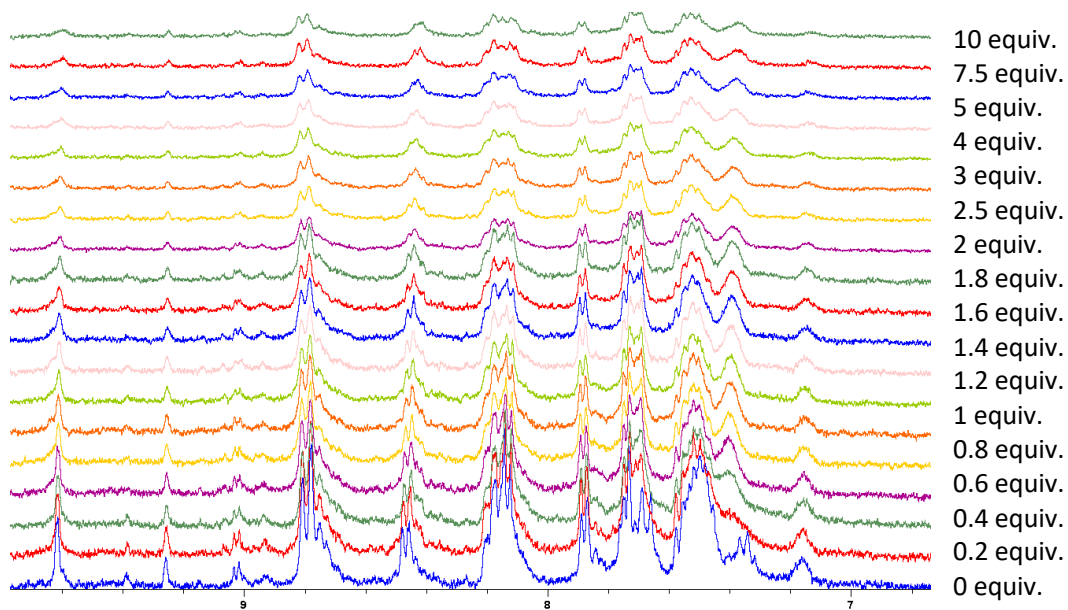
Appx. 70 – bbimbo phos
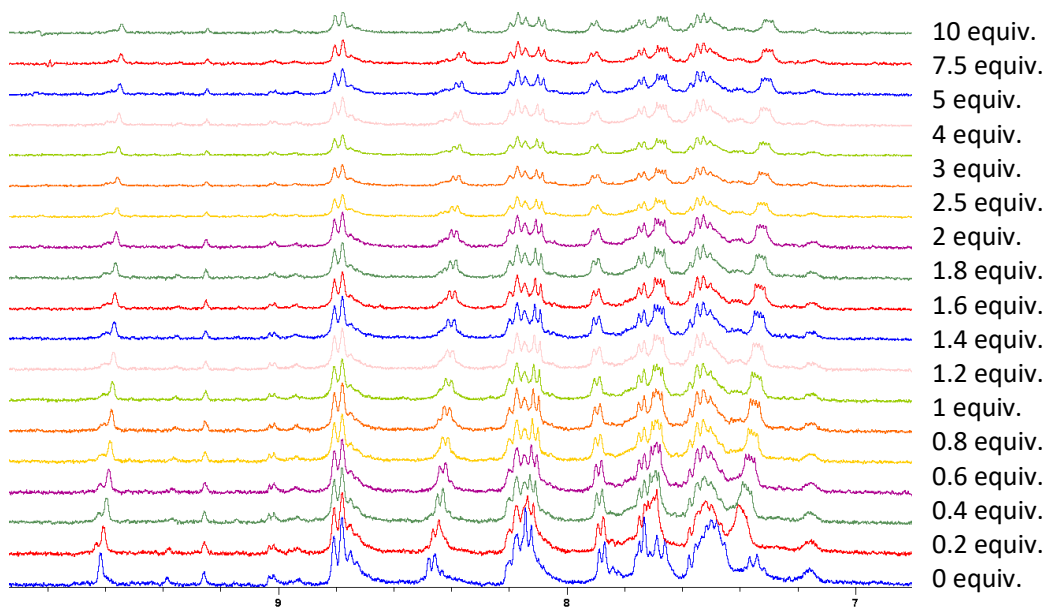
Appx. 71 – bbimbo ac
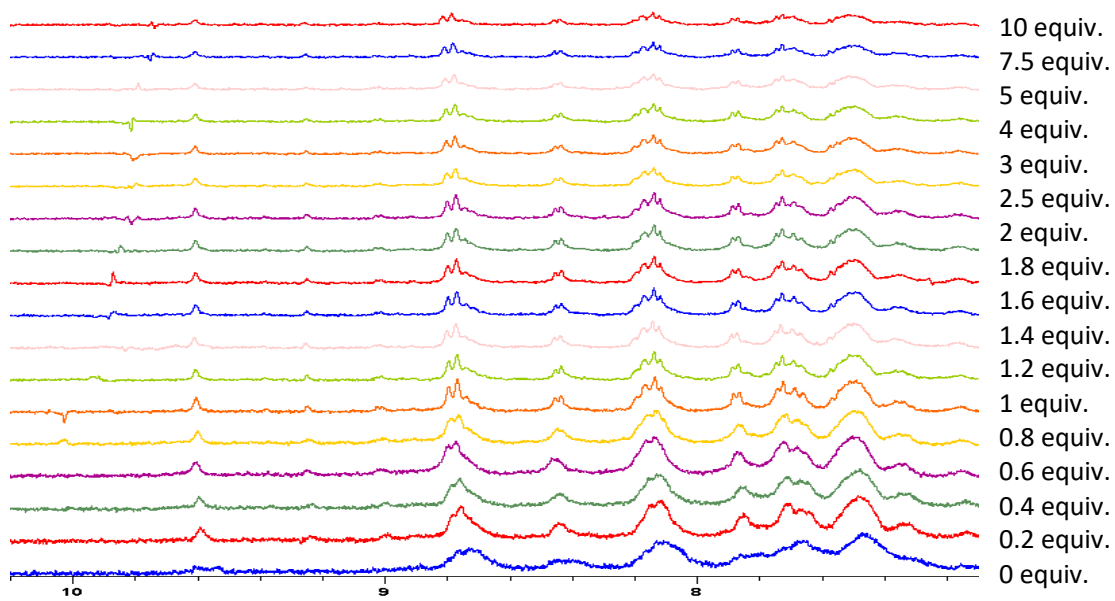
Appx. 72 – bbimbo cl

7.3.4 IR Spectra
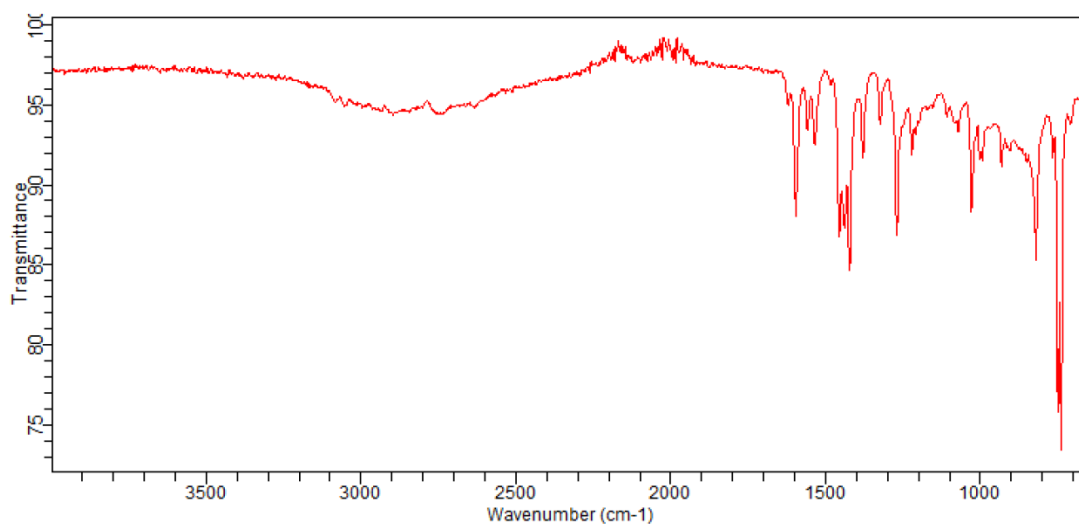
Appx. 73 – bbimb ligand
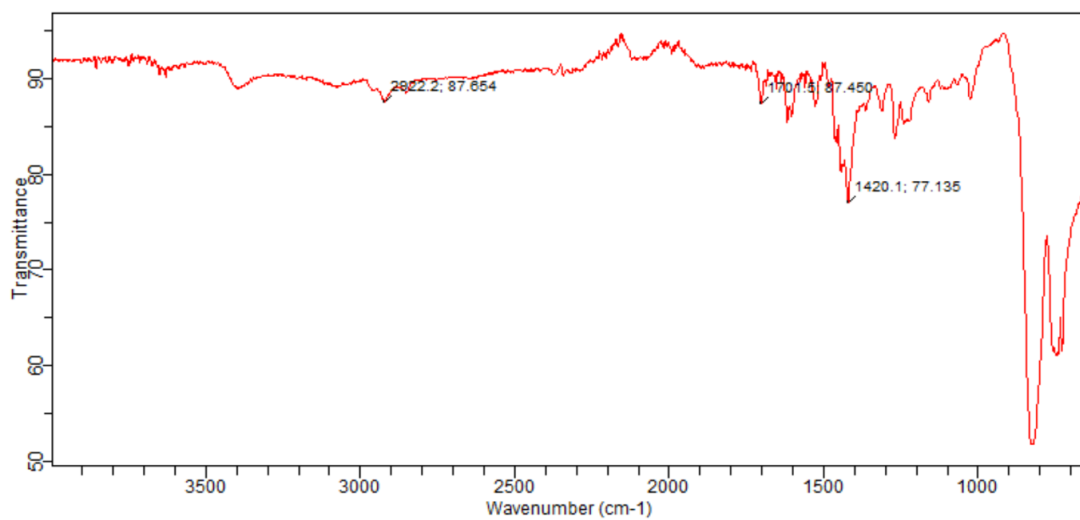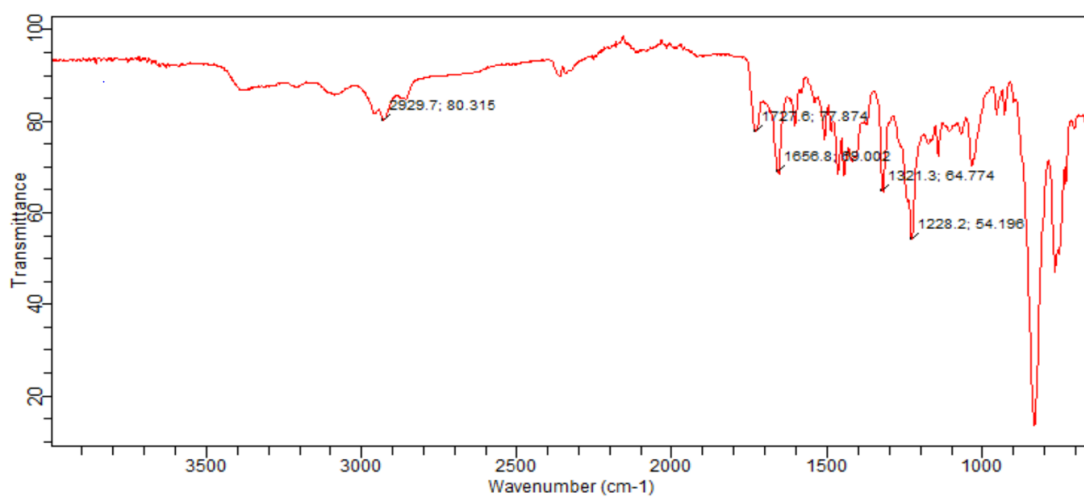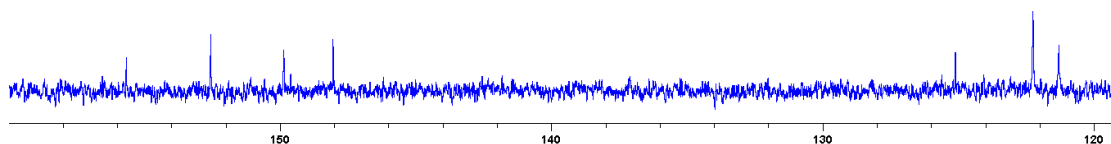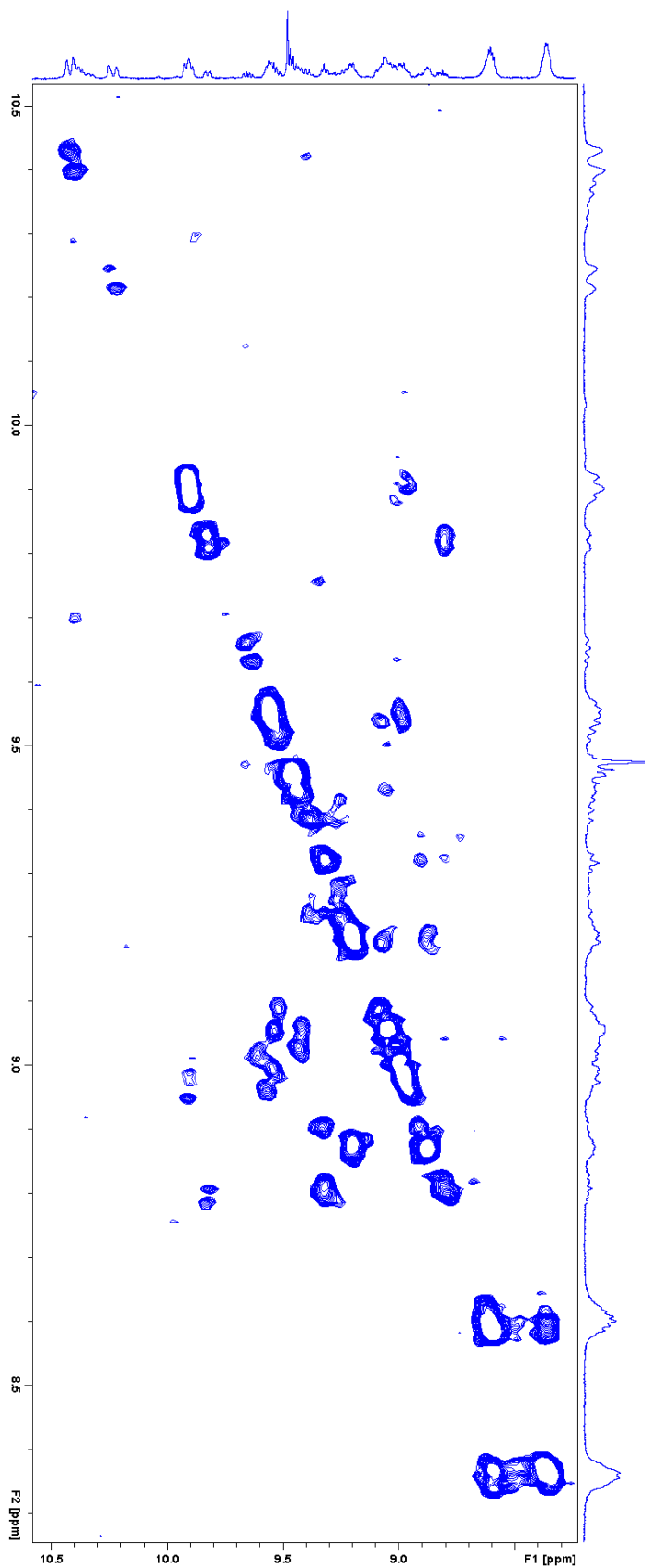
Appx. 74 - bbimb

Appx. 75 - bbimbo

7.3.5 ¹³C-NMR Spectra

Appx. 76 -

7.3.6 ¹H-NMR Spectra

Appx. 77 - *Rubpy2 bbimbo cosy*